

***In Vitro* Experiments Towards A
Mathematical Model of Solid Tumour
Treatment By Thermosensitive
Liposomes**



Michael D. Newsome
St Catherine's College

Supervised by

Professor Robert C. Carlisle
Professor Stephen J. Payne
Professor Constantin-C. Coussios
Department of Engineering Science

University of Oxford

A thesis submitted for the degree of Doctor of Philosophy

October 16, 2023

Abstract

Thermosensitive Liposomes (TSLs) are at a crossroads as a delivery platform. Recent attempts at clinical translation have had mixed outcomes. The HEAT and OPTIMA trials, using TSL doxorubicin and radiofrequency ablation (RFA) as a heating modality did not demonstrate improved outcomes compared to RFA alone. In contrast, the TARDOX trial demonstrated for the first time that the delivery of TSL doxorubicin with localised ultrasound-mediated mild hyperthermia of a deep-seated tumour was safe and feasible, as well as finding elevated levels of intratumoural doxorubicin after heating. Most notably, despite the fact many of the patients had diagnoses which would not ordinarily be expected to respond to doxorubicin therapy, a majority of patients had a localised radiological response following only a single cycle of treatment.

Several key parameters in the TARDOX trial (such as infusion duration, TSL dose, and heating duration) were chosen based on limited prior experimentation and practical considerations associated with an early stage trial. In this thesis, *in vitro* experiments and computational modelling are used to explore the effect of changing these variables on the likely treatment outcome, with a view to optimising the clinical translation of TSLs.

Three scales associated with the delivery of drug to tumours are identified: the clearance scale, which describes the concentration of drug in the systemic plasma; the delivery scale, which describes the extravasation of drug from the tumour vasculature and its transport through the extracellular space; and the pharmacodynamic scale, describing the cellular uptake and cytotoxic effect of the drug.

In the first chapter, a compartment model is used to demonstrate that literature data (from the delivery and pharmacodynamic scales) can be used to accurately resolve treatment of tumours with TSLs in man, comparing the model outputs to the clinical measurements obtained in the TARDOX trial. An initial optimisation is performed considering only the clearance and pharmacodynamic scales, and a sensitivity analysis shows that the predicted optimal treatment parameters are robust to fluctuations in parameters, however the predicted intratumoural concentrations do fluctuate more substantially with changing cellular uptake parameters.

The second research chapter therefore focuses on the pharmacodynamic scale, using experiments to quantify the beneficial effects of mild hyperthermia on cellular uptake and cytotoxicity of doxorubicin in CT26 cells, and provide improved parameters for the computational treatment model. It is found that the addition of mild hyperthermia results in significant increases in both uptake and cytotoxicity, with the cells exhibiting increased sensitivity to intracellular doxorubicin (compared to cells treated at normothermic conditions).

Finally, in the third research chapter, the aforementioned experimental data is used in a model which includes spatial heterogeneity (i.e., the delivery scale). It is demonstrated that spatial heterogeneity is not a substantial issue for doxorubicin TSLs, however in treatment with drugs that exhibit more rapid cellular uptake, this may be more limiting.

Overall, the work in this thesis demonstrates that TSLs should be able to bring a clinical benefit to patients, as increased delivery of drug is predicted with TSLs (compared to non-liposomal forms).

Statement of Originality

I hereby declare that this submission is my own work and, to the best of my knowledge, it contains no materials previously published or written by another person, or substantial proportions of material which have been accepted for the award of any other degree or diploma at the University of Oxford or any other educational institution, except where due acknowledgement is made in the thesis.

Any contribution made to the research by others, with whom I have worked at the University of Oxford or elsewhere, is explicitly acknowledged in the thesis.

I also declare that the intellectual content of this thesis is the product of my own work, except to the extent that assistance from others in the project's design and conception or in style, presentation and linguistic expression is acknowledged.

MD Newsome

Michael Newsome

June 2023

Acknowledgements

The first thanks must go to my three supervisors. Professor Constantin Coussios, for teaching me to look at the big picture (and sanity check my arguments by using poppadoms as a preferred unit of concentration). Professor Robert Carlisle, for agreeing to supervise me mid-way through - your support on cell culture and HPLC was vital in seeing this project through to the end. Professor Stephen Payne, whose guidance through the project, particularly in some of the more challenging times around the pandemic was invaluable.

I have been very lucky to have had the support of many brilliant members of both BUBBL and the Cerebral Haemodynamics Group. I am grateful to Dr Paul Lyon, for answering some of my early questions about the TARDOX trial. Laura Spiers was brilliant to work and laugh with through the slightly strange experience of sticking probes into porcine pancreata (also Laura, thank you for teaching me that this is the correct plural form). Alex, Cameron, Catherine, Tammy, Veerle, Colin, and Wahbi were all very helpful and provided much friendly advice and laughter throughout the process. The most thanks must go to Luca Bau, who dealt with my near-constant (and occasionally well-warranted) anxiety surrounding the HPLC, and who was frequently my first port-of-call for lab troubleshooting of all kinds (ahem, the plate reader works fine now thank you, ahem).

Outside of the lab, thanks are definitely due to Will, for showing me how hard running away from your research problems is, and being a great sounding board in the process. Ben & Emma, thanks for checking in when it got hard, and some good masked-up fun in the bad old days. Similarly, Joe Taylor for organising any number of daft Zoom quizzes (remember those?), stupid games, and socially-distanced barbecues during the pandemic and beyond.

Teaching undergraduates has been a large part of my DPhil experience which has helped me to develop my skills and critical thinking. Thanks are therefore due to Professor Antonis Papachristodoulou who first suggested I tried teaching, and supported me to apply for this DPhil in the first place. Special

thanks must go to Dr Brian Tang for encouraging my professional development as a tutor, as well as providing me with insight on both SCR dining(!) and how to complete a DPhil.

Mum, Dad, and Anna, thank you for your support throughout the last 4 years (and the 22 before that, come to mention it). This might not be model trucks, but I hope it makes you proud. Dad, please don't look too hard for split infinitive phrases at this stage.

Johanna, thank you for encouraging me through all the ups and downs of the last four years. Talking our strange mix of science and silly always makes me happy, and I look forward to that continuing for many years to come!

Statement of Contributions

Chapter 1

- This introductory section is entirely my own work.
- This chapter was reviewed by Professors Stephen Payne, Robert Carlisle, and Constantin Coussios prior to submission.

Chapter 2

- This literature review is entirely my own work.
- This chapter was reviewed by Professors Stephen Payne, Robert Carlisle, and Constantin Coussios prior to submission.

Chapter 3

- The results in this section are entirely my own work.
- This chapter was reviewed by Professors Stephen Payne and Constantin Coussios prior to submission.

Chapter 4

- The devising of the use of a BCA assay in place of trypan blue exclusion for cell counting was done in collaboration with Professor Robert Carlisle.
- Sample collection and preparation was entirely my own work.
- The original HPLC protocol was devised by Dr Luca Bau, and the sample preparation steps were devised in collaboration with Dr Luca Bau.

- HPLC data processing was performed in MATLAB based on an original script by (and with guidance from) Dr Luca Bau.
- Advice on statistical testing was received from Dr Luca Bau, Professor Malavika Nair, and Professor Robert Carlisle. Otherwise data processing was entirely my own work.
- Fitting the experimental data to a mathematical model was performed with guidance from Dr Luca Bau.
- This chapter was reviewed by Professors Stephen Payne, Robert Carlisle, and Constantin Coussios prior to submission.

Chapter 5

- The results in this section are entirely my own work.
- This chapter was reviewed by Professors Stephen Payne, and Constantin Coussios prior to submission.

Chapter 6

- This concluding chapter and suggestions for further work are entirely my own work.
- This chapter was reviewed by Professors Stephen Payne, Robert Carlisle, and Constantin Coussios prior to submission.

Appendix A

- The results in this section are entirely my own work.
- This chapter was reviewed by Professors Constantin Coussios and Stephen Payne prior to submission.

Appendix B

- The results in this section are entirely my own work.
- This chapter was reviewed by Professors Stephen Payne, Robert Carlisle and Constantin Coussios prior to submission.

Appendix C

- The work in this section was completed in an equal collaboration with Dr Laura Spiers.
- Fresh *ex vivo* tissue was provided by Dr Tamsyn Clark.

Dissemination

Peer-Reviewed Journal Papers

Newsome, M.D., Payne, S.J., Carlisle, R.C., Coussios, C-C. *'Mathematical Models of the Effect of Hyperthermia on the Cytotoxicity and Cellular Uptake of Doxorubicin in CT26 Cells'* (in preparation)

Conference Presentations

Newsome, M.D., Bau, L., Payne, S.J., Carlisle, R.C., Coussios, C-C. *'Uncovering the Relationship between Extracellular Drug Dose, Hyperthermia Time and the Resulting Intracellular Dose and Cell Kill'* (Poster), European Society of Hyperthermic Oncology, Gothenburg, Sweden, 14-17 September 2022

Newsome, M.D., Coussios, C-C., Payne, S.J. *'Compartmental Modelling of Cancer Treatment with ThermoDox®'* (Oral Presentation), 7th International Conference on Computational and Mathematical Biomedical Engineering, Milan, Italy, 27-29 June 2022

Contents

1	Introduction	1
1.1	Background	1
1.2	Synopsis	4
2	Literature Review	6
2.1	Solid Tumours	6
2.2	Chemotherapy	7
2.2.1	Pharmacokinetic Models	9
2.3	Drug Delivery Systems	11
2.3.1	Enhanced Permeability and Retention (EPR) Effect	12
2.4	Thermosensitive Liposomes	14
2.5	Doxorubicin	18
2.5.1	Pharmacodynamic Modelling	21
2.6	Hyperthermia, Solid Tumours, and Small Molecule Therapeutics	23
2.6.1	Heating Modalities	25
2.7	Mathematical Modelling of Chemotherapy	26
2.7.1	Previous Compartment Model Studies	26
2.7.2	Including Spatial Heterogeneity	30
2.8	Aims of the Present Work	32
3	Compartment Models of Thermosensitive Liposomal Doxorubicin Delivery	33
3.1	Introduction	33
3.2	The Compartment Model	34
3.2.1	Non-Ideal Heating	36
3.3	Comparison to Clinical Results	41
3.3.1	Sensitivity Analysis	45

3.4	Optimisation of Treatment	47
3.4.1	Optimisation of Infusion Duration with Concurrent Hyperthermia	52
3.4.2	Optimisation of Infusion Duration for Fixed Hyperthermia Duration	52
3.4.3	Global Sensitivity Analysis of the Optimal Infusion Duration	53
3.5	Variations in Model Input	55
3.5.1	When to Heat - During or After Infusion?	55
3.5.2	Altering the Total Administered Dose	57
3.5.3	Exploring Alternative Cellular Uptake Models	59
3.6	Summary	61
4	Characterising the Link Between Cytotoxicity and Intracellular Doxorubicin Concentration	63
4.1	Introduction	63
4.2	Studying Cell Viability: Materials and Methods	65
4.2.1	Cell Culture	65
4.2.2	Cell Counting	66
4.2.3	Doxorubicin and Choice of Treatment Conditions to be Assayed	66
4.2.4	Achieving Hyperthermia	67
4.2.5	Assaying for Cell Viability	68
4.3	Faster Cell Viability Assays	68
4.3.1	Assessment of Cell Viability with Trypan Blue	68
4.3.2	Assessment of Cell Viability with an MTS Assay	69
4.3.3	Assessment of Cell Viability with an Imaging Cytometer	72
4.3.4	Summary	76
4.4	Clonogenic Assay	76
4.4.1	Protocol	76
4.4.2	Results	79
4.5	Cell Viability Data Discussion	81
4.5.1	Mechanism of Action of Doxorubicin	82
4.5.2	Strengths and Weaknesses of the Clonogenic Assay	85
4.6	Determination of Intracellular Concentration	86
4.6.1	Results	90
4.6.2	Comparing Cell Counting with Trypan Blue Exclusion and the Bicinchoninic Acid Assay	90

<i>CONTENTS</i>	xii
4.7 Combining Viability and Intracellular Concentration	94
4.7.1 Intracellular Concentration - An Acceptable Metric for Cell Kill?	94
4.7.2 Mathematical Models for Cellular Uptake of Doxorubicin in CT26 Cells	95
4.7.3 Combining Uptake and Cell Survival	104
4.8 Summary	108
5 Optimised Thermosensitive Liposomal Drug Delivery to Patients Accounting for Spatial Variations	110
5.1 Introduction	110
5.2 Compartment Model with Hyperthermia	111
5.2.1 Optimal Free Doxorubicin Treatments	111
5.2.2 Optimal TSL Delivery	114
5.2.3 TSL Delivery with Non-Ideal Heating	114
5.2.4 Idarubicin - The Future of TSLs?	117
5.2.5 Liposomal Extravasation as a Delivery Mechanism	121
5.3 Krogh Cylinder Models - An Introduction	122
5.4 Free Doxorubicin Infusion - A 1D Krogh Model	124
5.5 TSLs and spatial variations	129
5.6 Cylinder Models with Axial Variations	132
5.7 Summary	138
6 Conclusions	140
6.1 Future Work	141
Appendices	145
Appendix A Global Sensitivity Analysis and Lessons For Using Small Animal Models	146
A.1 Example Elementary Effects Test: Interpreting the Results	146
A.1.1 Sensitivity Analysis on Model Output	148
A.2 Non-Optimal Infusion Durations - Effect on Intracellular Concentrations	152
A.3 <i>In vivo</i> models and Compartment Models	152
A.3.1 Comparing LTSL and Free Drug Delivery <i>In Vivo</i>	155
Appendix B Justification of Experimental Parameters	158
B.1 Acceptable Level of Doxorubicin Solvent	158
B.2 Consideration of Doxorubicin-Protein Binding	160

B.3	When to Assay for Cell Viability	164
B.4	Demonstrating Linearity and Choosing Incubation Period for the MTS Assay	165
B.5	Determination of Seeding Density and Incubation Time for the Clonogenic Assay . . .	166

Appendix C Microdialysis as a Method to Quantify Transport of Doxorubicin in *Ex Vivo*

Porcine Tissue		169
C.1	Microdialysis	169
C.1.1	Extraction Efficiency	169
C.2	Porcine Pancreas	172
C.3	Biopsies	172
C.4	Fluorescence Imaging	176
C.5	Summary	176

List of Figures

1.1	The different scales involved with the problem of optimising drug delivery to tumours.	4
2.1	Photo showing the distribution of doxorubicin (blue) in a murine mammary adenocarcinoma, with the blood vessels stained red and regions of hypoxia shown in green. Scale bar: 100 μm . Reproduced with permission from [42].	9
2.2	An example of a compartment model from Dawidczyk et al. [46], reproduced with permission.	11
2.3	Diagram of Doxil reproduced from [52] with permission, showing the lipid bilayer, encapsulated doxorubicin and surface-bound MPEG (this is a PEGylated liposome), to increase circulation half life by avoiding MPS clearance.	13
2.4	Adapted from [93] with permission. A) Survival fraction of murine L-929 fibroblasts compared with duration of exposure at constant extracellular concentration; and B) compared with mean intracellular fluorescence	20
2.5	Typical dose-response curves for a cytotoxic agent, modelled with a Hill equation: $V = \frac{1}{1+(K/c)^s}$, where V is the viability, c is the relevant concentration of the drug, K represents the concentration at which $V = 0.5$ (in these plots, $K = 0.5$), and s , is the slope of the curve. The larger the magnitude of s , the steeper the response.	21
2.6	A compartment model similar to that used by McKenna et al. [104], with irreversible nuclear binding. k_{EF} is the first order rate constant of free doxorubicin transport from the extracellular space to the intracellular compartment, while k_{FE} represents the reverse process. k_{FN} is the first order rate constant between the intracellular space and the nucleus; a process which is modelled here as irreversible.	23
2.7	Simulation results from [67], reproduced with permission. The curves are labelled with the simulated infusion duration of free doxorubicin.	28
2.8	Illustration of microvascular network used in time-dependent Green's function method, adapted from [127] with permission.	31

3.1	Compartment model. Doxorubicin molecules (red), are infused into the systemic plasma compartment, encapsulated in thermosensitive liposomes (dark blue). Both liposomal and free doxorubicin can enter the tumour extracellular space, but only free doxorubicin can then enter the tumour cells. Blue compartments denote the encapsulated drug, green compartments denote the unencapsulated, 'free' drug. Encapsulated doxorubicin is assumed not to accumulate in the peripheral tissue owing to its size. This is a typical assumption of such models [e.g. 65].	34
3.2	Results from the TARDOX compartment model simulation, $PIR_s = 0.5$, weighted arithmetic mean. Tumour concentrations are shown on the left plot and systemic concentrations are shown on the right plot.	38
3.3	Results from the TARDOX compartment model simulation, $PIR_s = 1$, weighted arithmetic mean. Tumour concentrations are shown on the left plot and systemic concentrations are shown on the right plot.	39
3.4	Results from the compartment model simulation, $PIR_s = 1$, weighted geometric mean. Tumour concentrations are shown on the left plot and systemic concentrations are shown on the right plot.	40
3.5	Plot showing the predicted peak tumour intracellular and extracellular concentrations as PIR_s is varied between 0.1 and 1 in the idealised TARDOX protocol, using both the weighted arithmetic and weighted geometric approaches. PIR_t is not shown on this plot owing to the more complex definition of PIR_t , i.e. that it requires a time block, and the specification of whether hyperthermia is initially on or off.	42
3.6	Plot showing the tumour concentrations resulting from the compartment model simulation of the TARDOX trial with $PIR_t = 0.5$, using a time block of 5 minutes of hyperthermia with heating initially on.	43
3.7	Comparison of the patient data points from the TARDOX trial and the predictions made by the compartment model for a 30 minute initial infusion, followed by 60 minutes of hyperthermia with $PIR_t = 0.5$, using a hyperthermia time block of five minutes.	45
3.8	Results of an elementary effects test performed on the peak intracellular concentration in units of $\mu\text{g}/\text{mL}$ resulting from the idealised version of the TARDOX protocol used in this chapter, with $PIR = 1$. The number of effects sampled for each input, r , was 50.	48
3.9	Plot showing how the peak intracellular concentration in $\mu\text{g}/\text{mL}$ changes as the cell volume is varied across the range specified in Table 3.2.	48

3.10 Plot showing how the peak intracellular concentration in $\mu\text{g/mL}$ changes as V_{max} is varied across the range specified in Table 3.2.	49
3.11 Plot showing how the peak intracellular concentration in $\mu\text{g/mL}$ changes as $k_{e,lip}$ is varied across the range specified in Table 3.2.	49
3.12 A plot of the maximum predicted intracellular concentration using LTSL and free doxorubicin with concurrent infusion and hyperthermia, as a function of the infusion duration. $\text{PIR}_s = 0.5$ for LTSL drug delivery.	53
3.13 Plot showing the peak intracellular concentrations achieved with 90 minutes of hyperthermia from $t = 0$ minutes and $\text{PIR}_s = 0.5$, as well as the peak intracellular concentrations achieved with an infusion of free doxorubicin.	54
3.14 Results from the elementary effects test with the output of the optimal infusion duration (in minutes), for the case of 90 minutes of hyperthermia beginning at $t = 0$ minutes, with the optimal infusion time being selected as that which results in the largest value of peak intracellular concentration ($r = 10$).	55
3.15 Plots showing how the optimal infusion duration based on peak intracellular concentration varies for 90 minutes of hyperthermia varies over the range of input values for a) $K_{m,extra}$ and b) R_{37} . The plots are not smooth owing to the discrete nature of both the parameter variation and the infusion times tested. 50 values of the parameter were sampled with a linear spacing in the stated range, while infusion time was sampled with a timestep of 1 minute from 1 minute to 360 minutes.	56
3.16 Plot showing the resulting tumour intracellular (solid lines) and extracellular (dashed lines) of free doxorubicin in the tumour for the idealised TARDOX protocol (30 minute infusion, followed by 60 minutes of heating), PANDOX protocol (30 minute infusion with 90 minutes of heating starting at $t = 0$ minutes), and a protocol which used a 30 minute infusion and 60 minutes of heating also starting at $t = 0$ minutes as blue, black, and red lines respectively. $\text{PIR}_s = 0.5$	58
3.17 A plot of the maximum values of relevant concentrations as total patient dose is varied, using a saturable model of cellular uptake. The vertical black dashed line represents the dose given in the TARDOX trial. ($\text{PIR}_s = 0.5$)	59
3.18 Plot showing how peak intracellular concentration still has a saturable relationship with dose across the therapeutic range, even with the inclusion of a linear uptake term, $\text{PIR}_s = 0.5$	61

- 4.1 A schematic of the experimental procedures used in this chapter to obtain mathematical models of cellular uptake and cytotoxicity of doxorubicin in CT26 cells. Created with BioRender.com. 64
- 4.2 Cell viability assessed by MTS assay measured 24 hours after exposure to varying doxorubicin concentration for 15 minutes. Brown squares represent the mean of five independent wells and the error bars the standard deviation. Standard deviation of negative control (i.e. zero doxorubicin), not shown due to logarithmic scale, was 4.77%. 'Viability (%)' calculated as described in Section 4.3.2. 71
- 4.3 Cell viability assessed by MTS assay measured 24 hours after exposure to varying doxorubicin concentration for 30 minutes. Brown squares represent the mean of five independent wells and the error bars the standard deviation. Standard deviation of negative control (i.e. zero doxorubicin), not shown due to logarithmic scale, was 4.04%. 'Viability (%)' calculated as described in Section 4.3.2 72
- 4.4 Results of an experiment to check how the MTS assay resolves an expected 'complete' cell death. Cells were treated for 72 hours with 1.8 $\mu\text{g}/\text{mL}$ doxorubicin, positive control (70% EtOH), or a negative control. The MTS assay was performed immediately after removal of treatment and the subsequent wash steps. Usual data processing was not followed here - two standard deviations of the negative control were not added to the noise signal to avoid a negative viability in the doxorubicin treatment group. Error bars represent the standard deviation, $n = 5$. Tukey's multiple comparisons test was performed in GraphPad PRISM and found that both treatment groups were significantly different from the negative control ($p < 0.0001$), but the treatment groups were not significantly different from each other ($p = 0.3785$). 73
- 4.5 Representative Celigo brightfield image of a sample of (left) an untreated well, and (right) a well treated for 30 minutes with 64 $\mu\text{g}/\text{mL}$ doxorubicin, 48 hours after the removal of doxorubicin-free media. Both scale bars 200 μm 73
- 4.6 Cell viability assessed by Celigo automated cell counting, 48 hours post exposure to varying doxorubicin concentration for 30 minutes. Red squares represent the mean of five independent wells and the error bars the standard deviation. Standard deviation of negative control (i.e. zero doxorubicin), not shown due to logarithmic scale, was 2.4%. Viability was calculated as the number of cells counted in the treatment wells/number of cells counted in the negative control wells. 74

- 4.7 The sample images in Figure 4.5, with the results from the Celigo cell count overlaid in green. The top image is a wider view of the left-hand image in Figure 4.5, which was an image of an untreated control well, while the bottom image is a similarly widened view of the right-hand image, which was treated with 64 $\mu\text{g}/\text{mL}$ for 30 minutes, 48 hours prior to imaging. Both scale bars 200 μm 75
- 4.8 Plot of the median colony sizes (error bars are the interquartile range) from three negative control wells (200 cells plated) and the corresponding three treatment wells, treated with 4 $\mu\text{g}/\text{mL}$ at 37°C for 60 minutes (1000 cells plated), as shown in Figure 4.9. Colony sizes were obtained by the CountPHICS macro. 83
- 4.9 GelCount scan of clonogenic assay plate. The top row contains the negative control wells, which all had 200 cells plated, and each well contained 113 colonies (in all other sets of negative control wells, the number of colonies across the three was not consistent). The bottom row had 1000 cells plated and was treated with 4 $\mu\text{g}/\text{mL}$ at 37°C for 60 minutes, before being washed twice, and returned to the incubator with fresh media for a week, before being fixed and stained as in Section 4.4. The number of colonies counted in these wells were 75, 108, and 67. 84
- 4.10 A diagram of the full protocol used to determine the intracellular concentration of doxorubicin in CT26 cells *in vitro*. 87
- 4.11 The full data-set of obtained intracellular concentrations. The top panel shows the mean and standard deviation of the measured concentrations ($n = 4$, except for the 60 minute normothermic 0.25 and 1 $\mu\text{g}/\text{mL}$ groups, where $n = 3$ due to lost samples). The bottom panel describes the treatment condition (extracellular concentration and exposure duration) to which the measured intracellular concentration shown in the top panel corresponds. 91

4.12 Intracellular concentrations of doxorubicin against exposure time. A) shows all of the measured data points together, B) shows only the normothermic data, C) shows only the hyperthermic data. D) and E) are a breakdown of the full data set. D) shows only the intracellular concentrations measured at the extreme extracellular concentrations (i.e. 0.25 and 64 $\mu\text{g}/\text{mL}$), and E) shows the remaining three concentrations. This was done to aid data visualisation, as it can be observed more clearly here than in A, that at all data points, the mean concentration measured for a given treatment condition at mild hyperthermia is greater than the corresponding normothermic treatment, with the exception of the two points which can clearly be seen in D, the 30 minute, 64 $\mu\text{g}/\text{mL}$ and the 60 minute 0.25 $\mu\text{g}/\text{mL}$ exposures. In all plots the data plotted are the mean and standard deviation of $n = 4$ (except for the 60 minute normothermic 0.25 and 1 $\mu\text{g}/\text{mL}$ groups, where $n = 3$ due to lost samples).	92
4.13 The results from the clonogenic assays plotted against the intracellular concentrations determined from the HPLC assay.	94
4.14 The same results as plotted in Figure 4.13, with the two Hill Model fits for survival also shown.	95
4.15 Plot of the separate fits of cellular uptake of doxorubicin for (i) normothermia and (ii) hyperthermia against time, with data points shown as mean and range of $n = 4$ (except for the 60 minute normothermic 0.25 and 1 $\mu\text{g}/\text{mL}$ groups in which $n = 3$).	98
4.16 Plot of the separate fits of cellular uptake of doxorubicin for (i) normothermia and (ii) hyperthermia against extracellular concentration, with data points shown as mean and range of $n = 4$ (except for the 60 minute normothermic 0.25 and 1 $\mu\text{g}/\text{mL}$ groups in which $n = 3$).	99
4.17 Plot of the predicted rates of cellular uptake for the models without nuclear binding, i.e. $y = k_{in}c_e + \frac{V_{m,in}c_e}{K_{m,in} + c_e}$	102
4.18 Plot of the combined normothermic and hyperthermic fit without nuclear binding against time, with the data points shown as mean ($n = 8$, except for the 60 minute 0.25 and 1 $\mu\text{g}/\text{mL}$ groups in which $n = 7$) and range.	102
4.19 Plot showing the combined normothermic and hyperthermic fit without nuclear binding against time, with the mean values of the normothermic ($n = 4$, except for the 60 minute 0.25 and 1 $\mu\text{g}/\text{mL}$ groups in which $n = 3$) and hyperthermic ($n = 4$) data points are shown separately on the plot as stars and diamonds respectively.	103

4.20	Plot of the cell survival predicted by the obtained mathematical models in normothermic (left) and hyperthermic (right) conditions, using separate models for cellular uptake.	104
4.21	Plot of the predicted cell kill by the separate normothermic and hyperthermic models across a range of concentrations over a 90 minute exposure.	105
4.22	Plot of the predicted cell kill by the separate normothermic and hyperthermic models for a range of exposure times at a concentration of 10 $\mu\text{g}/\text{mL}$	105
4.23	The predicted cellular uptake as exposure time varies for a constant 10 $\mu\text{g}/\text{mL}$ extracellular concentration of doxorubicin, with 95% prediction intervals.	106
4.24	Results of the Elementary Effects Test on the log(survival) model for hyperthermic conditions. This represents of the mean of the elementary effects of the resulting survival from exposure at the conditions tested experimentally in this chapter (0.25, 1, 4, and 16 $\mu\text{g}/\text{mL}$ for 15, 30, 60, and 120 minutes).	108
4.25	Results of the Elementary Effects Test on the cellular uptake model for hyperthermic conditions. This represents of the mean of the elementary effects of the resulting survival from exposure at the conditions tested experimentally in this chapter (0.25, 1, 4, and 16 $\mu\text{g}/\text{mL}$ for 15, 30, 60, and 120 minutes).	109
5.1	Plot showing how infusion duration and hyperthermia duration affect the achieved peak intracellular concentration for an infusion of free doxorubicin, based on the 'separate' model obtained from experimental work in the previous chapter (Table 4.8).	113
5.2	Plot showing how infusion duration and hyperthermia duration affect the achieved peak intracellular concentration for an infusion of TSL doxorubicin, based on the model obtained from experimental work in the previous chapter (Table 4.8, combined fit). . . .	115
5.3	Plot showing how the intracellular concentration of doxorubicin varies with time for optimal infusions when $\text{PIR} = 1$, and $\text{PIR}_t = 0.5$ with 5 minute time blocks. The optimal infusion durations were 18 minutes for the case where $\text{PIR} = 1$, and 26 minutes for $\text{PIR}_t = 0.5$. Heating ceases at 90 minutes. Peak values are 13.48 and 9.26 $\text{ng}/10^5$ cells respectively.	116
5.4	Plot of the tumour extracellular concentrations predicted for $\text{PIR}_t = 0.5$ with different time blocks of 5 and 15 minutes. For simplicity, the infusion times were kept the same at 25 minutes. The heating is initially off in this simulation and ceases at 90 minutes. .	117
5.5	Plot showing how the smaller of the two peak values of intracellular concentration vary when two halves of the tumour are alternately heated with the time block given on the y-axis, over an infusion duration given on the x-axis. ($\text{PIR}_t = 0.5$).	118

5.6	Tumour concentration profiles for an 'idarubicin' TSL, with $PIR = 1$ and an optimal infusion duration of 40 minutes, with 90 minutes of hyperthermia.	119
5.7	Plot showing how the intracellular concentration of 'idarubicin' varies with time for optimal infusions of 25 minutes for the case where $PIR = 1$ and 40 minutes for $PIR_t = 0.5$ with 5 minute time blocks. Heating ceases at 90 minutes. Peak values are 40.32 and 26.76 ng/ 10^5 cells respectively.	120
5.8	Plot showing how the smaller of the two peak values of intracellular concentration vary when two halves of the tumour are alternately heated with the time block given on the y-axis, over an infusion duration given on the x-axis for a TSL containing a drug with similar properties to idarubicin.	121
5.9	Obtained values of peak intracellular concentration following a 40 minute infusion of free doxorubicin, over a Krogh-style cylinder model with $r_c = 10\mu\text{m}$ and $r_t = 36.5\mu\text{m}$, using the combined uptake model. There is not a substantial decrease across the cylinder, which is consistent with <i>in vivo</i> literature, which shows fairly consistent levels of doxorubicin (total, not just intracellular) up to 100 μm from a capillary following doxorubicin release from TSLs [89]. Note that values plotted do not correspond to a single point in time, but rather the maximum intracellular concentration achieved at that distance from the capillary.	125
5.10	Obtained values of peak intracellular concentration following a 40 minute infusion of free doxorubicin, over a Krogh-style cylinder model with $r_c = 10\mu\text{m}$ and $r_t = 150\mu\text{m}$	126
5.11	The systemic plasma concentration following a 40 minute infusion of free doxorubicin, showing that the concentration remains relatively steady during the elimination phase, which lasts several hours.	127
5.12	Plot showing how the infusion duration of free doxorubicin affects the peak intracellular concentration predicted next to the capillary, in the middle of the cylinder, and at the outer edge of the cylinder for tissue radii of a) 36.5 μm and b) 150 μm	128
5.13	Plot of the predicted systemic free plasma concentration of doxorubicin (normothermic uptake model) for infusion durations of two minutes, 40 minutes, and 60 minutes. The concentration profile in the elimination phase is almost unaffected by the infusion duration.	130

5.14	Plot showing how temporal PIR affects the spatial distribution of peak intracellular doxorubicin concentration in the regular cylinder (a) and the larger cylinder (b). The infusion durations in both cases were chosen as those that were optimal according to the compartment model - 26 minutes for 5 minute time blocks, and 31 minutes for 15 minute time blocks. Hyperthermia was assumed to start immediately and lasted for 90 minutes, and the combined model for cellular uptake was used in this simulation.	131
5.15	Plot showing how temporal PIR affects the spatial distribution of peak intracellular concentration of 'idarubicin' in the regular cylinder (a) and the larger cylinder (b). The infusion durations in both cases were chosen as those that were optimal according to the compartment model - 40 minutes for 5 minute time blocks, and 46 minutes for 15 minute time blocks. Hyperthermia was assumed to start immediately and lasted for 90 minutes.	133
5.16	Plot of the concentrations resulting in the exponential phase of the washout problem, as defined in [186], which was used to confirm the implemented finite volume approach (the results from which are shown in Figure 5.16a) was working correctly. The literature results are reproduced from [186] with permission.	136
5.17	The concentrations at time $t = 40$ minutes into an infusion of free doxorubicin over 40 minutes, using the parameters from the compartment model in Chapter 3. The capillary flow speed was taken as $500 \mu\text{m s}^{-1}$, and a) shows the results from an 'average' tissue radius of $36.5 \mu\text{m}$, while b) shows the results from a larger tissue radius of $150 \mu\text{m}$	137
A.1	Results of an example sensitivity analysis, for the output as described by Equation A.1, with variables as in Table A.1. $r=10$	147
A.2	Results of the elementary effects test using the area under the curve of tumour plasma concentration of free doxorubicin from $t=0$ to $t=3$ hours as an output. $r = 1000$	148
A.3	Results of the elementary effects test using the area under the curve of systemic tissue concentration of free doxorubicin from $t=0$ to $t=3$ hours as an output. $r = 1000$	149
A.4	Plot showing how varying different parameters affects the tumour plasma AUC (left Y axis) and peak intracellular doxorubicin concentrations (right Y axis) for a) liposomal doxorubicin clearance, $k_{e,lip}$, b) Flow per tumour plasma volume, F , and c) tumour volume, with all parameters varied between the range as given in Table 3.2.	149
A.5	Plot showing how variation in BMI impacts both tumour plasma AUC of free doxorubicin (left axis) and peak intracellular concentration (right axis).	151

A.6	Results of the compartment model simulation for a murine model for a bolus dose of free doxorubicin (a) and LTSL doxorubicin (b), followed by one hour of hyperthermia. .	154
B.1	Analysis of the impact of a 2 hour exposure to DMSO on cell viability assessed by MTS assay 24 hours following removal of DMSO (Method: Section 4.3.2). Brown squares represent the mean of five independent wells, error bars represent standard deviations.	159
B.2	Analysis of the impact of a 24 hour exposure to DMSO on cell viability assessed by MTS assay immediately following removal of DMSO (Method: Section 4.3.2). Brown squares represent the mean of five independent wells, error bars represent standard deviations.	160
B.3	20x Magnification of cells after 1 hour of exposure to different concentrations of DMSO. A) DMSO-free control, B) 6.4 vol-% DMSO, C) 30 vol-% DMSO.	160
B.4	Representative brightfield Celigo images of cells in a 96 well plate with CT26 cells which have been exposed to 1 vol-% DMSO for 120 minutes (a), or DMSO-free control (b). Scale bar in both images is 200 μm	161
B.5	Viability measured by MTS, 28 hours after two hours in serum-free media (or complete media as a negative control). The cells were incubated with MTS reagent for 105 minutes. The error bars represent the standard deviation, $n = 5$. The difference between the groups was found to be significant ($p < 0.01$) with an unpaired t-test.	162
B.6	Viability measured by MTS 24 hours after 30 minutes in 10 $\mu\text{g}/\text{mL}$ doxorubicin in both serum-free and complete media compared to a negative control. The error bars represent the standard deviation, $n = 5$. P values from a one-way ANOVA (calculated in GraphPad PRISM) are included on the plot.	163
B.7	Graph of cell viability as obtained by trypan blue exclusion (Method: Section 4.3.1) assayed at the stated times post-exposure to 10 $\mu\text{g}/\text{mL}$ doxorubicin (0.1 vol-% DMSO) for 90 minutes. Error bars represent the standard deviation, $n = 3$	164
B.8	Viability of cells by MTS assay (method as described in Section 4.3.2), 24 hours (left) and 72 hours (right) after a 60 minute exposure to varying concentrations of doxorubicin as shown. Circles represent the mean of five independent wells, and the error bars the standard deviation. The standard deviations of the doxorubicin free wells (not shown due to logarithmic scale) were 26.29% and 18.02% for the 24 hour and 72 hour plates respectively.	165

B.9	Analysis of the impact of cell number plated on MTS absorbance signal generated. CT26 cells were plated at the stated densities in 96 well plates and exposed (24 hours later) to MTS reagent for 30 minutes (left) or 90 minutes (right) and measured for absorbance as described in Section 4.3.2. The absorbance was corrected by subtracting the background absorbance of the well (the mean value between 850 and 900 nm) from all wells, then subtracting the mean and two standard deviations of the resulting signal at 490 nm in the negative control wells. Brown squares represent the mean of five independent wells, error bars represent standard deviations, line of best fit as calculated using PRISM (using the standard deviations), $R^2 = 0.9204$ for the 30 minute incubation, and $R^2 = 0.8990$ for the 90 minute incubation.	166
B.10	Photograph of clonogenic assay plate to determine appropriate seeding density. The top three wells had 200 cells seeded, while the bottom wells had 400 cells seeded. The plate was incubated for 24 hours before being washed, returned to the incubator for an hour, then washed twice again before being returned to the incubator in complete media for seven days, and fixed and stained, as described in Section 4.4.	167
B.11	Photograph of a clonogenic plate that has been allowed 10 days to form colonies, rather than 7 days. 200 cells were plated in the top three wells, while 2000 cells were plated in the lower three wells, which were treated with 4 $\mu\text{g}/\text{mL}$ of doxorubicin for 2 hours at 37°C, as per the protocol described in Section 4.4 (except the incubation time).	168
C.1	The set up of the experiment designed to determine the extraction efficiency of recovery of the microdialysis probes for doxorubicin at 37°.	170
C.2	Extraction efficiency of 5 $\mu\text{g}/\text{mL}$ doxorubicin in stirred, deionised water at 37°C as a function of time. Samples every 10 minutes, with no sample at 50 minutes due to experimental error.	171
C.3	Photos which show how the condition of the pancreas section deteriorated over 2 hours immersed in PBS which was kept between 35.8°C and 38.3°C: a) shows the pancreas before the experiment, with the introducer needles and split tubing inserted, b) shows the pancreas after 2 hours, with the probes in place.	173
C.4	Photos which show a section of frozen pancreas embedded in agar in a holder: a) shows the pancreas prior to a two hour experiment, and b) shows the pancreas at the end of the experiment. Visually, there is much less change in the condition of the tissue than in the case in which the pancreas was unconstrained.	173
C.5	A biopsy punch used for tissue sampling, next to a 1.5 mL eppendorf for scale.	174

C.6 The holes left from 'round-the-clock' biopsy punch sampling in the experiment on a fresh, whole porcine pancreas. 175

List of Tables

2.1	The clinical data from the TARDOX trial, which consisted of a 30 minute infusion of a commercially available LTSL doxorubicin formulation, followed by up to 60 minutes of ultrasound-mediated hyperthermia. Plasma samples were taken from each patient before and after heating. Tumour biopsies were performed after heating in all patients, and before heating in a sub-set of patients. The plasma sample for patient I.01 was non-evaluative due to errors in sample processing.	19
3.1	Parameters used in the compartment model, chosen to replicate the TARDOX trial [21] as closely as possible.	37
3.2	Parameter ranges used in Sensitivity Analysis. ‘Standard approach’ refers to halving and doubling the literature value to obtain the range.	51
3.3	Parameters used in alternative uptake model	60
4.1	Percentage viability results obtained at normothermic conditions using the method of trypan blue exclusion (method as described in Section 4.3.1), assayed 48 hours following exposure to the given concentrations of doxorubicin for the stated durations, at normothermic (37°C). Values given are the mean \pm one standard deviation, n = 3. Grey entries were not assayed as it became clear that trypan blue exclusion was not resolving the cytotoxic effect of doxorubicin treatment.	69
4.2	Table showing the number of cells seeded for each treatment group in the clonogenic assays. For all plates, the negative control had 200 cells plated. Cells left blank are exposure time and concentration combinations which were not tested due to the likely very high or very low expected viabilities.	80
4.3	Viability (%) from clonogenic assays. Cells left blank are exposure time and concentration combinations which were not tested due to the likely very high or very low expected viabilities.	81

4.4	Ratio of the viabilities of cells treated with drug and hyperthermia compared to those treated with drug at normothermic conditions.	82
4.5	Intracellular concentrations resulting from a comparison between treating the cells in a 6 well plate format, using a BCA assay to estimate the number of cells, and treating the cells in a T75 flask, using cell counting with trypan blue to find the number of cells. The cells were treated with 4 $\mu\text{g}/\text{mL}$ of doxorubicin for one hour at 37°C. S.D. = Standard Deviation.	93
4.6	Parameters from the fitted Hill Models for cell survival	95
4.7	The Akaike Information Criterion for small sample size (AIC_c) values, calculated using Equation 4.7 for the four best fitting models.	97
4.8	Parameter values (and their 95% confidence intervals) obtained from the experimental data for the cellular uptake model defined by Equation 4.8.	100
5.1	Pharmacokinetic parameters used in the 'idarubicin' model, obtained from the data in [178].	119
5.2	The timescales involved in the spatially heterogeneous problem. Timescales are given to two significant figures.	129
A.1	Parameter ranges in the example sensitivity analysis.	147
A.2	The variation in peak intracellular concentration for different infusion times and values of R_{37} , with values rounded to the nearest 0.1 $\mu\text{g}/\text{mL}$. Cell volume taken as 10^{-9} mL, $\text{PIR}_s = 0.5$	152
A.3	Parameters used in the mouse model of LTSL doxorubicin delivery. All parameters not shown are unchanged from the values in Table 3.1.	156
A.4	The results obtained from simulating a mouse model with different infusion durations of free and LTSL doxorubicin. The increase in efficacy which appears when comparing the two bolus doses appears far more impressive than the comparative increase between the optimal protocols.	157
A.5	The results obtained from simulating (in man) different infusion durations of free and LTSL doxorubicin. The increase in efficacy which appears when comparing the two bolus doses appears far more impressive than the comparative increase between the PANDOX protocol and the optimal free doxorubicin infusion.	157

Chapter 1

Introduction

1.1 Background

There were 167,142 deaths from cancer in the UK from 2017 to 2019, with a substantial proportion of these deaths resulting from cancerous solid tumours (as opposed to blood cancers) [1]. Cancerous solid tumours begin with a single mutated cell, which undergoes uncontrolled division and avoids destruction by the immune system. These tumours often present clinically as new lumps (as in breast or skin cancer), or as symptoms associated with problems in the tumour-containing organ. As the tumours develop, cancer cells can enter the blood or lymphatic system and seed new tumours in other organs, which are termed metastases.

The first-choice treatment for solid tumours is usually surgical resection, which has been practised since ancient times, however the success of surgery depends on the ability of the surgeon to remove all cancerous cells to prevent a recurrence, and assumes the cancer has not yet metastasised. As many patients present with large, internal tumours, requiring a substantial operation, resection alone is often not a curative option. At the turn of the 21st century, in addition to surgery, chemotherapy (treatment with a drug, usually via systemic injection), radiotherapy (usually with gamma radiation to induce DNA damage and trigger cell death), hormone therapy (used for hormone sensitive cancers, such as some breast cancers), and ablative techniques (locally heating with ultrasound or radiofrequency/microwave probes to cause necrotic cell death) were all in clinical use alongside surgery.

Of these options, it could be argued that chemotherapy is the least specific treatment; the fraction of systemically administered small molecule (less than 900 Daltons) chemotherapeutic drug which reaches the tumour tissue is typically around only 0.01% [2]. Despite this, chemotherapy remains a

common treatment option for many cancers [3]. Systemic delivery of chemotherapeutics for cancer treatment began in the 1940s, with the administration of antifolates to treat non-Hodgkin's lymphoma [4]. In the decades that followed, scientists raced to discover chemical agents which could also cause remission from cancer. Using the knowledge that antifolates appeared to stop the proliferation of tumour cells, partial remissions of some solid tumours in response to methotrexate treatment were first recorded in 1951 [5]. Complete remission of choriocarcinoma (a rare solid tumour of the placenta) as a result of systemic methotrexate chemotherapy was reported in 1958 [6], and is the first recorded case of curing a metastatic cancer.

The reasons for the small fraction of drug reaching the tumour are the lack of specific targeting, combined with difficulties in extravasation from the tumour vasculature, and transport within the tumour tissue. Poor tumour penetration and accumulation is one of a multitude of reasons that the translation rate of drugs 'from bench to bedside' is so poor; just 3.4% of oncological drugs progress from phase I trials to the clinic [7]. *In vitro*, without the limitations of extravasation and transport through the tumour space, a therapeutic can show highly promising results, before subsequently failing to deliver on that therapeutic promise in humans.

Consequently, obtaining a mechanism whereby tumours can be treated systemically, while sparing the rest of the body became the major focus of research in oncological drug discovery and drug delivery. A variety of different cancer treatments have been developed over recent decades which achieve a more targeted approach. These can be split into two categories: biological therapies, and stimulus-responsive nanoparticles. The term nanoparticle encompasses a broad range of sizes, ranging from those with a diameter around 5 nm up to around a micron [8]; and the nanoparticles predominantly considered in this thesis (i.e. thermosensitive liposomes) are around 100 nm in diameter [9].

Biological therapies, or biologics, include immunotherapy [10] and antibody-drug conjugate (ADC) [11] approaches. The principle of cancer immunotherapy is that the body's immune system can be activated against cancer cells. This can be done (for example) by the delivery of checkpoint inhibitors (a type of monoclonal antibody) which prevents the cancer cells from blocking the immune response of the body [12]. ADCs represent a mechanism for targeting tumours which builds upon the decades of discovery of small molecule therapeutics. A monoclonal antibody for a tumour-associated antigen with limited or no expression in healthy cells is attached via a linker to a small molecule therapeutic. This small molecule therapeutic is released on antibody-antigen binding, thereby allowing for

localised release [13]. Both of these approaches have potential to improve treatment outcomes in specific cancers [e.g. 14], but their specificity limits their usage, and use of biologics can be prohibitively expensive. For instance, the average cost of treating a patient for a year with a biological therapy was around \$200,000 in the US in 2012 [15]. More recent numbers (post-2020) show that the cost has remained high, with a month of treatment with belantamab mafodotin, an ADC used to treat multiple myeloma costing \$23,800 [16]. By way of comparison, five cycles of CHOP chemotherapy with small molecule drugs cost the NHS under £4120 in 2016 [17].

Stimulus-responsive nanoparticles represent an alternative direction with potentially lower costs. The idea behind the concept is the use of external stimuli (including photosensitive, sonosensitive, magneto-electric and thermosensitive systems [18–20]) either to cause an accumulation of nanoparticles in the tumour, or to trigger drug release from a nanoparticle carrier at the tumour site. This concept offers versatility between cancer cell lines, since the stimulus for drug release is applied by the clinician, thereby neglecting the requirement in ADCs (for example) for tumour-specific antibody-antigen selection. Recent successes in clinical trials [21] of thermosensitive liposomal (TSL) drugs in liver tumours provide strong evidence that this technique can provide effective targeting.

TSLs release their payload at mild hyperthermia (typically defined as temperatures in the region of 40–43°C), which brings with it additional benefits. Mild hyperthermia is reported to improve tumour perfusion [22] and blood vessel permeability [23], both of which increase transport of drug into the tumour extracellular space. Furthermore, hyperthermia has been reported to increase the uptake of small molecule chemotherapeutics in cancer cell lines, and increase the cells' sensitivity to the drug once it has been internalised [24].

As clinical practice moves from administering drugs, to operating drug delivery systems, the number of decisions which must be made by clinicians and pharmaceutical manufacturers increases greatly. For example, delivery of a thermosensitive liposomal drug carries with it decisions on the total dose, infusion time, number of infusions and heating cycle. The pharmaceutical manufacturers must consider which of the many discovered small molecule drugs is likely to provide most therapeutic benefit inside the liposome, as well as design the liposomes release properties. The multiple combinations which result cannot all be tested experimentally; to do so would be time-consuming, expensive and unethical. Mathematical modelling represents a technique by which likely successful combinations of drugs, liposome properties and treatment protocols can be predicted [e.g. 25].

Therefore, the focus of the present work is to use a combination of *in vitro* and *in silico* experiments to obtain a mathematical model for treatment with TSLs, a class of stimulus-responsive nanoparticle, triggered by extracorporeal heating sources, such as ultrasound. This model is then used to provide certain recommendations for the clinical use of TSLs. Modelling of treatment with chemotherapy relies on the consideration of three different scales, which are shown in Figure 1.1. The clearance scale describes the concentration of drug in the systemic plasma, which is affected by the stability of the carrier as well as the rates of clearance of the free and encapsulated agent from the body. The delivery scale describes the extravasation of drug from the blood in the tumour into the tumour extracellular space and the spatial distribution of the drug within the extracellular space, which also incorporates the release characteristics of the drug from the carrier at hyperthermic conditions and the effectiveness of the hyperthermia. The pharmacodynamic scale describes the effect of the drug on cells; how the drug is taken up by cells and the timescales over which the cells are killed. It is clear that any model for treatment *in vivo* must be able to accurately describe behaviour on all three scales to be useful in TSL development or the clinic.

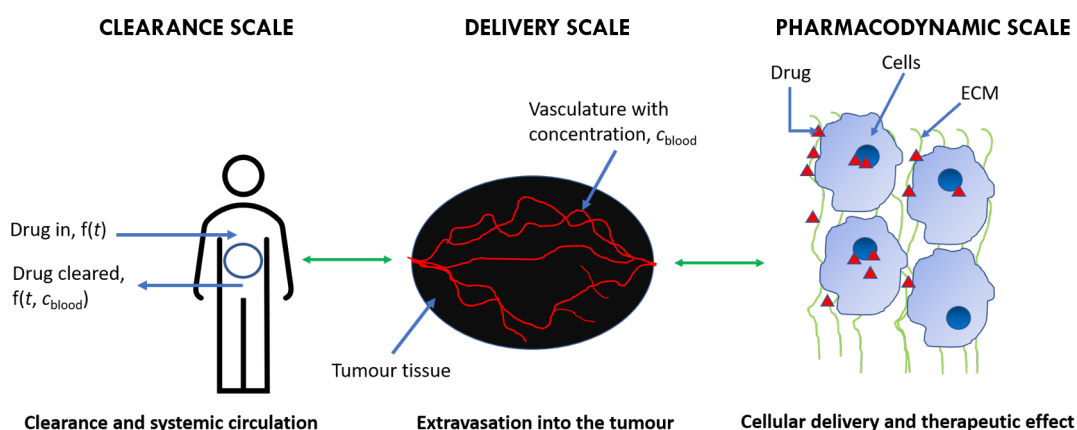


Figure 1.1. The different scales involved with the problem of optimising drug delivery to tumours.

1.2 Synopsis

Beyond this short introductory chapter, Chapter Two provides a more extensive literature review. The physiology of tumours which make them challenging targets for drug delivery is explored, and the need for drug delivery systems is discussed. The literature on thermosensitive liposomes (TSLs), doxorubicin (the drug which has been most commonly used in TSLs), and the bioeffects of hyperthermia are then examined. Finally, prior computational modelling work in this area is discussed, before the aims of the thesis are set out and justified.

In Chapter Three, a mathematical expression for cellular uptake from the literature is used in a compartment model for TSL treatment, and compared to the results from the TARDOX trial, representing the first time that results from such a model have been compared to clinical data. Optimal infusion durations (i.e. those predicted to maximise cancer cell kill) are found for a variety of different treatments with unencapsulated and TSL doxorubicin. As a further novel inclusion, the compartment model is updated to reflect non-ideal hyperthermia in both a spatial and a temporal sense. A global sensitivity analysis is performed to establish, not only the sensitivity of the predicted peak intracellular concentration to model parameters, but also the robustness of the obtained optimisations. Cellular uptake parameters are found to have a substantial impact on the predicted intracellular concentrations, although the findings of the optimisations are found to be fairly robust.

Chapter Four describes the *in vitro* work which was performed to quantify the effect of a variety of applied doxorubicin doses across a range of exposure durations at both 37°C and 42°C on a cancer cell line. The resulting data are used to fit a mathematical model of cellular uptake and cell kill by doxorubicin at both normothermic and hyperthermic conditions. It is established that hyperthermia increases cell kill, and demonstrated that the intracellular concentration of drug is correlated with cell kill. Cell kill was quantified via a clonogenic assay, which was found to be the most suitable approach compared to several other techniques. Cellular uptake of drug was quantified through High Performance Liquid Chromatography (HPLC).

The final research chapter, Chapter Five, explores how the compartment model optimisation problem is changed with use of the new cellular uptake data, and quantifies the likely therapeutic benefits of hyperthermia alone with unencapsulated doxorubicin. The use of a drug with more rapid cellular uptake kinetics is explored computationally. Spatial heterogeneity is then introduced into the model to answer questions about the validity of compartment model-based optimisation of treatment across the tumour, and assess the impact of segmenting the tumour for hyperthermia to facilitate sustained localised hyperthermia for the delivery of drug to cells.

Finally, in Chapter Six, the findings of the thesis are summarised, and limitations of the work are discussed. Future work which could be undertaken to address these limitations is then presented.

Chapter 2

Literature Review

2.1 Solid Tumours

According to the National Cancer Institute's Dictionary of Cancer Terms [26], a solid tumour is 'an abnormal mass of tissue that usually does not contain cysts or liquid areas.' They may be benign or malignant (cancerous), and are named after the type of cells which form them; for example, the two most common solid tumours are carcinomas and sarcomas, which are formed in the epithelial and connective tissues respectively [27]. In malignant solid tumours, the primary focus of this thesis, the initial set of mutations (resulting from cell damage) give rise to a set of cells which possess eight characteristics, as described in [28]:

1. A reduced dependence on external signals for growth.
2. Unresponsive to external signals inhibiting growth.
3. An avoidance of apoptosis/self-destruction, the body's usual defence-mechanism against cellular DNA damage.
4. Indefinite growth.
5. The induction of angiogenesis, the formation of a blood supply.
6. They may promote inflammation and an immune response.
7. A perturbed metabolism.
8. They can metastasise, or spread from their initial location in the body to create secondary tumours.

This combination of characteristics generally results in a rapid, uncontrolled growth of cells, with a highly irregular vascular structure [29]. Furthermore, this rapid growth causes elevated solid stress levels [30], compressing the local lymphatic system [31], reducing drainage from the tumour, and increasing the interstitial fluid pressure of the tissue. In healthy tissue, there is usually a net filtration pressure out of the capillaries between 1 - 3 mm Hg, whereas in tumour cells, negative values from -18 mm Hg (signifying a filtration pressure from the tissue into the capillary) to positive 2 mm Hg have been reported [32].

The metastasis of tumour cells represents a dangerous progression of the disease, in which cancer cells migrate from the primary tumour through the lymphatic or circulatory system, and begin proliferating in a new location. This represents a dangerous progression for the patient for two reasons; firstly, metastases are the major mechanism through which cancer proves fatal to patients. In 90% of cases, the primary tumour is not fatal [28], but rather, growing metastases prevent the proper functioning of vital organs. Secondly, the presence of secondary tumours makes surgical resection with curative intent unlikely (unless there are a small number of well-defined, accessible metastases), and so treatment options are thus reduced.

2.2 Chemotherapy

The features of tumour development described in the previous section combine to make tumours an extremely challenging target for drug delivery. Firstly, the convective transport of solutes out of the vasculature into the tissue is greatly reduced in solid tumours compared to in healthy tissues [29], as a result of the elevated interstitial fluid pressure. This reduces the extravasation of therapeutic at the site where it is required. One study quantified that the magnitude of convective transport is smaller than that occurring via diffusive mechanisms by at least an order of magnitude for small molecule therapeutics in tumours [33]; whereas, calculating the ratio of advective to diffusive transport (i.e. the Péclet number) for a typical small molecule drug with a diffusivity of $5.01 \times 10^{-11} \text{ m}^2\text{s}^{-1}$ [34], over a distance 100 μm , using the typical tissue fluid flow velocity given in [33] of $0.1 \mu\text{m s}^{-1}$, convective transport occurs around twice as fast as diffusive transport in healthy tissue .

Further to the elevated interstitial fluid pressure, the chaotic vascular structure and rapid cell division results in some cancerous cells being further from blood vessels than is the case for healthy tissue. To illustrate the scale of this issue, a study [35] by Baish et al. found that the maximum distance from

the vasculature in tissue sections was increased from around 35 μm in normal murine mammary tissue to around 115 μm in a murine mammary carcinoma. This is problematic, since by the nature of the diffusive transport process, the distal cells are exposed to lower concentrations of drug than those proximal to the blood vessels. Near complete cell-kill is often required for remission, owing to the indefinite growth potential which is a characteristic of malignant cells. This means that reaching these distal cells with a therapeutic dose is vital, and increasing tumour penetration is the primary aim of certain drug delivery systems [e.g. 36]. The issue of reduced drug concentrations reaching the distal cells is compounded by the fact that these cells, being further from the vasculature, are often hypoxic, and hypoxia has itself been shown to reduce the efficacy of several anti-cancer drugs [37]. Additionally, certain tumours, such as pancreatic ductal adenocarcinoma (PDAC), present a dense extracellular matrix (ECM) which further inhibits the diffusion of drugs through the extracellular space [38, 39].

Spatial heterogeneity in the doses of chemotherapeutic through the tumour has been observed *in vivo*, as is shown in Figure 2.1. The figure shows that doxorubicin (in blue) is not reaching the hypoxic regions (green) of the tumour, following an intravenous (i.v.) injection. The length of time between the injection and tumour excision is not explicitly given for this image. The reasons for poor transport through the extracellular space include the binding of drugs to the ECM [40], and (in the case of larger carriers) that the ECM provides a steric barrier [33] to tumour penetration. Distribution can also be affected by drugs being rapidly internalised by cells, as the cells nearest to the vasculature will reduce the concentration of free doxorubicin diffusing through the tissue [41] (in this context, rapid internalisation is internalisation which occurs on a timescale which is similar to or faster than the timescale associated with the transport of the drug across the tumour interstitium).

In addition to the problems posed by tumour physiology, chemotherapeutic agents used to treat tumours are cytotoxic and frequently have short circulation half lives, meaning that little separates therapeutic and toxic doses. Drug accumulates in other tissues, resulting in off-target toxicity, while the 'clearance organs' remove the drug from the systemic circulation for excretion. There are four major 'clearance organs' responsible for the physical processes removing drugs from the systemic circulation, the kidneys, liver, spleen, and lungs. The clearance pathway for a given therapeutic is related to its size (amongst other factors) [8]. The kidneys are mostly responsible for the clearance of small molecules with dimensions on the order of 5 nm and smaller, while the liver and spleen are responsible for the vast majority of the clearance of molecules between around 20 and 150 nm in size,

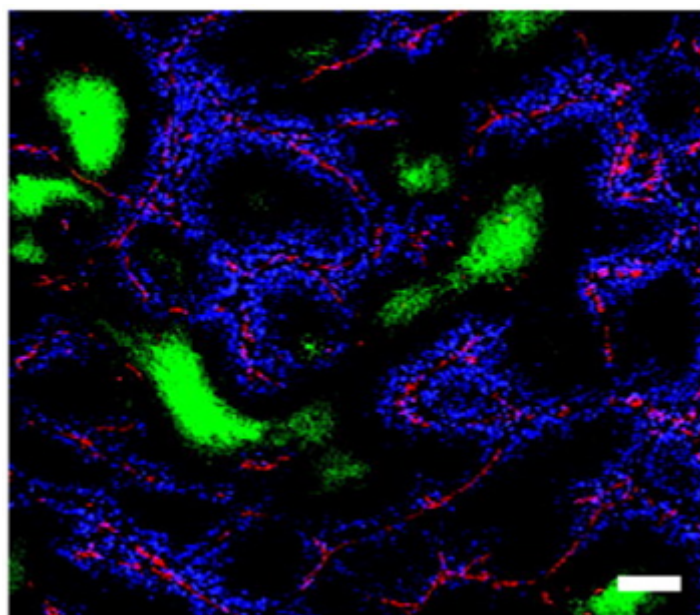


Figure 2.1. Photo showing the distribution of doxorubicin (blue) in a murine mammary adenocarcinoma, with the blood vessels stained red and regions of hypoxia shown in green. Scale bar: 100 μm . Reproduced with permission from [42].

with those between 5 and 20 nm being cleared by the kidneys and MPS. Together, the phagocytic cells in the liver and spleen are sometimes referred to as the reticuloendothelial system (RES) or mononuclear phagocyte system (MPS). Larger molecules (above 150 nm) are not considered here, but can also be cleared by the lungs as well as via the MPS [8]. Drugs can also be cleared through sweat glands [43], which

One interesting aspect of drug circulation is that drugs that are predominantly cleared by the liver can experience a saturation of their clearance rate [44]. This phenomenon is explained by Allen and Hansen [45], who describe that two separate timescales are involved in clearance by the MPS: the timescale over which "recognition, binding and uptake sites are occupied"; and the timescale over which such sites are recycled or re-synthesised. This makes quantifying clearance of such drugs with a single parameter challenging. The following subsection describes how the distribution of drugs throughout the body can be modelled mathematically.

2.2.1 Pharmacokinetic Models

Pharmacokinetics (PK) is the subdiscipline of pharmacology concerned with the movement of drugs within the body. Of particular interest here is the clearance of therapeutics; their metabolism and elimination from the systemic circulation, from which the concentration-time profile of a drug in the circulation can be estimated for a given infusion dose and duration. This is an important concen-

tration for two reasons: firstly, it is this concentration which drives transport into the tumour (and non-target tissues, causing toxicity); and secondly that it is a clinically measurable concentration in most situations.

Compartment models provide a mathematical framework for analysing the clearance of drugs from the body. A conventional compartment model considers the body as a series of spatially homogeneous blocks, with linear rates of transfer between them, as shown in Figure 2.2. Rate constants are derived retrospectively by fitting the exponential equations which result from compartmental systems to experimental data. The elimination from the central blood compartment (shown in Figure 2.2) typically occurs in the clearance organs, but as these organs are highly perfused this is an acceptable approximation. The equations to fit the two compartment model are shown below for illustration; the equations for the three compartment model are given in the supplementary information of [46].

$$V_b \frac{dc_b}{dt} = V_p k_d c_p - V_b (k_{el} + k_p) c_b \quad (2.1)$$

$$V_p \frac{dc_p}{dt} = V_b k_p c_b - V_p k_d c_p \quad (2.2)$$

in which $V_{b,p}$ are the volumes of the blood and peripheral compartments respectively, $c_{b,p}$ are the concentrations and $k_{p,d,el}$ are the rate constants as shown. A major benefit of compartment models is that the rate constants facilitate prediction of concentration-time profiles in the compartments for different dosing schedules. Despite this, the assumption of first order kinetics in these models can fail to represent the physiological reality (such as the saturation kinetics described above) and scaling from these models between species is difficult, something which has hindered their application in the clinic.

The plasma concentration profile which results from the two compartment model is a bi-exponential decay, split into an initial distribution phase, during which the drug is rapidly distributed into the peripheral tissue compartment, followed by a longer elimination phase, during which the drug is cleared from the body. In the elimination phase, drug concentration levels in the plasma can remain relatively steady for a comparatively prolonged period, owing to the intravasation of drug from the peripheral tissue back into the circulation. While the mathematical expression for the three compartment model is more complex, the plasma concentration profile will usually still approximate a biexponential decay, as the relative influence of the tumour compartment on the systemic pharmacokinetic profile of the drug (in humans) is usually very small [46].

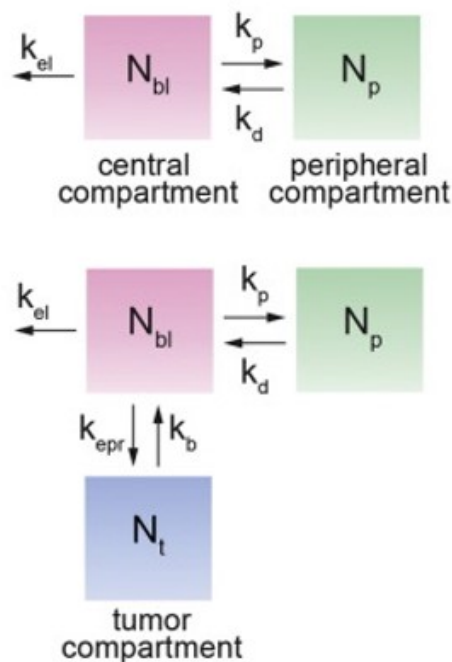


Figure 2.2. An example of a compartment model from Dawidczyk et al. [46], reproduced with permission.

Compartment models can be made more complex; for example, physiologically-based pharmacokinetic (PBPK) modelling includes individual compartments for the organs involved in the clearance of drugs. Some recent developments in this area include using normothermic perfused organ models to obtain organ specific PK parameters [47]. Other features which can be added to compartment models include the binding of drug to plasma proteins in the central blood compartment, with only unbound drug bioavailable [48]. This is not usually done however, as determination of rate constants in pharmacokinetic models is usually done on the basis of total blood concentration, which therefore already takes binding into account.

2.3 Drug Delivery Systems

Considering the small fraction of drug which reaches a tumour, and the fact that the side effect profile of chemotherapeutics often causes patients to question the value of life-extending chemotherapy [49], there is a clear clinical need for more targeted drug delivery. Consequently, multiple attempts have been made to achieve increased accumulation of drug in the tumour while sparing the rest of the body. Techniques for targeted delivery can either be passive (via the enhanced permeability and retention (EPR) effect, and prolonging the circulatory time of the drug), or active, such as the use of stimulus responsive and/or functionalised nanoparticles which preferentially deliver within the tumour volume.

2.3.1 Enhanced Permeability and Retention (EPR) Effect

One major difference between tumour and healthy vasculature results from tumour cells expressing vascular endothelial growth factor (VEGF), which causes looser cell junctions in the tumour endothelium than in normal tissue [50, 51]. This 'leaky' vasculature has been claimed to give rise to an EPR effect, which has been a key concept in several attempts to target drug delivery to solid tumours. The idea behind the EPR effect is that this hyperpermeability allows macromolecules to accumulate in tumour tissue but greatly reduces systemic toxicity, as the larger therapeutic size severely limits their permeation into healthy tissue [33]. The enhanced retention, the 'R' in EPR, was theorised to occur due to the lack of lymphatic drainage in tumours, reducing the clearance of nanoparticles once they had extravasated.

One of the first attempts to exploit this phenomenon was made by creating a liposomal form of an established small molecule therapeutic, doxorubicin, which had been in clinical use since the 1970s. Doxorubicin is described in more detail in Section 2.5, and was selected for much of the early research into the clinical development of a liposomal therapeutic. The reasons for this include its fluorescence, which facilitated the use of fluorescence-based quantification and imaging techniques, as well as its well-established efficacy and side-effect (cardiomyopathy). Development of liposomal doxorubicin began in the late 1970s, and in 1995, Doxil®, a liposomal form of doxorubicin, gained FDA approval [52]. Liposomes are 'spherical vesicles formed by a membrane bilayer usually composed by phospholipids' (see Figure 2.3). A major step in bringing liposomal drugs into the clinic was the PEGylation of liposomes, whereby polyethylene glycol (PEG) is grafted to the surface of the liposome, helping to prevent an immune response against the drug and thereby extending the circulation half life [53].

Doxil is used today to treat a variety of tumours and exhibits greatly reduced cardiotoxicity compared to the non-liposomal form of the drug [54] but has not replaced free doxorubicin entirely in the clinic. Despite the development of Doxil, the EPR effect remains controversial [55], and even the hypothesised leakiness of tumour vasculature was recently heavily contested [56]. It has been argued that liposomal drugs have failed to deliver the hoped for revolution in selectivity in the clinic [e.g. 53, 57], and although Doxil does reduce cardiotoxicity, it does not have an increased therapeutic effect compared to free doxorubicin in many cases. This was demonstrated by Petersen et al. in a recent meta-analysis which showed that there was no significant improvement in overall survival from liposomal formulations of doxorubicin in patients, despite the significant improvement in pre-clinical trials

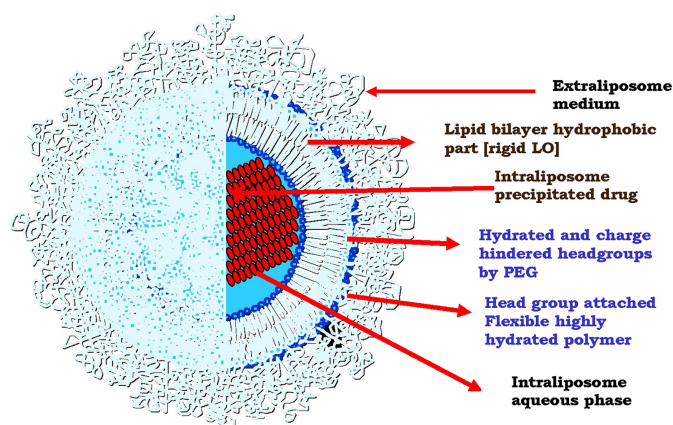


Figure 2.3. Diagram of Doxil reproduced from [52] with permission, showing the lipid bilayer, encapsulated doxorubicin and surface-bound MPEG (this is a PEGylated liposome), to increase circulation half life by avoiding MPS clearance.

of liposomal formulations in murine models [58]. Possible reasons for this discrepancy are discussed in the literature and include the use of different end-point criteria in man and *in vivo* [58] and the effects of comparatively large tumour volume fractions in mice compared to those seen in man [55]. In ‘EPR: Evidence and Fallacy’, Nichols and Bae argue that EPR should ‘only be invoked on a case by case basis, when clinical evidence suggests the tumor type is susceptible’ [53]. Such susceptibility is clearly present in the case of AIDS-related Kaposi’s sarcoma, one of the greatest clinical successes of Doxil. Kaposi’s sarcoma is known to be unusually well vascularised amongst tumours, making it ‘particularly favorable to the passive accumulation of nanocarriers, explained by the EPR effect’ [59].

One important potential drawback of liposomal formulations is that the liposomal form has a reduced cellular uptake and cytotoxic effect compared to the free form of the drug [60]; Seynhaeve et al. [61] found that Doxil was internalised by cells, but only 0.4% of internalised doxorubicin translocated to the nucleus when Doxil was internalised, compared to 26% of doxorubicin which translocated when the free drug was internalised by cells. This creates conflicting design requirements; liposomal formulations which are too stable fail to release sufficient therapeutic quantities into the target tissue [62], while those which are unstable suffer rapid drug clearance and produce more side effects. PEGylation further reduces interactions between cell membranes and the nanoparticle carriers; a problem recently reviewed by Zalba et al. [63], who detail attempts to circumvent this issue using (amongst other techniques) cleavable PEG, which is sensitive to the altered pH which is typical in solid tumours (solid tumours usually have an acidic extracellular pH, typically from 6.4 to 7.1, compared to healthy tissues, in which the equivalent pH is around 7.4 [64]).

The use of external stimuli to trigger drug release from a carrier represents an attractive alterna-

tive proposition, since it removes the dependence of drug delivery on the tumour microenvironment. The area of stimulus responsive nanomedicines is broad, and includes photosensitive, sonosensitive, magneto-electric and thermosensitive systems [18–20]. Of particular clinical interest recently has been the idea of thermosensitive liposomal delivery, whereby externally applied hyperthermia is used to trigger a release of drug from a liposome. The concept was first proposed in 1978 [20] and is discussed further in the following section.

2.4 Thermosensitive Liposomes

In their foundational 1978 paper, Yatvin et al. [20] suggested five mechanisms by which hyperthermia could be used to achieve greater therapeutic effect with liposomal drug formulations. These were:

1. "By promoting selective drug release at temperatures near that of the lipid phase transition of the liposomes"
2. "By increasing local blood flow"
3. "By increasing endothelial permeability to particles, thereby enhancing accumulation of liposomes in the target tissues"
4. "By increasing the permeability or susceptibility of target cells to the drug released from the liposomes"
5. "By increasing direct transfer of drug from vesicles to cells-for example, by fusion or endocytosis"

The idea of selective release has been shown to work in the clinic and is the only property which can be tuned by liposome design. Much of TSL design has therefore centred on achieving the most effective release of free drug at around 40-42°C. This release of drug at temperatures only a few degrees in excess of normal body temperatures is vital, as much above 42°C hyperthermia begins to cause irreversible damage to cells and also may cause vascular shutdown, limiting blood flow and transport of drug into the region [65].

Considering selective release, all TSLs work under the same basic principle; the release of encapsulated drugs at the melting phase transition temperature, T_m , of the liposome. Alterations to T_m are achieved by mixing the lipids used. In Yatvin's initial formulation, a mixture of DPPC¹ and DSPC²,

¹DPPC: Dipalmitoyl Phosphatidylcholine

²DSPC: Distearoyl Phosphatidylcholine

with transition temperatures around 41 °C and 55 °C respectively, was used to create a TSL which demonstrated a release rate 100 times greater at 44 °C than at 37 °C [20].

Different liposome formulations have different mechanisms by which release of free drug from TSLs occurs *in vivo*- intravascular (TSL-i), or extravascular (TSL-e) [66] release. The release of free drug from liposomes in the tumour vessels is termed intravascular release, while extravascular release occurs when the free drug is released following the accumulation of liposomes in the tumour tissue (employing the passive targeting hypothesised by the EPR effect). The predominant mechanism (as in any real system, both will be occurring [67]) depends on the design of the liposome and also on the heating regime, although TSL-i has been shown to give rise to better predicted outcomes, and so is the primary focus of this thesis [66].

The properties which are desirable in a thermosensitive liposomal (TSL-i) drug for cancer therapy are: a carrier which is stable at physiological temperature, as excessive leakage will limit the circulation time of the drug (since the free drug is generally cleared faster than the encapsulated form), and reducing the concentration of the encapsulated form in the systemic plasma will, in turn, reduce the concentration. A further risk with a short release time at physiological temperature is that this would be expected to increase the off-target toxicity experienced by the patient, which, in the case of doxorubicin, includes cardiomyopathy and congestive heart failure. Rapid release of the liposome contents upon heating is desirable, since excessively long release times will result in lower concentrations of free drug in the tumour plasma, reducing treatment efficacy. Additionally, if the drug were to remain in the carrier, the side-effects associated with conventional liposomal treatment, such as with Doxil, might be expected. This includes hand-foot syndrome, in which the hands and feet can swell, which is due to the PEGylated liposomal form of the drug being preferentially taken up by eccrine sweat glands; which are most dense in the hands and feet [68]. The encapsulated therapeutic should be cytotoxic, with a good degree of binding to the tumour cells; poor tumour binding would result in substantial transport of drug from the tumour back in to the blood stream [46].

In terms of liposome design, the rate of release of the free drug is the main factor in determining the release mechanism (i.e. TSL-e vs TSL-i). Although not strictly a good indicator of transit time in capillaries, the mean transit time through most tumours is on the order of seconds [69]³. This means that, as TSL-i treatment requires a sudden accumulation of high concentrations in tumour

³The mean transit time is not necessarily a reliable indicator of transit time through capillaries, since the mean transit time accounts for all vessels, with different flow velocities.

vasculature, liposomes with fast release are a pre-requisite for a predominantly TSL-i treatment. In 'Traditional TSLs' (or TTSLs [70]), as originally created by Yatvin et al., typical release of free drug is around 40% release after 30 minutes at 42°C [71], which favours use as a TSL-e technology.

A much more rapid release was found to be possible with the incorporation of lysolipids into the lipid bilayer, creating so-called lysolipid-containing low temperature TSLs (LTSLs) [71]. The lysolipids facilitate the creation of stabilised pores in the membrane around T_m , allowing for a rapid release of drug [70]. One recent study with a microfluidic device found that around 90% doxorubicin was released within 2 seconds from LTSLs [72]. A recent study with TSL-i doxorubicin in pigs demonstrated a 15-fold improvement in drug delivery between heated and unheated tissue [73], clearly showing the potential of LTSLs as a delivery platform.

One particular LTSL with similar release characteristics has undergone numerous clinical trials in recent years - ThermoDox®, a PEGylated LTSL containing doxorubicin. The clinical trials [e.g. 21, 74–76] have employed a variety of heating mechanisms, four of which are discussed here. The first trial, the DIGNITY study, was a phase I/II trial with microwave-induced hyperthermia which demonstrated the safety of ThermoDox in patients for the first time [74, 77] and paved the way for future trials. Two subsequent phase III trials of note, HEAT and OPTIMA, compared Radio Frequency Ablation (RFA) with ThermoDox and placebo infusions in patients with non-resectable hepatocellular carcinoma (HCC). The standard of care for this disease is RFA, which results in a median progression free survival of around 12 months. The recurrence of the disease is due to failing to kill all of the cancer cells, so the aim of including LTSL doxorubicin was to see if the addition of the drug increased survival through preventing or significantly delaying recurrence. The HEAT [75] trial could not demonstrate a clearly improved outcome between the groups receiving the placebo and the drug across 701 patients (with 354 participants being randomised to the treatment arm of the trial). However, a statistically significant improvement between the RFA and LTSL, and the RFA-only groups was noticed in those receiving the RFA for a duration greater than 45 minutes [78]. OPTIMA, the second Phase III trial, was then established to discover if a clear therapeutic benefit could be obtained when RFA duration exceeded 45 minutes [76], but in July 2020, Celsion Corporation (responsible for ThermoDox) received notification to consider stopping the trial owing to a futility threshold having been crossed [79]. In February 2021, the study was terminated, with no demonstrable benefit resulting from the addition of ThermoDox to RFA [80].

Reasons for the lack of success of the HEAT trial have been discussed in the literature, in particular by [81]. In this review, the authors give six potential reasons for the failure of the HEAT trial to reach its primary endpoint (Progression Free Survival, or PFS). These include firstly, that the control arm (RFA only) performed unusually well, with a median PFS of 13.9 months, compared to 12 months, which has historically been the median. More pertinently to the problem of providing patient benefit with LTSLs, the chosen cancer (Hepatocellular Carcinoma – HCC) is not very responsive to conventional chemotherapy, and is particularly insensitive to doxorubicin. Alternative possible indications for ThermoDox are suggested by Dou et al., such as breast cancer, which is known to be more responsive to doxorubicin than HCC. In the opinion of the author, however, the single greatest contributing factor to the failure of the HEAT trial was related to the use of RFA as a heating modality. This is also identified in [81] to some extent, in which it is stated that, there was “no published preclinical data on the effectiveness of ThermoDox® in combination with RFA for treatment of HCC prior to initiation of the HEAT clinical trial.”. The author believes that RFA is not an optimal heating modality to use in combination with LTSLs, since many of the benefits of treatment which are well documented for mild hyperthermia in the range of 40 – 43°C, such as increased cellular uptake of drug, increased tumour perfusion and increased blood vessel permeability, are unlikely to occur at the hotter temperatures initiated by RFA; indeed, vascular shutdown is expected to result from RFA [82]. This further motivates the use of other heating methods, as discussed further below, and in Section 2.6, such as microwave heating, and ultrasound.

Other thermosensitive carriers are also at various stages of development, examples of which include ThermoSome®, another TSL formulation, which does not use lysolipids or PEGylation, but rather a novel lipid, 1,2-dipalmitoyl-sn-glycero-3-phosphoglyceroglycerol (DPPG2), which has exhibited improved performance compared to LTSLs in some pre-clinical studies [73, 83]. Lu et al. [84] have developed ‘Smart Drug Delivery System’ (SDDS), which similarly does not make use of lysolipids and exhibits improved retention of drug at physiological temperatures (i.e., it is less leaky than LTSL formulations), which is being used with idarubicin in pre-clinical studies [85].

Whilst treatment with TSLs and RFA does not appear to have been a success, there remain reasons to be optimistic of a more successful combination of TSLs and ultrasound-mediated hyperthermia. The heating obtained with RFA is far in excess of the mild hyperthermia required for drug release and will be greatly reducing blood flow to the region through vascular shutdowns. However, in ultrasound treatments, one would expect the perfusion of the tumour to increase [86] owing to the far milder

heating. Indeed, the recent TARDOX trial [21, 87], which was run at the University of Oxford between 2015 and 2017 reported positive findings, demonstrating safety and elevated tumour doxorubicin concentrations after heating with ultrasound. This trial was believed to be ‘the first to investigate the safety and feasibility of extracorporeally triggered drug release in oncology and to quantify the potential benefits of this approach in terms of the drug dose, distribution, and cellular delivery’ [21].

The TARDOX trial provides a valuable data-set against which a computational model of LTSL drug delivery can be validated. Samples were taken from patients plasma after a 30 minute infusion of LTSL, and following (up to) 60 minutes of heating; the relevant data from [21] are summarised in Table 2.1. Additionally, this trial highlights some of the difficulties in using TSLs in the clinic which place bounds on the delivery optimisation problem. The treatment of tumours in the liver (and by extension, in other abdominal organs) requires general anaesthesia to facilitate the use of high frequency jet ventilation in order to minimise the movement of the target tissue, which does currently represent a major challenge to larger-scale clinical adoption [88].

Given the advanced stage trials with ThermoDox compared to other TSLs, doxorubicin is the primary small molecule therapeutic considered in this thesis. Its action is considered in the next section. It should be noted that recent work has examined the potential of using idarubicin in a TSL formulation [89]. Idarubicin is a drug which in its free form, is not suitable for systemic administration to treat solid tumours, owing to its rapid binding to plasma proteins, which severely limits its tumour accumulation. This represents an exciting potential application of TSLs, and the use of idarubicin is explored computationally in the final research chapter as a result. Ramajayam et al. [41] have also published a mathematical model of the uptake of four drugs (doxorubicin, idarubicin, pirarubicin, and aclarubicin) in three different cell lines at 37°C, showing in a computational model that idarubicin represents the best choice for inclusion in a TSL.

2.5 Doxorubicin

Doxorubicin is an anthracycline (drug derived from the *Streptomyces* bacterium) which has been used in the clinic against a wide variety of tumours since the 1970s. Its natural fluorescence has facilitated the study of its distribution and action *in vitro* and *in vivo*. As a highly effective, well-researched cytotoxic small molecule drug, doxorubicin was a natural choice to use in a nanoparticle formulation. These factors make it the primary therapeutic of interest throughout this thesis.

Patient ID	Plasma Concentrations ($\mu\text{g/g}$)		Biopsy Concentrations ($\mu\text{g/g}$)	
	Post-Infusion	Post-Heating	Post-Infusion	Post-Heating
I.01	N/E	N/E	2.56	5.32
I.02	26.2	23.5	1.78	13.20
I.03	19.9	6.0	4.09	7.89
I.04	26.2	5.4	1.59	2.09
I.05	23.7	8.0	2.23	11.50
I.06	26.8	11.8	1.79	6.41
II.01	31.9	19.3	N/A	6.65
II.02	29.8	16.0	N/A	6.84
II.03	30.2	12.9	N/A	3.89
II.04	21.7	12.9	N/A	21.80

Table 2.1. The clinical data from the TARDOX trial, which consisted of a 30 minute infusion of a commercially available LTSL doxorubicin formulation, followed by up to 60 minutes of ultrasound-mediated hyperthermia. Plasma samples were taken from each patient before and after heating. Tumour biopsies were performed after heating in all patients, and before heating in a sub-set of patients. The plasma sample for patient I.01 was non-evaluable due to errors in sample processing.

Despite the drug having been widely studied, there remains debate in the literature regarding the mechanism of action of doxorubicin against tumour cells. An oft-cited review of the topic suggests that it seems likely that cytotoxic effect is achieved by different mechanisms at different concentrations [90], although the mechanisms proposed are nearly all intracellular. Two of the most commonly described mechanisms for the action of doxorubicin are topoisomerase-II inhibition [e.g. 91] and the inhibition of macromolecular synthesis via DNA intercalation [e.g. 92].

Some of the clearest evidence for intracellular doxorubicin being a good indicator of therapeutic effect was published by Durand and Olive [93]. In their study, flow cytometry was used to assess the intracellular doxorubicin concentrations obtained after a variety of exposure times. The intracellular concentration was then compared to cell survival, assessed via a clonogenic assay, as shown in Figure 2.4, and a clear correlation between survival and intracellular concentration can be seen.

A possible extracellular mechanism of action, whereby doxorubicin achieves a cell kill through binding to the cell membrane is evidenced by experiments such as [94]. In this study, doxorubicin was covalently bonded to microspheres (which cannot penetrate into cells) and was still found to have a cytotoxic effect. As a result, extracellular mechanisms have been included with intracellular mech-

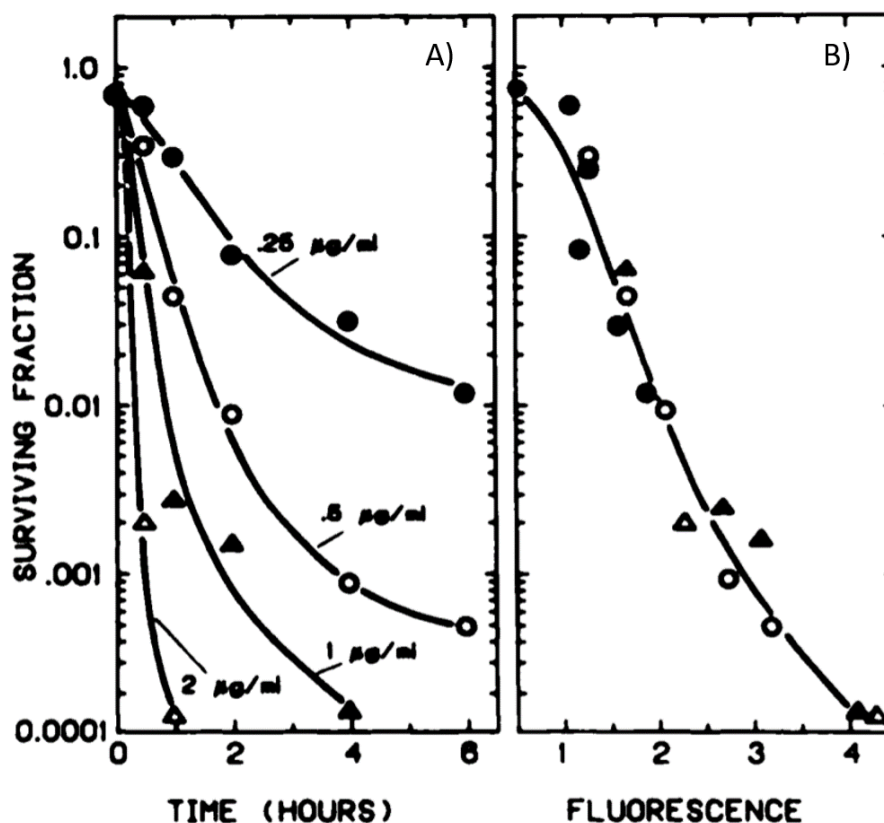


Figure 2.4. Adapted from [93] with permission. A) Survival fraction of murine L-929 fibroblasts compared with duration of exposure at constant extracellular concentration; and B) compared with mean intracellular fluorescence

anisms in previous time-dependent pharmacodynamic models [95]. Another study of immobilised drug [96] provided further evidence for the existence of an extracellular mechanism, but it was also shown that the magnitude of this effect was small compared to the effect of free drug at the same, physiologically relevant concentrations.

In light of this, Gerwitz's critical review of proposed doxorubicin mechanisms [90] acknowledges that extracellular mechanisms exist, but expresses doubt that such mechanisms are relevant at concentrations that occur in the clinic. However, as is discussed in Section 2.7.1, the release of drug from a thermosensitive liposome has resulted in a change in the concentrations which can be considered clinically relevant. Regardless of the possible existence of extracellular mechanisms, the predominance of intracellular mechanisms mean that mathematical models of intracellular uptake will almost certainly form a large part of the finished optimisation.

In terms of toxicity, the dose-limiting side-effect is cardiomyopathy, for which a number of causative routes have been suggested [97, 98]. The desire to avoid this side effect (and its poor prognosis), is what limits the cumulative lifetime dose of doxorubicin to around 450 mg/m^2 [99]. Peak plasma

concentration is also often limited in an effort to avoid cardiotoxicity and other side effects such as myelosuppression [100].

2.5.1 Pharmacodynamic Modelling

Pharmacodynamic models describe the interaction of drugs with their targets. In the case of doxorubicin TSLs, we are concerned with modelling the uptake kinetics of doxorubicin and obtaining a suitable metric for therapeutic effect which can be calculated. Traditional pharmacodynamic models assess only the concentration of drug required to inhibit cell growth by a percentage for a set exposure time. These data are often fitted to models similar to a Hill model, which was originally used to describe the binding of ligands to macromolecules. For viability, V , such an expression can be written as $V = \frac{1}{1+(K/c)^s}$, where c is the relevant concentration of the drug, K represents the concentration at which $V = 0.5$, and s , is the slope of the curve. This relationship is plotted for a variety of slopes, with $K = 0.5$ in Figure 2.5. This type of model is useful for assessing the effectiveness of new compounds, but does not provide a means of assessing the effect of a drug delivered *in vivo* due to the spatio-temporally varying concentration field that results.

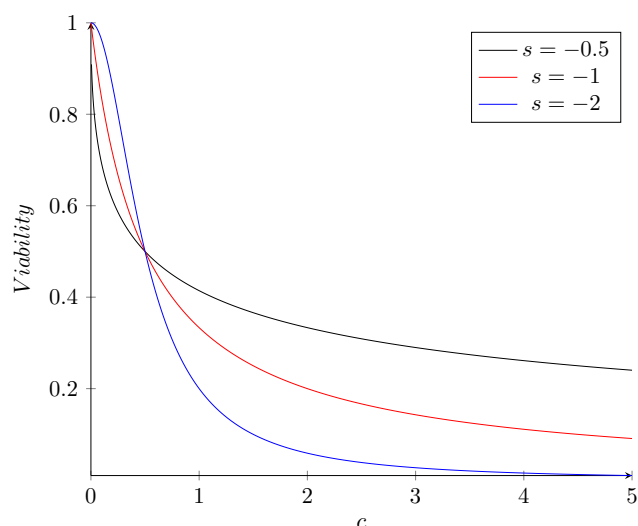


Figure 2.5. Typical dose-response curves for a cytotoxic agent, modelled with a Hill equation: $V = \frac{1}{1+(K/c)^s}$, where V is the viability, c is the relevant concentration of the drug, K represents the concentration at which $V = 0.5$ (in these plots, $K = 0.5$), and s , is the slope of the curve. The larger the magnitude of s , the steeper the response.

The creation of a mathematical model which enables such predictions requires a knowledge of the mechanism(s) by which doxorubicin achieves a therapeutic effect. Debate in the literature regarding the physical processes behind cellular uptake of doxorubicin mean that there is no clear ‘best model’.

A degree of saturable uptake is exhibited in most available data sets, which is possibly suggestive of a carrier-mediated transport component, which limits the maximal rate of drug transport into the cell when the carriers are saturated (as there are a finite number of carriers). An alternative explanation is that doxorubicin has been observed to self-associate (i.e. form larger, polymer-like molecules) at elevated concentrations, which are too large to be transported effectively across the cell membrane. This can give rise to the features of carrier-mediated (or saturable) transport, as is further discussed in [101]. In addition to saturable uptake mechanisms, Fickian diffusion, which would give rise to linear diffusive components in a mathematical model also have mechanistic basis [e.g. 101]. As a result, models in the literature typically combine linear and/or saturable influx and efflux terms.

Cellular uptake models are fitted to data, such as those obtained by Durand and Olive [93] in L-929 fibroblasts and Kerr et al. [102] in non-small cell lung tumour cells. This latter dataset is the basis of most *in silico* models of TSL doxorubicin delivery. For example, in an early work on optimisation, El-Kareh and Secomb [67] fitted the non-small cell lung tumour data to the following equation, assuming that both cellular influx and efflux were saturable:

$$\frac{dc_i}{dt} = V_{max} \left(\frac{c_e}{c_e + K_e} - \frac{c_i}{c_i + K_i} \right) \quad (2.3)$$

where c_i represents the intracellular concentration of drug, V_{max} is the maximum possible uptake rate, while K_e and K_i represent the concentrations at which influx and efflux respectively are at $0.5V_{max}$. In a subsequent paper [95], the same authors fit data from a variety of cell lines to the following uptake model, combining instead a linear and saturable influx with a purely linear efflux:

$$\frac{dc_i}{dt} = k_1 c_e + \frac{k_2 c_e}{K_e + c_e} - k_3 c_i \quad (2.4)$$

where $k_{1,2,3}$ are rate constants with units of s^{-1} , and all other quantities are as previously defined. This study also attempted to fit the same model to data from other cell lines, which highlighted that the uptake characteristics cannot be assumed to be similar from one cell line to the next (although several of these studies did not include uptake data, and El-Kareh and Secomb inferred uptake data from cytotoxicity data).

A small number of models include the intranuclear doxorubicin concentrations. Amongst the reasons for this are the difficulty in obtaining accurate measurements (doxorubicin fluorescence is known to be quenched by nuclear binding [103]) and the lack of clear data linking intranuclear concentration

and cell survival. One study which did include nuclear binding was that of McKenna et al. [104], who studied the effect of doxorubicin on triple negative breast cancer cells. This method was based on a three compartment model, as shown in Figure 2.6. One feature of this model, shared with most others is that they permit higher concentrations in cells than in the extracellular space; this is not necessarily non-physical, but indicative of either active transport processes into the cells and binding processes in the cells. In general, higher concentrations of drug such as doxorubicin are seen in the cells than outside the cells; there are several reasons for this, including the fact that a greater fraction of the drug inside the cell is bound to proteins or DNA, as well as changes in the protonation state of doxorubicin as a result of the transmembrane pH change (protonated doxorubicin cannot cross the cell membrane as freely as the unprotonated form) [105]. While it would be possible to include more intracellular compartments, such as endosomal, mitochondrial, cytoplasmic, and nuclear drug, as the total intracellular drug has been shown to be well correlated with cell kill [93], this is generally not done in modelling which incorporates the clearance scale (Figure 1.1). This is because it adds complexity without increasing the clarity of the desired output (i.e. the likely cell kill).

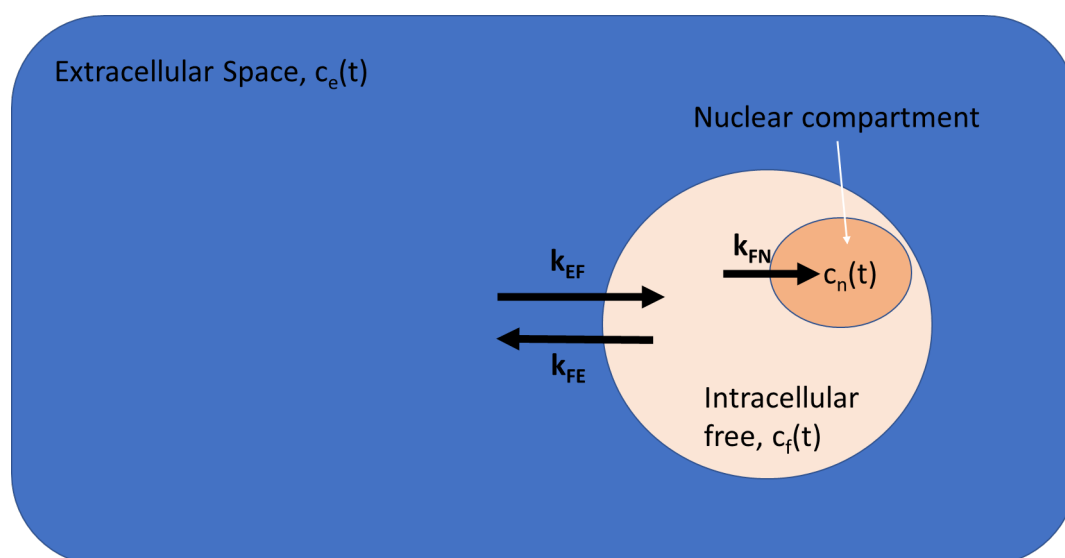


Figure 2.6. A compartment model similar to that used by McKenna et al. [104], with irreversible nuclear binding. k_{EF} is the first order rate constant of free doxorubicin transport from the extracellular space to the intracellular compartment, while k_{FE} represents the reverse process. k_{FN} is the first order rate constant between the intracellular space and the nucleus; a process which is modelled here as irreversible.

2.6 Hyperthermia, Solid Tumours, and Small Molecule Therapeutics

A recent systematic review [106] found 235 ongoing clinical studies investigating hyperthermia and cancer treatment. These were divided into five categories depending on the type of hyperthermia; whole-body (WBHT), hyperthermic intraperitoneal chemotherapy (HIPEC), regional (typically a hy-

perthermic infusion into a cavity other than the peritoneum, such as intrathoracic or intravesicle), local, and unknown.

These investigations are almost all performed without the use of thermosensitive drugs, but rather look to explore the number of bio-effects that can be beneficial to treatment with either chemotherapy or radiotherapy (sometimes termed thermochemotherapy and thermoradiotherapy). These effects have been the subject of numerous reviews, including by van Rhoon et al. [107] and Dewhirst et al. [108]. The most notable macroeffects of mild hyperthermia (typically defined as temperatures in the 39°C - 42°C [109]) which improve the efficacy of treatment are increasing the tumour perfusion and increasing the permeability of the vascular endothelium. The increased perfusion increases the oxygenation of the tumour tissue [107] (i.e., alters the tumour microenvironment), which is in turn likely to have a positive impact on treatment outcome. Increased permeability of the vascular endothelium aids the extravasation of therapeutics from the blood stream into the extracellular space, increasing the extraction fraction [85] of the drug (this is defined as the fraction of drug which extravasates on its first-pass through the tumour).

Cells themselves have been shown to be sensitised to small molecule therapeutics by mild hyperthermia. The inhibition of DNA repair has been shown to be a key mechanism in inducing cell death at lower concentrations than would be expected at normothermia; this inhibition is a well-accepted mechanism for the enhanced effectiveness of thermoradiotherapy compared to conventional radiotherapy [110]. Recent research in this area suggests that specifically, mild hyperthermia degrades the BRCA2 protein, which is a mediator of the RAD51 protein, required for homologous recombination, the process by which cells repair double DNA strand breaks, which (in this case) have been caused by radiotherapy (for thermoradiotherapy) or a cytotoxic agent (thermochemotherapy) [111]. Salvador et al. [112] showed that hyperthermia decreased cell viability when combined with doxorubicin in A375 and MNT-1 melanoma cells, although not in all conditions. Similarly, Maurici et al. [113] demonstrated that hyperthermia reduced the IC50 in different PDAC cell lines for 5-fluorouracil, cisplatin, and gemcitabine (for 6, 12, and 24 hour exposure durations). In a recent review, the cellular heat stress response, which is responsible for protecting cells from the adverse effects of hyperthermia was identified as a potential limiting factor in the use of hyperthermia in oncology, as repeated treatments can render cells thermotolerant; overcoming thermotolerance is another area of active research [114].

Furthermore, hyperthermia has been shown to increase the uptake of doxorubicin by certain cells. Sharma et al. [24] demonstrated that hyperthermia caused an increase in cellular uptake of doxorubicin, as well as an increase in cytotoxicity which was not explained by the elevated uptake alone; i.e. the inhibition of DNA repair acts synergistically with the elevated uptake. Reasons for the elevated uptake of drug include increased cell membrane permeability at elevated temperature [24], enhanced passive diffusion [115], and modulation of cellular efflux pumps [116]. Sharma et al. [24] also propose increased generation of reactive oxygen species as a potential mechanism for the enhanced toxicity of doxorubicin when combined with mild hyperthermia.

2.6.1 Heating Modalities

There are several techniques which can be used to achieve heating within a target tissue (sometimes described as locoregional hyperthermia), which are summarised more fully in [117] (except RFA). Firstly, in many pre-clinical studies, regional, superficial heating is applied using a water bath. This technique works well in pre-clinical studies, in which mice have tumours implanted in known locations, but will not translate to the clinical setting. Secondly, it is possible to use external electromagnetic (microwave) applicators for heating. These are non-invasive, but have a limited penetration depth of around 3 cm, and so are only suitable for tumours close to the surface. Minimally invasive microwave probes are also available for localised hyperthermia. Multiple probes can be used at once for heating, unlike with RFA (see below), but the use of probes is constrained to tumours in accessible locations (such as the prostate). Microwave power is adjustable, which can be used to control the rate of heating.

As was used in the TARDOX [21], focused ultrasound (FUS) is a non-invasive heating modality which can be used to achieve localised hyperthermia, at greater depths than is possible with external microwave applicators. Ultrasound is also . However, challenges associated with ultrasound-mediated hyperthermia including heating a large volume, such as a whole tumour volume, as the focus for heating is small in comparison to the tumour volume; the transducer used in the TARDOX trial had a transverse 3-dB beam-width of 1.2 mm and an axial 3-dB length of 9.5 mm [118]. Perhaps the biggest challenge with ultrasound, however, is the movement of internal organs due to the oscillatory motion of the diaphragm when a patient breathes. This meant that, in the TARDOX trial, patients were under general anaesthetic with high frequency jet ventilation to control the timing and magnitude of these oscillations, so as to facilitate the targeting of the tumours. This also required an involved treatment planning process for each patient [87], far in excess of what is required to microwave heating with a

probe.

Finally, as used in the HEAT and OPTIMA trials discussed in Section 2.4, Radiofrequency Ablation (RFA) can be used to heat the tissue. RFA is a minimally invasive technique, involving the insertion of a probe into the tumour. This probe delivers a high frequency electrical current (between 350 and 750 MHz), causing the local temperature to rise to around 70°C, as a result of the current flowing into the tissue, and tissue ions being agitated [119]. The heating mechanism (which is reliant on the completion of an electrical circuit) means that the use of multiple probes at once is not possible.

2.7 Mathematical Modelling of Chemotherapy

2.7.1 Previous Compartment Model Studies

Although many compartment models neglect spatial heterogeneity in tumour dose, such models can still have utility. The study by Dawidczyk et al. [46] (comparing delivery of free and liposomal doxorubicin) is a good example of both what can and cannot be learned from compartmental models. The study fitted a three compartment model, as shown in Figure 2.2 to the administration of liposomal doxorubicin in mice with different tumour xenografts, the data clearly showing that some tumours had a greater uptake of the drug than others. Additionally, the study assessed how fluctuations in the obtained rate constants would affect tumour accumulation. Unsurprisingly, reducing k_{el} increased tumour concentrations, with 10 fold reductions in k_{el} equating to 2.5 fold increases in tumour concentrations. However, less intuitively, intravasation from the tumour back into the vasculature (k_b) was also identified as a ‘rate-limiting step’, with 10 fold reductions in k_b increasing tumour concentrations by a factor of three. This suggests that drug delivery systems should aim to mitigate against transport back into the vasculature, either by binding to cells (active targeting) or through more prolonged elevated concentrations of free drug in the tumour vasculature, as is realisable with TSL delivery. This is used to hypothesise that idarubicin may be a good drug to use in a TSL-i formulation, as its rapid binding reduces the amount of drug re-entering the blood stream [Figure 6 of 89].

The work of El-Kareh and Secomb [67] is an early study which sought to optimise treatment with free doxorubicin by obtaining an optimal infusion duration. They optimised the peak intracellular

concentration and used a plasma concentration approximated by a single compartment model fit:

$$c_b(t) = \begin{cases} \frac{c_0}{\alpha T}(1 - e^{-\alpha t}) & t \leq T \\ \frac{c_0}{\alpha T}(e^{\alpha T} - 1)e^{-\alpha t} & t > T \end{cases} \quad (2.5)$$

where T is the infusion time of the drug and α is the clearance rate constant for doxorubicin. The extracellular drug concentration (c_e) of drug was modelled by:

$$\frac{dc_e}{dt} = PS(c_b - c_e) - R(t) \quad (2.6)$$

where PS is the permeability-surface area product, and $R(t)$ denotes the drug entering the intracellular compartment (there was no spatial variation in tumour dose considered). The uptake model was as described by equation 2.3, the authors having fitted uptake parameters to non-small cell lung tumour data [102].

For the chosen parameters, an optimal infusion time of free doxorubicin of around 100-150 minutes was obtained (see Figure 2.7). Shorter infusion times saw higher extracellular concentrations with saturated cellular uptake limiting the peak intracellular concentrations, while longer infusion times saw cellular uptake limited by lower extracellular concentrations. The implications of this for TSL delivery are that short doses achieving high extracellular concentrations do not necessarily equate to a greater therapeutic effect. TSL doxorubicin delivery was also considered by El-Kareh and Secomb, although assumption of TSL-e as the primary delivery mechanism limits the utility of their findings in optimising treatment with ThermoDox.

Examining the studies which explore TSLs specifically, Huang et al. [25] used a compartment model for doxorubicin and topotecan TSLs to explore the effects of changing the drug release rate from the TSL, and how this might give rise to preferential treatment regimens (although the same model of cellular uptake was used in both cases). Gasselhuber et al. published three papers between 2010 and 2012, which used compartment modelling. The first of these papers modelled treatment with doxorubicin and TSL doxorubicin in combination with RF ablation [65]. The second paper compared conventional doxorubicin, liposomal doxorubicin, and two different TSLs (one with predominantly intravascular release, and the other with predominantly extravascular release) *in silico* [66], finding that TSL-i offered the greatest potential intracellular concentrations. The treatments with free doxorubicin had a peak extracellular concentration around 2 $\mu\text{g/g}$; whereas peak extracellular concentrations

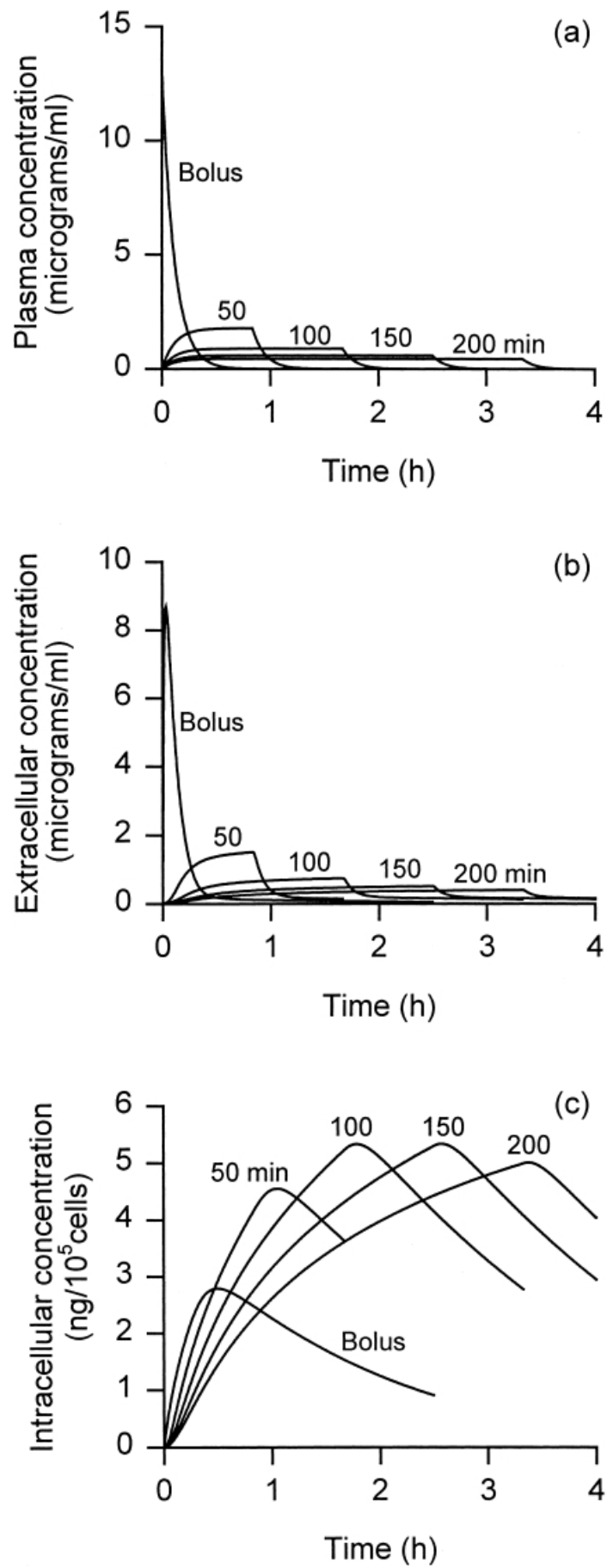


Figure 2.7. Simulation results from [67], reproduced with permission. The curves are labelled with the simulated infusion duration of free doxorubicin.

from TSL-i delivery varied (depending on parameter values) between 10 and 130 $\mu\text{g/g}$. This increase over orders of magnitude changes the bounds of what might previously have been considered physiologically relevant concentrations. This, alongside the fact that the cellular uptake data used in these models comes from a lung cancer cell line, when lung cancer is an unlikely target for LTSL doxorubicin delivery (in the case of ultrasound-mediated hyperthermia, because of the challenges associated in delivering ultrasound through the lungs due to the large amount of energy reflected at the tissue/air boundary), provides a clear need for experimental work in cells to verify the validity of using intracellular concentration as a metric for cell kill. The final paper demonstrated good agreement between predicted drug concentration from a compartment model and a preliminary *in vivo* experiment in a rabbit [120] in terms of spatial concentration profile.

In 2015, Liu and Xu [121] performed a local sensitivity analysis on a compartment model of TSL doxorubicin delivery (which did not include liposomal accumulation in the extracellular space), finding that the parameters which gave rise to the greatest change in the predicted peak intracellular concentration, when increased by 10% from their initial values were liposomal release rate, liposomal clearance, tumour perfusion, maximum cellular efflux, and tumour vascular permeability. Asemani and Haemmerich [122] extended this model to include tumour accumulation of the liposomal doxorubicin, and further assessed how the predicted intracellular doxorubicin concentrations varied when different parameters were varied one at a time (i.e. a local sensitivity analysis). Another improvement made by this study was the inclusion of a model of drug release from the liposomes which more accurately characterised their behaviour. Another improved model of drug release from TSLs (i.e. not simply first-order release kinetics) was also suggested by Lu and ten Hagen in 2020 [123].

Some of the most promising developments in this field have been published recently. In 2021 ten Hagen et al. [85], published work in which they used *in vivo* experiments to obtain a parameter set for a compartment model, which was then validated using intravital microscopy and delivery of carboxyfluorescein (rather than doxorubicin). This paper demonstrated that compartment models could be used for prediction of *in vivo* experiments. Furthermore, a global sensitivity analysis identified the tumour transit time, liposomal release rate, and permeability surface-area product as the parameters which gave rise to the greatest output variance, defined as the root-mean-square error of the tumour interstitial concentration calculated over 20 minutes in comparison to the reference tumour interstitial concentration calculated using the default parameter values.

2.7.2 Including Spatial Heterogeneity

Spatial heterogeneity of tumour drug dose is included in some computational studies, and, as has been shown experimentally (as in Figure 2.1), can be an important part of the problem. Mathematically, general transport processes are governed by the advection-diffusion-reaction equation. Advective mass transport is due to bulk motion of the fluid phase; the mass flux due to an advective term is therefore given by the product of the fluid flux, q and the local solute concentration, c :

$$\frac{\partial c}{\partial t} + \nabla \cdot (qc - D\nabla c) = R(c) \quad (2.7)$$

D is the diffusion coefficient of the solution through the tissue, while $R(c)$ represents the reaction of the drug (usually its uptake by cells). This is often simplified to neglect the advective component which is an acceptable approximation due to the poor lymphatic drainage in tumours, meaning that diffusive transport typically dominates [33]. This means that the value of D is now a ‘lumped element’ diffusivity; in other words, multiple transport processes are being approximated using a purely diffusive model. This simplification was made in both [65] and [120], in which spatial heterogeneity was considered. The latter paper further used a mathematical model for heating with HIFU which included modelling the spatial variation in the drug delivered to the tumour, and demonstrated that the achieved fluorescence profile of doxorubicin showed good agreement with the concentration predicted by the mathematical model of heating in a rabbit model following TSL doxorubicin delivery ($n = 1$).

More complex models simulate spatial heterogeneity considering transport at multiple scales [e.g. 124]. In these cases, mass flux across the vascular endothelium is usually assumed to be proportional to the difference in concentration on either side of the membrane, as it is in the compartment model. This approximation is widely used in the literature [e.g. 67, 124]; using a more complex model is difficult due to a lack of parameter values. The incorporation of spatial heterogeneity on the microvascular scale has been argued to be important owing to differences between different regions of solid tumours [125], which often present with a more poorly-vascularised necrotic core [28].

Modelling this computationally is non-trivial. The use of finite volume or finite difference numerical codes usually invokes strict stability requirements on the timesteps and grid spacing required, while discretising a realistic microvascular geometry is not easy within the confines of a structured grid system. Forward Euler methods are limited by the Courant-Friedrichs-Lewy condition [126], while

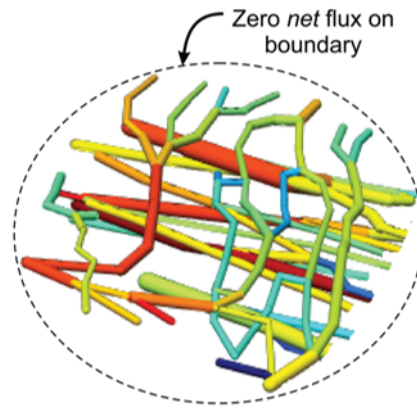


Figure 2.8. Illustration of microvascular network used in time-dependent Green's function method, adapted from [127] with permission.

the matrix inversion associated with backward Euler methods becomes prohibitively computationally expensive for large domains, which are required for physiologically-relevant geometries.

One approach which avoids the stability requirements of finite difference code, is the time-dependent Green's function method of Secomb [127]. The principle behind the method is that 'the diffusive transport of the solute is computed by convoluting [sic] the previous solute distribution with the solution of the diffusion equation for the spread of an instantaneous point source over the given time step' [127]. Microvascular geometries for certain tissues, including some tumours, are available in the literature [e.g. 128], where the blood flow rates were estimated counting the passage of fluorescently labelled red blood cells with intravital microscopy and vascular structure was obtained via confocal fluorescence microscopy. Solutions are obtained over a network set in a finite domain, as shown in Figure 2.8. Zero net flux is imposed over the boundary, allowing for simulations to be run over an infinite domain (as opposed to applying zero flux on the boundary):

$$\int_{\Omega} \left(\frac{\partial C_{e,a}^T}{\partial t} - \Psi_a(\mathbf{x}, t) \right) dV = 0 \quad (2.8)$$

where Ω represents the boundary and $\Psi_a(\mathbf{x}, t)$ is a time-dependent distribution of sources and sinks for a solute a . This simplifies the Green's function solution to the diffusion equation and avoids the accentuation of hypoxic regions at the boundary of the domain.

2.8 Aims of the Present Work

The recent failures of the HEAT [75] and OPTIMA [76] phase III trials of ThermoDox represent a significant set-back for TSL technology. Success in future trials is therefore vital for the clinical future of both ThermoDox and TSL delivery. The TARDOX trial [21, 87] demonstrated that TSL technology can have significant positive impacts on intracellular uptake and therapeutic response through using ultrasound-mediated hyperthermia as opposed to RFA. Further recent developments regarding the use of idarubicin as the encapsulated agents represent an alternative utilisation of TSLs which represent an interesting new direction for the treatment of tumours with a drug which was not previously suitable for this purpose due to its rapid plasma protein binding [89].

The aim of this work is to use *in vitro* and *in silico* techniques to obtain a mathematical model for the treatment of solid tumours in patients with LTSLs, and to use these models to explore the effect of changing key parameters, such as the dose, hyperthermia duration, and infusion duration of the drug. As such, the main aims of the project are:

1. To establish whether or not computational modelling can accurately resolve the results of clinical treatment with ThermoDox, a TSL formulation of doxorubicin, which was used in the TARDOX trial (Chapter Three).
2. To assess how the outputs (such as peak intracellular drug concentration) vary with fluctuations in the inputted parameters with a global sensitivity analysis (Chapter Three).
3. To verify that peak intracellular concentration is an acceptable metric for cell kill with doxorubicin (Chapter Four).
4. To quantify the uptake of doxorubicin in a cancer cell line at normothermic and mildly hyperthermic conditions (Chapter Four).
5. To use these data to establish a model of cellular uptake (Chapter Four).
6. To quantify the spatial variations in tumour drug dose resulting from delivery of drug from TSLs. (Chapter Five).
7. To use this modelling to explore the effect of changing key parameters, such as the dose, hyperthermia duration, and infusion duration of the drug.(Chapter Five).

Chapter 3

Compartment Models of Thermosensitive Liposomal Doxorubicin Delivery

3.1 Introduction

As discussed in the literature review, compartment models can be used to explore different treatment protocols with both free drug and TSL drug. In the case of TSL drug delivery, for a given nanoparticle and encapsulated agent, the clinicians must choose the dose, infusion duration, and hyperthermia duration; three variables well-suited to optimisation with computational modelling. The optimisation of encapsulated agent, nanoparticle shape/size and various PEGylation strategies are not considered in this modelling, but it is important to remember that these variables exist when trying to obtain the best possible treatment. Unless otherwise stated, optimisation in this chapter is performed to maximise the peak intracellular concentration of doxorubicin, as this has been shown [e.g. 93] to be correlated with cell kill by doxorubicin.

In this chapter, the governing equations of the model are presented, and the implementation of non-ideal heating (i.e. that which does not uniformly heat the target region to the therapeutic temperature for the entire treatment duration, which would be expected when ultrasound-mediated hyperthermia is used in the clinic) is explored, before the results of the model are compared to clinical data from the TARDOX trial. A global sensitivity analysis is used to explore the parameters which give rise to the most uncertainty in the model predictions. The infusion duration is then optimised for two separate cases: first, in which the infusion is concurrent with hyperthermia; and second, in which the hyper-

thermia duration is fixed. The robustness of these predictions is tested with a further global sensitivity analysis of the optimum infusion duration. Finally, the effects of varying three factors are considered: firstly, the timing of the heating with respect to the infusion; secondly, the total administered dose; and thirdly, using a different form of cellular uptake model. The resulting findings are then used to inform the experimental work performed in the next chapter.

3.2 The Compartment Model

A compartment model, similar to those used in the studies described in the literature review, for delivery of LTSL doxorubicin is used in this chapter, and illustrated in Figure 3.1. The cellular uptake model used here is the same as that used in [67], which was fitted to uptake data obtained by Kerr et al. [102] for non-small cell lung cancer cells. This model was chosen for use in these compartment models as it was the simplest available in the literature (in terms of the number of parameters), and the results of El Kareh and Secomb's study provided a good test case to check that the code was correct. The validity of this choice is discussed extensively in the next chapter.

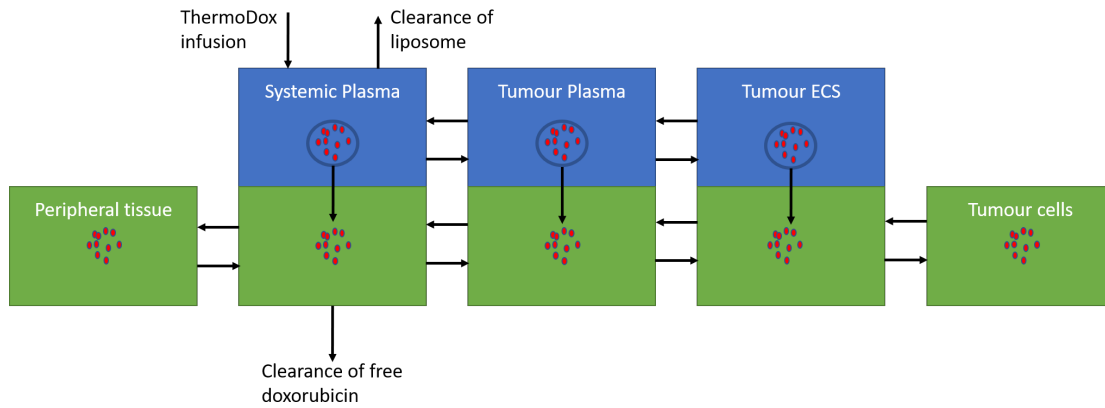


Figure 3.1. Compartment model. Doxorubicin molecules (red), are infused into the systemic plasma compartment, encapsulated in thermosensitive liposomes (dark blue). Both liposomal and free doxorubicin can enter the tumour extracellular space, but only free doxorubicin can then enter the tumour cells. Blue compartments denote the encapsulated drug, green compartments denote the unencapsulated, ‘free’ drug. Encapsulated doxorubicin is assumed not to accumulate in the peripheral tissue owing to its size. This is a typical assumption of such models [e.g. 65].

The governing equations for the systemic plasma and peripheral tissue concentrations are:

$$V_P^S \frac{dL_P^S}{dt} = -V_P^S k_{e, lip} L_P^S - V_P^S r_{37} L_P^S + V_P^T F(L_P^T - L_P^S) + (1 - \mathcal{H}(t - T_{inf})) \frac{\Psi}{T_{inf}} \quad (3.1)$$

$$V_P^S \frac{dc_P^S}{dt} = -V_P^S k_e c_P^S + V_P^S r_{37} L_P^S + V_P^T F(c_P^T - c_P^S) - V_P^S k_p c_P^S + V_{tis}^S k_t c_{tis}^S \quad (3.2)$$

$$V_{tis}^S \frac{dc_{tis}^S}{dt} = V_P^S k_p c_P^S - V_{tis}^S k_t c_{tis}^S \quad (3.3)$$

where V is the volume of the compartment, with the subscripts P , and tis representing the plasma and tissue respectively, while L and c denote whether the concentration is liposomal or free doxorubicin. The superscripts S and T denote the systemic level and tumour compartments. k_e denotes the clearance of free drug from the central blood compartment ($k_{e,lip}$ being the liposomal equivalent), while k_p and k_t denote the rate constants for mass transfer to and from the peripheral tissue compartment - for free doxorubicin only. F is the plasma flow per tumour plasma volume, and r is the release rate of free doxorubicin from its liposomal form. Ψ is the total amount of drug administered over an infusion time, T_{inf} , and $\mathcal{H}(t)$ is a Heaviside step function.

In the tumour plasma:

$$V_P^T \frac{dL_P^T}{dt} = V_P^T F(L_P^S - L_P^T) - V_P^T L_P^T r - V_{tot}^T P_{Lip} S(L_P^T - L_e^T) \quad (3.4)$$

$$V_P^T \frac{dc_P^T}{dt} = V_P^T F(c_P^S - c_P^T) + V_P^T L_P^T r - V_{tot}^T P S(c_P^T - c_e^T) \quad (3.5)$$

PS and $P_{Lip}S$ denote the permeability-surface area product for free and liposomal doxorubicin respectively, while r denotes the release rate of doxorubicin from the TSL, which takes the value of r_{37} in normothermic (37°C) conditions and r_{42} in mildly hyperthermic (42°C) conditions. V_{tot}^T is the total tumour volume. In the tumour tissue:

$$V_e^T \frac{dL_e^T}{dt} = V_{tot}^T P_{Lip} S(L_P^T - L_e^T) - V_e^T L_e^T r \quad (3.6)$$

$$V_e^T \frac{dc_e^T}{dt} = V_{tot}^T P S(c_P^T - c_e^T) + V_e^T L_e^T r - V_i^T \left(\frac{dc_i}{dt} \right) \quad (3.7)$$

where the subscript i denotes the intracellular compartment. The intracellular uptake is initially modelled as

$$\frac{dc_i}{dt} = V_{max} \left(\frac{c_e}{c_e + K_e} - \frac{c_i}{c_i + K_i} \right) \quad (3.8)$$

in which V_{max} , K_e and K_i are constants in the uptake model, as fitted in [67] and discussed above.

The TARDOX trial provides a suitable data-set for the task of assessing whether compartment models can accurately resolve the effects of treatment by LTSL doxorubicin, as biopsies were taken following the end of a 30 minute infusion, and after (up to) 60 minutes of heating. The parameters used in this chapter are presented in Table 3.1, and the treatment protocol was chosen to replicate *in silico*, an

idealised version of the TARDOX trial. This table includes the volume fractions in the tumour which are extracellular space (v_e^T), intracellular space (v_i^T), and plasma (v_p^T) respectively, with the total tumour volume also specified. In simulating the TARDOX trial, the infusion duration, T_{inf} is set to 30 minutes, and hyperthermia is applied (i.e. $r = r_{42}$, rather than r_{37}) from $t = 30$ minutes to $t = 90$ minutes.

3.2.1 Non-Ideal Heating

One aspect of the TARDOX trial which is important to consider in the model is that the ultrasound-mediated hyperthermia used does not result in ideal heating, owing to the challenges associated with maintaining the entirety of an internal tumour at 42°C for the duration of the treatment. In [87, Table E3], a Proportion In Range (PIR), that is, the mean volume fraction of the tumour which was successfully heated to between 39.5°C and 47.0°C during the treatment is reported for each patient. The average value is 0.473 (range: 0.276 - 0.600), which is different to many pre-clinical studies, in which the tumours are typically smaller, and closer to the skin, allowing for either more effective heating with focused ultrasound, or the use of immersion in a water bath to achieve hyperthermia.

There are several different ways in which non-ideal heating could be included in a compartment model. The first is in a spatial-average sense. In this case, we can use the PIR to reduce the release constant proportionally (i.e. as a weighted arithmetic average), replacing the term r in equations 3.4 to 3.7 with $r_{42}\text{PIR}_s + r_{37}(1 - \text{PIR}_s)$. The subscript s denotes the fact that this is a spatial-average sense of PIR, and the four equations for tumour plasma and tumour tissue concentrations of free and encapsulated drug are thus altered to become:

$$V_P^T \frac{dL_P^T}{dt} = V_P^T F(L_P^S - L_P^T) - V_P^T L_P^T [r_{42}\text{PIR}_s + r_{37}(1 - \text{PIR}_s)] - V_{tot}^T P_{Lip} S(L_P^T - L_e^T) \quad (3.9)$$

$$V_P^T \frac{dc_P^T}{dt} = V_P^T F(c_P^S - c_P^T) + V_P^T L_P^T [r_{42}\text{PIR}_s + r_{37}(1 - \text{PIR}_s)] - V_{tot}^T P S(c_P^T - c_e^T) \quad (3.10)$$

$$V_e^T \frac{dL_e^T}{dt} = V_{tot}^T P_{Lip} S(L_P^T - L_e^T) - V_e^T L_e^T [r_{42}\text{PIR}_s + r_{37}(1 - \text{PIR}_s)] \quad (3.11)$$

$$V_e^T \frac{dc_e^T}{dt} = V_{tot}^T P S(c_P^T - c_e^T) + V_e^T L_e^T [r_{42}\text{PIR}_s + r_{37}(1 - \text{PIR}_s)] - V_i^T \left(\frac{dc_i}{dt} \right) \quad (3.12)$$

with the other equations in the model unchanged. The concentrations resulting from this simulation with $\text{PIR}_s = 0.5$ and 1 respectively are shown in Figures 3.2 and 3.3. It can be seen that the inclusion

Parameter	Value	Source
Dose (mg)	90	50 mg/m ² dose [21], assumes 1.8 m ² .
V_p^s (L)	2.9	Assumed 70 kg human with 79 g blood/kg [129]. Blood density 1050 kg/m ³ m [130], haematocrit 0.45 [131].
F (s ⁻¹)	0.196	Based on typical liver perfusion [132], $w = 0.018$ s ⁻¹ . $F = w \times \frac{1-Hct}{v_p^T}$ Tumour haematocrit (Hct) is 0.19 [133].
P_{lip} (ms ⁻¹)	3.42×10^{-9}	[134]
P (ms ⁻¹)	3.4×10^{-7}	Similar molecule to doxorubicin [135]
S (mm ² /mm ³)	15	Value taken for larger tumours [136].
Tumour Volume (mL)	50	Target treatment region volume in [21].
V_{tis}^S (L)	64.5	70 kg patient, 7.9% blood (as in V_p^T). Tissue density approximated as 1000 kg m ⁻³ .
v_e^T	0.454	Representative value from [137].
v_i^T	0.454	Representative value from [137].
v_p^T	0.07452	$(1 - \text{Tumour Haematocrit}) \times (1 - v_e^T - v_i^T)$ Tumour haematocrit taken as 0.19 [133].
k_e (s ⁻¹)	1.1×10^{-3}	Fitted to data from [138] by [65].
$k_{e, lip}$ (s ⁻¹)	2.228×10^{-4}	Fitted to data from [139] by [65].
k_p (s ⁻¹)	1.6×10^{-3}	Fitted to data from [138] by [65].
k_t (s ⁻¹)	4.68×10^{-5}	Fitted to data from [138] by [65].
R_{37} (s ⁻¹)	3×10^{-4}	[25]
R_{42} (s ⁻¹)	1.6	Figure 5b of [72] suggests 80% release in 1 second.
Cell Volume (mL)	10 ⁻⁹	[67]
V_{max} ([μg/mL] s ⁻¹)	0.04667	Based on [67], using the above cell volume to convert between ng/10 ⁵ cells and μg/mL.
$K_{m, intra}$ (μg/mL)	13.7	Based on [67], using the above cell volume to convert between ng/10 ⁵ cells and μg/mL.
$K_{m, extra}$ (μg/mL)	0.219	[67]

Table 3.1. Parameters used in the compartment model, chosen to replicate the TARDOX trial [21] as closely as possible.

of PIR in this way has minimal effect on the tumour intracellular and extracellular concentrations, which is not consistent with what would be expected to occur with non-ideal heating in reality. This is because the release rate is an exponent, and the values at 37°C and 42°C vary by several orders of magnitude. As a result, even with a PIR of 0.1, the release rate remains very rapid when using weighted arithmetic means.

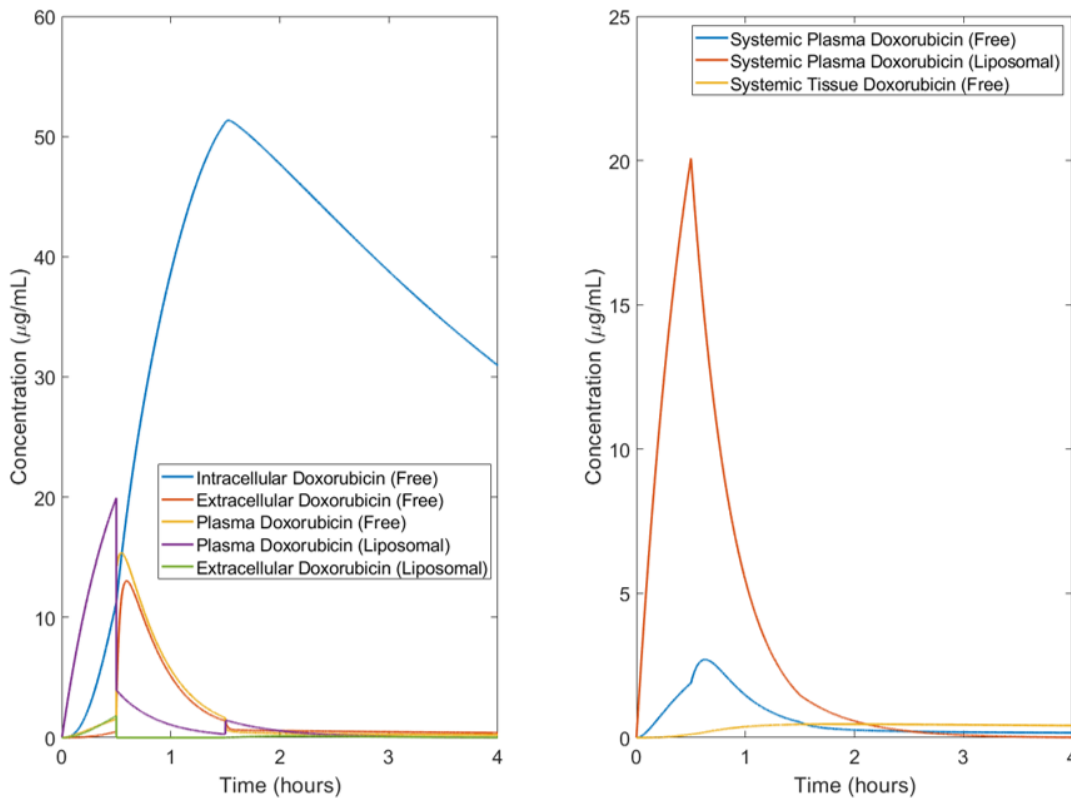


Figure 3.2. Results from the TARDOX compartment model simulation, $PIR_s = 0.5$, weighted arithmetic mean. Tumour concentrations are shown on the left plot and systemic concentrations are shown on the right plot.

An alternative spatial-averaging approach is to use weighted geometric means; i.e., replacing the terms $[r_{42}PIR_s + r_{37}(1 - PIR_s)]$ in equations 3.9 to 3.12 with $[(r_{42})^{PIR_s} (r_{37})^{1-PIR_s}]$. The results of applying $PIR_s = 0.5$ in this way are shown in Figure 3.4; from which it can clearly be seen that this has a more substantial impact on the intracellular and extracellular free doxorubicin concentrations in the tumour compartment. Compared to the case where $PIR = 1$, the peak intracellular and extracellular concentrations are decreased by 22.5% and 85.0% respectively; the intracellular concentration is reduced by a smaller factor as a result of the fact that the transport into the cells is saturated ($K_m = 0.219 \mu\text{g/mL}$) for much of the time in the $PIR = 1$ case.

The maximum tumour intracellular and extracellular concentrations that are achieved in the simulated

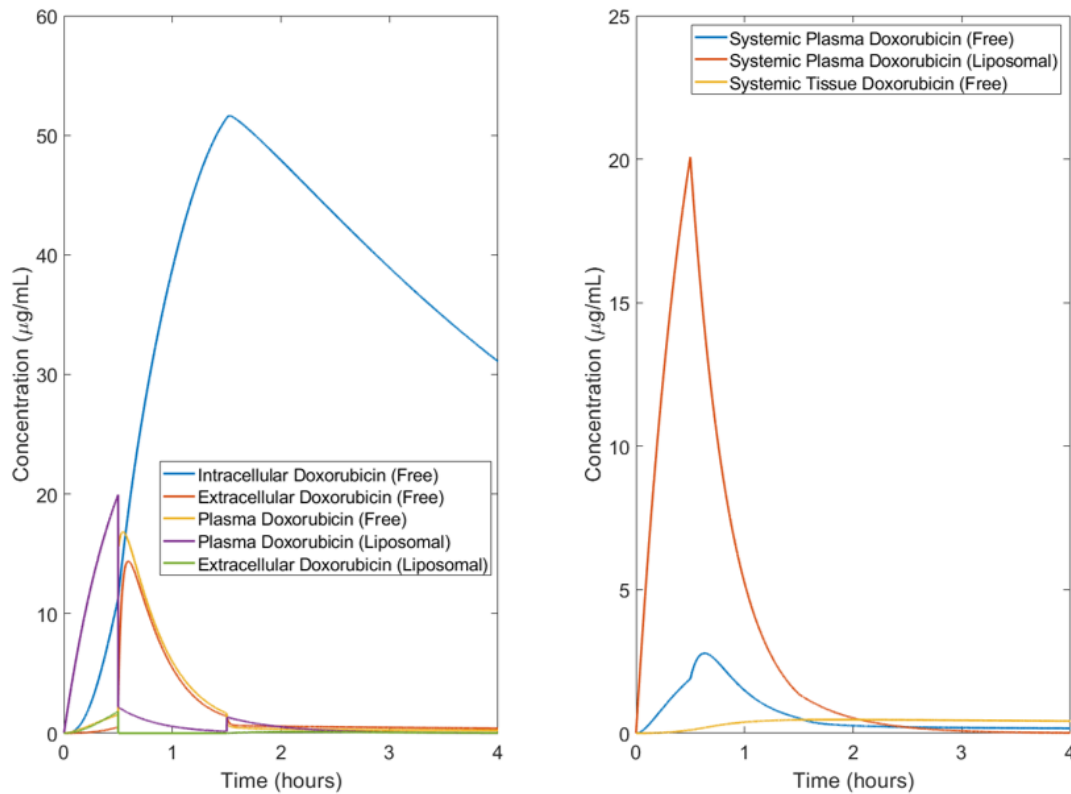


Figure 3.3. Results from the TARDOX compartment model simulation, $PIR_s = 1$, weighted arithmetic mean. Tumour concentrations are shown on the left plot and systemic concentrations are shown on the right plot.

TARDOX protocol are shown as a function of both weighted arithmetic and weighted geometric PIR_s in Figure 3.5. This shows more clearly that the use of weighted arithmetic mean is inappropriate, as this fails to resolve the expected effects of reducing the heating efficiency from 1 to 0.5. While the weighted geometric mean does resolve this effect, it too displays behaviour which is unlikely to resolve the true situation well. For example, the extracellular concentrations achieved below heating efficiencies of 0.5 are low, given that one would expect higher peaks, which may result in increased predicted intracellular drug concentrations (particularly given non-saturable cellular uptake models). In other words, PIR_s fails to capture the clinical situation of an ultrasound beam sweeping over the treatment volume, such that different regions of the tumour experience mild hyperthermia at different times.

An alternative approach, therefore, is to apply PIR in a temporal sense (PIR_t). In this method of incorporating uneven heating, the elevated release rate is only applied for the fraction of the hyperthermia time given by the PIR_t in distinct time blocks. Considering the literature detailing the focused ultrasound used in the TARDOX trial, five minutes is of the right order of magnitude for a time block when trying to recreate the results of the TARDOX trial: in [87], Gray et al. give the maximum transla-

tion speed of the beam as being fixed at 6 mm s^{-1} with slice thickness and slice skips of 2 and 8 mm respectively. This means that the time taken to pass through a 50 mL cube with example dimensions $45.6 \text{ mm} \times 45.6 \text{ mm} \times 24 \text{ mm}$ would be 8.74 minutes. The tumour concentrations for this implementation of PIR are shown in Figure 3.6, in which the effect of the passage of the ultrasound beam on the extracellular and tumour plasma concentrations can be seen more clearly.

Temporal PIR can certainly be argued to provide extracellular concentration profiles which more closely resemble those which would be expected to be seen by individual cells, and thus, the extracellular concentration profiles resulting from applying PIR_t are a more appropriate input to the cellular uptake model. However, the use of PIR_t is more complex to implement, requiring the specification of a period for which heating can be modelled as ‘on’ and ‘off’ (referred to hereinafter as the ‘time block’). Further complexity arises when considering dividing the hyperthermia time in the case where the product of the total hyperthermia duration and PIR_t is not a multiple of the time block. Additionally, the heating being initially ‘on’ instead of ‘off’ can affect the results in a non-negligible way, particularly in the case of ‘infuse-then-heat’, as in the TARDOX trial; something which is further discussed in Chapter Five.

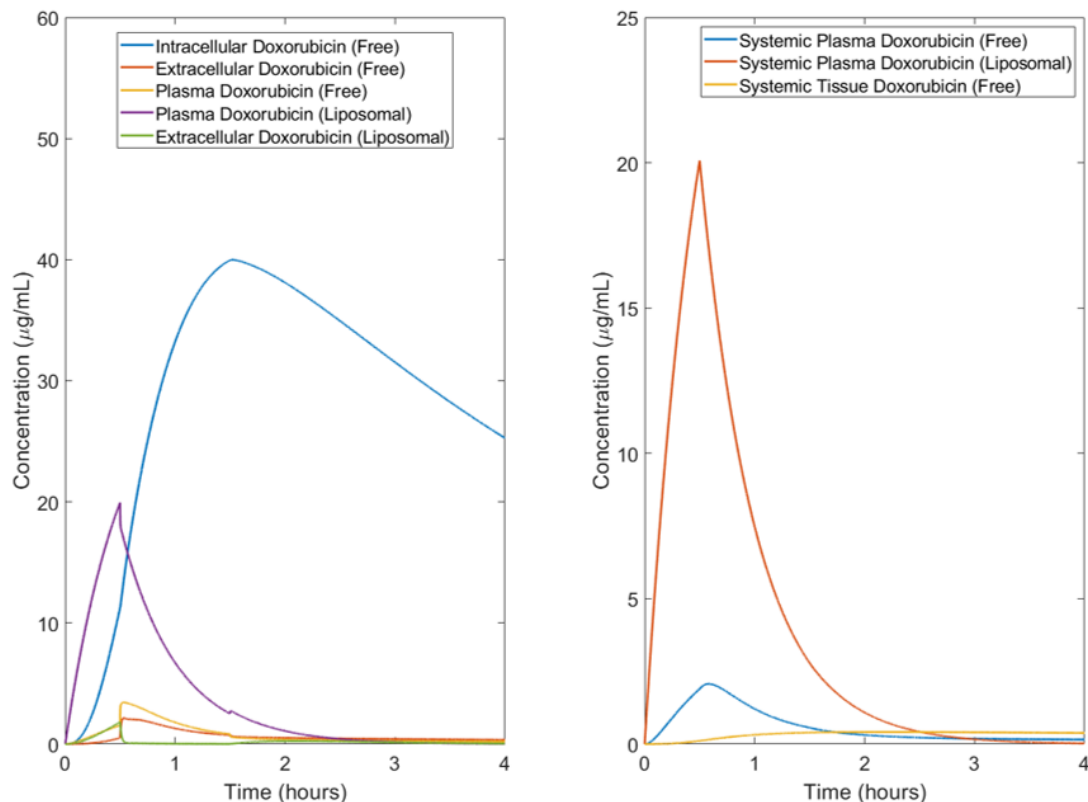


Figure 3.4. Results from the compartment model simulation, $\text{PIR}_s = 1$, weighted geometric mean. Tumour concentrations are shown on the left plot and systemic concentrations are shown on the right plot.

In summary, these three different approaches for including non-ideal heating in a compartment model each have their own merits and drawbacks. The weighted arithmetic PIR_s is a simple way of including uneven heating, but most likely under-estimates its effect, with a PIR_s of 0.5 not really having a discernible impact on the relevant concentrations¹. Using the weighted geometric mean PIR_s does have a more notable effect on the achieved peak intracellular and extracellular concentrations, which suggests that it may be a better metric, however the low levels of achieved peak extracellular concentration achieved for lower values of PIR_t , as seen in Figure 3.5 are also unlikely to be correct considering that the passage of an ultrasound beam over a region of tumour will result in briefly elevated extracellular concentrations, as is seen with temporal PIR. In the case of a model of cellular uptake which is not purely saturable (see Section 3.5.3), failure to resolve this behaviour would result in inaccurate predictions of intracellular concentration.

It is acknowledged that a weakness of all of the above models of non-ideal heating is that they do not account for the possibility of off-target heating; which is occurring in clinical and pre-clinical studies. For example, Partanen et al. [140] found that the targeted centre of treatment was offset by between 0.6 and 4.8 mm in a Rabbit model of treatment with MR-HIFU. A further inaccuracy of this model is that the release models described here fail to incorporate the non-complete release of payload which is characteristic of LTSLs [66]. This is a feature which is incorporated by a model similar to that proposed by Asemani and Haemmerich [122], and is an improvement which could be made to these models in the future, however this does further increase the amount number of parameters and the experimental data required to implement the model.

3.3 Comparison to Clinical Results

Applying $PIR_t = 0.5$, with the heating initially on, the model was used to provide equivalent values to the plasma samples and biopsies that were taken from patients in the TARDOX trial [21]. In the trial, as described in the literature review, tumour biopsies and plasma concentration samples were taken from patients following a 30 minute infusion with LTSL doxorubicin, and after (up to) 60 minutes of hyperthermia, which began after the infusion had ceased. The biopsy concentrations from the computational model were calculated as the weighted sum of the free and liposomal drug in the tumour intracellular and extracellular compartments at 30 minutes and 90 minutes respectively. The model predicted plasma concentrations are taken as the sum of the model predicted liposomal and

¹When PIR_s is stated in the rest of this thesis, it is the weighted arithmetic PIR_s .

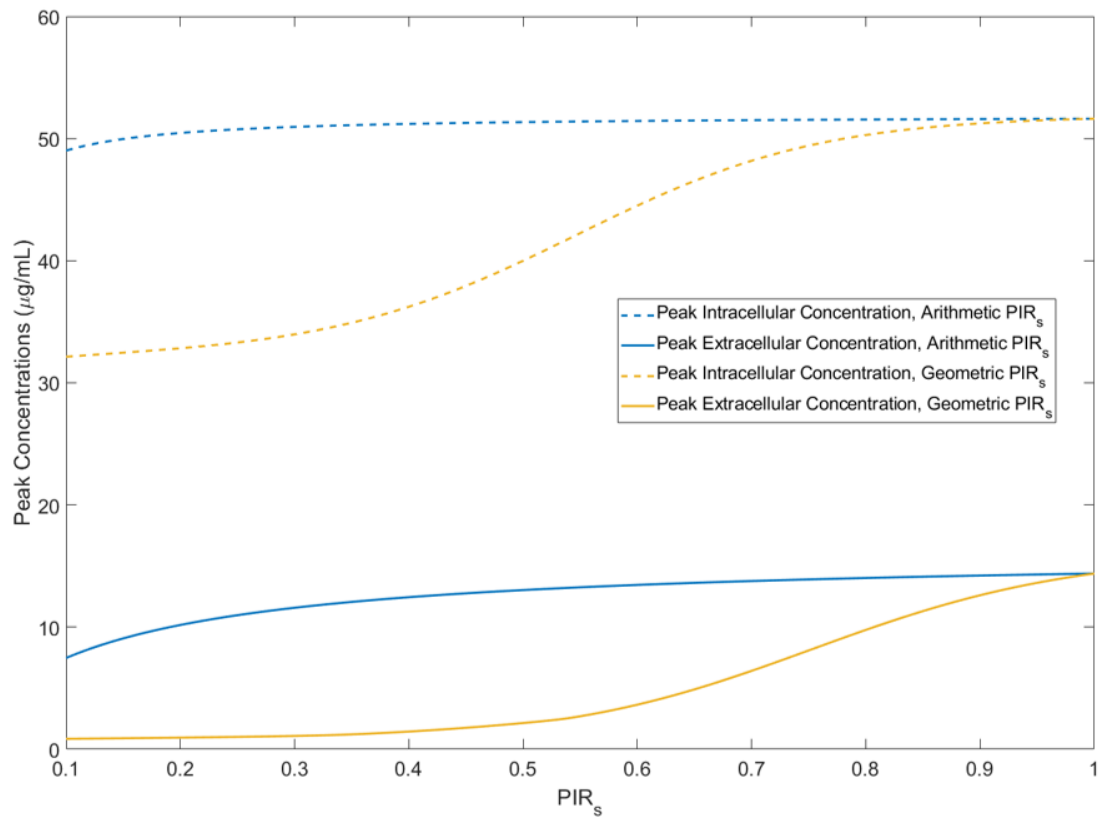


Figure 3.5. Plot showing the predicted peak tumour intracellular and extracellular concentrations as PIR_s is varied between 0.1 and 1 in the idealised TARDOX protocol, using both the weighted arithmetic and weighted geometric approaches. PIR_t is not shown on this plot owing to the more complex definition of PIR_t , i.e. that it requires a time block, and the specification of whether hyperthermia is initially on or off.

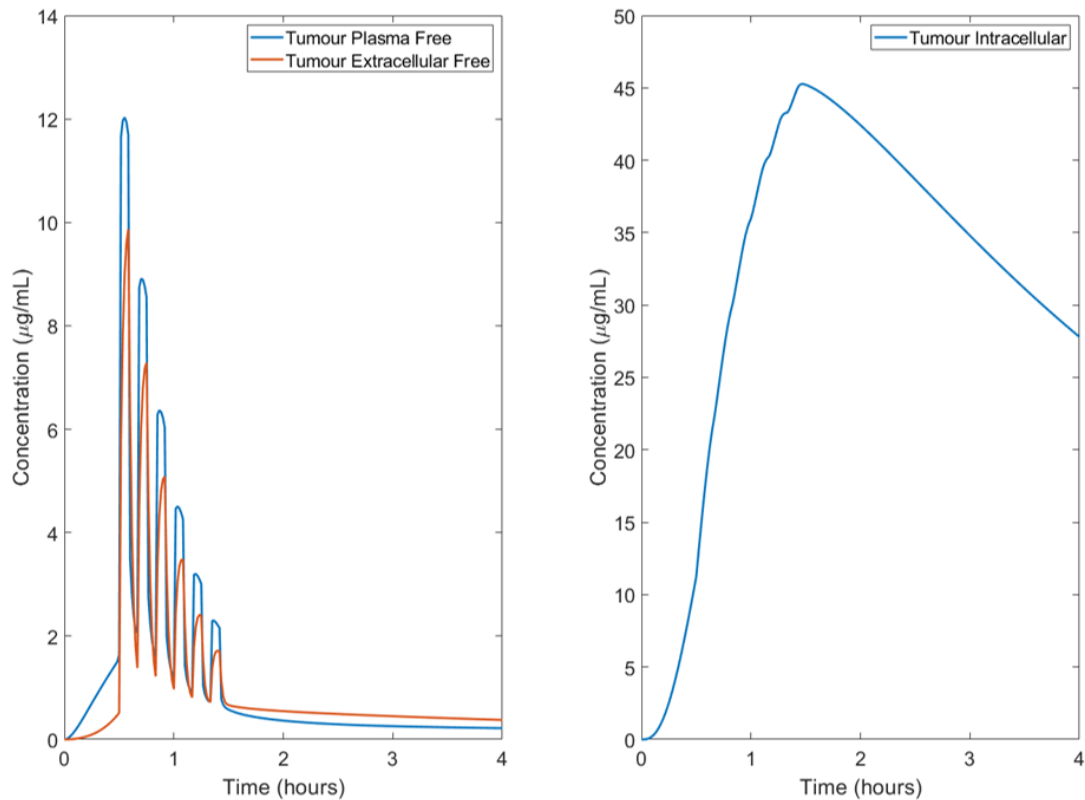


Figure 3.6. Plot showing the tumour concentrations resulting from the compartment model simulation of the TARDOX trial with $PIR_t = 0.5$, using a time block of 5 minutes of hyperthermia with heating initially on.

free drug concentrations in the systemic plasma at the same timepoints. To provide a comparison between the reported clinical trial results in $\mu\text{g/g}$ and the model results in $\mu\text{g/mL}$, a tissue density of 1.05 g/mL was assumed [141]. The results from the model are plotted against the results from the clinical trial in Figure 3.7.

The main observation to be made from this figure is that both biopsy values demonstrate acceptable agreement with the concentrations found in the trial, albeit at the higher end (with the post-infusion biopsy value falling slightly outside the reported range). Considering the post-heating biopsy, it would be expected that the concentrations predicted by this model are at the upper-end of those reported in the TARDOX trial. The main reason for this is that 60 minutes of hyperthermia represents the upper end of the 30-60 minutes aimed for in the TARDOX trial, and lower biopsy concentrations would be expected with less heating. Additionally, as can be seen from Supplementary Table 5 of [21], the biopsies were performed a few minutes after the end of heating (owing to the practicalities of treatment which are evidently not present in the *in silico* model), which is likely to result in a slight decrease in concentrations reported in the clinical case. Furthermore, the lack of spatial heterogeneity in the model provides an additional reason to treat the compartment model as an upper estimate of the

biopsy concentrations; this is a possible reason why the predicted post-infusion biopsy concentration is higher than the clinical data points.

Considering the plasma predictions, it can be observed that the predicted value for the systemic plasma concentration post-infusion and before heating is inside the range found in the clinical trial, albeit at the lower end. Post-heating, the systemic concentration predicted by the model is outside the range from the clinical trial, being lower than the values obtained in TARDOX. Again, this is likely related to the fact that the heating in this model is at the upper-end of that achieved in the TARDOX trial. However, there are two additional factors which should be considered, given that the other model prediction for systemic plasma concentration is low, which is that the parameters used in the model are over estimating elimination of the drug. The author postulates two possible reasons: firstly, that the liver is responsible for much of the clearance of the liposomal form of the drug [8], and that it is known that these patients had diseased livers, which may have reduced the clearance of the drug. Secondly, the impact of general anaesthesia on the pharmacokinetics of chemotherapeutics is not well-characterised [142], but is likely to reduce blood pressure, which in turn might be expected to reduce clearance of the free drug from the kidneys.

The results of this simulation can also be used to provide an indication of the degree of improvement of targeting of delivery compared to that of free doxorubicin by considering the maximum percentage of the initial dose (often written as % I.D.) which is contained within the tumour (taken in this case to be the intracellular and extracellular compartments), and the peripheral tissues. For this simulation of the TARDOX trial, a maximum of 1.17 % I.D. was found to be in the tumour, while the equivalent figure for the systemic tissue was 31.2% I.D.. In contrast, for an equivalent delivery of free doxorubicin (30 minutes infusion), the corresponding values are 0.9524 % I.D. and 55.78 % I.D.. This clearly shows that while targeting is improved, and less drug enters the peripheral tissues in LTSL delivery, in both cases far more of the drug still enters the peripheral tissues than the tumour.

In summary, although inter-patient variation, as shown in Figure 3.7, is clearly very large, the findings demonstrate that a compartment model provides results that display the correct trends (that is, an increase of drug in the tumour after heating). Further, it is established that, even using literature data, the predicted value for the tumour concentration after treatment falls inside the range of values obtained in the clinical trial. This suggests that compartment models can resolve the effects of treating solid tumours with ultrasound-mediated hyperthermia and LTSL doxorubicin. A further discussion of

the challenges involved in using compartment models, in particular with small animal models is made in Section A.3.

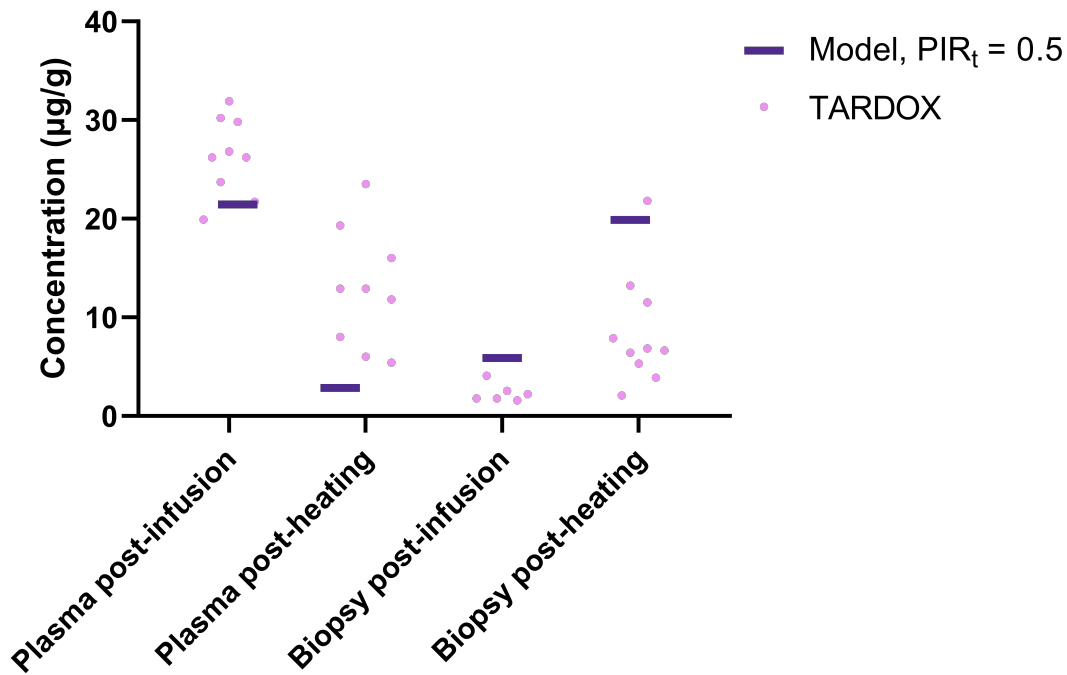


Figure 3.7. Comparison of the patient data points from the TARDOX trial and the predictions made by the compartment model for a 30 minute initial infusion, followed by 60 minutes of hyperthermia with $PIR_t = 0.5$, using a hyperthermia time block of five minutes.

3.3.1 Sensitivity Analysis

To determine which variables had the most effect on the outcome of the mathematical model (with various ‘outcomes’ being assessed, so a singular mathematical outcome is not defined here) of the TARDOX trial, a global sensitivity analysis was performed in MATLAB using the SAFE toolbox [143], with the elementary effects (EE) test, using Latin Hypercube Sampling (so as to ensure a more representative sample of input parameters than could be guaranteed by random sampling) to vary the model parameters within the ranges given in Table 3.2. Where a reasonable range of parameters from the literature is difficult to determine, the parameter was varied between half and double the value used in the model, as this was felt an appropriate level of uncertainty to include. A guide to interpreting the results fully is included in Appendix A, but briefly, an elementary effect, d_i , is defined as:

$$d_i = \frac{\Delta_i(y(x_1, x_2, \dots, x_i + \delta, \dots, x_n) - y(x_1, x_2, \dots, x_i, \dots, x_n))}{\delta} \quad (3.13)$$

where Δ_i is the range over which variable i can vary, and δ is its perturbation from the initial values.

r effects are sampled for each input, so the total number of function evaluations required is $r(p + 1)$, where p is the number of parameters - so there are r vectors of initial values about which each parameter is varied in turn. The mean is then defined as

$$\mu_i = \frac{1}{r} \sum_{j=1}^r |d_i(X^{(j)})| \quad (3.14)$$

where $X^{(j)}$ is the j -th input vector in which the variable of interest, i , is varied. The standard deviation is defined as

$$\sigma_i = \sqrt{\frac{1}{r-1} \sum_{j=1}^r (d_i(X^{(j)}) - \mu_i)^2} \quad (3.15)$$

This term captures interaction, since the r elementary effects are calculated with respect to different initial vectors. A radial design (as opposed to one based on trajectories) is specified, which means that each variable is perturbed in turn from the same starting vector, before a new set of starting vectors is chosen [144, 145].

The computational model was slightly altered to perform the sensitivity analysis such that the model inputs reflect measurements which are more akin to those which would be used by a clinician when deciding on the treatment options. For example, instead of varying the total dose, as is usually done in a computational study, in this case the physical characteristics of the patient are used as variables. New relationships used in the sensitivity analysis are:

- Dose in mg is calculated from the product of the dose in mg/m² and the patient surface area (as this is frequently how dose is calculated in the clinic [146]).
- The patient surface area is calculated from a given weight and BMI. Patient height in metres is the square root of the mass divided by BMI. Patient surface area is then approximated from the Du Bois formula² [147]
- Tumour plasma fraction was varied through a combination of the tumour blood fraction and the tumour haematocrit.
- Tumour intracellular fraction was then calculated from the relationship $1 - v_e^T - v_B^T$, where v_B^T is the tumour blood volume.

²[Area (m²)] = 0.007184([Mass (kg)]^{0.425} [Height (cm)]^{0.725})

- Systemic plasma volume was calculated by varying body mass (M), blood/body mass (β), and haematocrit (H), through $V_p^S = M\beta(1 - H)$

The results of the global sensitivity analysis considering the peak intracellular concentration in units of $\mu\text{g/mL}$ achieved are displayed in Figure 3.8. In all Figures presenting sensitivity analysis results, the legend lists from top to bottom, left to right, the variable with the greatest mean EE. It is clear that the parameter which gives rise to the most uncertainty in output is the cellular volume, followed by the cellular uptake parameters. In Figures 3.9, 3.10 and 3.11, the effects of varying the cell volume, V_{max} , and $k_{e, lip}$ independently over the ranges given in Table 3.2 are plotted. Considering first Figure 3.9, the cell volume varying by a factor of almost four has a large influence on the conversion of concentration in $\text{ng}/10^5$ cells to $\mu\text{g/mL}$; this represents a challenge makes any sort of validation of this model extremely challenging; any work aiming to validate intracellular concentration determination *in vivo* should consider using as a model parameter the density of cells within the tumour tissue and approximating this directly from samples taken from a biopsy. Further implications of these findings for validation in small animal models are included in Appendix A, alongside further sensitivity analyses.

Considering Figure 3.10, the variation in model output as V_{max} is perturbed from the value used in the comparison to the TARDOX trial, also gives rise to variation by a factor of two, which suggests that the cellular uptake parameters are the parameters in the model which give rise to the biggest uncertainty in the magnitude of the outputted peak intracellular concentration. Finally, the parameter with the largest mean elementary effect which is unrelated to cellular uptake is the clearance of the liposome, which gives rise to a variation in the output on the order of 10% as plotted in Figure 3.11, which is much less than the variation associated with the cellular uptake parameters. This suggests that refined estimates of the cellular uptake parameters are needed to give more confidence in the outputs of the computational model, but that the other parameters are known to an acceptable degree of accuracy for optimising treatments with confidence.

3.4 Optimisation of Treatment

As described in the introduction, clinicians treating patients with LTSL doxorubicin must choose the dose, infusion duration, and hyperthermia duration. In this section, the optimal infusion durations are obtained for the cases of concurrent infusion and hyperthermia, and for a fixed hyperthermia duration. The robustness of these optimisations is then considered. The effect of not beginning heating immediately (as in the TARDOX trial) is also quantified, before the effect of varying the delivered dose

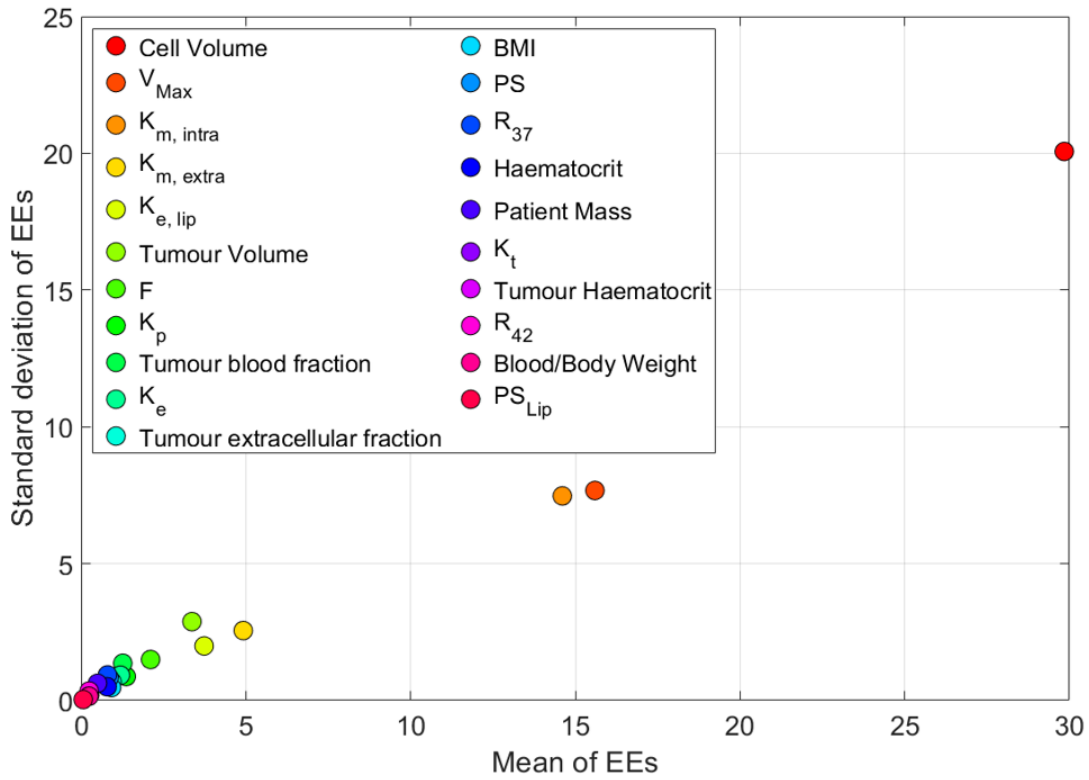


Figure 3.8. Results of an elementary effects test performed on the peak intracellular concentration in units of $\mu\text{g}/\text{mL}$ resulting from the idealised version of the TARDOX protocol used in this chapter, with $\text{PIR} = 1$. The number of effects sampled for each input, r , was 50.

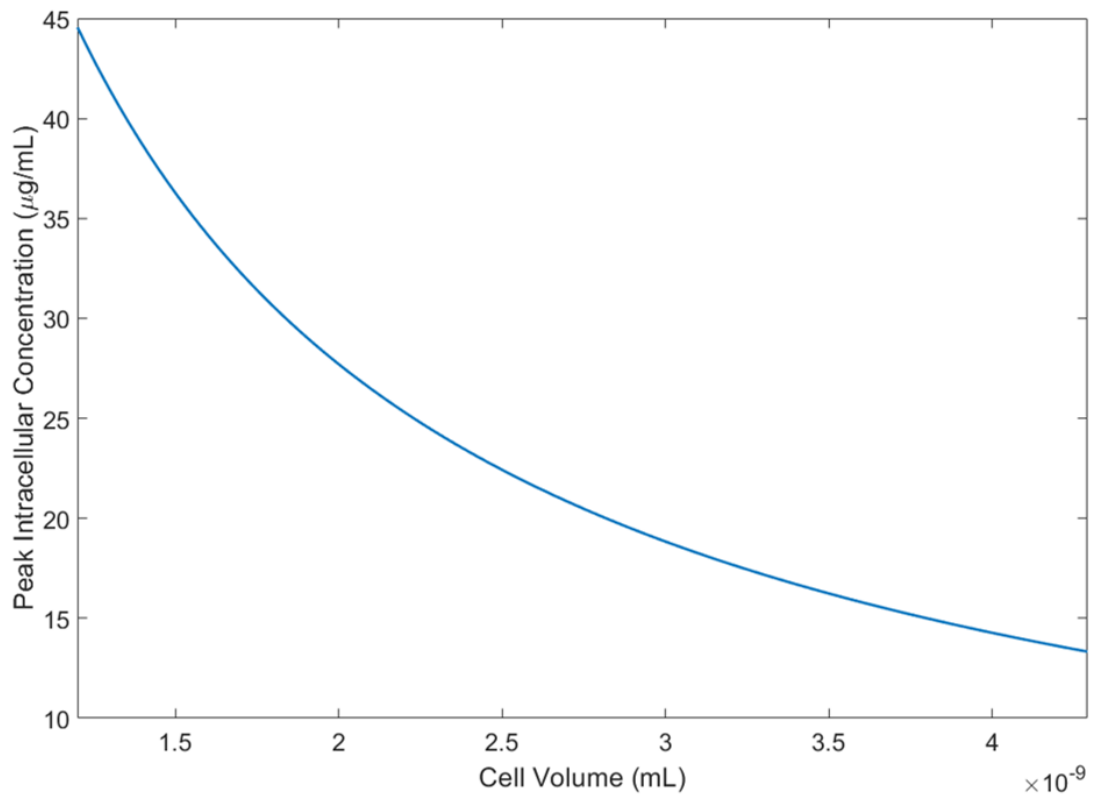


Figure 3.9. Plot showing how the peak intracellular concentration in $\mu\text{g}/\text{mL}$ changes as the cell volume is varied across the range specified in Table 3.2.

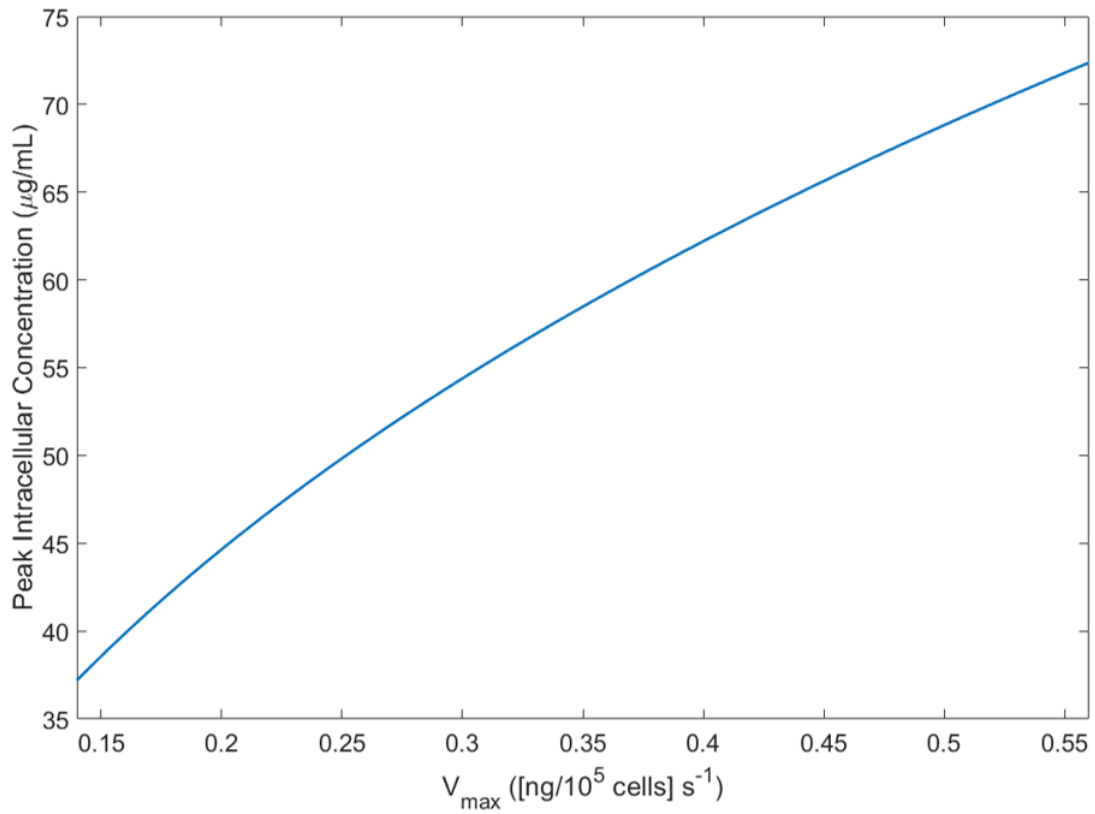


Figure 3.10. Plot showing how the peak intracellular concentration in $\mu\text{g/mL}$ changes as V_{max} is varied across the range specified in Table 3.2.

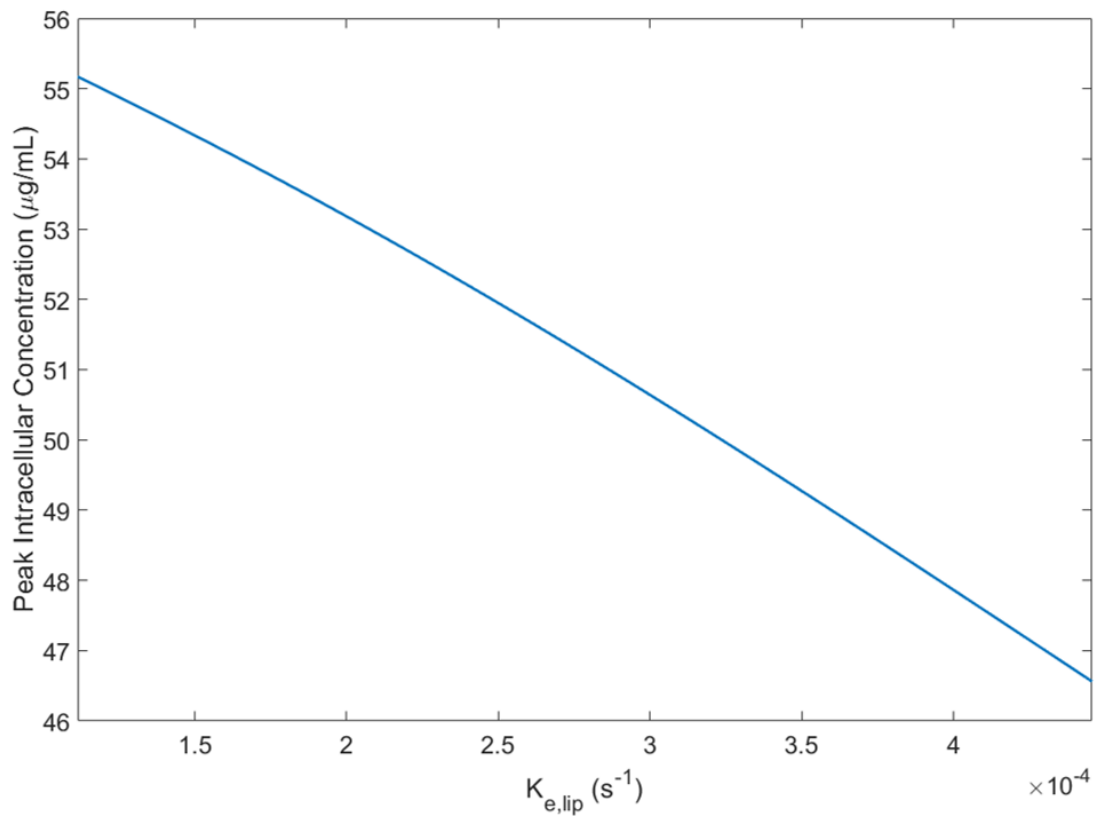


Figure 3.11. Plot showing how the peak intracellular concentration in $\mu\text{g/mL}$ changes as $k_{e,lip}$ is varied across the range specified in Table 3.2.

Parameter	Range	Reasoning
Patient Mass (kg)	61.3 - 98.21	Average weight for men in the UK is 85.4 kg, and for women is 72.1 kg. These bounds are these values $\pm 15\%$.
Tumour Volume (mL)	10 - 100	Those treated in TARDOX had treatment volumes from 10.5 - 90.9 mL (although some tumours were larger than this). From [21] supplementary materials
BMI (kg/m ²)	18 - 30	A BMI range from just underweight (18.5), to the top end of overweight (30). There is perhaps an argument for increasing this range into the obese range (30-39)
Tumour blood fraction	0.054 - 0.153	Range reported in [148]
v_e^T	0.33 - 0.6	Range of values reported for different rat tumour models [137]
PS (ms ⁻¹)	$(2.55 - 10.2) \times 10^{-3}$	Standard approach to default value (see Table 3.1)
PS_{lip} (ms ⁻¹)	$(2.57 - 10.3) \times 10^{-5}$	Standard approach to default value (see Table 3.1)
F (s ⁻¹)	0.112 - 0.4473	50 - 200 mL/min/100 g is a reasonable perfusion for primary colorectal malignancies in humans [149]. Assuming a tissue density around 1 kg/L, this gives a perfusion rate (w_{blood}) of 0.0083 - 0.033 s ⁻¹ . This is converted to F as $F = w_{blood}/v_p^T \cdot v_p^T$ is taken as the value in Table 3.1 (0.07452).
R_{37} (s ⁻¹)	$(1-3) \times 10^{-4}$	The lowest found literature value was around 1×10^{-4} using Figure 5a of [72], which suggests around 6% release in 10 minutes. The value of 3×10^{-4} is used in [25]
Blood/Body Weight (mL/kg)	65 - 70	Range from literature [150]

Parameter	Range	Reasoning
R_{42} (s^{-1})	0.8 - 3.2	A value of $1.6 s^{-1}$ was obtained by examining Figure 5b of [72], based on the 80% release of doxorubicin in 1 second. A standard approach was then applied. Previous modelling studies have used values outside of the ranges for R_{37} and R_{42} , such as [25], which took $0.114 s^{-1}$ as R_{42} , although this is not based on a ThermoDox-style liposome.
k_e , (s^{-1})	$(0.55 - 2.2) \times 10^{-3}$	Standard approach, as data in Table 3.1 was not obtained under anaesthesia, and with co-administration of paclitaxel.
$k_{e,lip}$ (s^{-1})	$(1.114 - 4.456) \times 10^{-4}$	Standard approach, as data in Table 3.1 was not obtained under anaesthesia.
k_p (s^{-1})	$(0.8 - 3.2) \times 10^{-3}$	Standard approach, as data in Table 3.1 was not obtained under anaesthesia, and with co-administration of paclitaxel.
k_t (s^{-1})	$(2.34 - 9.36) \times 10^{-5}$	As above
Tumour Haematocrit	0.08 - 0.27	Reported interquartile range in [133]
Haematocrit	0.36 - 0.5	[151]
Cell Volume (mL)	$(1.2 - 4.29) \times 10^{-9}$	BNID 103725 [141]
V_{max} ($[ng/10^5 \text{ cells}] s^{-1}$)	0.14 - 0.56	Standard approach applied to value from [67].
$K_{m,intra}$ ($ng/10^5 \text{ cells}$)	0.685 - 2.74	Standard approach applied to value from [67].
$K_{m,extra}$ ($\mu g/mL$)	0.1095 - 0.438	Standard approach applied to value from [67].

Table 3.2. Parameter ranges used in Sensitivity Analysis. ‘Standard approach’ refers to halving and doubling the literature value to obtain the range.

is explored. In all cases, $PIR_s = 0.5$, and the maximised metric is the peak intracellular concentration achieved.

3.4.1 Optimisation of Infusion Duration with Concurrent Hyperthermia

To perform this optimisation, the infusion and hyperthermia durations were varied between 1 and 340 minutes with a temporal resolution of one minute. The resulting peak intracellular concentration is plotted as a function of the infusion/hyperthermia duration in Figure 3.12. Also plotted on the same figure are the resulting peak intracellular concentrations from an infusion of the same dose of unencapsulated doxorubicin.

The optimum infusion time was found to be 269 minutes, although there is not much difference in predicted peak intracellular concentration between 250 and 300 minutes. This yielded an intracellular concentration of $78.5 \mu\text{g/mL}$, although clinically such an infusion and hyperthermia duration would be a very demanding procedure owing to the general anaesthesia and high frequency jet ventilation requirements for ultrasound-mediated hyperthermia of deep-seated tumours. Taking three hours as a challenging but perhaps achievable upper limit for infusion duration, the predicted peak intracellular concentration is $74.7 \mu\text{g/mL}$, which represents a 1.58-fold increase in predicted peak intracellular concentration compared to an optimal free doxorubicin infusion (which is 117 minutes in duration). It can also be seen from the plot that a concurrent infusion and hyperthermia in excess of 47 minutes (discounting durations greater than 340 minutes, where the concentration achieved from LTSL delivery is decreasing as infusion duration increases) results in improved drug delivery to the intracellular compartment compared to an optimal free doxorubicin infusion, which achieves a peak intracellular concentration of $47.3 \mu\text{g/mL}$.

3.4.2 Optimisation of Infusion Duration for Fixed Hyperthermia Duration

Given that it is acknowledged that the prolonged hyperthermia determined as optimum in the previous section is clinically challenging to attain, an alternative question can be posed: what is the optimal infusion duration for a set hyperthermia duration? If this duration is taken to be 90 minutes, which is felt to be clinically achievable considering the anaesthesia duration in the TARDOX [21]. The predicted peak intracellular concentrations are plotted as a function of infusion duration (alongside the equivalent values for an infusion of free doxorubicin) in Figure 3.13. In this case, as long as the infusion of LTSL is less than 154 minutes, LTSL doxorubicin provides a greater intracellular concentration, and the optimal delivery of LTSL doxorubicin results in predicted intracellular concentrations of 57.8

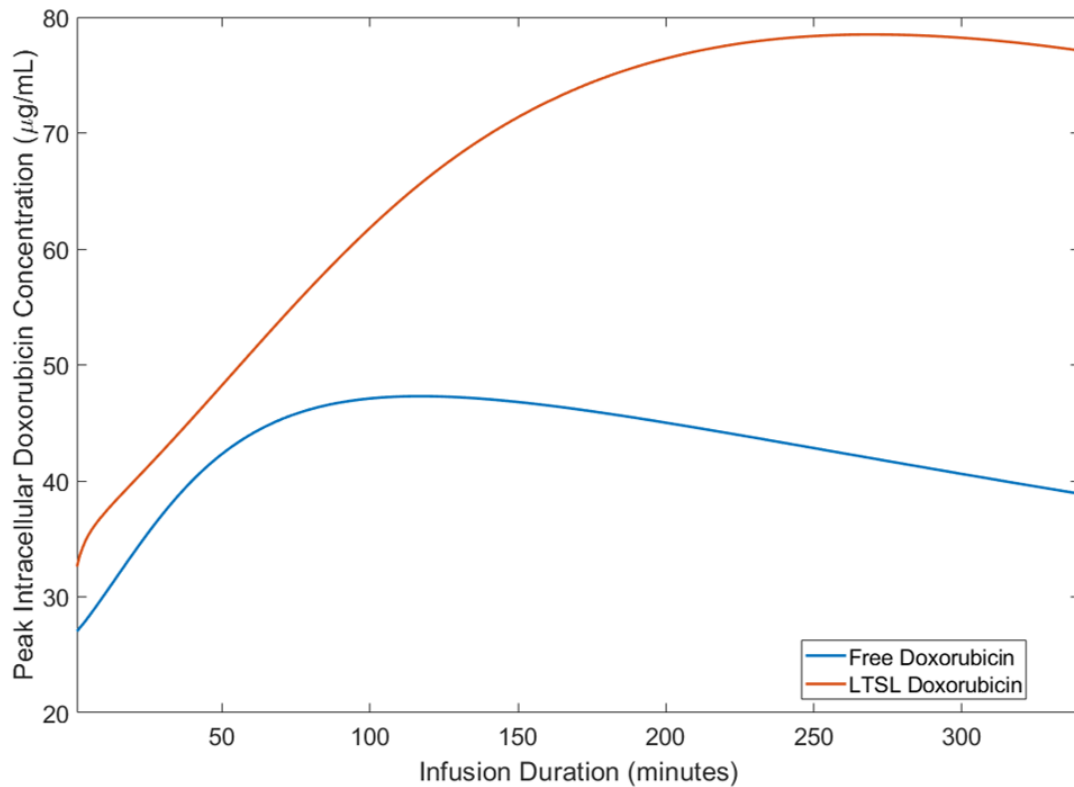


Figure 3.12. A plot of the maximum predicted intracellular concentration using LTSL and free doxorubicin with concurrent infusion and hyperthermia, as a function of the infusion duration. $PIR_s = 0.5$ for LTSL drug delivery.

$\mu\text{g/mL}$, which represents an increase by a factor of 1.2 on the optimal delivery of free doxorubicin.

3.4.3 Global Sensitivity Analysis of the Optimal Infusion Duration

In order to assess the sensitivity of the obtained optimum infusion durations to variation in the parameters, a further global sensitivity analysis was performed on the obtained optimum infusion time, using the same approach as in Section 3.3.1. In these sensitivity analyses, PIR_s was also varied between 0.25 and 0.75, as this was felt to be a reasonable range in light of the results reported in [87]. The results from the sensitivity analysis for a fixed hyperthermia duration of 90 minutes are presented in Figure 3.14.

From this, it can be seen that the release rate at 37°C has the greatest mean elementary effect, and can therefore be considered as the variable which has the most effect on the optimum infusion duration. Fluctuations in the cellular uptake parameters have less impact on the optimal infusion duration than they do when the peak intracellular concentration is considered as an output in its own right. The results of varying both $K_{m,extra}$ and R_{37} on the optimal infusion duration are shown in Figure 3.15a and 3.15b respectively. It can be seen that lower values of $K_{m,extra}$ lengthen the optimal infusion time. This happens because as $K_{m,extra}$ decreases, influx into the cell tends towards zero-

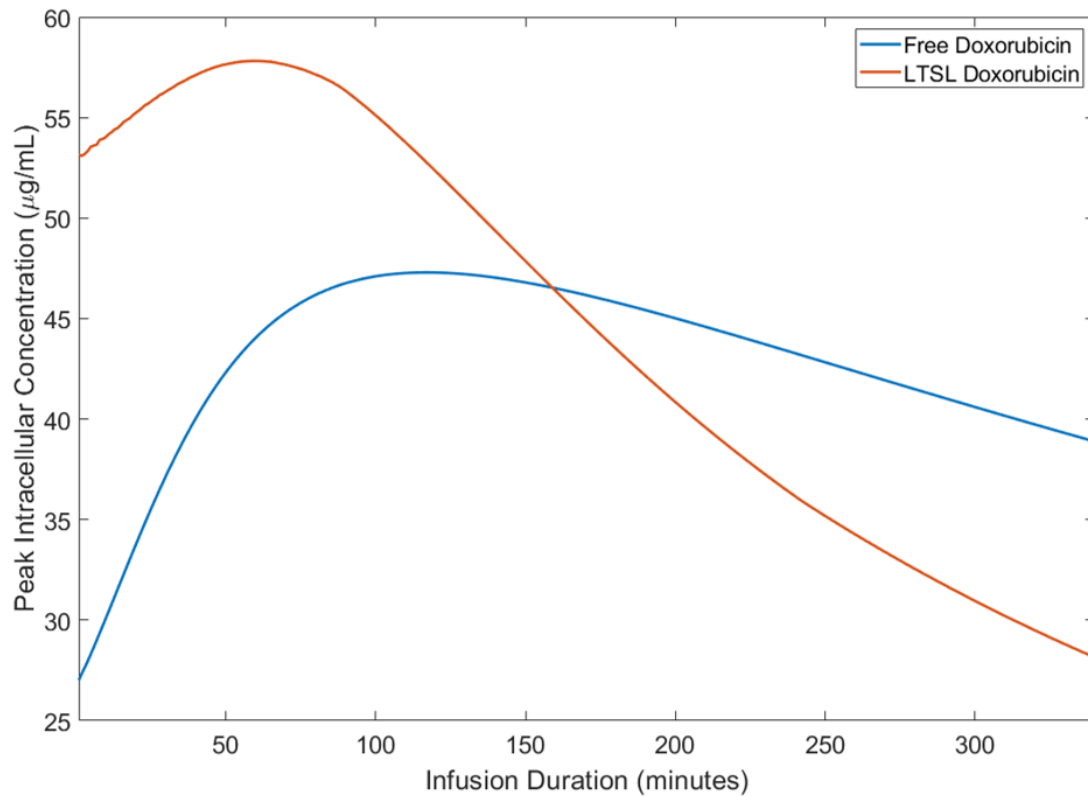


Figure 3.13. Plot showing the peak intracellular concentrations achieved with 90 minutes of hyperthermia from $t = 0$ minutes and $PIR_s = 0.5$, as well as the peak intracellular concentrations achieved with an infusion of free doxorubicin.

order kinetics (given the form of cellular uptake equation); so prolonging the exposure to extracellular doxorubicin, even at lower levels, becomes beneficial, acting to increase the achieved intracellular concentrations. Outside of these parameters however, the variation in predicted optimal infusion time is on the order of ± 10 minutes; which is certainly robust enough to continue to use computational models to optimise treatments.

Examining Figure 3.15b, larger values of R_{37} also increase the predicted optimum infusion duration, as increases in the leakage rate from the liposome necessitate a longer infusion to maintain levels of liposomal drug in the tumour (where release is locally triggered). The variation in this case is within 15 minutes of the optimal infusion time calculated using the parameters in the middle of the parameter range. The variability exhibited when $K_{m,extra}$ is varied over the selected range is seemingly large, but it should be noted that the behaviour displayed for smaller values of $K_{m,extra}$ in this range is unlikely to match the physical reality, and would be countered by the behaviour exhibited in the alternative models discussed in the next section. If it could be known with certainty that $K_{m,extra}$ was above $0.2 \mu\text{g/mL}$, then the variation in the optimal infusion time due to this parameter over this range is fairly minimal, and the optimisation could be said to have a good degree of robustness overall.

Interestingly, the optimal infusion times are always longer than those used in the TARDOX trial, and those in the proposed, but now cancelled PANDOX trial, which proposed a 30 minute infusion, and 90 minutes of hyperthermia beginning with the infusion [152]. Details of how intracellular concentrations are affected by using non-optimal infusion durations as a result of parameter variations are presented in Appendix A.

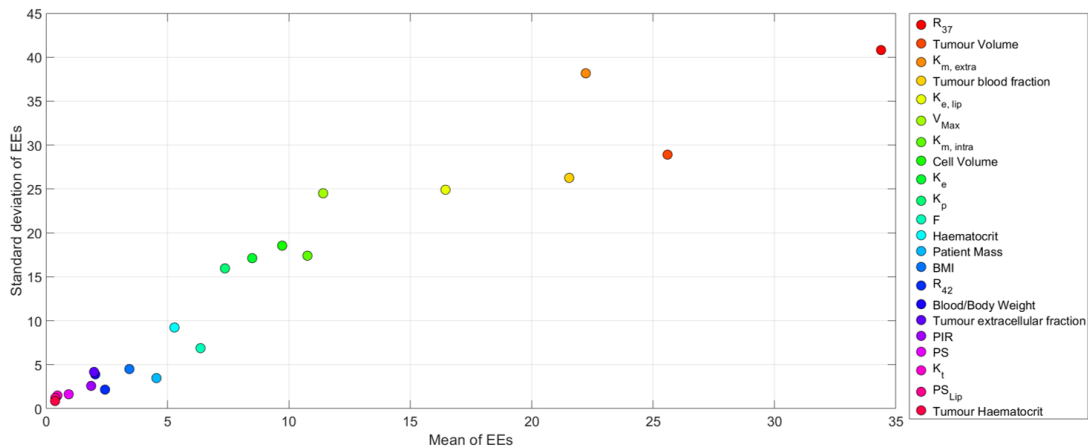


Figure 3.14. Results from the elementary effects test with the output of the optimal infusion duration (in minutes), for the case of 90 minutes of hyperthermia beginning at $t = 0$ minutes, with the optimal infusion time being selected as that which results in the largest value of peak intracellular concentration ($r = 10$).

3.5 Variations in Model Input

In this section, the effects of varying the timing of the hyperthermia (with respect to the infusion), the total dose administered to the patient, and the cellular uptake model used are considered.

3.5.1 When to Heat - During or After Infusion?

One question which should be asked is whether beginning hyperthermia with the infusion, as opposed to infusing first then treating, as in the TARDOX trial, brings with it substantial benefit in terms of the peak intracellular concentration. The tumour intracellular and extracellular concentrations for a protocol with an hour of heating beginning with a 30 minute infusion and the TARDOX protocol, in which the heating begins after the infusion are plotted in Figure 3.16. The figure also shows the idealised PANDOX protocol of a 30 minute infusion and 90 minutes of heating for comparison.

For a single hour of heating, a similar peak intracellular concentration is achieved whether the heating begins with the infusion or after infusion. This is because the concentration profile of liposomal doxorubicin in the tumour plasma (not shown) is not dissimilar between these two protocols, although

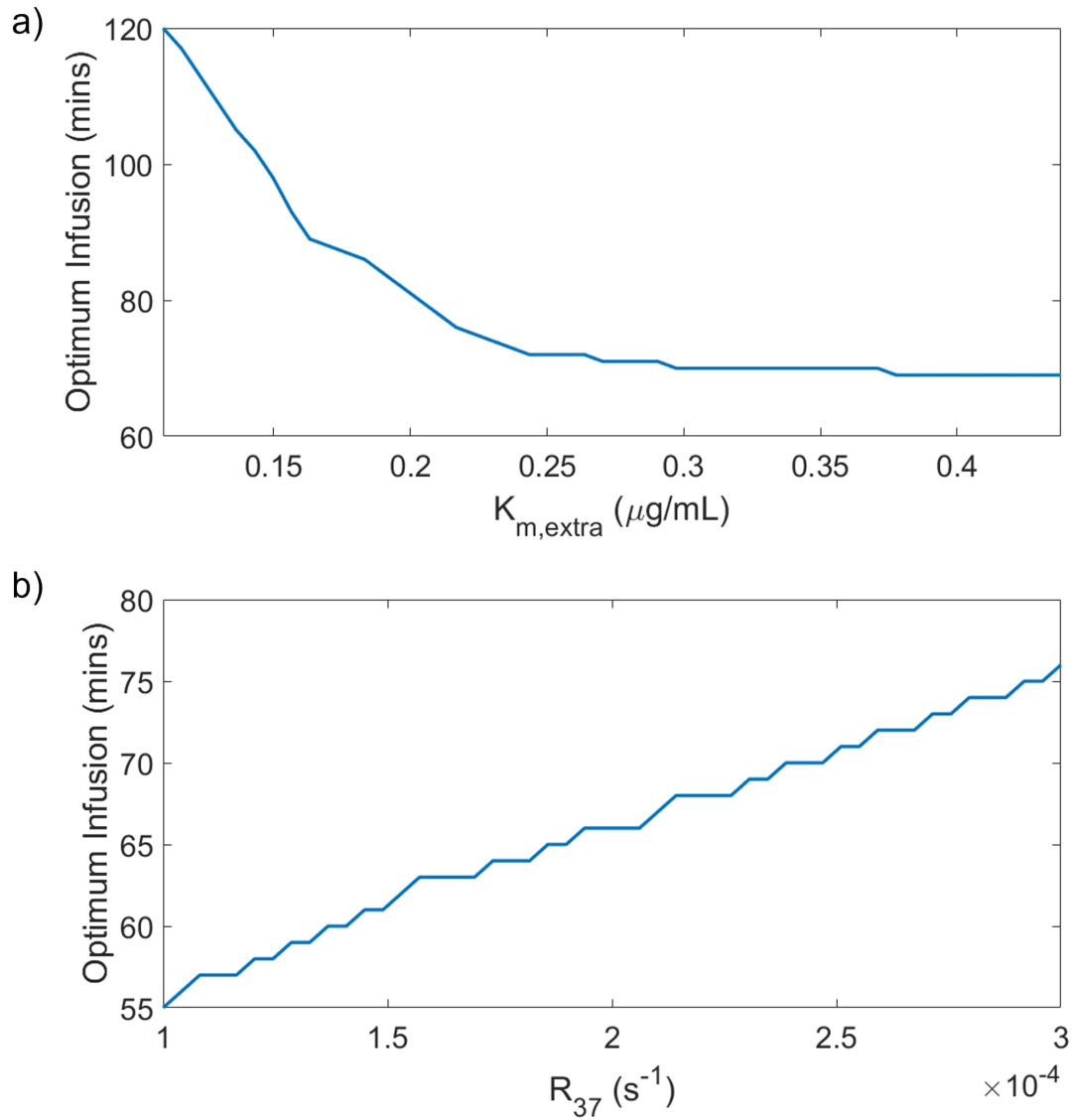


Figure 3.15. Plots showing how the optimal infusion duration based on peak intracellular concentration varies for 90 minutes of hyperthermia varies over the range of input values for a) $K_{m,extra}$ and b) R_{37} . The plots are not smooth owing to the discrete nature of both the parameter variation and the infusion times tested. 50 values of the parameter were sampled with a linear spacing in the stated range, while infusion time was sampled with a timestep of 1 minute from 1 minute to 360 minutes.

the concentrations achieved with heating beginning concurrently with infusion are slightly higher. In practice, the delay between beginning to heat the treatment volume and hyperthermia being achieved means that future clinical treatments should aim to begin hyperthermia with the infusion (so in practice, the method of heating should begin before the infusion to ensure the target region is at a therapeutic temperature from the beginning of the infusion). In the TARDOX trial, it was reported (in the subset of patients in which the temperature was actively measured with a thermocouple) that the target region reached therapeutic temperatures in around 5 minutes from the beginning of ultrasound heating [87, see Figure 3b].

The concentration profiles presented in the PANDOX case demonstrate that the additional 30 minutes of hyperthermia provide a substantial improvement over the TARDOX protocol. While there will be a duration of hyperthermia beyond which additional heating does not provide additional delivery (an idea explored further in Chapter Five), it is clear that there should be a focus on ensuring that hyperthermia can begin with the infusion and last as long as possible to ensure maximal patient benefit. Further emphasising the point that hyperthermia should begin concurrently with infusion, is the result that if the 90 minutes of hyperthermia in the PANDOX protocol is delayed to start at the end of the infusion, the peak intracellular concentration achieved falls by $7 \mu\text{g}/\text{mL}$ from $60.4 \mu\text{g}/\text{mL}$ (as in Figure 3.16) to $53.4 \mu\text{g}/\text{mL}$ (results not shown).

3.5.2 Altering the Total Administered Dose

Another question of clinical interest is the effect of varying the dose on the treatment outcome. Again, using peak intracellular concentration as a measure of efficacy, the model was used (applying the idealised TARDOX protocol) to simulate a range of applied doses, up to $60 \text{ mg}/\text{m}^2$, and the results are shown in Figure 3.17 ($\text{PIR}_s = 0.5$). Unsurprisingly (given the chosen cellular uptake model), there is a saturation in cellular uptake, with diminishing returns seen as the dose is escalated. This has potential implications for patients with previous doxorubicin exposure, or who are otherwise less suitable for the standard dose of chemotherapy, since it can be seen from these results that if the dose of doxorubicin given to patients is reduced by 20% from the dose administered in the TARDOX trial, the reduction in predicted peak intracellular dose is only 6.6% lower - a reduction from $48.8 \mu\text{g}/\text{mL}$ to $45.6 \mu\text{g}/\text{mL}$.

The choice of cellular uptake model however, as discussed below, means that care must be taken not to over-interpret these results, since cellular uptake models which are not purely saturable will

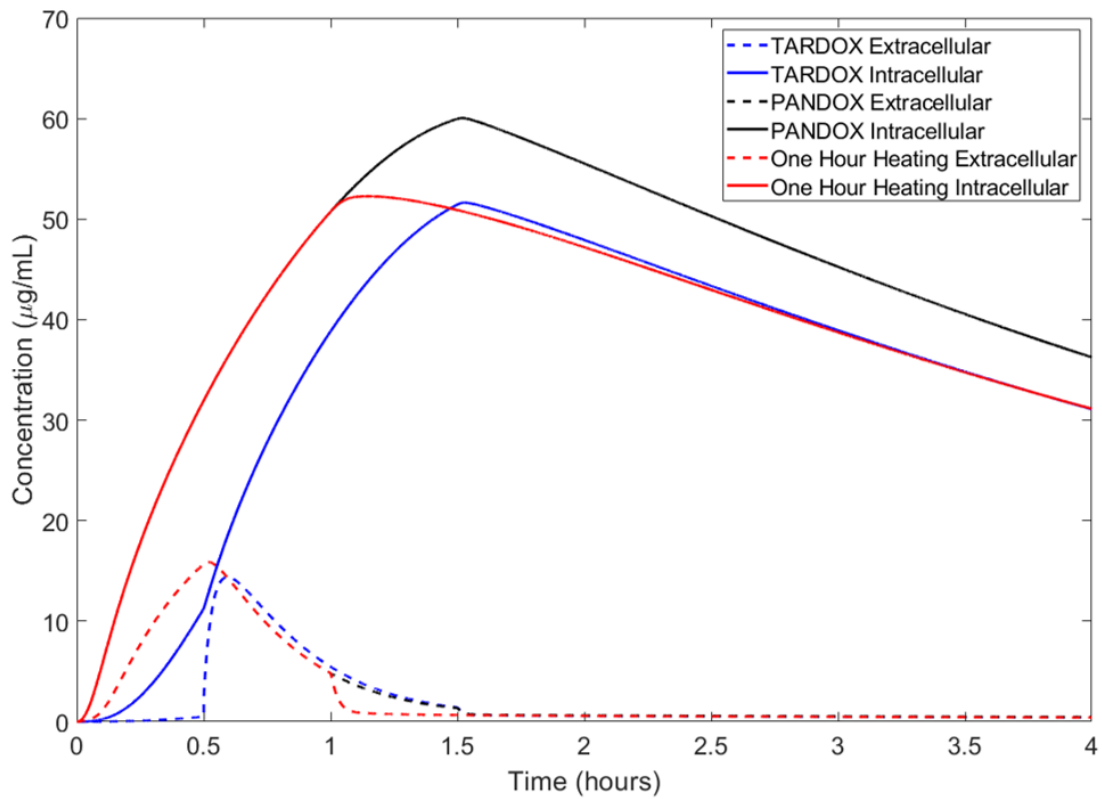


Figure 3.16. Plot showing the resulting tumour intracellular (solid lines) and extracellular (dashed lines) of free doxorubicin in the tumour for the idealised TARDOX protocol (30 minute infusion, followed by 60 minutes of heating), PANDOX protocol (30 minute infusion with 90 minutes of heating starting at $t = 0$ minutes), and a protocol which used a 30 minute infusion and 60 minutes of heating also starting at $t = 0$ minutes as blue, black, and red lines respectively. $PIR_s = 0.5$.

provide a different relationship. This notwithstanding, the finding that elevated extracellular concentrations do not necessarily translate to improved intracellular delivery (and thus greater treatment efficacy) supports the recent work which has been done in developing LTSLs containing drugs which display more rapid cellular uptake characteristics, as in [85].

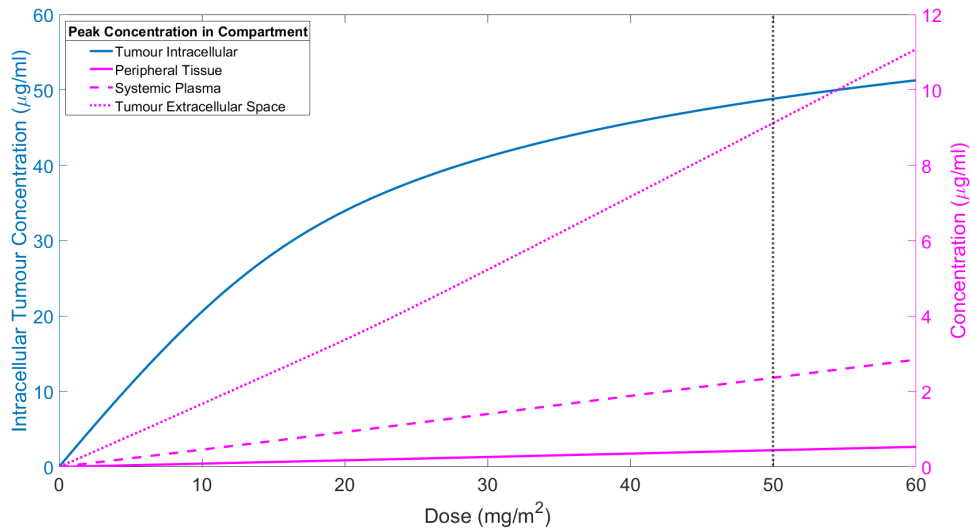


Figure 3.17. A plot of the maximum values of relevant concentrations as total patient dose is varied, using a saturable model of cellular uptake. The vertical black dashed line represents the dose given in the TARDOX trial. ($PIR_s = 0.5$)

3.5.3 Exploring Alternative Cellular Uptake Models

The cellular uptake model described was chosen as it was shown to give results which were a reasonable match to the clinical reality in [67], and had fewer parameters than other models. Over the course of this research, it has become apparent that such a form of cellular uptake model is not accurate; there is no reason for the maximum rates of transport of drug into and out of the cell to be the same, and there should certainly be an element of passive diffusion (which would be represented mathematically with a linear influx/efflux term), which one would perhaps expect to be non-negligible at concentrations which are well above the Michaelis constants.

Other models of cellular uptake are used in the literature, with the following model being used by (amongst others) Gasselhuber [65]:

$$\frac{dc_i}{dt} = k_{in}c_e + \frac{V_{max}c_e}{c_e + K_m} - k_{out}c_i \quad (3.16)$$

where $k_{in,out}$ represent linear influx and efflux terms, and there is a saturable cellular influx term as

Parameter	Value
k_{in} (s^{-1})	6.333×10^{-4}
V_{max} ($[\mu\text{g}/\text{mL}] s^{-1}$)	0.01268
K_m ($\mu\text{g}/\text{mL}$)	0.5285
k_{out} (s^{-1})	2.8056×10^{-4}

Table 3.3. Parameters used in alternative uptake model

before, but no saturable efflux. The model was altered to allow this form of cellular uptake model and run using the same parameters (but with $PIR = 1$) as [65], which are still based on the same cellular uptake data from non-small cell lung cancer cells [102]. These cellular uptake parameters are given in Table 3.3. These parameters actually improves the fit to the clinical data, reducing the predicted biopsy concentration after infusion to $4.35 \mu\text{g}/\text{g}$ (from $5.87 \mu\text{g}/\text{g}$ with the purely saturable model). The predicted biopsy concentration following hyperthermia is also reduced to $14.45 \mu\text{g}/\text{g}$ (from $19.87 \mu\text{g}/\text{g}$ with the purely saturable model), which is closer to being representative of the biopsies obtained in the TARDOX trial (which are shown in Figure 3.7).

At concentrations which are relevant to LTSL doxorubicin delivery, saturable uptake still dominates this model; for example, at a concentration of $5 \mu\text{g}/\text{mL}$, the saturable term represents 78% of the cellular uptake. As a result, when the dose is varied with this model, the peak intracellular concentration still exhibits diminishing returns as the administered dose increases (Figure 3.18), although to a slightly lesser extent than the fully saturable uptake model. However, models of different cancer cell lines have different characteristics predicted [e.g. 95], and it is reasonable to expect completely different characteristic behaviour from cell lines with reduced ratios of linear/saturable uptake at therapeutic concentrations.

In summary, the choice of cellular uptake model can have a non-negligible effect on the outcome of compartment models. Notably, the data set of Kerr et al. [102] (on which most of these models are based) use a maximum extracellular concentration of $7.5 \mu\text{g}/\text{mL}$, which is exceeded in simulations of LTSL delivery of doxorubicin, so the model is being extrapolated beyond its intended range. Furthermore, there has also not yet been a study which has attempted to quantify the impact of there being different cellular uptake parameters in hyperthermic conditions in a compartment model of doxorubicin delivery from LTSLs. This suggests a need for further experimentation to obtain a model of appropriate complexity on a clinically relevant cell line - which forms the basis of the next chapter of this thesis.

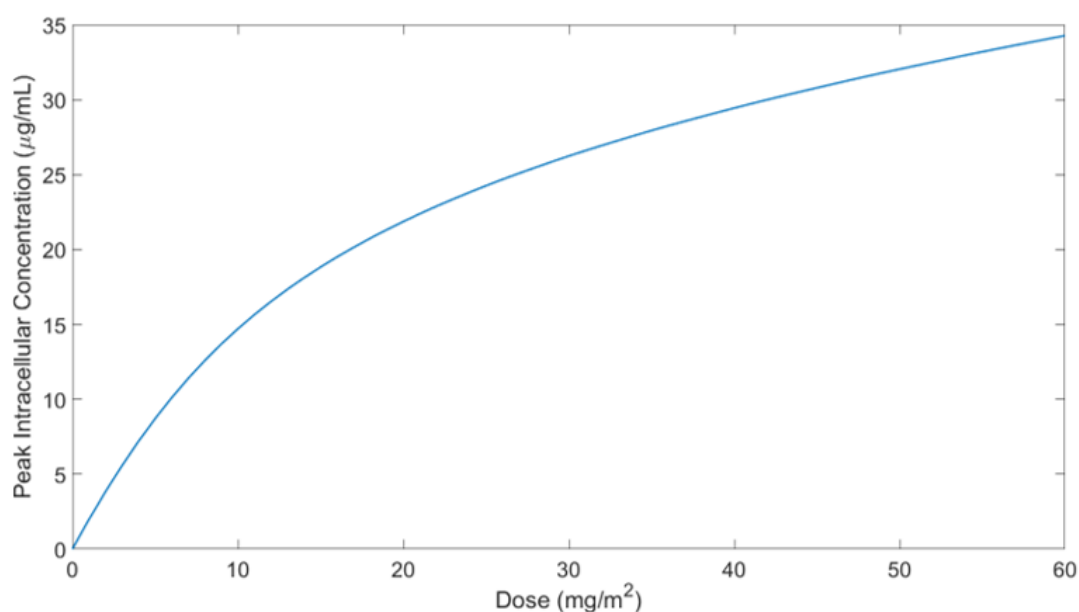


Figure 3.18. Plot showing how peak intracellular concentration still has a saturable relationship with dose across the therapeutic range, even with the inclusion of a linear uptake term, $PIR_s = 0.5$.

3.6 Summary

In this chapter, existing literature data are used to demonstrate that compartment models of delivery of doxorubicin from thermosensitive liposomes can provide a predicted value for tumour drug concentration after hyperthermia which falls inside the range of values obtained in a clinical trial. While good agreement has been shown with *in vivo* tests previously [85, 120], to the best of the author's knowledge, this is the first time that such a model has been compared to results from a clinical trial.

A potential improvement to the way the compartment model resolves the effect of partial hyperthermia was discussed. It is given that ultrasound-mediated hyperthermia will give rise to fluctuating extracellular concentrations, which are captured by incorporating the PIR in a temporal sense. Considering this finding within the broader context of research currently ongoing in LTSL drug delivery, the use of PIR_t may be an important inclusion in future models of idarubicin TSLs, as idarubicin is more rapidly taken up by cells than doxorubicin [41]. This means that the resulting intracellular concentrations (and therefore, therapeutic effect) may be more influenced by these fluctuations. This is explored further in Chapter Five.

Two global sensitivity analyses were presented; the first on the predicted peak intracellular concentrations, which found that the model output was highly dependent on parameters associated with the cellular uptake of drug. The second sensitivity analysis (on the optimal infusion duration) found that despite the uncertainty in the magnitude of the intracellular concentration highlighted by the first

sensitivity analysis, the optimal infusion duration was surprisingly robust to changes in parameter values.

Given the variation in the predicted magnitude of the output, and the fact that the cellular uptake model is based on data (at 37°C only) which does not include the higher concentrations seen during LTSL drug delivery, the aim of the next chapter is to determine parameters for cellular uptake which are more appropriate for this sort of modelling.

Chapter 4

Characterising the Link Between Cytotoxicity and Intracellular Doxorubicin Concentration

4.1 Introduction

As explained in the previous chapter, the use of computational models to predict intracellular concentration (which is used as a metric of likely therapeutic efficacy), is highly dependent on the cellular uptake model. This chapter describes the experimental work undertaken in this thesis, which broadly aims to provide a mathematical model which is better-suited to the optimisation of TSL delivery of doxorubicin. A further aim is to quantify the impact of mild hyperthermia on the action of doxorubicin in terms of both cytotoxicity and cellular uptake.

Firstly, it is established whether intracellular concentration remains an acceptable proxy for cell kill in CT26 cells, making use of both a clonogenic assay, and a novel assay for the determination of intracellular concentration of drug. The intracellular concentrations are then used to fit a mathematical model of cellular uptake of doxorubicin at both normothermic (37°C) and mildly hyperthermic (42°C) conditions. The set of experiments are represented together schematically in Figure 4.1.

CT26 Murine Colorectal Carcinoma (CT26.WT CRL-2638, American Tissue Culture Collection) cells were selected for use in this work for two reasons: firstly, its use in pre-clinical *in vivo* studies involving LTSL doxorubicin [e.g. 153]; and secondly its prior use in BUBBL facilitated access to cell line-specific expertise. The work in this thesis is performed using monolayer cell culture, as opposed

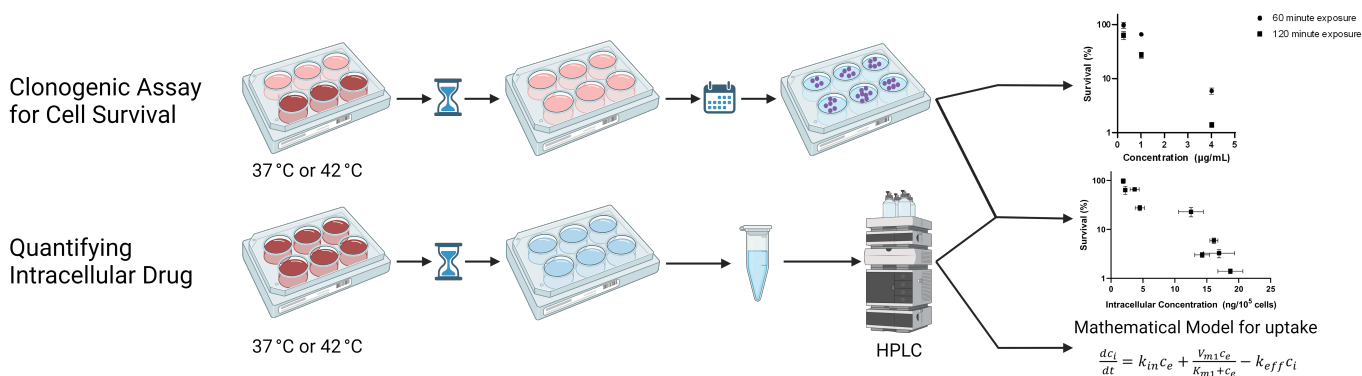


Figure 4.1. A schematic of the experimental procedures used in this chapter to obtain mathematical models of cellular uptake and cytotoxicity of doxorubicin in CT26 cells. Created with BioRender.com.

to more advanced 2.5D or 3D cell culture techniques [154]. The primary reason for this is that, although the latter techniques may provide measurements which are closer to the clinical reality, the number of measurements required to be able to construct a mathematical model of drug uptake and cell kill necessitates the use of (simpler) monolayer cell culture. The major limitation of monolayer cell culture, when compared to more advanced techniques, is the lack of interaction between cells and proteins in an extracellular matrix (ECM). It has been demonstrated that ECM can alter the sensitivity of cancer cell lines to doxorubicin [155]. Even without the presence of ECM, the cell density, and treatment of adherent cells while suspended (rather than adhered), have both been shown to have a non-negligible effect on transport of doxorubicin into cells [93], so it is important going forwards that the cells are treated while adhered, and at consistent densities.

Perhaps one of the more significant limitations of cell culture in general, when compared to the replication of tumour cells in humans, is that cells grown *in vitro* have had media optimised to ensure maximal cell growth and viability. In comparison, the tumour microenvironment is poorly regulated, spatially diverse, and nutrient-poor; indeed, a necrotic core occurring beyond the limit of sufficient oxygen diffusion is a well-recognised feature of solid tumour physiology [e.g. 156]. This means that the cell viabilities which result from experiments in a monolayer culture are unlikely to match those *in vitro*, but the observed trends (such as an increase in cell kill at hyperthermic conditions) are likely to be clinically relevant, since clonogenic assays have been shown to be a good predictor of *in vivo* performance [157].

In the following sections, the cell culture technique is outlined, and the different approaches to assess cell viability are described. Initially, three rapid assays (trypan blue exclusion, an assay of cell

metabolism, and the use of an imaging cytometer) are detailed, before the literature gold-standard clonogenic assay is performed. Subsequently, a novel assay to determine intracellular doxorubicin concentration is presented, and the results of both sets of experiments are then modelled.

4.2 Studying Cell Viability: Materials and Methods

4.2.1 Cell Culture

CT26 cells were cultured in Roswell Park Memorial Institute (RPMI) 1640 Medium (ATCC Modification, ThermoFisher Scientific Catalogue no. A1049101) with 10% Fetal Bovine Serum (FBS) (ThermoFisher Scientific Catalogue no. 10270106) in 75 cm² cell culture flasks (Corning Catalogue no. 430641U) and maintained in an incubator (Sanyo MCO-17AIC Incusafe CO₂ Incubator) at 37°C and 5% CO₂.

On reaching confluency, the medium was aspirated, and the cells were washed once with 5-6 mL of Dulbecco's Phosphate Buffered Saline (DPBS) (ThermoFisher Scientific Catalogue no. 14190250), before 2.5 mL of Trypsin EDTA (0.05%) (which had previously been made up from DPBS and Trypsin EDTA (0.5%) (ThermoFisher Scientific Catalogue no. 15400054)) was added to the flask. The flask was then returned to the incubator for five minutes, before being examined under an inverted microscope. If the cells were not fully detached, they were returned to the incubator for a further two minutes. Once detachment had been observed, 10 mL of medium was then added to the flask to neutralise the trypsin, before the contents were aspirated into a 50 mL centrifuge tube and spun down into a pellet at 125 x g for five minutes in a centrifuge at 22°C (Heraeus Labofuge 400R). The tube was returned to the hood, excess medium was aspirated, then the pellet was resuspended in 10 mL of media. Typically 2 mL of this suspension was added to a new flask, with 8 mL of fresh media (a 1:5 split).

Cells typically required passaging every three to four days, depending on the seeding density. Unless stated otherwise, media, trypsin, and PBS were all heated to 37°C, or 42°C prior to by immersion in a water bath.

The transmembrane pH differential has a large impact on the transport of doxorubicin into cells, and indeed its efficacy in cells; increasing the extracellular pH from 6.5 to 7.5 has been shown to more than double the intracellular doxorubicin concentrations achieved in HCT116 colon cancer cells

[105]. This is due to the fact that doxorubicin is a weakly basic drug, and becomes protonated at a lower pH, which greatly reduces its ability to pass through the lipid cell membrane. Cell culture medium is often buffered with a bicarbonate buffer, which relies on the dynamic equilibrium between carbonic acid and carbonate/hydrogen ions. CO_2 reacts with the water in cell culture media to form carbonic acid: H_2CO_3 . This in turn partly dissociates to give bicarbonate and hydrogen ions, which make the solution more acidic. As a result of this, on removal from a 5% CO_2 atmosphere, media buffered in this way will rapidly become more basic. Such a change in media being added is not physiologically relevant and may cause discrepancies over the shorter exposure times required.

Consequently, the selected medium uses an alternative buffer, HEPES. HEPES has more buffering capacity than sodium bicarbonate, and crucially should remain stable for longer when the media is not in an incubator, as the system does not depend on the presence of carbon dioxide. The pH of the media at 37°C and 42°C was tested with and without the addition of 1% penicillin-streptomycin (as is used in the clonogenic experiments described later), and there were no substantial changes in pH (readings varying from 7.30 - 7.32).

4.2.2 Cell Counting

Trypan blue is a dye which cannot permeate into the membranes of live cells, but can cross the membranes of dead cells, resulting in a clear differentiation between live and dead cells under a microscope, that can be used to estimate the total number of viable and dead cells in a sample [158]. To estimate the concentration of cells in a sample to allow plating of a known standardised number, a representative sample of a cell suspension was taken. A 100 μL sample was mixed with 100 μL of 0.4% Trypan Blue (ThermoFisher Scientific, 15250061) in an Eppendorf tube (FisherScientific, 10718894). 20 μL of this was then drawn up and slowly pipetted into the first chamber of a Countess® Cell Counting Chamber Slide (ThermoFisher, C10228). This was repeated for the second chamber, before inserting the slide into a Countess Cell Counter (Invitrogen). The focus was adjusted to ensure optimal counting, before an average of both readings were taken as the final value.

4.2.3 Doxorubicin and Choice of Treatment Conditions to be Assayed

The results of initial compartment modelling in the previous chapter, suggests that typical extracellular concentrations of doxorubicin for delivery via an LTSL was around 16 $\mu\text{g}/\text{mL}$ [65]. Similarly, in the TARDOX trial, the average doxorubicin tissue concentration following ultrasound exposure results was 8.56 $\mu\text{g}/\text{g}$ of tissue – although the maximum found was 21.08 $\mu\text{g}/\text{g}$. A selection of concentra-

tions increasing logarithmically was therefore selected to ensure that extrapolation beyond the tested range was not required, and that there was reasonable resolution at the lower concentrations which are more frequently seen clinically: 0.25, 1, 4, 16, and 64 $\mu\text{g}/\text{mL}$.

The exposure durations chosen were 15, 30, 60, and 120 minutes. Exposure times less than an hour are rarely found in the literature, but are particularly relevant in the case of TSL drug delivery, as the highest concentrations persist for shorter periods of time. 15 minutes was felt to be the shortest time practicable for treatment to ensure that consistent conditions (i.e. temperature and CO_2 level) were maintained. A maximum duration of 120 minutes was chosen, as it was observed that at this exposure duration the cells remained adhered to the plate, and so intracellular concentration could still be assayed. This duration is also appropriate since, as discussed in the previous chapter, this time would represent a clinically challenging, but feasible upper limit of ultrasound-mediated hyperthermia of a deep-seated tumour. Not all combinations of the above durations and concentrations were tested, but only those most appropriate to the problem (i.e. the lower concentrations were not assayed for the shortest exposure times and so on).

100 mg of doxorubicin hydrochloride (BID0120, Apollo Scientific Ltd) was dissolved in 2 mL of dimethyl sulphoxide (DMSO), to create a stock solution of 50 mg/mL. The stock was then aliquoted to create stock solutions of 6.4, 1.6, 0.4, 0.1, and 0.025 mg/mL of doxorubicin to facilitate easy spiking of media to create solutions with 64, 16, 4, 1, and 0.25 $\mu\text{g}/\text{mL}$ of doxorubicin, which all had a constant (1 vol-%) DMSO content. All vials were kept stored at -70°C between experiments, with vials only being thawed when necessary, and at all times protected from light. Maintaining a constant vol-% of DMSO was found to be an important control, with 1 vol-% deemed an acceptable level (see Section B.1).

4.2.4 Achieving Hyperthermia

For any treatments involving hyperthermia, the set temperature of a separate incubator was turned up to 42.2°C and allowed to equilibrate. All plates were treated on the top shelf, where the temperature was verified through placing a METRIA TP3001 Digital Thermometer on the shelf before the experiments and checking the temperature through the inner glass door of the incubator five minutes after first opening the door; the temperature was in good agreement with the display temperature on the incubator, and hyperthermic conditions had been established. During the experiments, the door was not opened throughout, as the incubator temperature had good agreement with that displayed

on the thermometer, but the temperature was checked for consistency on the removal of the plate at the end of the incubation duration. The temperature was set slightly above 42°C, since opening the door lowers the temperature inside the incubator, and a slightly higher setting was found to be required to sustain an average temperature of around 42°C. Across all hyperthermic treatments, the temperature never fell below 41.3°C, or rose above 42.3°C.

4.2.5 Assaying for Cell Viability

Four distinct methods were attempted to determine the viability of cells treated with doxorubicin. Although recognised in the literature as the gold standard [159], the clonogenic assay was not attempted initially, as it is a more time consuming and technically challenging protocol, and the faster collection of more (albeit less accurate) data points is preferable for the construction of a mathematical model. The findings from these 'faster' assays (namely trypan blue exclusion, an assay of cell metabolism, and an imaging cytometer) are presented first, before the results from a clonogenic assay are presented in a later section.

4.3 Faster Cell Viability Assays

In this section, the three methods used to estimate cell viability initially are presented. Although they are shown to be inappropriate, they are included in the work as the results provide valuable insight into the mechanisms of doxorubicin. In all cases, the presented results were obtained by performing the stated assays 48 hours following treatment of the cells with doxorubicin, a duration obtained following preliminary experiments detailed in Appendix B (Section B.3).

4.3.1 Assessment of Cell Viability with Trypan Blue

In addition to being used to count cells for plating, trypan blue counting was also used to provide a quick estimate of cell viability following exposure to doxorubicin. For a single reading, six T25 flasks were seeded with 1×10^6 cells, and incubated for 24 hours in 2.5 mL of media. After incubation, the media was aspirated, the cells were gently washed with 1 mL of DPBS, before the addition of doxorubicin-spiked media ($n = 3$), or a negative control. The cells were then incubated for the stated treatment time, before the media was again aspirated, the cells were washed twice, before media was again added and the flasks were returned to the incubator.

Cell counting was then performed 48 hours post treatment, by trypsinising the flasks with the ad-

Normothermia Viability (%)	0.25 $\mu\text{g/mL}$	1 $\mu\text{g/mL}$	4 $\mu\text{g/mL}$	16 $\mu\text{g/mL}$	64 $\mu\text{g/mL}$
15 minutes				41.4 \pm 9.2	39.0 \pm 8.9
30 minutes					
60 minutes	118.2 \pm 21.7	102.3 \pm 24.3	49.0 \pm 29.5		
120 minutes	79.2 \pm 32.1	63.1 \pm 15.5			

Table 4.1. Percentage viability results obtained at normothermic conditions using the method of trypan blue exclusion (method as described in Section 4.3.1), assayed 48 hours following exposure to the given concentrations of doxorubicin for the stated durations, at normothermic (37°C). Values given are the mean \pm one standard deviation, $n = 3$. Grey entries were not assayed as it became clear that trypan blue exclusion was not resolving the cytotoxic effect of doxorubicin treatment.

dition of 1 mL of trypsin solution, incubating, then adding 3 mL of complete media to neutralise the trypsin when the cells have fully trypsinised (as checked under the microscope). This solution can then be counted as described above. If the two counts differed by more than 15%, or viability was below 85% (for non-treated cells), a second count was performed. An approximate 'relative survival' can be calculated by dividing the average of the counts in the treatment flasks by the average of the counts in the negative control flasks.

The results are presented in Table 4.1, and demonstrate that, even with this limited data set, the full cytotoxic effect of the drug is clearly not resolved by this method, and the standard deviation of measured viabilities was very large (albeit with only $n = 3$). Consequently, a complete data-set with this protocol was not obtained.

4.3.2 Assessment of Cell Viability with an MTS Assay

The MTS (3-(4,5-dimethylthiazol-2-yl)-5-(3-carboxymethoxyphenyl)-2-(4-sulfophenyl)-2H-tetrazolium) assay is an assay of cell metabolism which relies on the reduction of a tetrazolium compound to a formazan product by the mitochondria of metabolically active cells [160]. The formazan product has an absorbance peak at 490 nm, the magnitude of which correlates with the number of cells present (demonstrated in Appendix B, Section B.4).

Quantification of cell survival following treatment with doxorubicin was performed as follows: cells were rescued from a flask and counted, before being diluted to 1×10^5 cells/mL. 1×10^4 cells ($100 \mu\text{L}$) were seeded as required in the wells of a flat-bottomed 96 well plate (FisherScientific, 10695951), and incubated for 24 hours to ensure the cells had adhered. The outermost wells on the plates were

not used to generate data and were instead filled with DPBS to minimise evaporation from the experimental wells. The medium was then aspirated from the treatment wells, which were then gently washed with 50 μL DPBS, before the addition of either doxorubicin-spiked media or negative control. At the end of the treatment time, this media was again aspirated, the wells were gently washed twice with DPBS, before the addition of fresh media, after which the plate was returned to the incubator for 48 hours. Subsequently, the MTS reagent, CellTiter 96® AQueous One Solution (Promega, G3580), was prepared by diluting the reagent in a 1:5 mixture with complete media in a reservoir. The plate was removed from the incubator, media aspirated, and wells gently washed once with PBS. 120 μL of reagent-media mixture was then pipetted into each experimental well (and an additional set of cell-free control wells) with a multichannel pipette. The plate was then returned to the incubator for 90 minutes (a timing chosen following a preliminary experiment - see Section B.4).

After 90 minutes, the plate was removed from the incubator and shaken for 5 minutes at 320 min^{-1} on an orbital shaker (KS 130 Basic, IKA England Ltd.) to ensure that the formazan product was uniformly distributed in each individual well. Any bubbles large enough to affect the absorbance reading were burst with a fine gauge needle, before the plate was placed in a plate reader (FluoStar Omega, BMG LABTECH), and an absorbance spectrum was taken for each well. The viability of treatment wells was then calculated as follows.

- The absorbance value for each well at 490 nm was calculated by subtracting the background value of absorbance (the mean value between 850-900 nm) for that specific well.
- The mean absorbance at 490 nm due to natural turnover of the MTS substrate in the cell-free control wells was calculated, as well as the standard deviation of the background wells.
- From each treatment well and doxorubicin-free well, the mean absorbance of cell-free control plus two standard deviations of this were subtracted, to ensure that the remaining signal does not contain any background.
- The viability was then defined as the corrected mean absorbance of the treatment group divided by the corrected mean absorbance of the doxorubicin-free wells

Cytotoxicity results from the MTS assay were obtained for 37°C exposures only, with results for 15 and 30 minute exposures shown in Figures 4.2 and 4.3. The results do not show the anticipated levels of cell kill considering literature data on doxorubicin cell kill in CT26 cells. For example, Na et al. [161] reported a 50% inhibitory concentration of 1.8 $\mu\text{g}/\text{mL}$ doxorubicin in CT26 cells for a 72 hour

exposure using a similar metabolic assay (MTT). Although the exposure durations here are very brief in comparison, higher levels of cell kill would be expected than were obtained for 16 and 64 $\mu\text{g}/\text{mL}$ in particular.

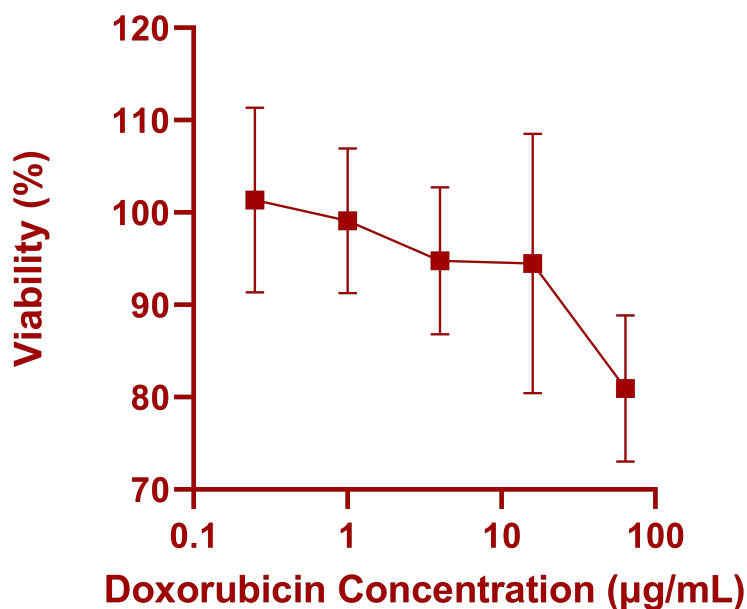


Figure 4.2. Cell viability assessed by MTS assay measured 24 hours after exposure to varying doxorubicin concentration for 15 minutes. Brown squares represent the mean of five independent wells and the error bars the standard deviation. Standard deviation of negative control (i.e. zero doxorubicin), not shown due to logarithmic scale, was 4.77%. 'Viability (%)' calculated as described in Section 4.3.2.

Therefore, in order to ensure this assay is being performed correctly and to isolate the duration of drug incubation as the differentiating factor between the results obtained in Figures 4.2 and 4.3 and the described literature results, the protocol was then repeated with a 1.8 $\mu\text{g}/\text{mL}$ concentration of doxorubicin incubated for 72 hours (a 50% inhibitory concentration according to [161]) and a positive control of 70% Ethanol (EtOH). In this case the MTS reagent was added immediately after the removal of the drug (rather than waiting for another 48 hours), owing to the prolonged exposure.

The results from this experiment, shown in Figure 4.4, evidence that 1.8 $\mu\text{g}/\text{mL}$ for 72 hours results in complete loss of metabolic activity, and demonstrate the impact of extended exposure to be even greater than may have been suggested by the results of [161]. Secondly, although the positive control signal has a large standard deviation, the MTS results do suggest that there is complete cell death.

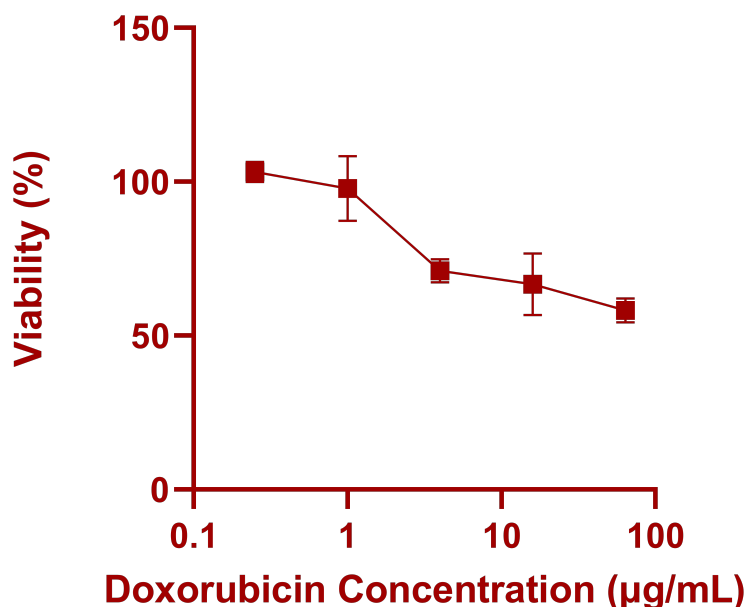


Figure 4.3. Cell viability assessed by MTS assay measured 24 hours after exposure to varying doxorubicin concentration for 30 minutes. Brown squares represent the mean of five independent wells and the error bars the standard deviation. Standard deviation of negative control (i.e. zero doxorubicin), not shown due to logarithmic scale, was 4.04%. 'Viability (%)' calculated as described in Section 4.3.2

4.3.3 Assessment of Cell Viability with an Imaging Cytometer

A whole-well image cytometer (Nexcelom Bioscience, Celigo) was used to provide additional insight into the other assays being performed. Additionally, an attempt was made to use the Celigo's bright-field imaging to count the number of adherent cells in a 96 well plate, thereby providing an easy estimate of viability between treatment and control wells.

The plate treated with the full range of doxorubicin concentrations (0.25 - 64 $\mu\text{g/mL}$, $n = 5$) for 30 minutes and assayed (48 hours later) for viability with MTS (with the results as shown in Figure 4.3), was subsequently imaged with the Celigo, with some representative images shown in Figure 4.5. The plate was scanned using the settings recommended by Nexcelom for adherent cells in a 96 well plate format. A plot of the obtained cell count, which can be seen in Figure 4.6, appeared to be reasonable; viability decreases with increasing concentration, and does not seem inconsistent with literature values. Viability is defined as the cell count in the treatment group divided by the cell count in the control group.

Manually reviewing the images however, showed that there were discrepancies between the counts - specifically, changes to cell morphology meant that cells were not being detected in the treatment

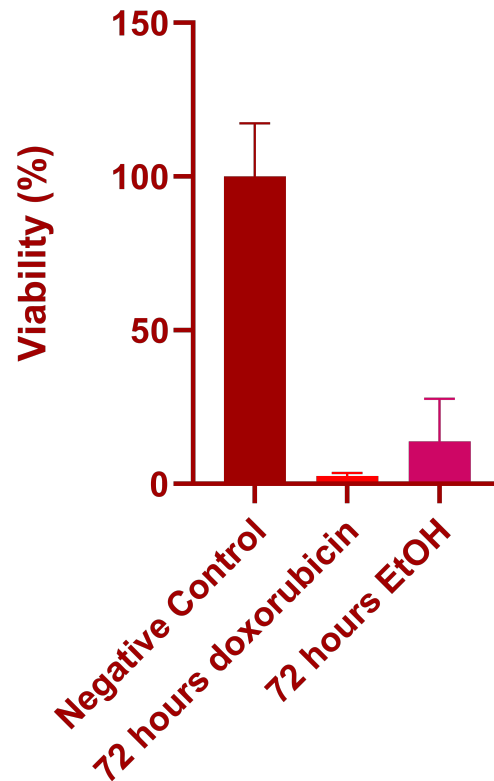


Figure 4.4. Results of an experiment to check how the MTS assay resolves an expected 'complete' cell death. Cells were treated for 72 hours with $1.8 \mu\text{g}/\text{mL}$ doxorubicin, positive control (70% EtOH), or a negative control. The MTS assay was performed immediately after removal of treatment and the subsequent wash steps. Usual data processing was not followed here - two standard deviations of the negative control were not added to the noise signal to avoid a negative viability in the doxorubicin treatment group. Error bars represent the standard deviation, $n = 5$. Tukey's multiple comparisons test was performed in GraphPad PRISM and found that both treatment groups were significantly different from the negative control ($p < 0.0001$), but the treatment groups were not significantly different from each other ($p = 0.3785$).

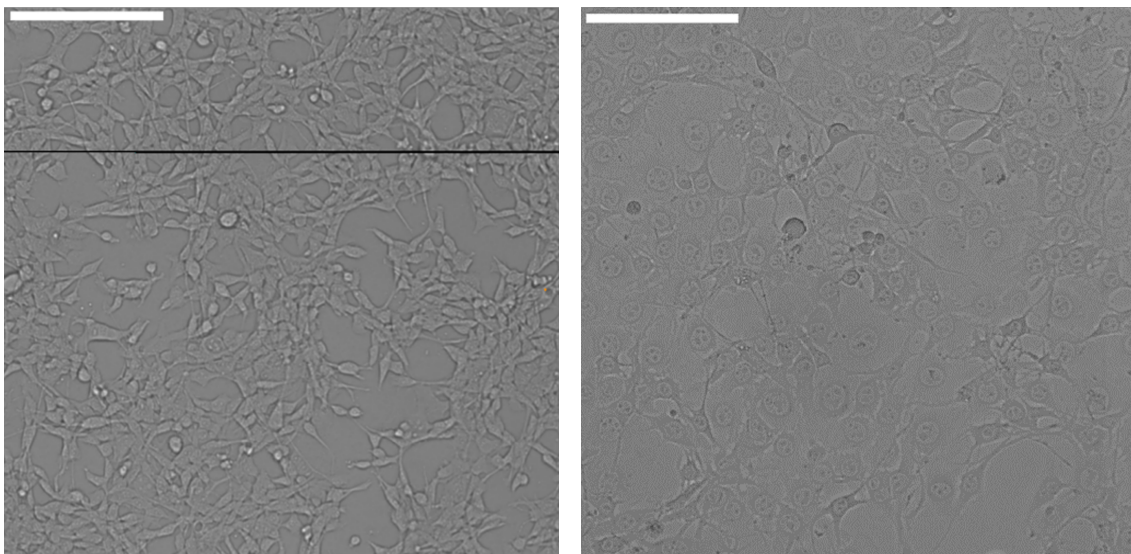


Figure 4.5. Representative Celigo brightfield image of a sample of (left) an untreated well, and (right) a well treated for 30 minutes with $64 \mu\text{g}/\text{mL}$ doxorubicin, 48 hours after the removal of doxorubicin-free media. Both scale bars $200 \mu\text{m}$.

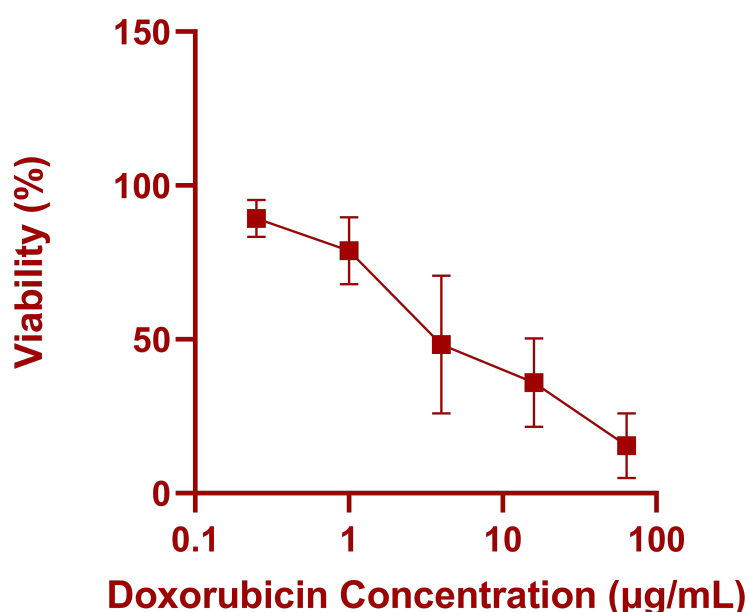


Figure 4.6. Cell viability assessed by Celigo automated cell counting, 48 hours post exposure to varying doxorubicin concentration for 30 minutes. Red squares represent the mean of five independent wells and the error bars the standard deviation. Standard deviation of negative control (i.e. zero doxorubicin), not shown due to logarithmic scale, was 2.4%. Viability was calculated as the number of cells counted in the treatment wells/number of cells counted in the negative control wells.

wells, or sometimes were counted several times, as the algorithm detected several of a cell's organelles, as can be seen in Figure 4.7. The high quality of the Celigo images allowed visualisation of some of the effects of doxorubicin (as in the treated well in Figure 4.5). For instance, it appears that at the higher doses, cells have become multi-nucleated, or possibly formed vacuoles, which can occur in mammalian cells following treatment with certain drugs [162]. Altering the settings to increase minimum cell size and change the detection threshold proved futile, as solving one detection problem gave rise to several others. In the negative control well, the algorithm struggled to segment cells properly, owing to their confluency, and so the Celigo's brightfield cell counting was not pursued further to obtain viability data in isolation.

The images obtained from the Celigo provide some insight into the findings of the MTS and trypan blue exclusion assays. The cellular damage and changes to cell morphology which were clearly observed here may well be irreparable (and thus prevent further replication), but would not necessarily result in the membrane being permeable to trypan blue, nor the cell failing to metabolise the MTS assay reagent. The implications of these findings with respect to the overall mechanism of cell kill by doxorubicin are discussed further in Section 4.5.1.

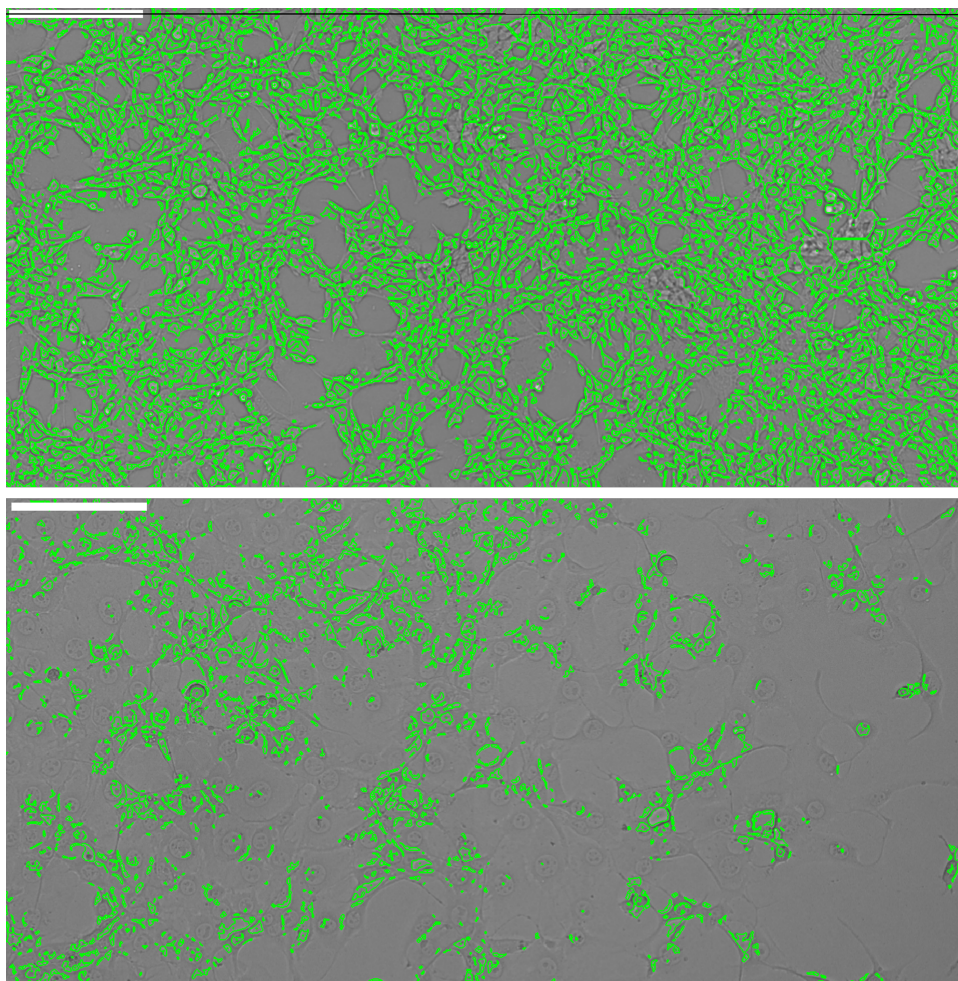


Figure 4.7. The sample images in Figure 4.5, with the results from the Celigo cell count overlaid in green. The top image is a wider view of the left-hand image in Figure 4.5, which was an image of an untreated control well, while the bottom image is a similarly widened view of the right-hand image, which was treated with 64 $\mu\text{g/mL}$ for 30 minutes, 48 hours prior to imaging. Both scale bars 200 μm .

4.3.4 Summary

None of the techniques described above can be used with confidence to determine the cytotoxic effect of doxorubicin with the required precision for creating a mathematical model. Being able to distinguish between 95% and 99% cell kill is clinically important, but neither the MTS or Trypan Blue assays would be able to satisfactorily resolve this difference owing to the magnitude of their standard deviations. Because of this, the same is likely true of these techniques for building mathematical models of the action of other therapeutics. Further doubt is cast upon the ability of these assays to resolve the cytotoxic effects of doxorubicin by the images obtained by the Celigo imaging cytometer. The differences in results between the different techniques are not surprising in and of themselves, since the different methods use different metrics for cell viability; generally, as long as like methods are compared, the findings of experiments comparing alternative treatments could be considered to be valid, however the microscopy images strongly suggest that these cells are not healthy. It is therefore necessary to use a clonogenic assay to measure more directly whether these cells still have the ability to replicate, which could be considered as the desired clinical outcome of chemotherapy, since it would prevent further tumour growth and metastasis. As a result, a clonogenic assay was performed to collect the final data used in the mathematical model and is described in the next section.

4.4 Clonogenic Assay

4.4.1 Protocol

A clonogenic assay for cell survival was performed to quantify cell survival, based on the protocol of Franken et al. [163]. The final protocol (following some preliminary experiments, see Section B.5) was as follows:

- Cells were grown in complete media with the addition of 1% Pencillin-Streptomycin (ThermoFisher, 15070063) to prevent infection during the prolonged incubation period.
- Cells were rescued from the flask and pelleted, before being resuspended, as in Section 4.2.
- A count was performed, and the suspension was diluted to a suspension in the range 1000-4000 cells/mL. The general idea of this step is to never take less than 50 μ L of any suspension, and to recount if an intermediate suspension is used - for treatment with high drug concentrations, sometimes, suspensions with higher cell densities were required to seed the treatment wells. In

this case, this suspension was the one subsequently diluted to the range 1000-4000 cells/mL to seed the negative control.

- 200 cells were plated in each negative control well of a six well plate (Corning, Costar® 6-well Clear TC-treated Multiple Well Plates, 3516) adding media such that the total volume in the well was 2.5 mL. An appropriate number of cells (see Table 4.2) was then seeded in the same way, with the same total volume in the treatment wells. Any unused wells (for example, if the treatment group was for doxorubicin + hyperthermia, so the negative control needed to be treated at a different temperature) were filled with the same volume of DPBS to ensure similar evaporation across the plates.
- The plates were returned to the incubator for 24 hours.
- After 24 hours, the media and DPBS were warmed to 37°C in a waterbath. The doxorubicin stocks were protected from light and defrosted. When the medium was at the required temperature and the doxorubicin had defrosted fully, spiked solutions of media at treatment concentrations were prepared in the tissue culture hood in centrifuge tubes protected from light. The resulting spiked media solutions were well mixed by inverting the tube. The plate was removed from the incubator, and the media carefully aspirated through a 5 mL stripette. The wells were then gently washed once with 900 μ L DPBS (with a sterile 1 mL pipette tip). 2 mL of spiked-media or negative control were then gently added to each well, and the plate was returned to the incubator for the treatment time.
- At the end of the treatment time, the medium was aspirated from the wells, which were then twice washed with 900 μ L DPBS. 2.5 mL of medium was then added to each well, and the plates were again returned to the incubator for seven days.
- The plates were then fixed and stained using a mixture of 6% (v/v) glutaraldehyde (Merck, 820603), 0.5% (w/v) Crystal Violet (Sigma-Aldrich, C0775), and dH₂O. The medium was aspirated from the plates, which were then gently washed once with DPBS, before 2 mL of the staining solution was added. The staining solution was left on the plates for 1-2 hours.
- The staining solution was then aspirated gently using a 5 mL stripette. The plate was then immersed and shaken vigorously in a tub containing tap water to remove excess crystal violet staining. Plates were then left to air-dry overnight.
- Colonies were then visible on the plates.

The well plates were scanned using a GelCount™ scanner (Oxford Optronix) at 1200 dpi. The images were then analysed using the CountPHICS ImageJ macro [164]. The CountPHICS macro works as follows:

- The image is split into its RGB intensities, and the image with the highest standard deviation (i.e. the most contrast between background and colonies) is taken forward for analysis.
- A Gaussian Blurring Filter is then applied to remove random noise (the standard deviation of this filter can be set automatically by the macro, or chosen by the user)
- A rolling ball algorithm is applied to remove smooth background noise (due to variations on the amount of incident light on the plate). The rolling ball radius, as with the standard deviation of the Gaussian filter, can be set automatically, or manually.
- Finally, values for minimum colony size and circularity are set, again, either manually or automatically.
- A region of interest is selected manually.
- The image is thresholded; with this threshold intensity being set automatically based on the standard deviation of the region of interest.
- A watershed algorithm is applied to separate overlapping colonies.
- The separate colonies are counted; the number of colonies, and a list of their sizes are outputted in a .txt file.

The macro parameters were adjusted to provide good agreement with manual counts on several wells. The rolling ball radius and automatic thresholding values suggested by the macro were used, as manually changing these values did not provide any improvement in algorithm performance. The Gaussian blur standard deviation was set to 4, and the circularity to 0.2. The minimum colony size was set based on a measurement of cell size with the Celigo, in which the smallest healthy cells in the sample measured around 60 x 10 microns. This means that the minimum area of 50 cells would be $30,000 \mu\text{m}^2$ - which corresponds to a minimum colony size of 67 pixels after GelCount scanning, assuming a perfect packing of the smallest cells. As a result, this slightly over-counted, and 100 pixels was found to give the best agreement with the manual count. As an example of the agreement between the macro and a manual count with these parameters, a manual count of the negative control wells on one plate was 62, 73, and 76, while CountPHICS outputted 59, 75 and 74.

For two plates, weak crystal violet staining meant that the resulting scans of the plate did not have sufficient contrast to be analysed computationally, and so were manually counted, using a microscope to check colony size.

To calculate the survival fraction, a plating efficiency (PE) was calculated for the negative control well:

$$PE = \frac{N_{c,NC}}{N_{s,NC}} \quad (4.1)$$

where $N_{c,NC}$ is the number of colonies counted in the negative control wells, and $N_{s,NC}$ is the number of cells seeded in those wells. The plating efficiency was then used to calculate the survival fraction (SF) of the treatment well:

$$SF = \frac{N_{c,T}}{N_{s,T} * PE} \quad (4.2)$$

where, $N_{c,T}$ and $N_{s,T}$ refer to the number of colonies counted in the treatment wells and the number of cells seeded in the treatment wells respectively.

The clonogenic assay has become a gold standard technique for assessing the long term response of monolayer cultures to chemical or radiation insult. This technically challenging assay requires seeding density to be optimised to avoid merging of adjacent colonies (which occurs when seeding density is too high) or loss of dynamic range (which occurs when seeding density is too low). Following preliminary experiments (See Section B.5), it was established that 200 cells would be seeded in the negative control well, and that seven days would be left between treatment and the fixing and staining of cells.

To ensure that the assay was able to resolve the therapeutic effect precisely across the variety of planned treatment conditions, the number of cells plated in the treatment wells was varied depending on the treatment concentration, but kept the same between corresponding normothermic and hyperthermic exposures. The seeding densities used for treatment are shown in Table 4.2.

4.4.2 Results

The results for both normothermic and hyperthermic conditions are shown in Table 4.3. The clonogenic data were analysed in GraphPad PRISM using a two-way ANOVA, grouping the exposure time

Exposure Duration	0.25 $\mu\text{g/mL}$	1 $\mu\text{g/mL}$	4 $\mu\text{g/mL}$	16 $\mu\text{g/mL}$	64 $\mu\text{g/mL}$
15 minutes				5000	5000
30 minutes			400	5000	
60 minutes	200	500	1000		
120 minutes	500	1000	2000		

Table 4.2. Table showing the number of cells seeded for each treatment group in the clonogenic assays. For all plates, the negative control had 200 cells plated. Cells left blank are exposure time and concentration combinations which were not tested due to the likely very high or very low expected viabilities.

and extracellular concentrations as a categorical variable ('treatment condition'), with the temperature condition 'hyperthermic' or 'normothermic' being treated as the other independent variable. The dependent variable was the cell survival, which was log transformed to normalise the error distribution. Mild hyperthermia was found to have a significant effect on cell kill for given treatment conditions ($p < 0.001$), while treatment group (unsurprisingly) has a significant effect on cell kill for a given temperature ($p < 0.001$). There was a significant interaction between hyperthermic effect and treatment condition on survival, suggesting that the effect is not uniform ($p < 0.001$).

The two-way ANOVA was deemed the best way to analyse the data set. A QQ plot and homoscedasticity plot were produced to verify that the log transformed data were approximately normal, meaning that an ANOVA was appropriate. A three-way ANOVA is not appropriate in this instance as the relatively small number of samples effectively results in over-fitting. A three-way ANOVA would have been a preferred analysis had a higher throughput approach, such as the MTS assay, given acceptable results.

The effect of hyperthermia in the absence of drug was also tested, and shown to have a minimal effect on cell viability with the same washing steps as the full protocol. Wells exposed to 120 minutes of hyperthermia had a $98.37 \pm 10.39\%$ viability, while those exposed for 15 minutes had a $91.19 \pm 8.96\%$ viability when compared to the equivalent negative controls ($p > 0.05$ in both cases, unpaired t-test performed on the colony numbers). This suggests that exposure to mild hyperthermia alone, over the given exposure times, is not lethal for the cells.

One result that is worthy of further discussion is the difference observed between a 30 minute and a 60 minute exposure at 4 $\mu\text{g/mL}$ in hyperthermic conditions. The cell viability at 30 minutes is an order of magnitude greater than that seen at 60 minutes. This is likely due to the sharp nature of the

Exposure Duration (%)	0.25 $\mu\text{g/mL}$	1 $\mu\text{g/mL}$	4 $\mu\text{g/mL}$	16 $\mu\text{g/mL}$	64 $\mu\text{g/mL}$
Normothermic Viability					
15 minutes				1.79 \pm 0.18	0.83 \pm 0.40
30 minutes			22.90 \pm 4.87	3.27 \pm 0.64	
60 minutes	97.22 \pm 10.91	65.80 \pm 5.74	14.75 \pm 3.14		
120 minutes	63.60 \pm 11.59	27.43 \pm 3.42	9.09 \pm 0.16		
Hyperthermic Viability					
15 minutes				0.99 \pm 0.18	0.49 \pm 0.16
30 minutes			10.06 \pm 2.69	0.55 \pm 0.04	
60 minutes	91.07 \pm 16.25	41.12 \pm 2.62	1.38 \pm 0.46		
120 minutes	85.98 \pm 5.53	11.62 \pm 0.53	1.18 \pm 0.39		

Table 4.3. Viability (%) from clonogenic assays. Cells left blank are exposure time and concentration combinations which were not tested due to the likely very high or very low expected viabilities.

Hill response often seen when assessing the effect of therapeutics, as well as possibly reflecting the fact that the DNA repair-inhibiting effects of hyperthermia may not have affected all cells at only 30 minutes, and that there is likely less drug inside the cells considering the shorter exposure.

4.5 Cell Viability Data Discussion

The general trends which can be seen in these data are unsurprising, yet important; increasing exposure time to a given concentration of drug increases the cell kill, and increasing the concentration of drug for a given exposure time also increases the cell kill. Comparing the hyperthermic treatments to their normothermic equivalents; the effect of adding hyperthermia resulted in between a 1.35 fold increase in cell survival (0.25 $\mu\text{g/mL}$, 120 minutes) to a decrease in survival by a factor greater than 10. As shown in Table 4.4, of the 10 conditions compared, hyperthermia decreased cell viability in nine.

The lack of increased kill at 0.25 $\mu\text{g/mL}$ is difficult to explain. Given the small number of replicate wells, it is certainly possible that this result is not reflective of the true impact of hyperthermia on the cytotoxic effect of doxorubicin for this exposure duration. However, antagonisms between hyperthermia and small molecule therapeutics at certain concentrations have also been reported in other studies [113], so it would be wrong to assume (without further study) that this finding is erroneous.

Exposure Duration	0.25 $\mu\text{g/mL}$	1 $\mu\text{g/mL}$	4 $\mu\text{g/mL}$	16 $\mu\text{g/mL}$	64 $\mu\text{g/mL}$
15 minutes				0.55	0.58
30 minutes			0.44	0.17	
60 minutes	0.93	0.63	0.09		
120 minutes	1.35	0.42	0.13		
Viability decreases with hyperthermia					
Viability increases with hyperthermia					

Table 4.4. Ratio of the viabilities of cells treated with drug and hyperthermia compared to those treated with drug at normothermic conditions.

4.5.1 Mechanism of Action of Doxorubicin

One feature of the above results which is unambiguous across all methods of attempting to resolve the cytotoxic effect of doxorubicin is the time delay between the addition of drug and the effect being observed. This is consistent with literature data across different methods of assessing cytotoxicity of doxorubicin, including when cells were treated in suspension before being analysed by a live-dead stain using flow cytometry [165]. This study also found that the measured cell kill was greatest 48 hours after treatment.

The images from the Celigo show clear evidence of changes to cell morphology, which are not consistent with an end-stage of apoptotic cell death being the major cause of cell kill following treatment with doxorubicin under these conditions. Apoptotic cell death is characterised by membrane blebbing and the formation of apoptotic bodies; which cannot clearly be seen in the right-hand image in Figure 4.5. Instead, cells appear to be enlarged and multi-nucleated, and the MTS assay results suggest that at least some cells remain metabolically active. This is consistent with cell death through mitotic catastrophe [166], during which ‘cells proceed into mitosis after a transient cell cycle arrest and fail to separate, leading to catastrophic cell division’ [167]. Although cell death through mitotic catastrophe is not mentioned in Gewirtz’s review of doxorubicin’s mechanisms, such a cell death has previously been reported to have occurred following treatment of cells *in vitro* with doxorubicin [e.g. 168].

A further mechanism of action of doxorubicin becomes apparent when examining the results of the clonogenic assay more closely. One benefit of using the CountPHICS macro is that a plot of the measured colony sizes can be obtained; a representative plot, showing the results from the plate

treated for 60 minutes with 4 $\mu\text{g}/\text{mL}$ at 37°C are shown in Figure 4.8. An image of the plate itself is also shown in Figure 4.9. A reduction in colony size can clearly be seen between the treated and drug-free wells, which, when seen under the microscope demonstrated that phenotypic changes were being expressed in addition to cell death. In addition to the generally smaller colonies in treatment wells, there were often individual cells (and many small groups of cells which clearly began dividing, but did not replicate sufficiently to become a colony) on the plates. As these were not washed off prior to fixing and staining, this suggests that the cells were viable (since dead cells would be expected to detach on washing), and thus it can be concluded that doxorubicin is inducing cellular senescence.

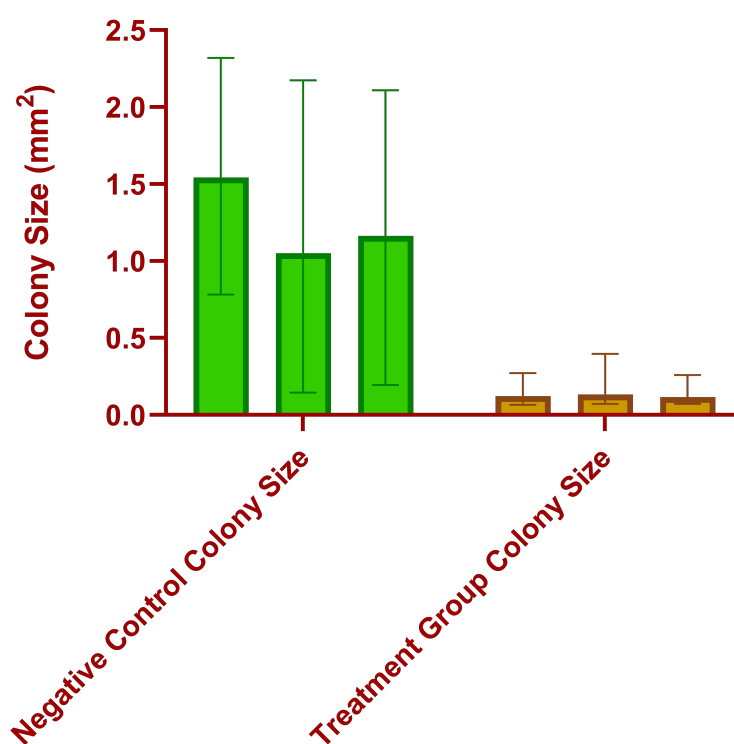


Figure 4.8. Plot of the median colony sizes (error bars are the interquartile range) from three negative control wells (200 cells plated) and the corresponding three treatment wells, treated with 4 $\mu\text{g}/\text{mL}$ at 37°C for 60 minutes (1000 cells plated), as shown in Figure 4.9. Colony sizes were obtained by the CountPHICS macro.

The induction of cellular senescence by doxorubicin has been reported in the literature [e.g. 169, 170]; and is (similarly to mitotic catastrophe) associated with multi-nucleated, giant cells [171], which can be seen clearly in the image of the treated well, on the right-hand side of Figure 4.5. Indeed, one study reported that treatment with doxorubicin induced either a 'senescence-like phenotype' or mitotic catastrophe in a variety of cells following treatment with low doses of doxorubicin [172], which is in many ways consistent with the results in this chapter. Of note is that the doses in [172] were an order of magnitude lower in concentration than those used in this chapter, but these lower doses

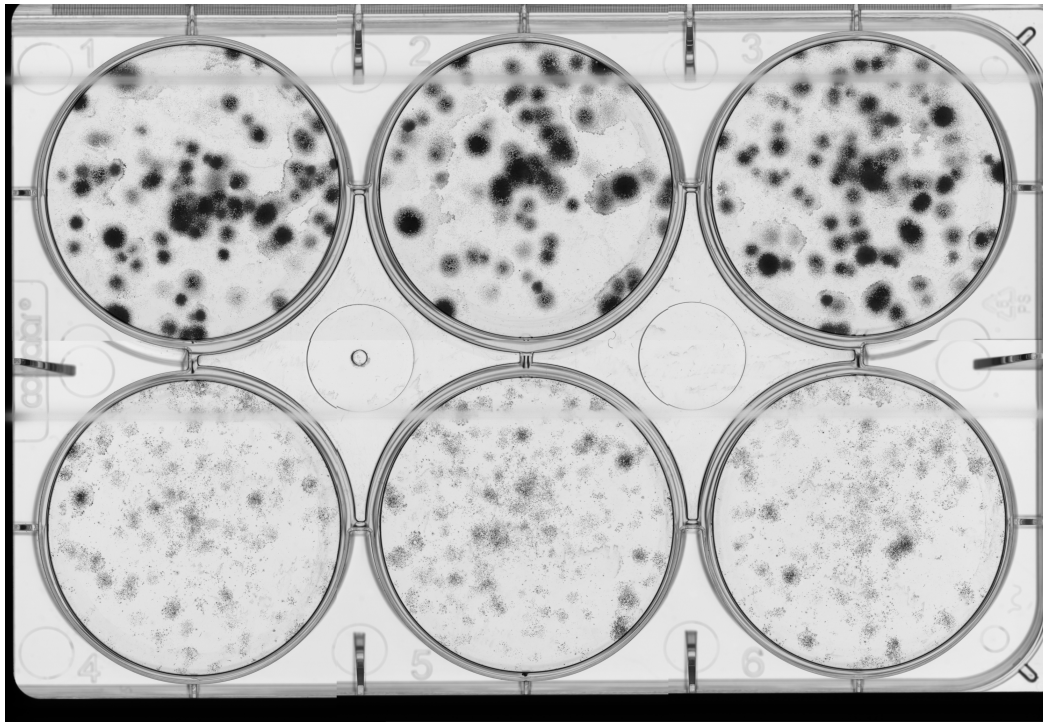


Figure 4.9. GelCount scan of clonogenic assay plate. The top row contains the negative control wells, which all had 200 cells plated, and each well contained 113 colonies (in all other sets of negative control wells, the number of colonies across the three was not consistent). The bottom row had 1000 cells plated and was treated with 4 $\mu\text{g}/\text{mL}$ at 37°C for 60 minutes, before being washed twice, and returned to the incubator with fresh media for a week, before being fixed and stained as in Section 4.4. The number of colonies counted in these wells were 75, 108, and 67.

were applied for exposure times on the order of days rather than minutes. This further emphasises the importance of both concentration and exposure time in quantifying cell death as a result of doxorubicin treatment.

It is clear that doxorubicin has several mechanisms of inducing cell death. Topoisomerase inhibition, which will inhibit DNA replication by preventing torsional release and strand separation of the DNA, has been described as being primary amongst these, but interaction with mRNA and direct free radical induced damage have also been reported. Notably, the timing and scale of these toxicities will vary depending on the cell cycle (i.e. topoisomerase impact will be most impactful at cell division) and the background mutation profile of the cells being treated. It should be noted that loss of apoptotic control is a 'hallmark' of cancer and yet the level and point in the pathway at which apoptosis control is lost varies greatly between cells. As a result, the specific mode of the cytotoxic effect of doxorubicin may change between cells or even within the same cell type at different time points after exposure. As these assays essentially address the question of viability via different metrics at different time points it is perhaps not surprising that there is not a single unifying output.

4.5.2 Strengths and Weaknesses of the Clonogenic Assay

The results from the clonogenic assay represent the so-called 'gold-standard' measurement for cytotoxicity, as a direct measure of the proliferative ability of cells. Despite this, it remains subjective, since colonies must be manually defined (although the process was automated here to remove bias). Indeed, it is difficult at the more extreme insults to distinguish between colonies and clusters of plated cells, since phenotypic changes are being expressed, and cells and colonies become smaller.

The cell survival percentages from the clonogenic assay on CT26 cells presented in this chapter are (particularly at the higher concentrations) an order of magnitude or so larger than the most directly comparable results in the literature, i.e., those published by Sharma et al. [24]. These differences can be explained by differences in the clonogenic assay protocol; the published data rely on a clonogenic assay in which cells are treated in a flask, then rescued and seeded (i.e. the work in this chapter follows a 'plate-then-treat' style assay, whereas [24] is a 'treat-then-plate' style assay).

'Treat-then-plate' represents a significant confounding insult to the cells, as the cells which have been exposed to a doxorubicin insult are then required to withstand further damage resulting from the protease activity of trypsin, and then to reattach to a new plate. This is not necessarily to say that the approach taken in this chapter is better, as seeding cells before treating results in a potential source of inaccuracy which is not present in the method used by Sharma: namely, that plating before treatment leads to more ambiguity in defining exactly what a colony is. In the approach taken by Sharma, plating increased numbers of treated cells is more likely to result in the development of healthy colonies from the few cells which successfully adhere to the dish and begin to proliferate, whereas the development of senescence-like phenotypes in a 'plate-then-treat' assay, as in this chapter, has less clarity. In any case, both assays resolve an effect as a result of hyperthermia and doxorubicin, and give results consistent with the clinical reality, and are acceptable given the intrinsic weaknesses of monolayer cell culture as an approach for estimating clinical outcomes.

One additional weakness of both styles of clonogenic assays is that there is an intrinsic difference between the negative control wells and the treatment wells, in that higher initial seeding densities in treatment wells may lead to higher plating efficiencies in treatment wells compared to the drug-free control wells, as a result of increased cell-cell interaction and, therefore, more effective adhesion to the plate. This may lead to underestimates of plating efficiency in the treatment wells, and thus, an overestimate of survival (recent studies have shown that this effect is not necessarily negligible

[159]). This effect could be partially counteracted in future assays by using conditioned media (that which has already been used to grow cells) in the seeding step.

One substantial drawback of using a monolayer cell culture to study the cytotoxic effect of doxorubicin, is that the cells are, in theory, identical, and so there is no selection for populations of cells which are resistant to doxorubicin insult, as happens in real tumours. This would increase the survival fractions with each successive cycle of doxorubicin treatment. In the context of using LTSL doxorubicin in the clinic, the development of these populations of cells is a reason to combine LTSL doxorubicin with additional chemotherapeutic agents, such as in the CHOP chemotherapy regimen [17], in which doxorubicin is administered alongside cyclophosphamide, vincristine, and prednisolone. Regimens such as CHOP are used with the idea that, if the cancer cells are resistant to one or two of the administered drugs, they are unlikely to be resistant to all. If LTSL doxorubicin is being used as a neoadjuvant therapy, this does mean that any recurrence is more likely to have developed a resistance to doxorubicin, which may reduce treatment options at this later stage – although this is true for whatever small molecule therapeutic (or combination thereof) that is used for neoadjuvant therapy.

4.6 Determination of Intracellular Concentration

The general principles behind the final protocol used to determine the intracellular concentration are to establish an estimate of the number of cells in each treated sample by quantifying the protein content using a BCA assay and comparing the resulting absorbance to a previously obtained standard curve. The doxorubicin concentration in the sample was measured using High Performance Liquid Chromatography (HPLC). The protocol (shown diagrammatically in Figure 4.10) was as follows:

Cells were rescued from a flask, pelleted, and counted, as in Section 4.2, before being seeded at a density of 1×10^6 cells/well in each well of a 6 well plate, in 2.5 mL of complete media. The plate was then placed in the incubator for 24 hours to allow the cells to fully adhere and recover from any effects resulting from the protease activity of the trypsin. The cells were then removed from the incubator, washed, and 2 mL of doxorubicin-spiked media was then added to four of the wells, as in the clonogenic assay (but without the addition of antibiotics). The other two wells were used as negative controls for the purposes of creating a standard curve for HPLC analysis and checking that the numbers of cells in the treated wells was not substantially different from the control (i.e. that cells were not being killed very rapidly and being removed in the wash step, thus affecting the results).

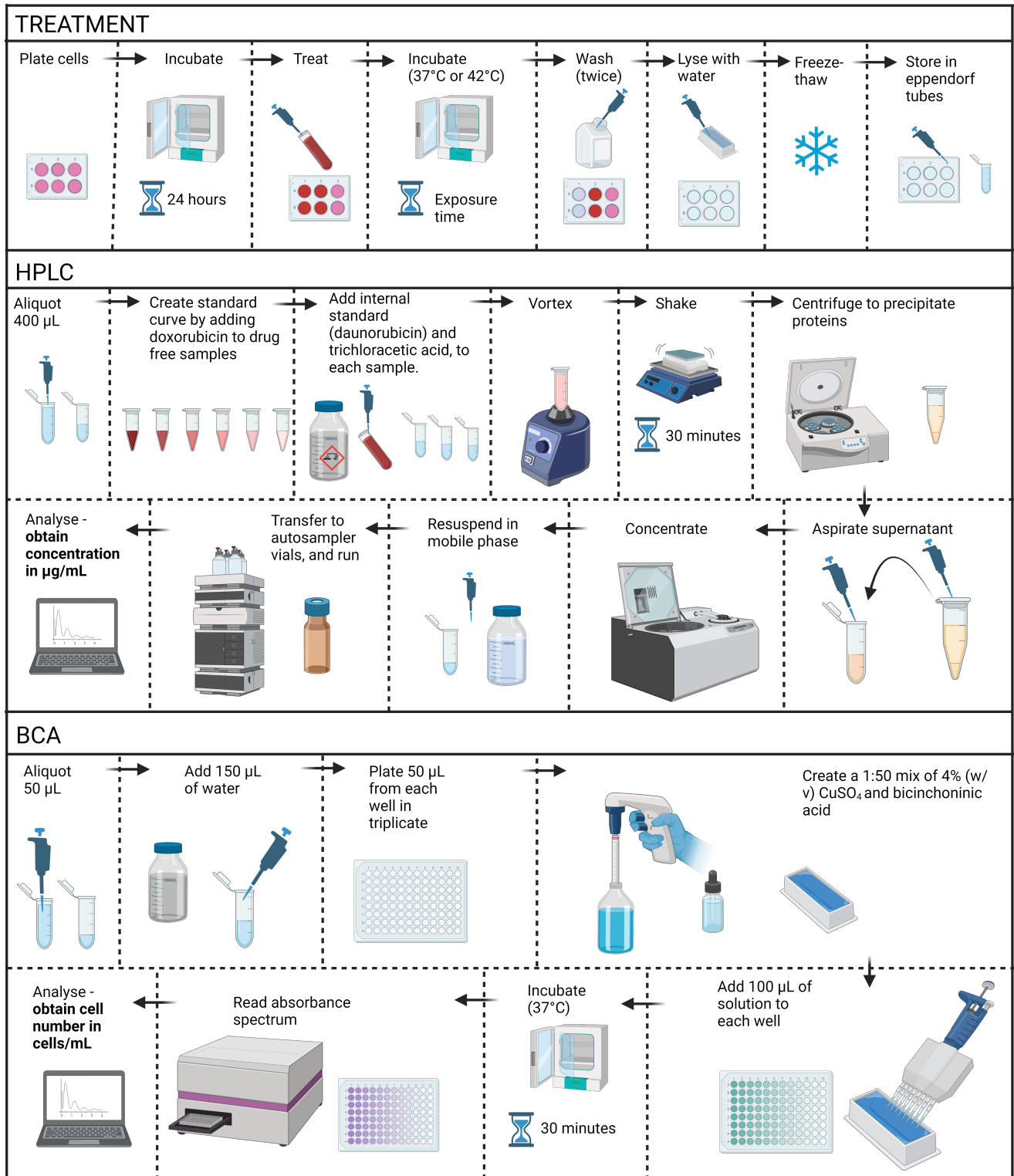


Figure 4.10. A diagram of the full protocol used to determine the intracellular concentration of doxorubicin in CT26 cells *in vitro*.

Following the second PBS wash after the removal of the drug, 1 mL of dH₂O was added to each well. The well plate was then immediately transferred to a -80 °C freezer.

The bicinchoninic acid (BCA) assay was used to provide an estimate of the number of the cells in the sample. 50 μ L of each sample was aliquoted into a new Eppendorf tube, and diluted with the addition of 150 μ L of deionised water. 50 μ L of this dilution was pipetted into three wells of a flat bottom 96 well plate (Corning 96-well Clear Flat Bottom Polystyrene TC-treated Microplates, Corning), and 100 μ L of a 1:50 mix of 4% (w/v) copper sulfate solution (Merck, C2284) and bicinchoninic acid (Merck, B9643) was added to each sample. The well plate was then incubated at 37 °C for 30 minutes, before an absorbance spectrum of each well was measured on a plate reader (Fluostar Omega, BMG Labtech).

To create the calibration curve, three 6 well plates were prepared from different flasks of CT26 cells, with 0, 0.4, 0.8, 1, 1.2 and 1.4 million cells per well. These flasks were incubated for 24 hours, before being washed gently twice with PBS, and lysed with 1 mL of deionised water, as in the cell culture protocol for treatment. The samples were prepared as above, and absorbance spectra measured for each sample. A calibration curve was produced by defining the BCA signal as the value obtained by subtracting the background absorbance (taken to be that at 700 nm) from the absorbance peak due to the BCA assay at 562 nm.

The HPLC analysis was performed using 400 μ L of lysate. First, the standard curve was prepared, by spiking the lysate with doxorubicin in methanol, and making up the final volume of all the standards to 500 μ L with methanol. The standard concentrations were 0, 0.2, 0.4, 0.6, 0.8, 1.0 and 2.0 μ g/mL. All samples were then also made up to 500 μ L with the addition of 100 μ L of methanol, before adding 10 μ L of 100 μ g/mL of daunorubicin solution to all samples and standards such that all samples and standards had a total volume of 510 μ L with 1 μ g of IS.

A 35% stock solution of trichloroacetic acid (TCA) was made up in water, and 90 μ L was added to each sample and standard. This results in each sample and standard having a TCA concentration of just over 5%, which is consistent with literature values for this sort of sample preparation. This preparation was done in a cold room (4 °C), as the process is more efficient when the reagents are cold [173].

Each sample and standard was then vortexed and shaken for 30 minutes at 320 min^{-1} on an orbital shaker (KS 130 Basic, IKA England Ltd.) while protected from light, before being spun at $18000 \times g$ for 15 minutes to pellet the proteins. $450 \mu\text{L}$ of the supernatant was aspirated into a fresh eppendorf tube, and the samples were concentrated using a centrifuge concentrator (Eppendorf Concentrator Plus, Eppendorf), increasing the vacuum level applied gradually to avoid sample loss - the vacuum level was set first for highly volatile solvents for 10 minutes, then for alcohols for 20 minutes, and then for aqueous solvents. Initially, the concentrator was left to run for 80 minutes on the highest setting, then run for 20 minutes at a time until the samples were dry.

The samples were then resuspended in $25 \mu\text{L}$ of 20% acetonitrile (ACN), 79.9% water and 0.1% formic acid (FA). The tubes were then shaken for 30 minutes again at 320 min^{-1} , before being gently centrifuge at $300 \times g$ for two minutes to ensure the liquid was at the bottom of the tube. The samples and standards were then pipetted in HPLC sample vials (Merck, SU8611362) and placed into autosampler vials. The presence of the formic acid is common in reversed-phase chromatography, as it minimises the negative charge on the stationary phase by protonating the silanols. The HPLC method was an isocratic elution, with 24.95% ACN and 74.95% water with 0.1% FA, at a flow rate of 0.6 mL/min , with $4 \mu\text{L}$ of each sample being injected. The autosampler was protected from light and refrigerated to 4°C during the run. The column oven was heated to 40°C , with a C18 column (ZORBAX RRHD Eclipse Plus C18, 95\AA , $2.1 \times 50 \text{ mm}$, $1.8 \mu\text{m}$, Agilent Technologies).

The run-time for each sample was set to seven minutes, which was found to be sufficient to allow both the doxorubicin and daunorubicin to elute. The samples were resuspended in a weaker solvent than was used for the mobile phase, as is standard practice in HPLC sample preparation (a weaker solvent in this case has more water and less ACN (or organic solvent), and is called weak because it has less ability to strip analyte from the column). This is because resuspension in a stronger solvent than the mobile phase means that locally, some analyte will remain in the solvent, and its behaviour in the column will become unpredictable, resulting in multiple peaks.

The analytes were passed through both UV and fluorescence detectors, with only the data from the fluorescence detector (Agilent, G7121B) being analysed. The fluorescence detector had excitation-emission wavelengths of 480 and 560 nm respectively. The signals were then processed in MATLAB, with appropriate integration limits for doxorubicin and daunorubicin being identified from plots of the fluorescence trace. For each trace, an average background signal was subtracted, then the MATLAB

function 'trapz' was used to integrate the curve between the limits. The ratio of the areas between the peaks corresponding to doxorubicin and daunorubicin was taken to account for loss of drug during sample preparation. These ratios were then used to calculate a standard curve, which was fitted in MATLAB using the Curve Fitting Toolbox (Mathworks, 2022), minimising the sum of squared residuals. Once the concentrations in each of the vials had been calculated, these were used to find the total amount of drug in each sample.

4.6.1 Results

The full data-set of concentrations is presented in Figure 4.11. For all treatment conditions and temperatures, $n = 4$, except for the 60 minute normothermic 0.25 and 1 $\mu\text{g}/\text{mL}$ groups in which $n = 3$, as one sample from each group was lost during processing. A further plot of the results, plotted against time, and further broken down into several sub-plots is shown in Figure 4.12.

A two-way ANOVA was performed on the log-transformed intracellular concentration against treatment condition (i.e. doxorubicin concentration and exposure duration) and hyperthermia/normothermia, in a way that is analogous to the ANOVA performed for the cell viability data. There was a significant increase in intracellular doxorubicin between hyperthermic and normothermic treatment for given treatment conditions ($p=0.008$). There was also a significant difference ($p<0.001$) between treatment conditions, which is to say that cells treated with different concentrations and exposure times had different intracellular concentrations (which was expected). The interaction between treatment condition and mild hyperthermia/normothermia was not found to be significant ($p=0.2647$), suggesting that the increase in uptake at elevated temperature is not a function of treatment condition.

4.6.2 Comparing Cell Counting with Trypan Blue Exclusion and the Bicinchoninic Acid Assay

For a number of test plates, the bicinchoninic acid assay approach was compared to a cell count. Three wells were treated as above, while the remaining three were rescued with 0.5 mL of trypsin solution for five minutes, before 2 mL of complete media was added to each well, and 100 μL of the resulting suspension was counted with trypan blue as previously described. The resulting cell counts gave results which were similar (albeit with slightly less variation) than those from the corresponding BCA assays.

Additionally, two sets of T75 flasks ($n = 3$) were treated with 4 $\mu\text{g}/\text{mL}$ for one hour in normothermic

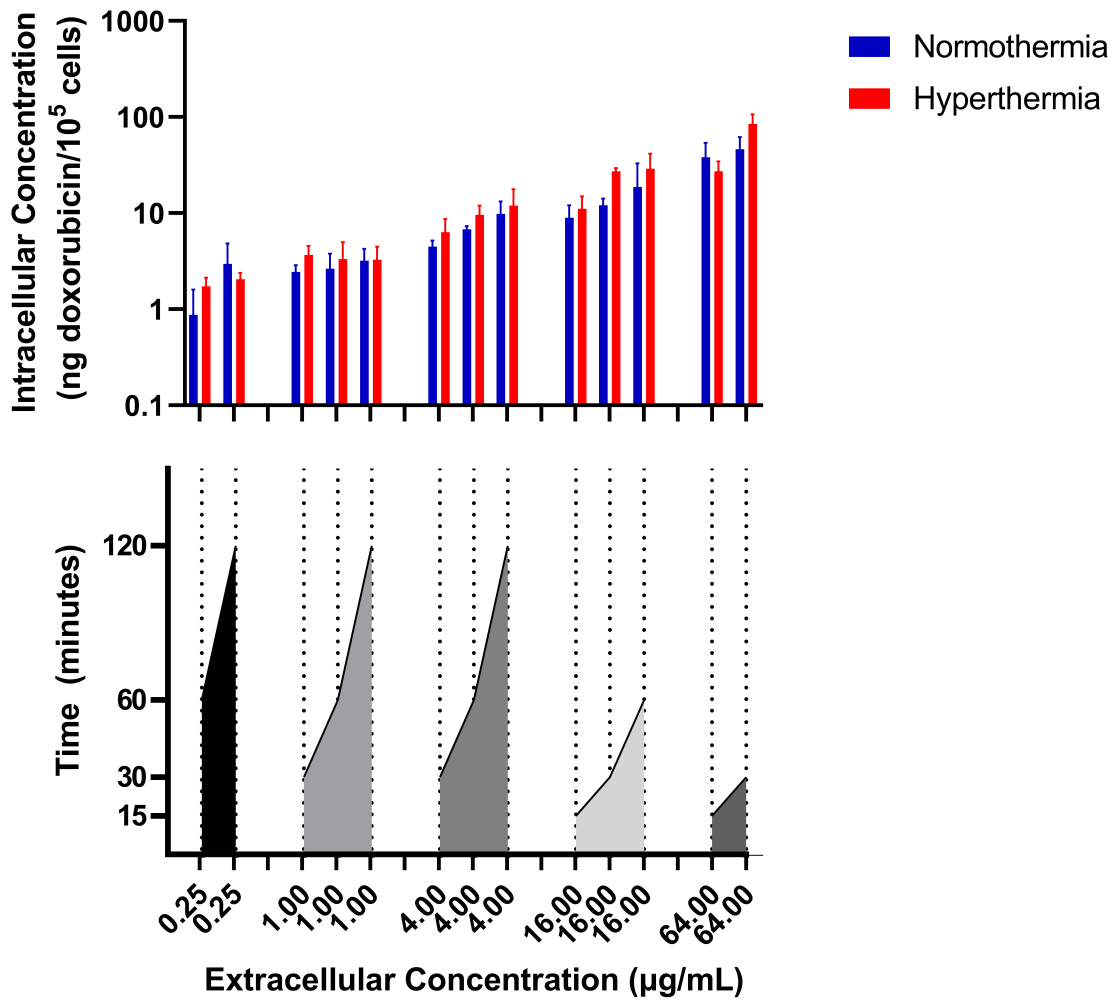


Figure 4.11. The full data-set of obtained intracellular concentrations. The top panel shows the mean and standard deviation of the measured concentrations ($n = 4$, except for the 60 minute normothermic 0.25 and 1 $\mu\text{g/mL}$ groups, where $n = 3$ due to lost samples). The bottom panel describes the treatment condition (extracellular concentration and exposure duration) to which the measured intracellular concentration shown in the top panel corresponds.

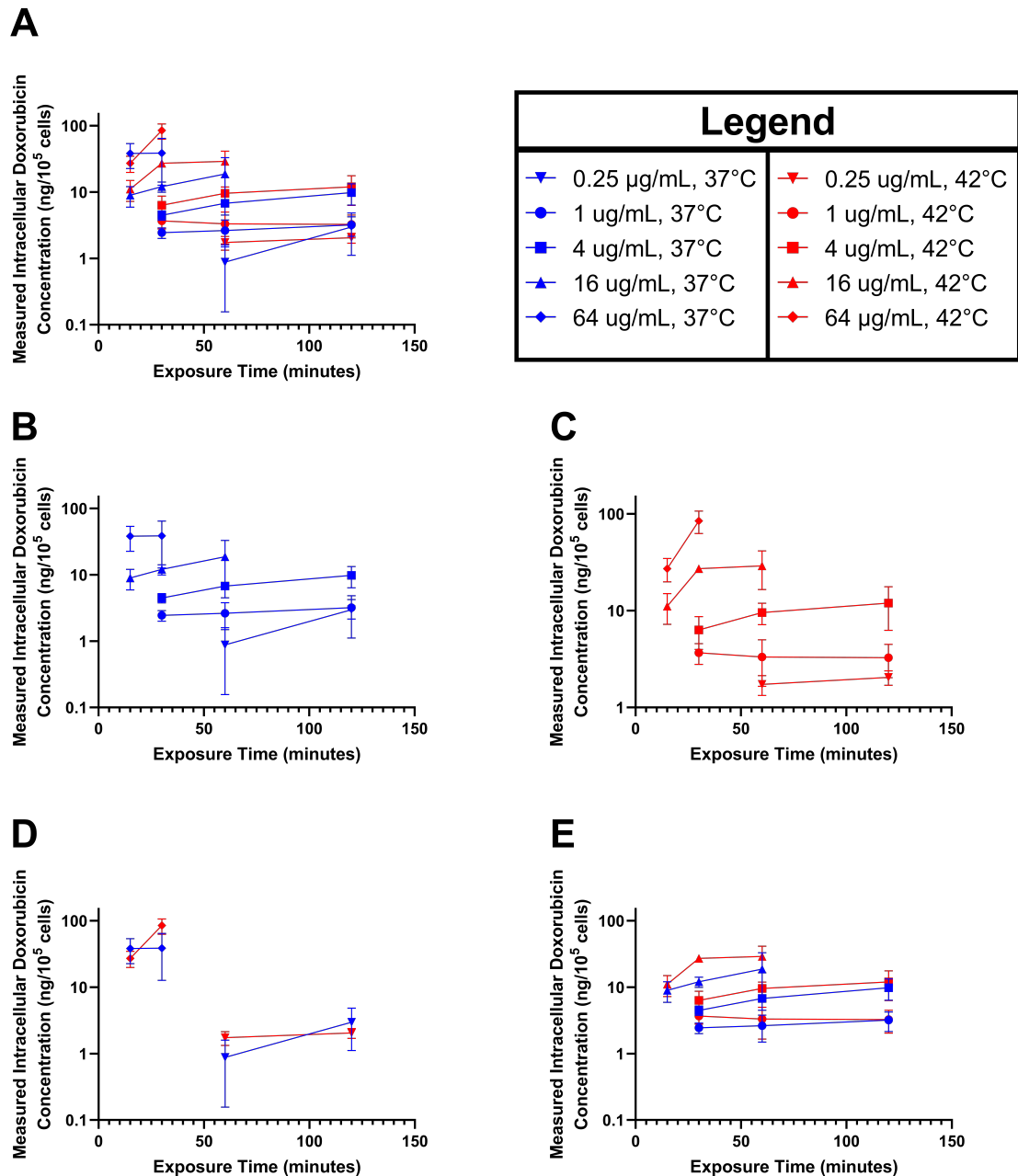


Figure 4.12. Intracellular concentrations of doxorubicin against exposure time. A) shows all of the measured data points together, B) shows only the normothermic data, C) shows only the hyperthermic data. D) and E) are a breakdown of the full data set. D) shows only the intracellular concentrations measured at the extreme extracellular concentrations (i.e. 0.25 and 64 μ g/mL), and E) shows the remaining three concentrations. This was done to aid data visualisation, as it can be observed more clearly here than in A, that at all data points, the mean concentration measured for a given treatment condition at mild hyperthermia is greater than the corresponding normothermic treatment, with the exception of the two points which can clearly be seen in D, the 30 minute, 64 μ g/mL and the 60 minute 0.25 μ g/mL exposures. In all plots the data plotted are the mean and standard deviation of $n = 4$ (except for the 60 minute normothermic 0.25 and 1 μ g/mL groups, where $n = 3$ due to lost samples).

		BCA Assay	Trypan Blue
Normothermia	Mean (ng/10 ⁵ cells)	6.76	5.01
	S.D.	0.54	0.85
Hyperthermia	Mean (ng/10 ⁵ cells)	9.56	9.92
	S.D.	2.38	1.15

Table 4.5. Intracellular concentrations resulting from a comparison between treating the cells in a 6 well plate format, using a BCA assay to estimate the number of cells, and treating the cells in a T75 flask, using cell counting with trypan blue to find the number of cells. The cells were treated with 4 μ g/mL of doxorubicin for one hour at 37°C. S.D. = Standard Deviation.

and hyperthermic conditions. This protocol is more similar to that used by previous studies (which could, therefore, be considered the literature ‘gold-standard’), such as [102]. It is important, therefore, to ensure that the results from the BCA assay approach were similar to this.

The results of the experiment comparing the data obtained from cell counts performed by rescuing the cells with trypsin and staining with trypan blue against the method used in this thesis, of approximating the cell number via a BCA protein assay are shown in Table 4.5. Comparing the BCA assay to the trypan blue counting, the hyperthermic results are clearly in good agreement with each other. The normothermic results are slightly different, with the mean concentration in the trypan blue group being lower than that from the BCA group. This may be expected, since rescuing the cells with trypsin represents a ten minute period during which the cells are effectively in perfect sink conditions (five minutes while being trypsinised, then an additional five minutes while being spun down so that the pellet can be lysed with water), during which the elevated internal concentrations would result in an efflux of drug from the cells. This would represent a particularly problematic part of the protocol for 15 and 30 minute exposures. However, considering the results together, and acknowledging that different protocols cannot be expected to produce identical results (considering, for example, the different rates of thermal equilibration of the media in the incubator in the T75 flasks used for trypan blue staining compared to the smaller fluid volumes in the 6 well plate format used with the BCA assay), the mean values are close enough that the new protocol used here, employing a BCA assay, is acceptable.

4.7 Combining Viability and Intracellular Concentration

4.7.1 Intracellular Concentration - An Acceptable Metric for Cell Kill?

The data from the experiments to determine intracellular concentration for given exposure conditions are plotted against the survival data obtained from the clonogenic assays in Figure 4.13. The data show that intracellular concentration is correlated with cell kill, as expected, meaning that maximising the intracellular concentration of doxorubicin is an appropriate metric by which to optimise treatment with thermosensitive liposomal doxorubicin as presented in the next chapter.

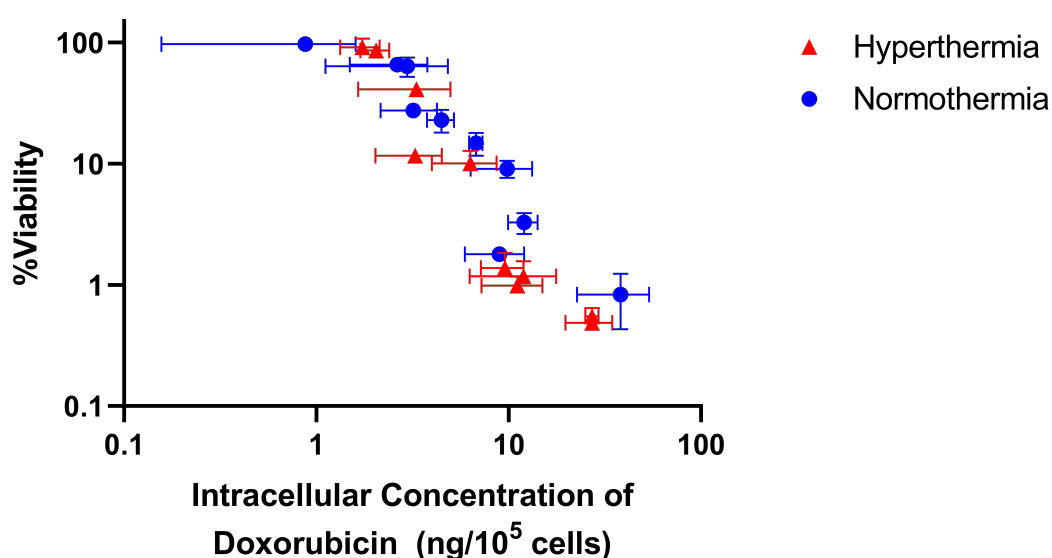


Figure 4.13. The results from the clonogenic assays plotted against the intracellular concentrations determined from the HPLC assay.

Hill models were fitted to the normothermic and hyperthermic data, as well as for a 'grouped' model, fitted on all the data points, and the two separate models are shown in Figure 4.14. The equation was fitted to the log transformed survival data, using a least squares regression in GraphPad PRISM, i.e.

$$\log Y = \log \frac{100}{1 + \left(\frac{IC_{50}}{X}\right)^s} \quad (4.3)$$

where Y is the % survival, X is the measured intracellular concentration, IC_{50} is the intracellular concentration associated with 50% cell kill, and s is the Hill Slope. The fitting did not take the uncertainty in the intracellular concentration into account. An extra sum-of-squares F test was used to compare the choice of a single grouped model or two separate models for temperature condition.

	Hyperthermia	Normothermia
IC50 (ng/10 ⁵ cells) (95 % Confidence Interval)	1.904 (1.428, 2.443)	2.290 (1.690, 2.944)
Hill Slope (95 % Confidence Interval)	-2.195 (-2.534, -1.879)	-1.902 (-2.249, -1.575)

Table 4.6. Parameters from the fitted Hill Models for cell survival

The null hypothesis, that the improvement in the fit as a result of two separate models was down only to chance was rejected, with a p-value of 0.0003. This suggests that, if the Hill Model is an appropriate form, cell kill has a different dependence on intracellular concentration under normothermic conditions compared to under conditions of mild hyperthermia. This is not unexpected, as the literature suggests that mild hyperthermia inhibits DNA repair [110]; from which one would expect a lower IC50, since the same amount of intracellular drug would result in the same or increased kill under hyperthermic conditions when DNA repair is inhibited. The parameter values are displayed in Table 4.6, from which it can be seen that the fitted value of IC50 is lower in the hyperthermic group, however care must be taken not to over-interpret this owing to the unaccounted for uncertainty in intracellular concentration and the substantial overlap in the 95% confidence intervals for the two IC50s.

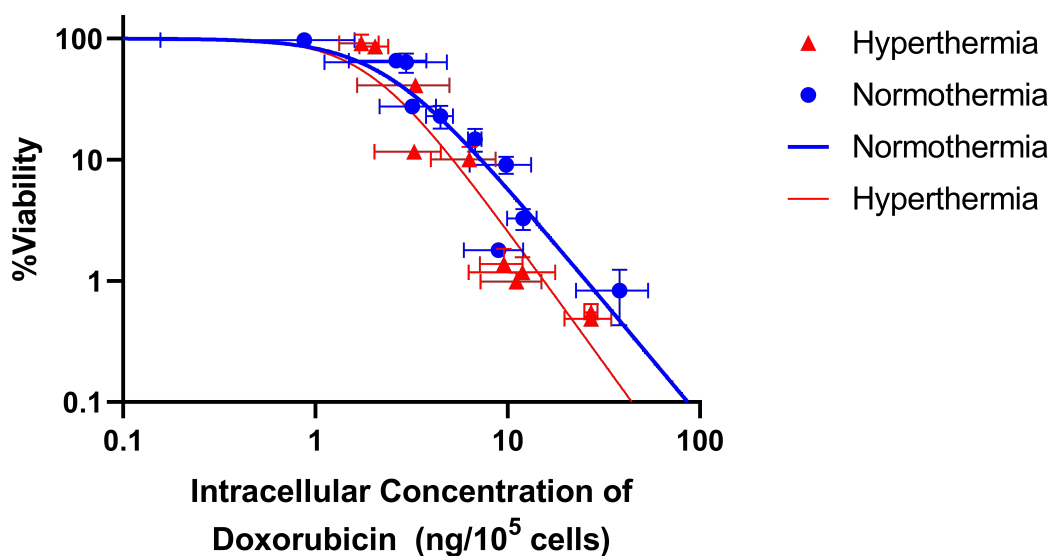


Figure 4.14. The same results as plotted in Figure 4.13, with the two Hill Model fits for survival also shown.

4.7.2 Mathematical Models for Cellular Uptake of Doxorubicin in CT26 Cells

To fit the cellular uptake data, all possible combinations of the following model, involving at least one influx and one efflux term were fitted to the data:

$$\frac{dc_i}{dt} = k_{in}c_e + \frac{V_{m,in}c_e}{K_{m,in} + c_e} - k_{out}c_e - \frac{V_{m,out}c_i}{K_{m,out} + c_i} - k_n c_i \quad (4.4)$$

$$\frac{dc_n}{dt} = k_n c_i \quad (4.5)$$

where k_{in} and k_{out} are terms associated with linear influx and efflux, $V_{m,in}$ is the maximum rate of saturable transport into the cell, and $V_{m,out}$ is the equivalent rate out of the cell. $K_{m,in}$ and $K_{m,out}$ are the Michaelis constants for transport into and out of the cell respectively, and represent the concentrations at which the contribution from the saturable term equals $\frac{V_m}{2}$. Contributions from nuclear binding were included using k_n ; in the case where nuclear binding was modelled the intracellular concentration was given by $c_i + c_n$, where c_n is the nuclear bound concentration of drug. These terms were used to reflect the saturable terms used by El-Kareh and Secomb [67], the linear and saturable combination used by Gasselhuber and others [66], and the nuclear binding model used by McKenna and others [104].

The model was fitted to the log-transformed data to normalise the error. The fit was conducted using MATLAB's `lsqcurvefit`, with the terms fitted as exponentials to constrain the values to be positive. For example, considering a purely linear model:

$$\frac{dc_i}{dt} = e^{(\theta_1 + \delta_{hyp}\theta_2)} c_e - e^{(\theta_3 + \delta_{hyp}\theta_4)} c_i \quad (4.6)$$

As can be seen from the above equation, the hyperthermic terms were fitted at the same time as the normothermic terms by means of including a delta function, δ_{hyp} , which takes a value of 0 when the data point being fitted was recorded at 37°C, and 1 when the value was recorded at 42°C. This has the effect of the hyperthermic constant functioning as a ratio between the normothermic and hyperthermic terms, so $\theta_1 = \log k_{in}$, $\theta_2 = \log\left(\frac{k_{in,hyp}}{k_{in}}\right)$, $\theta_3 = \log k_{out}$, and $\theta_4 = \log\left(\frac{k_{out,hyp}}{k_{out}}\right)$. The further advantage of this approach, is that if the 95% confidence interval for the ratio does not include one, it can be said that the term in the hyperthermic fit is significantly different from the corresponding term in the normothermic fit.

The model fits were compared using the AIC corrected for small sample size (AIC_c) [174]

$$AIC_c = N \log\left(\frac{\sum_i (\hat{y}_i - y_i)^2}{N}\right) + 2p + \frac{2p(1+p)}{N-1-p} \quad (4.7)$$

in which N is the number of samples, p is the number of parameters, \hat{y}_i is the model estimated value

Equation	AIC _c for Single Model for Both Conditions	AIC _c for Separate Models for Normothermic and Hyperthermic Conditions
$\frac{dc_i}{dt} = k_{in}c_e + \frac{V_{m,in}c_e}{K_{m,in}+c_e} - k_{out}c_i$	-160.8	-164.1
$\frac{dc_i}{dt} = k_{in}c_e + \frac{V_{m,in}c_e}{K_{m,in}+c_e} - k_{out}c_i - k_n c_i$ $\frac{dc_n}{dt} = k_n c_i$ $c_{i,total} = c_i + c_n$	-159.3	-165.8

Table 4.7. The Akaike Information Criterion for small sample size (AIC_c) values, calculated using Equation 4.7 for the four best fitting models.

of y_i . The four best fitting models (determined by the lowest AIC_c) had the AIC_cs presented below in Table 4.7.

These values of AIC_c are quite close together (especially compared to those generated by the other models). Clearly, the AIC_cs suggest that the most complicated of the four models in the above table is the best fitting, with the improved fit compensating for the increased number of parameters. However, with the small difference between the AIC_c values, choosing any of these models is justifiable; for instance, comparing the separate models for normothermia and hyperthermia with and without nuclear binding with an extra sum-of-squares F test yields a p-value of 0.0582; in other words, we cannot reject the hypothesis that the improvement in fit as a result of the nuclear binding term is down to chance using the conventional (and completely arbitrary) threshold of $p = 0.05$.

Considering the above arguments, it is worth considering if there are any other reasons not to use the model with the smallest AIC_c. There are two important considerations for choosing any model including a nuclear binding term. Firstly, that the nuclear binding model displays non-physical behaviour at longer times; the nucleus must, at some point, saturate, due to a limited number of binding sites, and creating a model including this behaviour would require an additional parameter. Secondly, although we know that nuclear binding is important in the mechanism of action of doxorubicin, there is insufficient literature data to know if this parameter value is reasonable, and the experimental data in this work provide no way of quantifying the nuclear doxorubicin. Consequently, given the closeness of the AIC_c values, the model without a nuclear binding term is chosen for use from this point onwards. An additional bonus of using this model, as opposed to one with nuclear binding, is the reduced complexity of implementation. Mathematically, the model is described by:

$$\frac{dc_i}{dt} = k_{in}c_e + \frac{V_{m,in}c_e}{K_{m,in} + c_e} - k_{out}c_e \quad (4.8)$$

with the parameter values (and 95% confidence intervals) as presented in Table 4.8. The model fits against time and concentration are presented in Figures 4.15 and 4.16.

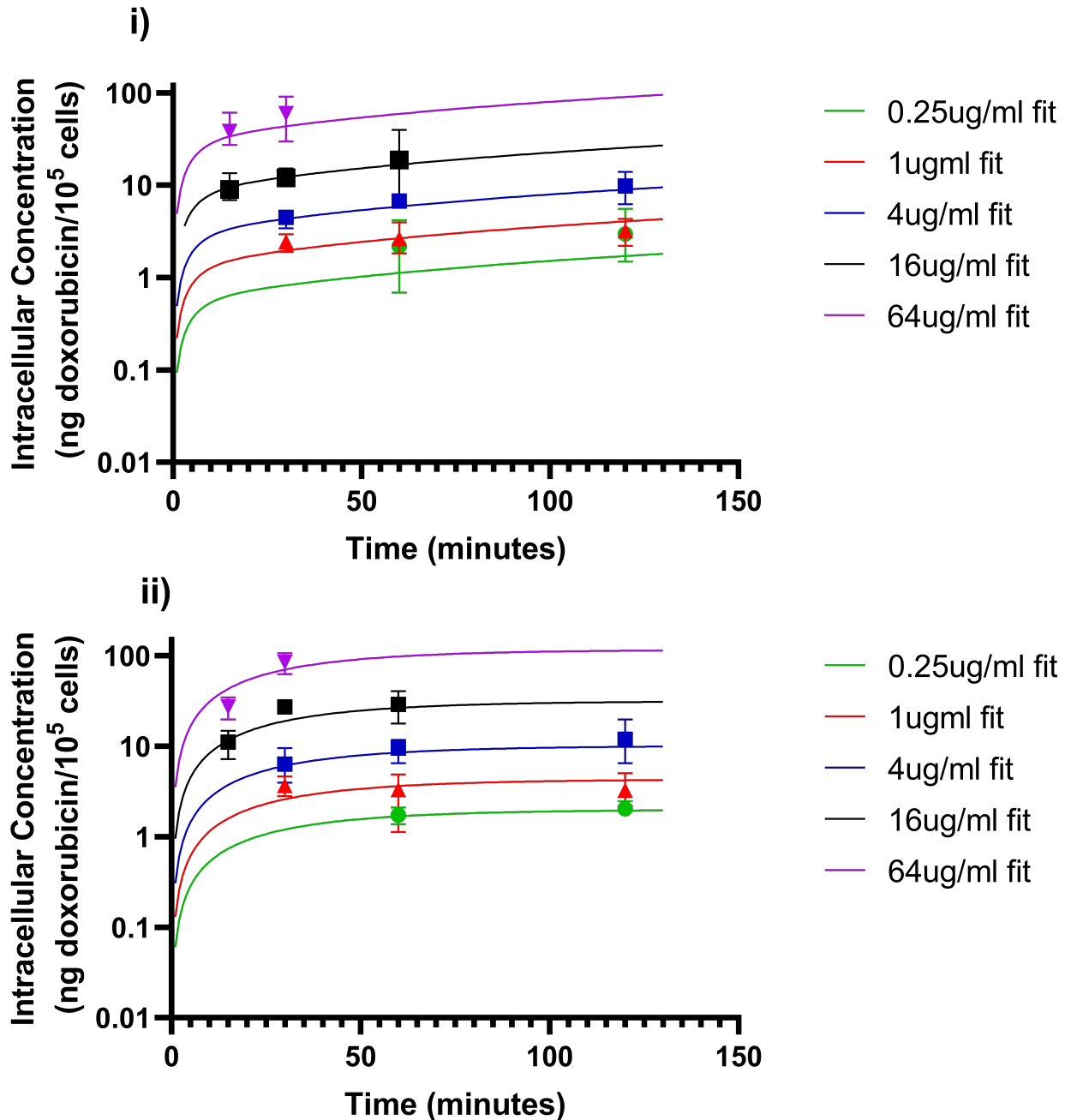


Figure 4.15. Plot of the separate fits of cellular uptake of doxorubicin for (i) normothermia and (ii) hyperthermia against time, with data points shown as mean and range of $n = 4$ (except for the 60 minute normothermic 0.25 and 1 $\mu\text{g}/\text{mL}$ groups in which $n = 3$).

First, examining the parameter values, it can be seen that the only ratio for which the 95% confidence

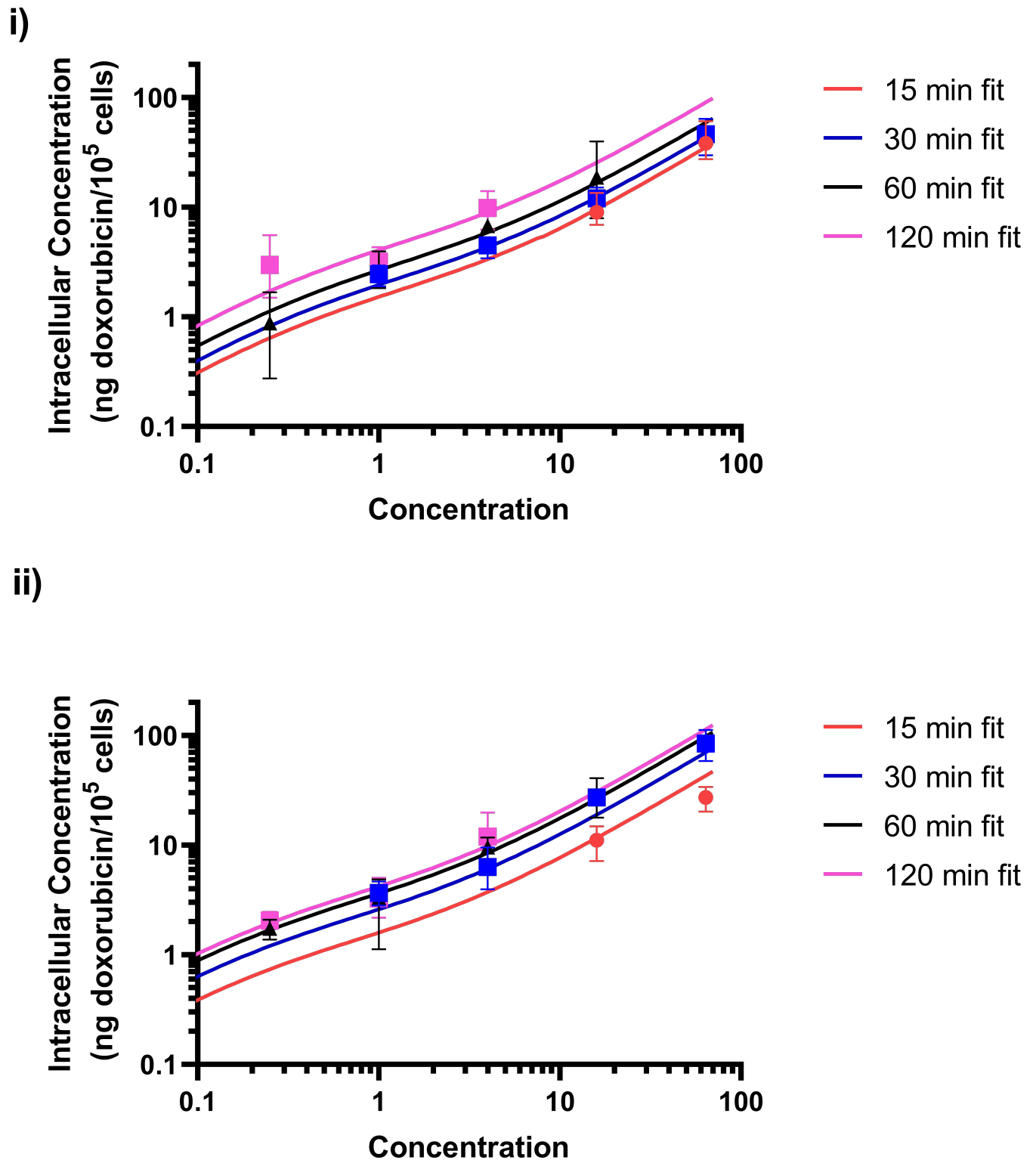


Figure 4.16. Plot of the separate fits of cellular uptake of doxorubicin for (i) normothermia and (ii) hyperthermia against extracellular concentration, with data points shown as mean and range of $n = 4$ (except for the 60 minute normothermic 0.25 and 1 $\mu\text{g}/\text{mL}$ groups in which $n = 3$).

Parameter	Units	Separate Model (95% CI)	Combined Model (95% CI)
k_{in}	$\frac{[\text{ng}/10^5 \text{ cells}]}{[\mu\text{g}/\text{mL}\cdot\text{min}]}$	0.03418 (0.02544 - 0.04593)	0.04342 (0.03466 - 0.05439)
$V_{m,in}$	$\frac{[\text{ng}/10^5 \text{ cells}]}{[\text{min}]}$	0.07786 (0.02984 - 0.20316)	0.09219 (0.04525 - 0.18782)
$K_{m,in}$	$\mu\text{g}/\text{mL}$	0.36040 (0.07455 - 1.74219)	0.31918 (0.09696 - 1.05076)
k_{out}	$\frac{1}{\text{min}}$	0.02409 (0.01253 - 0.04633)	0.02825 (0.01774 - 0.04498)
$\frac{k_{in,hyp}}{k_{in,norm}}$	-	1.59082 (1.03467 - 2.44592)	N/A
$\frac{V_{m,in,hyp}}{V_{m,in,norm}}$	-	1.27212 (0.31958 - 5.06379)	N/A
$\frac{K_{m,hyp}}{K_{m,norm}}$	-	0.74779 (0.07078 - 7.90072)	N/A
$\frac{k_{out,hyp}}{k_{out,norm}}$	-	1.27616 (0.51696 - 3.15028)	N/A

Table 4.8. Parameter values (and their 95% confidence intervals) obtained from the experimental data for the cellular uptake model defined by Equation 4.8.

interval does not include 1 is the linear influx term, which is significantly increased in the hyperthermic case; this is to be expected, since passive diffusion would be elevated at increased temperature. One notable outcome is that the predicted value of k_{out} is higher in the hyperthermic case, but by a lesser factor than k_{in} increases. This is supportive of the idea that mild hyperthermia modulates P-glycoprotein (efflux pump) activity, but 'the mechanism for hyperthermia-induced increase in drug uptake is mostly a result of enhanced membrane permeability' [116]. This is consistent with the increase in k_{out} observed here, as it is a lumped element term incorporating both passive diffusion across the membrane and active efflux.

The major consideration of the model output with regards to the bigger picture of improving delivery of doxorubicin from thermosensitive liposomes in the clinic is whether the effect of saturation has a large impact on the uptake of doxorubicin by cells. In all four of the models (with and without nuclear binding, with and without separate fits), linear uptake dominates the model at therapeutic concentrations. This is shown in Figure 4.17 for the model without nuclear binding. This suggests that cellular saturation should not be much of an issue going forwards in optimising delivery of doxorubicin (for example, transport of doxorubicin through the extracellular space may be a more important factor). It was considered during the analysis whether or not such a low saturable concentration could be a function of the selected data points, rather than explaining part of the biological process. This is possible, since the obtained Michaelis constants are not much above the smallest extracellular concentration used in the experiments, which means that the readings on which this term has the greatest influence are those measurements closest to the limit of quantification of the assay. As the obtained values are larger than the smallest tested concentrations, and there were five total data points at 0.25 and 1 $\mu\text{g/mL}$, this is acceptable, although it is acknowledged that future experiments should incorporate more samples in the 0.25 - 1 $\mu\text{g/mL}$ range.

The combined model is plotted against time in Figures 4.18 and 4.19, with the first plot showing all data points, while the second plot shows just the means of the normothermic and hyperthermic data points separately. The first figure shows that the combined model certainly provides a reasonable fit to the data, plotting the means of the two groups separately on the plot shows how there is an expected overprediction of concentration in the normothermic condition and underprediction of concentration in the hyperthermic condition. The two individual fits are clearly superior for the cases of having cells treated at the two conditions as described. However, going forwards into the next chapter, the combined model will be used. This decision is based on the fact that clinically treated

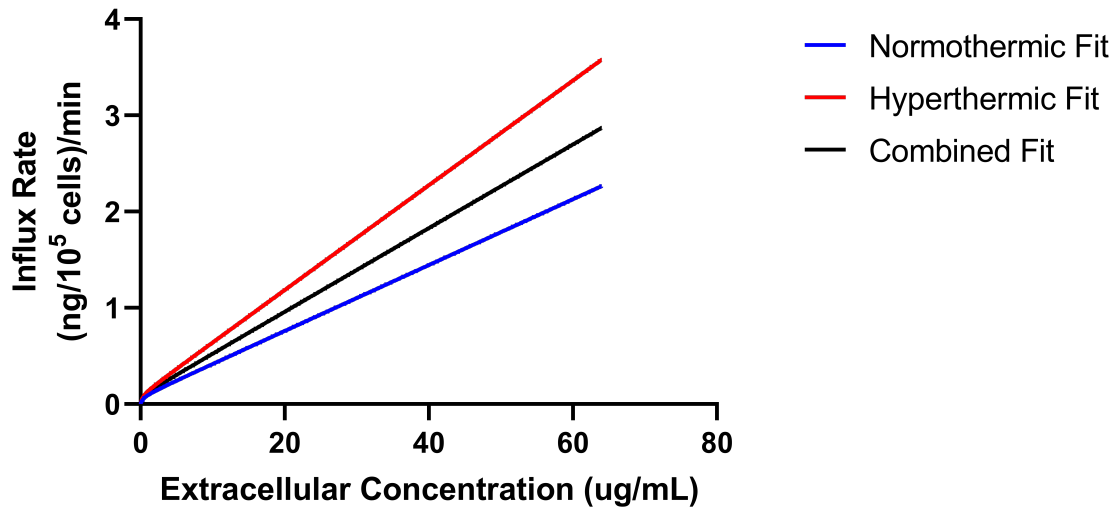


Figure 4.17. Plot of the predicted rates of cellular uptake for the models without nuclear binding, i.e. $y = k_{in}c_e + \frac{V_{m,in}c_e}{K_{m,in}+c_e}$.

solid tumours do not see a uniform state of normothermia, followed by hyperthermia, but rather cycle between the two, as the ultrasound beam passes across the tumour [87] (this argument extends to other heating modalities). Whilst it is certainly possible to model this by switching between the models during treatment, this adds complexity, and there is no evidence from these experiments what happens to cellular uptake of doxorubicin in the aftermath of reaching 42°C. This means there is no clear benefit to the accuracy of the model to introduce this complexity, and it has been decided that the best approach is to try and capture this behaviour with a grouped model.

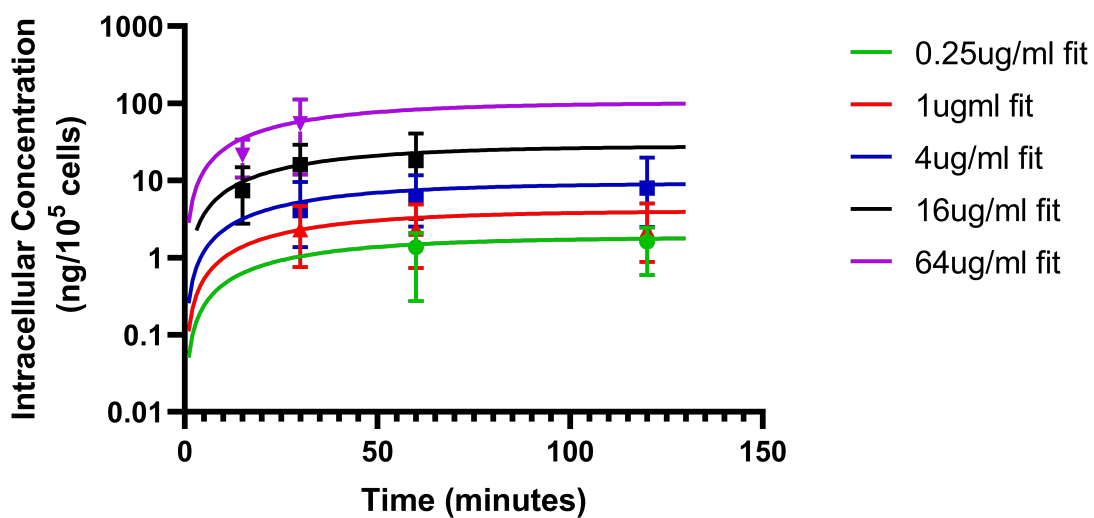


Figure 4.18. Plot of the combined normothermic and hyperthermic fit without nuclear binding against time, with the data points shown as mean ($n = 8$, except for the 60 minute 0.25 and 1 $\mu\text{g/mL}$ groups in which $n = 7$) and range.

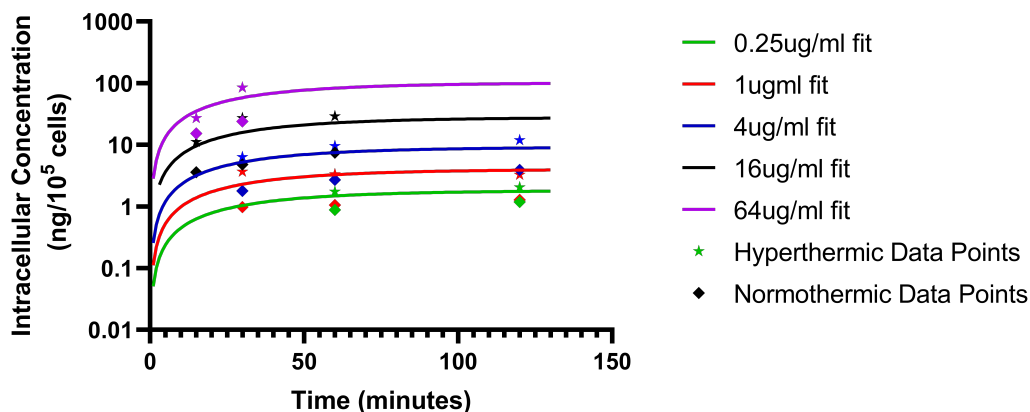


Figure 4.19. Plot showing the combined normothermic and hyperthermic fit without nuclear binding against time, with the mean values of the normothermic ($n = 4$, except for the 60 minute 0.25 and 1 $\mu\text{g}/\text{mL}$ groups in which $n = 3$) and hyperthermic ($n = 4$) data points are shown separately on the plot as stars and diamonds respectively.

One phenomenon which is observed in the experimental data is that it appears that equilibration may be being reached earlier in the hyperthermic case. Experimentally, this can be seen by examining Figure 4.12 D and E, which show that, except for the 64 $\mu\text{g}/\text{mL}$ data set, the hyperthermic concentrations appear to plateau earlier than the normothermic concentrations (if at all). The number of data points is too small to say anything of any certainty, except that this is something which would be interesting to investigate further. The idea of faster equilibration is seen in the mathematical models, since the solution at constant concentration is:

$$c_i = \left(k_{in}c_e + \frac{V_m c_e}{K_m + c_e} \right) \frac{(1 - e^{-k_{out}t})}{k_{out}} \quad (4.9)$$

which suggests that a characteristic time for the growth is given by $\frac{1}{k_{eff}}$; which is indeed smaller in the hyperthermic case, considering the values in Table 4.8. However further work is required to determine if this is a real effect, given the small number of data points and the lack of significant difference in the ratio between the normothermic and hyperthermic k_{eff} .

One assumption in the analysis - that the concentration of drug in the well can be modelled as approximately constant has been shown to be valid during the analysis of these results. For a two hour exposure to 0.25 $\mu\text{g}/\text{mL}$ the resulting intracellular concentration on the order of 1 $\text{ng}/10^5$ cells, means that the amount of drug inside cells is around 0.01 μg (based on a million cells/well). In 2 mL of spiked 0.25 $\mu\text{g}/\text{mL}$ media, there was initially 0.5 μg of doxorubicin, so 98% of the drug remains in the media, the concentration of which fell to 0.245 $\mu\text{g}/\text{mL}$. At the other end of the spectrum, considering 64 $\mu\text{g}/\text{mL}$ for 30 minutes, an intracellular concentration on the order of magnitude of 100 $\text{ng}/10^5$

cells is about $1 \mu\text{g}$ in the cells. $64 \mu\text{g/mL}$ equates to $128 \mu\text{g}$ in the well initially, so the percentage drop of the well concentration is even smaller in this case.

4.7.3 Combining Uptake and Cell Survival

It is possible to combine the expressions for cellular uptake and cell survival for a given extracellular concentration to obtain the required exposure time for $\alpha\%$ cell kill:

$$T = \frac{-1}{k_{out}} \log \left[1 - \left(\frac{IC50c_e}{k_{out}} \left(k_{in} + \frac{V_{m,in}}{K_{m,in} + c_e} \right) \right)^{-1} \left(\frac{\alpha}{100 - \alpha} \right)^{\frac{1}{s}} \right] \quad (4.10)$$

in which T is the time required to achieve the percentage cell kill, α . These can be plotted as isolines on a surface mapping cell survival, which is shown below in Figure 4.20.

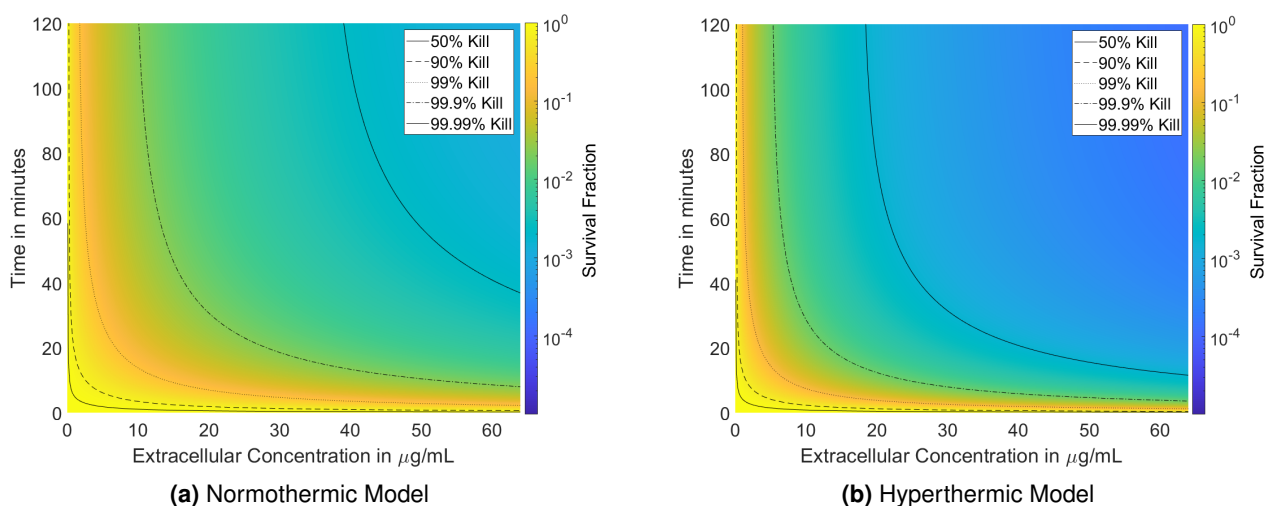


Figure 4.20. Plot of the cell survival predicted by the obtained mathematical models in normothermic (left) and hyperthermic (right) conditions, using separate models for cellular uptake.

Additionally, plots of projected survival for a 90 minute exposure across a range of extracellular concentrations and for $10 \mu\text{g/mL}$ exposure across a range of exposure times are plotted in Figures 4.21 and 4.22 respectively.

The mathematical models clearly predict a substantial increase in cell kill with hyperthermia in the window of concentrations which are most commonly seen therapeutically (around $5\text{--}10 \mu\text{g/mL}$ for 30 to 60 minutes). This is further demonstrated by the diverging survival curves in the two figures for a 90 minute exposure and $10 \mu\text{g/mL}$ exposure.

The marked effect is largely due to the sharp nature of the Hill curve cell kill relationship. This

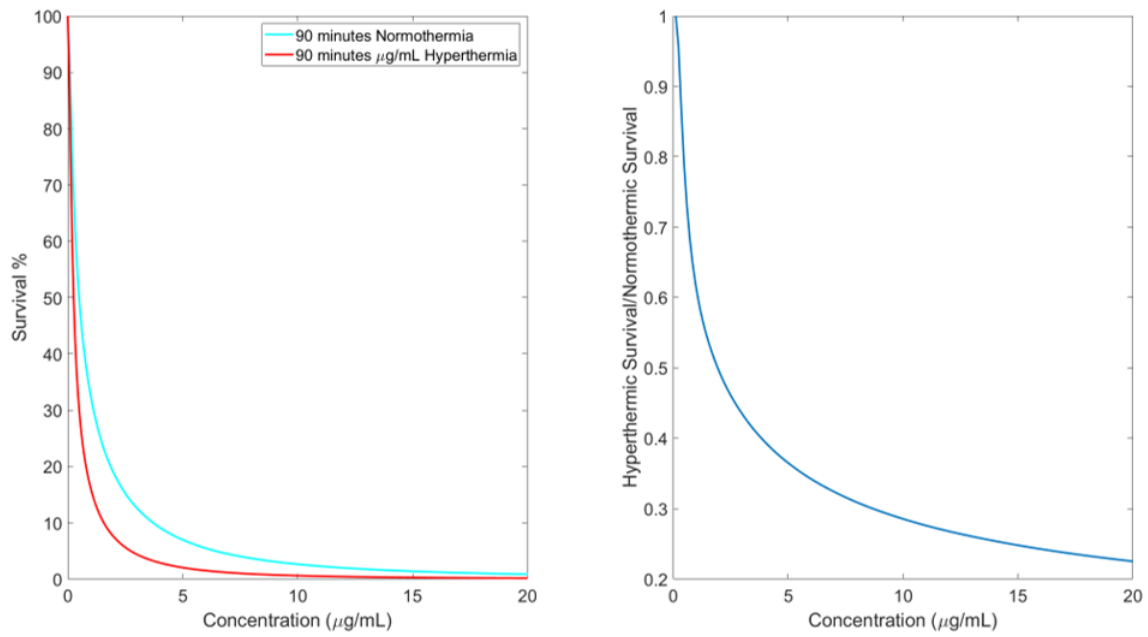


Figure 4.21. Plot of the predicted cell kill by the separate normothermic and hyperthermic models across a range of concentrations over a 90 minute exposure.

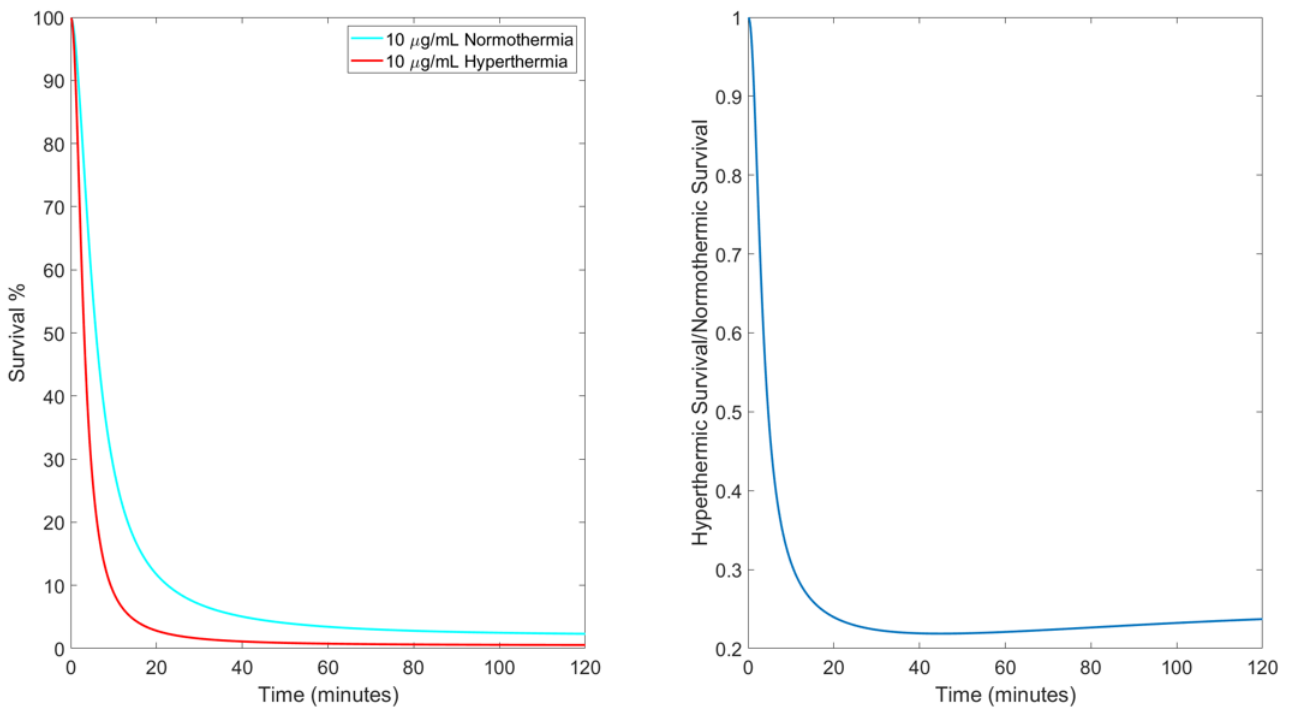


Figure 4.22. Plot of the predicted cell kill by the separate normothermic and hyperthermic models for a range of exposure times at a concentration of 10 $\mu\text{g/mL}$.

has resulted in the fact that although the individual effects (in terms of model parameters) may be small, their combined impact is important at clinically relevant concentrations. It is perhaps unfortunate that only one of the six corresponding pairs of parameters (four in each uptake model and two in each kill model) were significantly different between normothermic and hyperthermic conditions. With hindsight, given the non-linear nature of the model, only small changes in a few parameters would potentially be required to cause a large effect overall - and more data points would be required to ascertain which model parameters change for certain between hyperthermia and normothermia.

These findings are consistent with the wider literature around hyperthermia and treatment of cancer cell lines *in vitro* with doxorubicin, however, considering that these parameters are estimates, it is important to acknowledge the broad confidence intervals of the parameters. For cellular uptake at a constant extracellular concentration of 10 $\mu\text{g/mL}$, the 95% prediction bands (calculated using `nlpredci` in MATLAB) are plotted in Figure 4.23¹. Although different metrics discussed above suggest that separate models are justifiable, the relatively small data set in this thesis means that not too much weight should be given to the specific ratio values calculated in Figures 4.21 and 4.22.

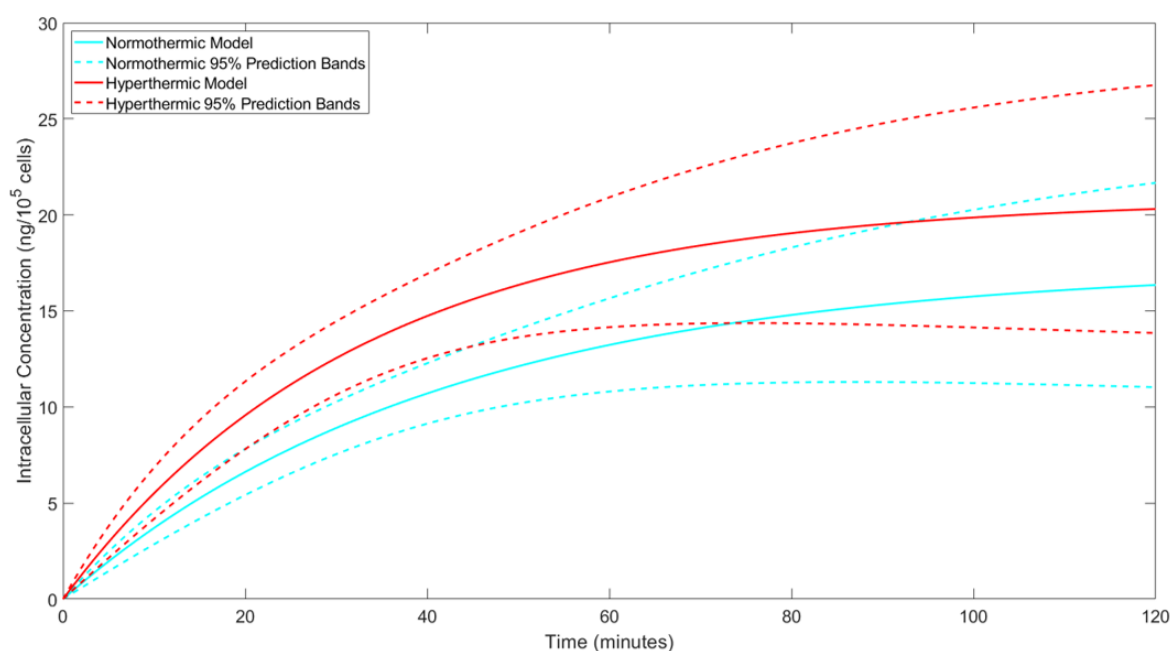


Figure 4.23. The predicted cellular uptake as exposure time varies for a constant 10 $\mu\text{g/mL}$ extracellular concentration of doxorubicin, with 95% prediction intervals.

The rationale for much of the work in this chapter began with a sensitivity analysis on the output of

¹Note that the plot in Figure 4.23 shows the range in which 95% of observations would be expected to fall; so is not a plot of a likely distribution of the 'true' model fits. An alternative approach would be to use bootstrapping to obtain a 95% confidence interval for the difference between the mean hyperthermic and normothermic intracellular concentrations for some given exposure conditions, although this has not been performed here, due to time limits.

a compartment model simulation of drug delivery through TSLs, which demonstrated that the uncertainty in the parameter values used in cellular uptake were the major causes of variability in the compartment model; this chapter ends with a similar sensitivity analysis on the mathematical models for cellular uptake of doxorubicin and cell kill by doxorubicin.

As in the previous chapter, the SAFE toolbox [143] was used to perform the sensitivity analysis, employing Latin hypercube sampling with a radial design, and $r = 1000$. The intracellular concentrations were calculated for the exposure durations and concentrations used in the experiments (0.25, 1, 4, and 16 $\mu\text{g}/\text{mL}$ for 15, 30, 60, and 120 minutes)². For each of these 16 conditions, the mean elementary effect and standard deviation were calculated ($r = 1000$), before the means of these values were calculated across the 16 different treatment conditions explored. The intracellular concentration in $\text{ng}/10^5$ cells was used as the output for the cellular uptake model (which was performed using the hyperthermic parameters), while \log_{10} of the % survival was used as the output for assessing the sensitivity of the survival prediction. The parameters were assumed to vary uniformly within the 95% confidence intervals that were obtained in this chapter.

The results are shown in Figures 4.24 and 4.25 for survival and intracellular concentration respectively. Considering the order of the Mean of EEs, although there is a little difference between the two plots, the two parameters (and associated ratios) which it would be most helpful to obtain more precise estimates of are V_m and k_{out} . The presence of V_m here is not very surprising, as the 95% confidence interval for V_m is very wide, spanning almost an order of magnitude. It would be valuable to consider sampling more data points closer to the estimated K_m , in order to provide closer bounds on the saturable term. As discussed in Future Work (Section 6.1), k_{out} could be better determined by separate experiments designed to look specifically at the efflux of drug from the cell.

The variation in the intracellular IC50 term is the Hill model parameter which causes the most variability in the survival output, and so, especially considering that the confidence interval for the IC50 parameter is underestimated in this chapter, it would also be beneficial to obtain a more precise estimate for this parameter. Researchers looking to more precisely determine the intracellular IC50 (which was not a primary motivator of this work) would be well-advised to use a protocol which allows the simultaneous measurement of cell kill and intracellular concentration, as opposed to determining these values in separate protocols; a good example of this is given in [175]. Furthermore,

²The sensitivity analysis was not performed using the higher 64 $\mu\text{g}/\text{mL}$ concentration, as it was felt that this represented an unusually high concentration which risked skewing the results of the analysis.

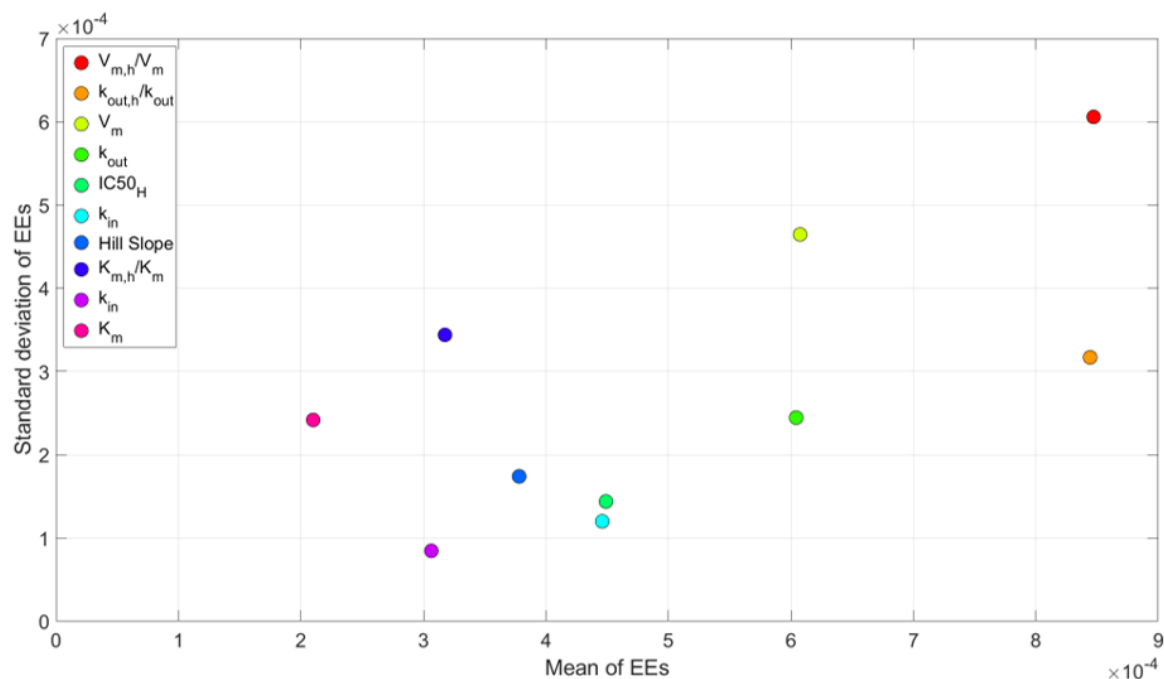


Figure 4.24. Results of the Elementary Effects Test on the log(survival) model for hyperthermic conditions. This represents of the mean of the elementary effects of the resulting survival from exposure at the conditions tested experimentally in this chapter (0.25, 1, 4, and 16 $\mu\text{g/mL}$ for 15, 30, 60, and 120 minutes).

combinations of exposure times and extracellular concentrations which give values of intracellular concentration close to the IC_{50} are necessary to refine this estimate, owing to the sharp nature of the Hill curve.

4.8 Summary

In this chapter, it was demonstrated that intracellular doxorubicin concentration is an acceptable metric for cell kill. A novel assay was used to determine the intracellular concentration of doxorubicin for a variety of extracellular concentrations at normothermic (37°C) and mildly hyperthermic (42°C) conditions.

In establishing cell viabilities, it was found that shorter-term assays for cytotoxicity, such as the MTS and trypan blue exclusion assays were not able to accurately resolve the cytotoxic effects of short term exposures to doxorubicin. A clonogenic assay, which measures the proliferative ability of cells more directly, reported much lower viabilities than either the MTS or trypan blue approaches, which is suggestive (in combination with the images of the cells obtained with a Celigo imaging cytometer) of some non-apoptotic mechanisms of cell death, such as mitotic catastrophe or the induction of cellular senescence. The clonogenic assay data demonstrate that cell kill by doxorubicin is significantly increased by the addition of mild hyperthermia.

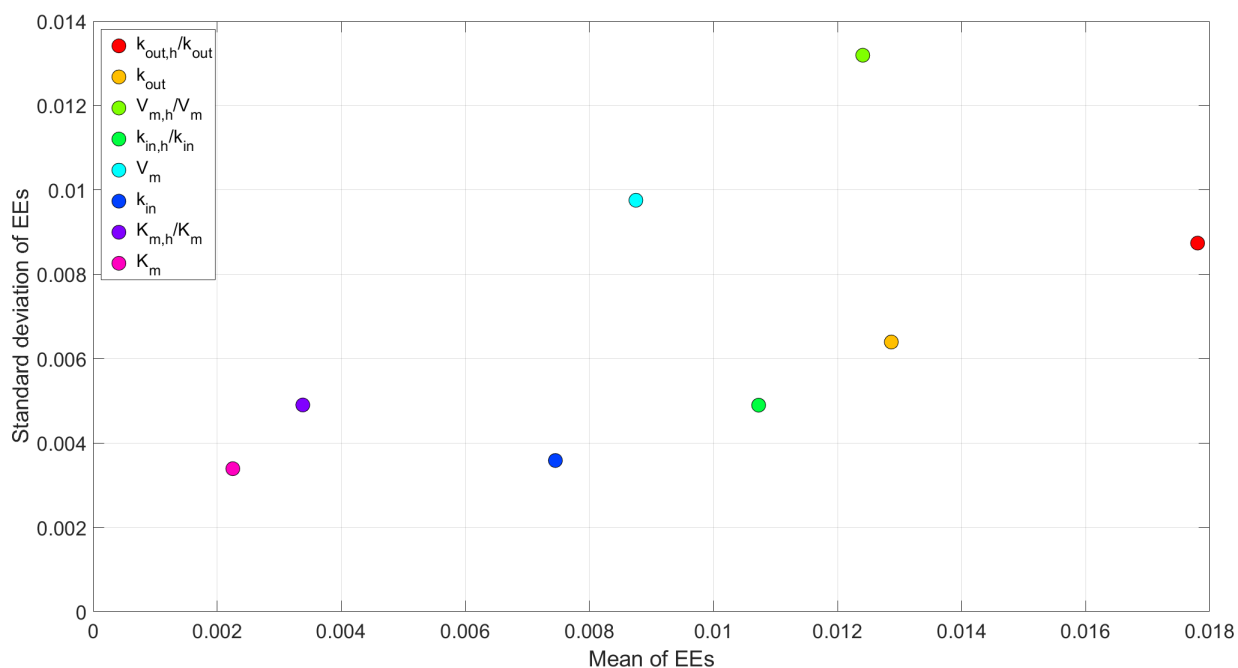


Figure 4.25. Results of the Elementary Effects Test on the cellular uptake model for hyperthermic conditions. This represents of the mean of the elementary effects of the resulting survival from exposure at the conditions tested experimentally in this chapter (0.25, 1, 4, and 16 $\mu\text{g}/\text{mL}$ for 15, 30, 60, and 120 minutes).

A mathematical model was fitted to the cellular uptake data, and the most appropriate mathematical model for cellular uptake of doxorubicin was found to include linear and saturable influx terms, and a linear efflux term, with the linear influx term being significantly increased by the addition of mild hyperthermia. Cellular uptake of doxorubicin by CT26 cells was found to be significantly increased by the addition of mild hyperthermia. A Hill model was fitted to the survival data with respect to intracellular drug concentration, in which the IC_{50} was lower in the hyperthermic case than in the normothermic case (although this was not significant).

Chapter 5

Optimised Thermosensitive Liposomal Drug Delivery to Patients Accounting for Spatial Variations

5.1 Introduction

The compartment model introduced in Chapter Three does not account for the spatial variations in concentration which are seen in real treatments as a result of the requirement for the drug to diffuse through the tissue following extravasation from the vasculature. Further causes of spatial heterogeneity include: uneven heat deposition, which will result in uneven quantities of drug released across the tumour; variations in cellular density in the tissue, as regions with higher cell density will see less drug per cell, which may limit penetration of the drug [e.g. 85]; and differences in vascularity through the tumour as more poorly vascularised regions with equivalent cell densities will similarly see reduced quantities of drug per cell.

In this chapter, the models of cellular uptake and cell kill obtained in the last chapter are used in a cylinder model to determine the importance of including spatial variations in the problem of optimising treatment with LTSL doxorubicin, and an LTSL formulation of a drug exhibiting more rapid uptake kinetics (such as idarubicin). These treatments are compared to the use of free doxorubicin, to establish whether (even with non-ideal heating) the use of LTSLs as a delivery platform should result in improved efficacy compared to the free drug alone.

In order to fairly compare the LTSL and unencapsulated treatments, the different optimal infusion

durations (assuming a fixed hyperthermia duration) must be determined for both therapies. As discussed further in Appendix A, this avoids the unfair comparison between a non-optimal use of unencapsulated drug and a near-optimal use of LTSL drug, such as comparing two bolus doses. Therefore, the optimal infusion durations for free and LTSL doxorubicin, as well as an LTSL form of a drug similar to idarubicin, are identified using a compartment model in the first section of this chapter. Ranges of infusion and hyperthermia durations which give rise to efficacious treatments are also identified.

The relative improvement in cell kill between the unencapsulated and LTSL forms is then calculated, before the predicted tumour plasma concentrations are used as inputs for cylinder models of the tumour. The impact of tissue radius and axial variation on the optimisation problem are then discussed. Finally, recommendations on how to optimise LTSL delivery and best use computational modelling to do so are presented.

5.2 Compartment Model with Hyperthermia

5.2.1 Optimal Free Doxorubicin Treatments

Using the new cellular uptake model described in the previous chapter, the compartment model from the first chapter was used to determine the optimum infusion duration (i.e. that which results in the largest peak intracellular concentration) for free doxorubicin, with parameters unchanged, except the cell volume, which was taken to be 2×10^{-9} mL, since, as discussed in Chapter 3, the previously used literature value is very small, and this has a large effect on the predicted biopsy concentrations. The peak intracellular concentration was obtained for infusion durations up to four hours, with a temporal resolution of one minute. By this metric, the optimal infusion duration was found to be 40 minutes, which corresponds to a peak intracellular concentration of $4.86 \text{ ng}/10^5$ cells. Using the Hill model for cell survival at normothermic conditions (Equation 4.3), this gives a survival fraction of 0.193. This represents the best possible treatment (in terms of peak intracellular concentration) with free doxorubicin alone.

A comparison between free doxorubicin and TSL doxorubicin should also be made for the case of free doxorubicin with hyperthermia. 90 minutes of hyperthermia was chosen in order to provide a quantitative comparison that was clinically feasible. For free doxorubicin with hyperthermia, the optimum infusion duration was 25 minutes, and the obtained peak intracellular concentration was

6.10 ng/10⁵ cells which, using the hyperthermic model of cell survival, gives a survival fraction of 0.072. The addition of 90 minutes of hyperthermia and the optimal use of free doxorubicin therefore facilitates a 1.26-fold increase in peak intracellular concentration, and a 2.68-fold reduction in cell survival. Interestingly, as long as the hyperthermia duration is 36 minutes or longer, the same peak intracellular concentration is found for infusions of 25 minutes.

A plot of the interaction between the infusion and hyperthermia duration is shown in Figure 5.1. This plot shows that as infusion duration increases, the required minimum length of hyperthermia required to maximise the peak intracellular concentration increases. This is expected, since the peak intracellular concentration is reached quite rapidly after the end of the infusion, which is associated with the peaks in plasma and extracellular concentrations of drug. This occurs despite the saturable uptake terms, as the linear terms dominate at the elevated concentrations, and the initial drop in concentration is very rapid following the cessation of infusion (i.e., the extracellular drug concentration decreases rapidly, as free drug returns to the vasculature, in a manner consistent with other studies [e.g. 46]). For the same reason, to maximise the peak intracellular concentration for a given infusion duration with free drug, the hyperthermia only needs to last a fraction longer than the infusion duration. In the plot, this is shown by the large yellow region from the bottom right of the plot, which has constant concentrations for a given infusion duration, since the peak intracellular concentration was reached earlier. If the hyperthermia is not long enough, the cellular uptake is decreased, as the enhanced uptake due to hyperthermia is not fully realised; this is shown in the bottom left hand corner of the plot.

These results demonstrate the potential of targeted hyperthermia alone (without the use of an LTSL delivery platform) to improve outcomes for patients in the clinic through both increasing intracellular concentrations of doxorubicin and reducing cell survival by inhibiting repair mechanisms. Considering the relative size of the two effects at the physiological concentrations predicted by the compartment model, it is possible to argue that the enhanced sensitivity to intracellular doxorubicin is the effect which has more impact on the outcome. The peak intracellular concentration and cell survival with normothermia only is 4.86 ng/10⁵ cells and 0.193. If the hyperthermic model of kill is used, the survival fraction more than halves to 0.088, and the maximum kill with hyperthermic uptake and cell kill is only further reduced by a factor of 1.22 (to 0.72). Making the same argument in reverse (i.e., applying both cell kill models to the concentration achieved with a hyperthermic uptake model) reveals that the hyperthermic and normothermic survival fractions for 6.10 ng/10⁵ cells are 0.072 and 0.134

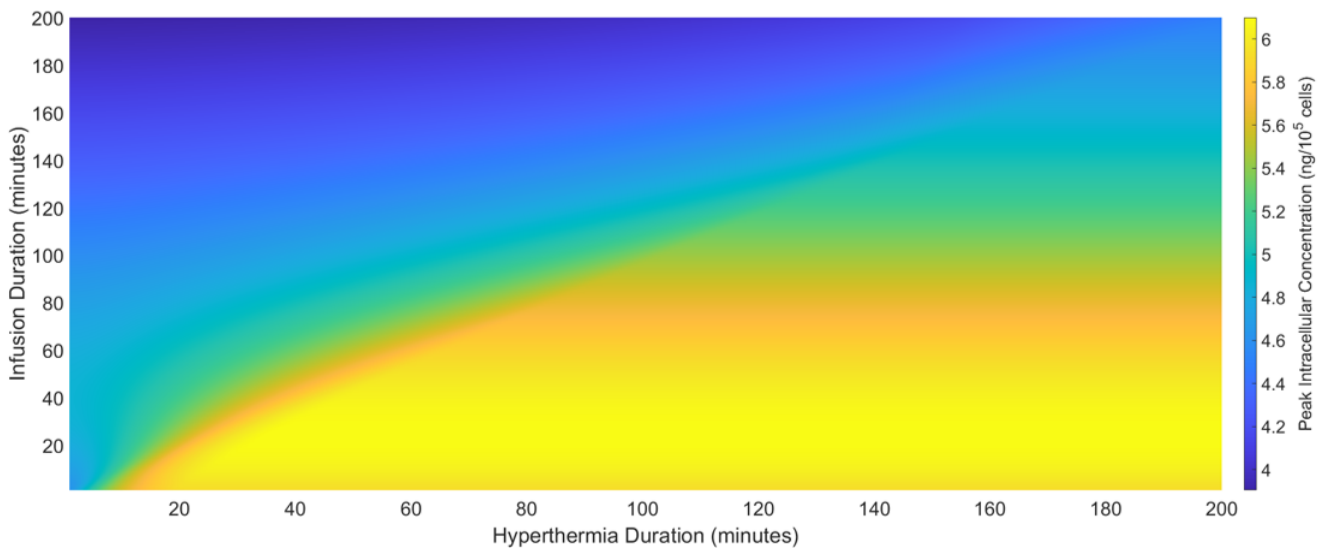


Figure 5.1. Plot showing how infusion duration and hyperthermia duration affect the achieved peak intracellular concentration for an infusion of free doxorubicin, based on the ‘separate’ model obtained from experimental work in the previous chapter (Table 4.8).

respectively; so the reduction in survival due to elevated uptake alone is 1.44-fold, and the reduction resulting from increased sensitivity is 1.86-fold.

Given that there is plenty of clinical evidence demonstrating that the use of hyperthermia with chemotherapy is beneficial, and that the clonogenic assay has previously been shown to be a good predictor of *in vivo* performance for a variety of therapeutics [157], the calculated 2.68-fold reduction in cell survival for an optimal treatment with hyperthermia is likely a reasonable estimate of the magnitude of the beneficial effect of hyperthermia. However, it is acknowledged that these survival fractions are unlikely to be accurate with respect to the clinical situation, given the large number of factors associated with treatment in the human body which it is not possible to include in this sort of model.

The optimal infusion time for free doxorubicin in this case (40 and 25 minutes at normothermia and hyperthermia respectively) is notably shorter than that obtained using El-Kareh and Secomb’s model, for which the optimal infusion duration was found to be 117 minutes [67]. The reason for this is that the uptake is no longer purely saturable, and at the achieved extracellular concentrations, linear uptake dominates as the concentration represented by the extracellular Michaelis constant is much lower than the achieved extracellular concentrations. This is a notable difference from the previous results, based on the non-small cell lung cancer cell line data reported by Kerr et al. [102], and does show how optimal treatment is likely to depend on the specific characteristics of the targeted tumour’s cells.

5.2.2 Optimal TSL Delivery

When considering optimal TSL delivery, the combined model of cellular uptake (i.e. that which was generated using both the data points at 37°C and 42°C, given in Table 4.8) was used throughout. This decision was taken because it is not reasonable (particularly when considering temporal PIR) to switch repeatedly between models, when the duration of the effect of hyperthermia on cellular uptake has not been studied in this thesis. The hyperthermic model is used for all predicted survival data, unless indicated, as there is clear evidence from the literature that hyperthermia before, during, or after treatment sensitises cells to therapeutics [e.g. 176].

For TSL doxorubicin delivery, an 18 minute infusion was found to be optimal for a given 90 minutes of hyperthermia, which results in a predicted concentration of 13.48 ng/10⁵ cells and a predicted survival of 0.013. A plot considering the full range of infusion and hyperthermia durations is shown in Figure 5.2. The results of this simulation reveal that for an 18 minute infusion, as long as the effect of hyperthermia on the cells lasts for longer than 49 minutes, this maximal concentration of 13.48 ng/10⁵ cells is achieved. Similarly to the case of optimising free doxorubicin delivery with hyperthermia, the hyperthermia duration should be longer than the infusion duration. It can also be observed that infusion durations shorter than the optimum infusion do not have a large effect on the predicted peak intracellular concentration (which makes sense, as the area under the curve (AUC) of the tumour plasma concentration-time plot for LTSL doxorubicin would be expected to be similar owing to the slower clearance of LTSL compared to free drug).

The predicted improvement in treatment between TSLs and free doxorubicin with hyperthermia when compared at optimal conditions is a 2.21-fold increase in intracellular doxorubicin and a 5.54-fold decrease in cell survival. The conclusion is clear - there should, with ideal heating, be a real patient benefit to using thermosensitive liposomal doxorubicin compared to free doxorubicin.

5.2.3 TSL Delivery with Non-Ideal Heating

It is important to assess whether or not this benefit is still present for the case of non-ideal heating. As previously, PIR_s is used to denote the spatial-sense and PIR_t is used for the temporal-sense of PIR. Unless otherwise stated, the peak intracellular concentrations given relate to the 'optimum' infusion duration with 90 minutes of hyperthermia.

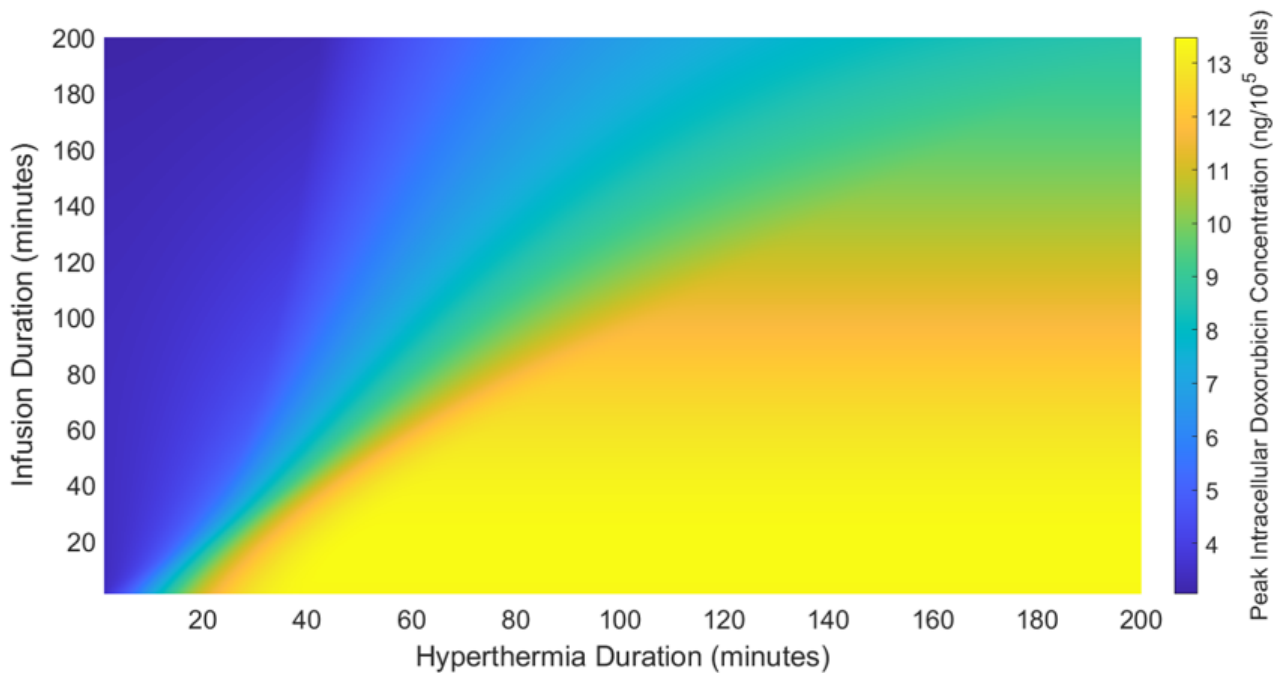


Figure 5.2. Plot showing how infusion duration and hyperthermia duration affect the achieved peak intracellular concentration for an infusion of TSL doxorubicin, based on the model obtained from experimental work in the previous chapter (Table 4.8, combined fit).

If a spatial PIR of 0.5 is applied, the peak intracellular concentration (with an infusion time of 17 minutes) achieved falls by 6% to $12.69 \text{ ng}/10^5 \text{ cells}$, which increases the survival fraction to 0.0153 (from 0.013); so as in Chapter One, it seems that the effect of uneven heating is still poorly resolved by PIR_S .

Applying $\text{PIR}_t = 0.5$ with a time block of 5 minutes, the peak intracellular concentrations achieved were dependent on whether the heating was initially on or off. Plainly, considering this as two separate blocks of the tumour, the infusion must be optimised for both; that is, to maximise the lower of the two concentrations. This occurs for an infusion duration of 26 minutes and predicts intracellular concentrations in the two parts of 9.26 and $9.27 \text{ ng}/10^5 \text{ cells}$ respectively. The reduction from the ideal case is now larger (and certainly more realistic, representing a reduction in peak intracellular concentration of 31.3%), but even this use of TSLs gives a predicted survival of 0.030, representing more than a halving of the predicted survival fraction from the ideal use of unencapsulated drug and hyperthermia. The predicted intracellular concentrations for the ideal infusions for the cases of $\text{PIR} = 1$ and $\text{PIR}_t = 0.5$ with a time block of five minutes are shown in Figure 5.3.

One question which is worth considering is whether it would be beneficial to patients to segment the tumour so that different sub-volumes are heated sequentially, rather than to heat the entire tumour in one go, especially if the tumour is large. Such a segmentation is possible with ultrasound-mediated

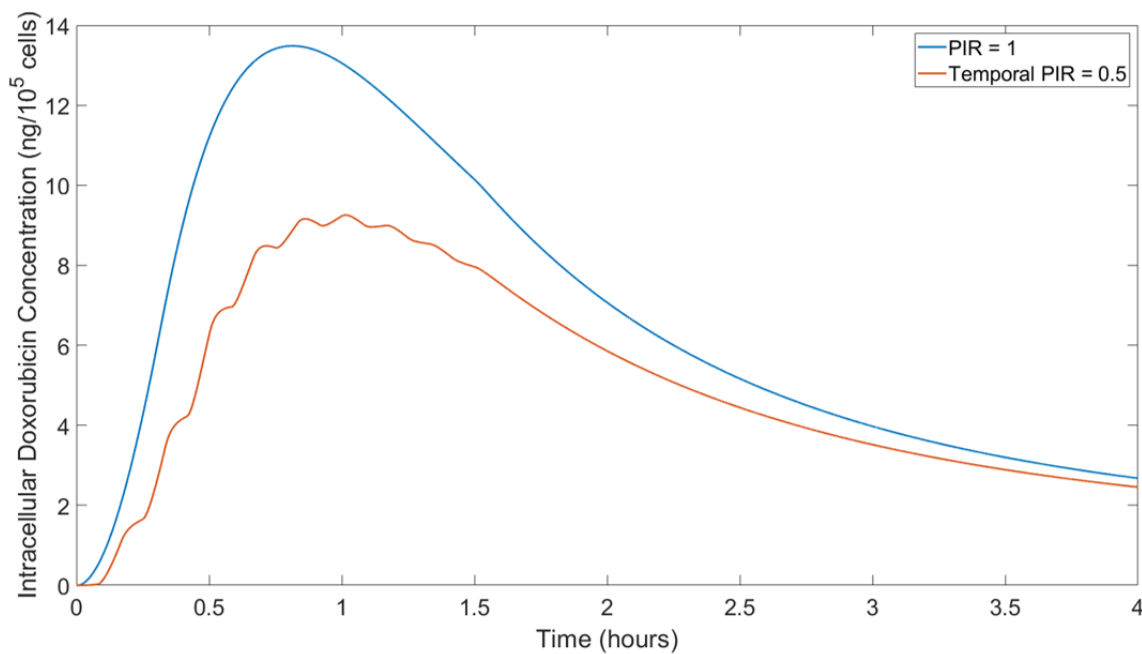


Figure 5.3. Plot showing how the intracellular concentration of doxorubicin varies with time for optimal infusions when $PIR = 1$, and $PIR_t = 0.5$ with 5 minute time blocks. The optimal infusion durations were 18 minutes for the case where $PIR = 1$, and 26 minutes for $PIR_t = 0.5$. Heating ceases at 90 minutes. Peak values are 13.48 and 9.26 $ng/10^5$ cells respectively.

hyperthermia by changing the volume swept through by the focus of the ultrasound beams to include only, say, half of the tumour for an initial period, then changing the swept volume to the complementary half of the tumour. This would result (in the model) in longer time blocks, which might be beneficial as the cells are exposed to elevated concentrations for longer. This is shown in Figure 5.4, which shows the predicted extracellular concentrations for optimised TSL doxorubicin delivery with $PIR_t = 0.5$ and time blocks of 5 and 15 minutes respectively. For doxorubicin, the prolonged elevated concentration does not cause a substantial increase in peak intracellular concentration. This is because the bonus of heating one section of the tumour for longer must be balanced with a longer infusion such that the other part of the tumour, seeing a complementary heating pattern receives a similar dose.

Figure 5.5 shows the lower of the two peak intracellular concentrations achieved in segments of the tumour receiving complementary heating patterns, with a time block on the y-axis, and an infusion duration on the x-axis. It can be seen that there is little difference in predicted peak intracellular concentration for longer time blocks (as long as the infusion is also prolonged). For longer hyperthermia time blocks, the infusion duration is required to be similar to, or double the hyperthermia block to ensure a maximisation of the peak intracellular concentrations (which are the largest two yellow bands aligning approximately with $y = x$ and $y = x/2$ on the Figure respectively). This makes sense, since although one segment of the tumour is being heated for longer, the other segment must similarly wait for longer to see hyperthermia; so if the hyperthermia time block duration is 30 minutes, and the

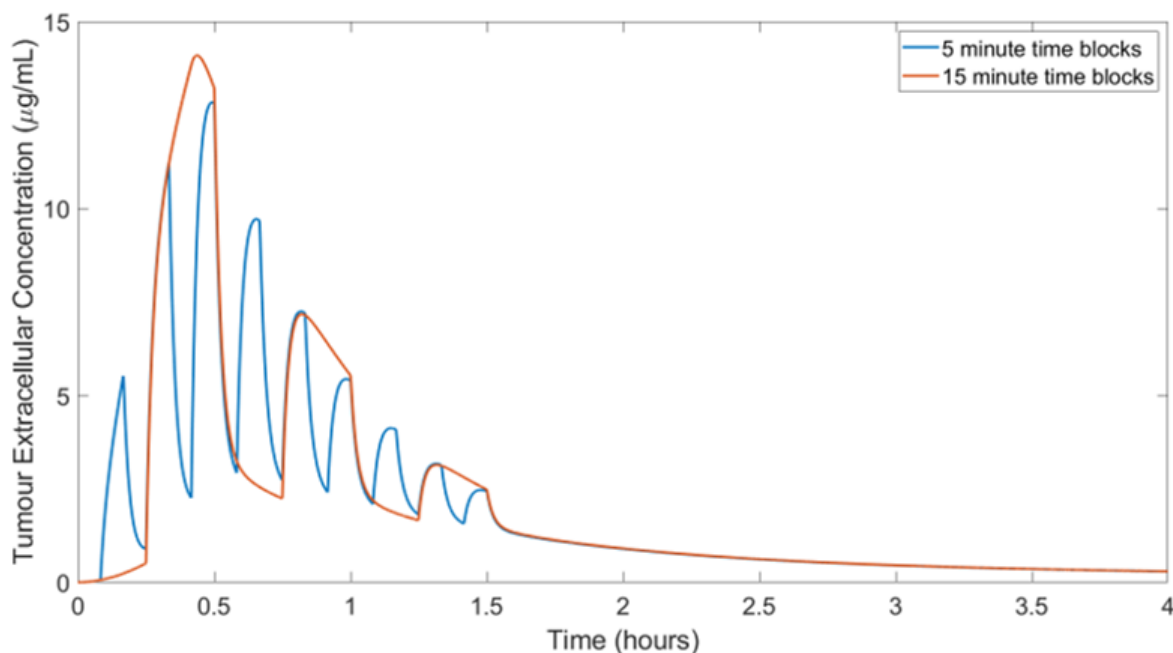


Figure 5.4. Plot of the tumour extracellular concentrations predicted for $PIR_t = 0.5$ with different time blocks of 5 and 15 minutes. For simplicity, the infusion times were kept the same at 25 minutes. The heating is initially off in this simulation and ceases at 90 minutes.

infusion duration is 35-40 minutes, the second block will receive a lower dose. However, it can be seen that for infusion durations around 30 minutes, there is not much difference for hyperthermia time blocks between 5 and 15 minutes. As a result, a recommendation to improve patient outcome would be to segment the tumour volume and perhaps use longer time blocks up to 15 minutes, since the predicted intracellular concentrations are not meaningfully lower for the increased time blocks, and prolonged hyperthermia is more likely to allow the therapeutic benefits of hyperthermia to be realised.

This modelling is of course, simplified, and the number of segments used here is assumed to be two, whereas for larger tumours, it may be that treating the whole volume in one go remains the best approach as the infusion time otherwise becomes too long and thus limits delivery. Another important conclusion that can be drawn from this figure is that the predicted intracellular concentrations, even with this non-ideal heating, remain substantially higher than those which can be achieved with unencapsulated drug.

5.2.4 Idarubicin - The Future of TSLs?

Some of the most interesting recent work in TSLs has been to explore the effect of changing the therapeutic agent encapsulated within the liposome. In particular, this has included the use of idarubicin, which is typically used to treat blood cancers, owing to its rapid-binding to blood cells. This property also means that as a free drug, it is poorly-suited to the treatment of solid tumours. As discussed in

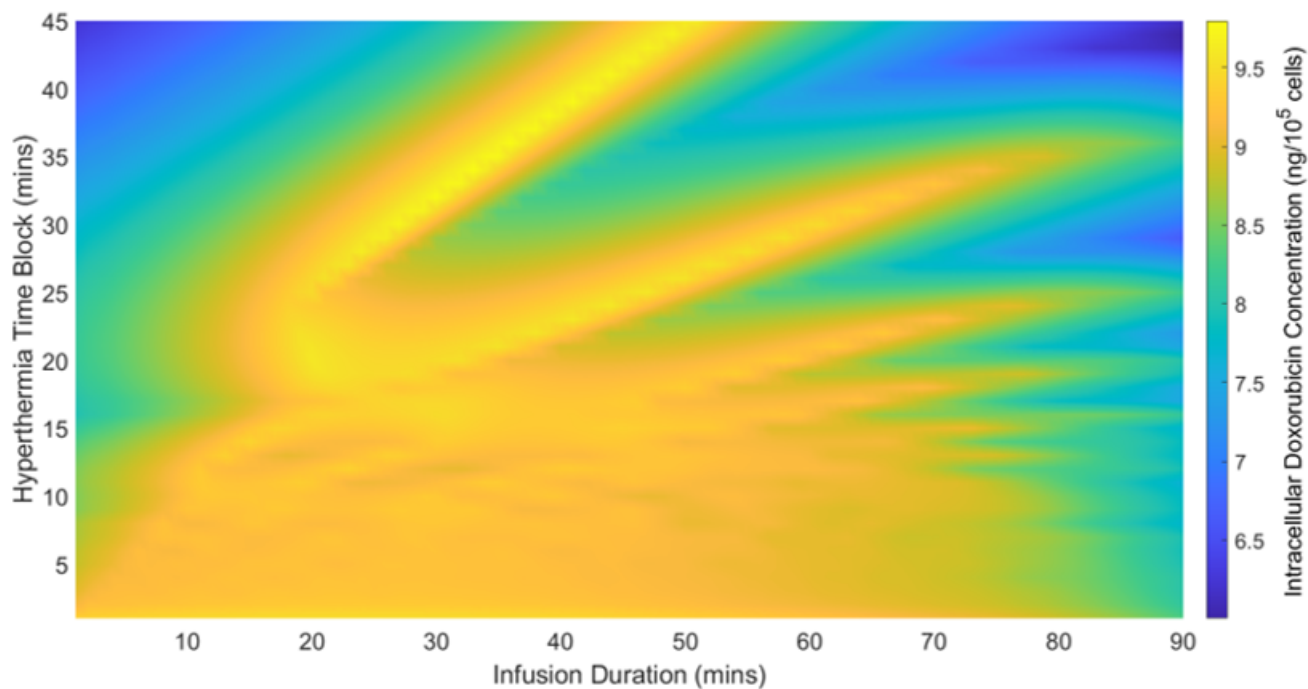


Figure 5.5. Plot showing how the smaller of the two peak values of intracellular concentration vary when two halves of the tumour are alternately heated with the time block given on the y-axis, over an infusion duration given on the x-axis. ($PIR_t = 0.5$).

the Literature Review, the less saturable nature of idarubicin's uptake kinetics means that the benefit of being able to rapidly release a large quantity of drug locally in the tumour plasma is potentially greater than for a drug such as doxorubicin, which displays more slower uptake kinetics (although the cellular uptake model derived in the previous chapter is less saturable than previously obtained literature models at concentrations relevant to LTSL delivery).

There is an assumption in the following work that peak intracellular concentration remains a good metric for therapeutic efficacy. This is assumed on the basis that idarubicin is also recognised as a topoisomerase inhibitor [177], although it is acknowledged that this finding should be validated experimentally (see Future Work, Section 6.1). Literature data for idarubicin uptake in CT26 cells is lacking, however a recent study [41] examined the potential of using different drugs in TSLs, and compared the uptake of doxorubicin and idarubicin (amongst others) in three different cell lines. A purely linear model (i.e. $\frac{dc_i}{dt} = k_{12}c_e - k_{21}c_i$) was fitted for each drug and cell line. It was found that the linear influx term, k_{12} increased by factors ranging from 7.75 to 62-fold, while the efflux term, k_{21} , increased between 1.01 and 11-fold. Therefore, an approximation of a drug exhibiting more rapid uptake, referred to from here as 'idarubicin' is modelled with the same parameters as doxorubicin, with a 10-fold increase in uptake (k_{in} and V_{max}) and 2-fold increase in efflux (k_{out}). For a $5 \mu\text{g/mL}$ extracellular concentration, this increases the equilibrium intracellular concentration by a factor of

Parameter	Value (s^{-1})
k_t	0.00631
k_p	0.01895
k_e	0.00661

Table 5.1. Pharmacokinetic parameters used in the ‘idarubicin’ model, obtained from the data in [178].

just over 5; so such behaviour is consistent with prior study, in which the intracellular concentration required for equilibrium with a given extracellular concentration increased by factors of 1.64, 5.6, and 7.7-fold for the three studied cell lines.

The model’s pharmacokinetic parameters were changed, with the values in Table 5.1 now being used. These were obtained from the two compartment model for idarubicin pharmacokinetics given in [178], using the relationships between the biexponential model and two compartment model, as can be found in [46]. The clearance parameter of the liposome was unchanged, as was the tumour vessel permeability. Considering the case where $PIR = 1$, using the same 90 mg of drug as used in the doxorubicin compartment model, the optimum ‘idarubicin’ TSL infusion is 25 minutes, giving a peak intracellular concentration of $40.32 \text{ ng}/10^5 \text{ cells}$; the tumour concentration profiles can be seen in Figure 5.6.

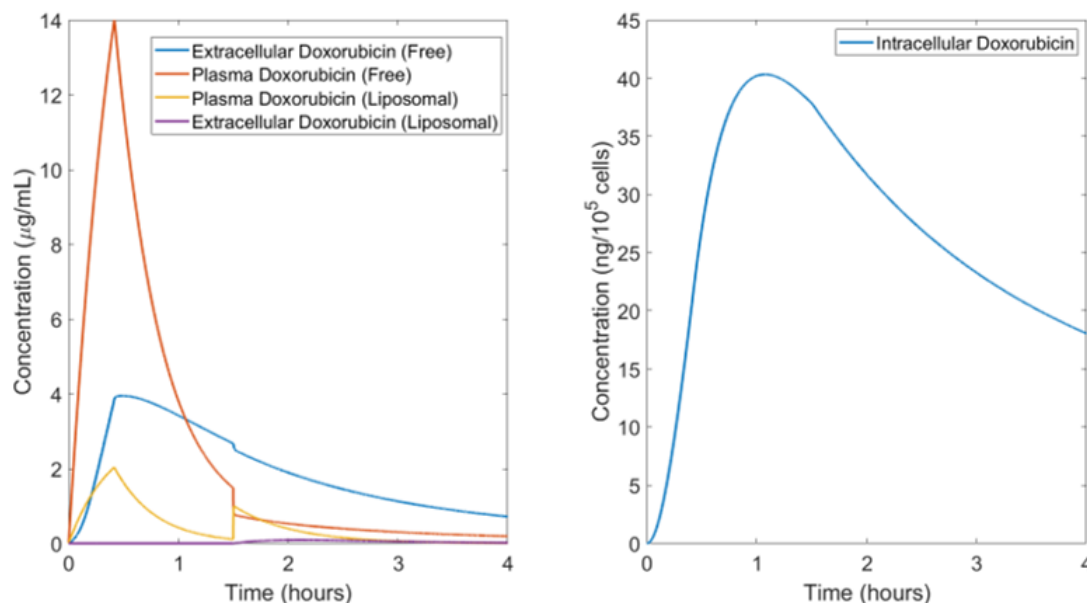


Figure 5.6. Tumour concentration profiles for an ‘idarubicin’ TSL, with $PIR = 1$ and an optimal infusion duration of 40 minutes, with 90 minutes of hyperthermia.

The effect of PIR_t is slightly greater in the case of a drug with more rapid uptake kinetics. The predicted intracellular concentration as a function of time is plotted in Figure 5.7, applying $PIR = 1$ and

$PIR_t = 0.5$, with the same 5 minute blocks as used in the doxorubicin analysis. The optimal infusion duration for $PIR_t = 0.5$ was 40 minutes when the time blocks were five minutes. The reduction in the peak value between the two cases is 33.6%, a slightly larger reduction than for doxorubicin (31.3%, shown in Figure 5.3). The impact of PIR_t therefore appears similar for a drug with more rapid pharmacokinetics and cellular uptake, however given the approximate nature of the cellular uptake parameters, this finding should not be over-interpreted.

If 15 minute blocks are used instead (for which the optimum infusion duration is found to be 46 minutes), the lower of the two peak intracellular concentrations achieved is slightly greater than for five minute blocks (26.95 compared to 26.76 $ng/10^5$ cells). This increase is not large, and similarly to the doxorubicin liposome case, a plot of the variation in peak intracellular concentration against infusion duration and heating blocks is shown in Figure 5.8. This demonstrates that there is not a large variation in peak intracellular concentration for extended heating time blocks (without considering spatial variations). In light of this, longer time blocks can also be recommended for 'idarubicin' TSLs, as there is a negligible effect on the level of intracellular drug, but the prolonged hyperthermia increases the chances of the other therapeutic benefits of mild hyperthermia being realised.

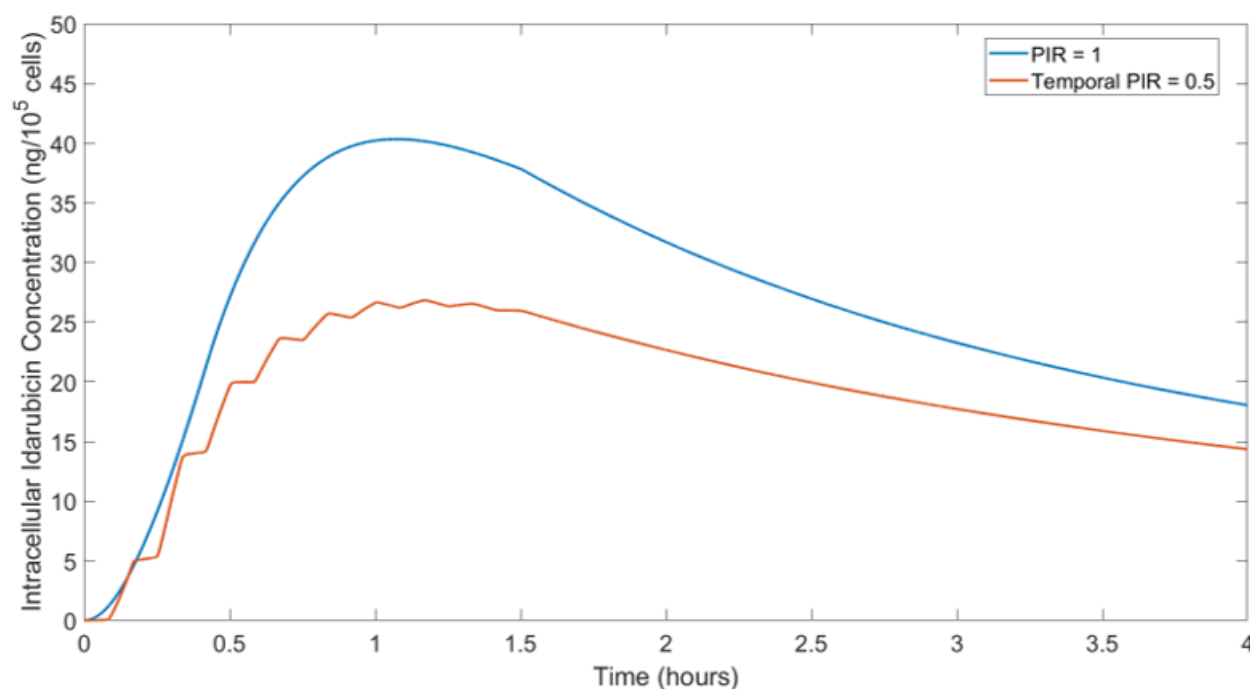


Figure 5.7. Plot showing how the intracellular concentration of 'idarubicin' varies with time for optimal infusions of 25 minutes for the case where $PIR = 1$ and 40 minutes for $PIR_t = 0.5$ with 5 minute time blocks. Heating ceases at 90 minutes. Peak values are 40.32 and 26.76 $ng/10^5$ cells respectively.

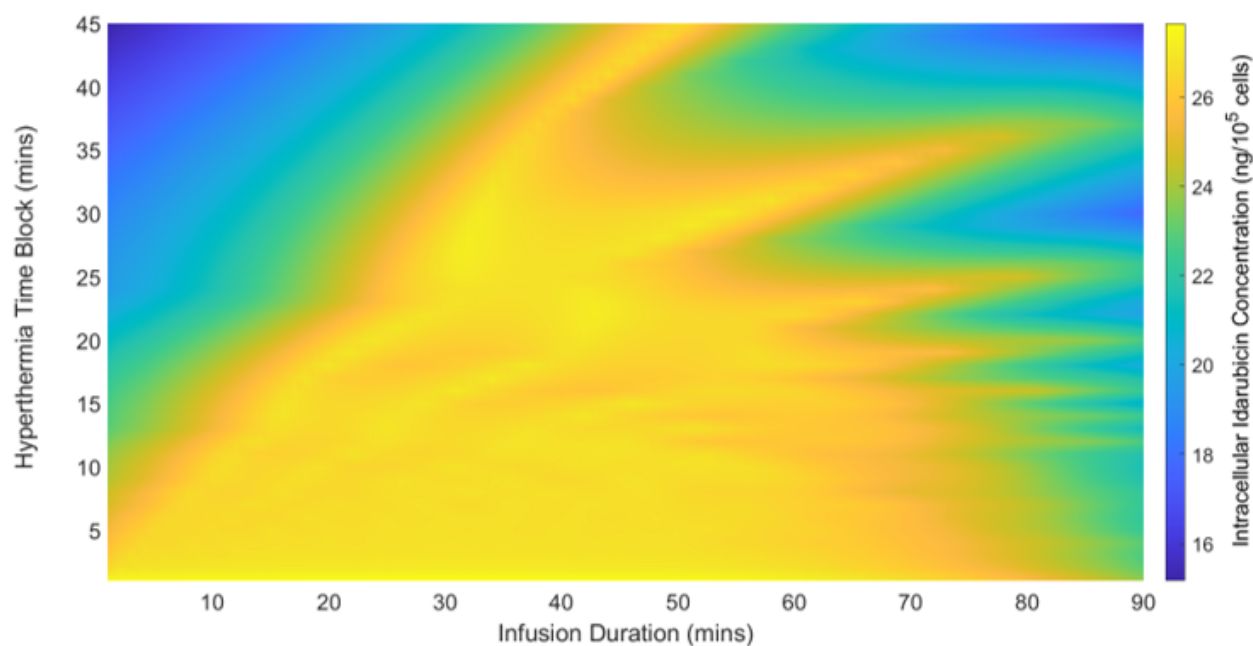


Figure 5.8. Plot showing how the smaller of the two peak values of intracellular concentration vary when two halves of the tumour are alternately heated with the time block given on the y-axis, over an infusion duration given on the x-axis for a TSL containing a drug with similar properties to idarubicin.

5.2.5 Liposomal Extravasation as a Delivery Mechanism

The compartment model was used to assess the reduction in peak intracellular concentration if liposomal extravasation was neglected (achieved by decreasing the permeability of the vessel wall to liposomes to 0 ms^{-1}). Comparing the optimal infusion of LTSL doxorubicin with 90 minutes of hyperthermia ($\text{PIR}_S = 0.5$), the peak intracellular concentration was decreased by 0.16% when the mechanism of liposomal extravasation was turned off. This suggests that liposomal extravasation into the extracellular space is not a substantial mechanism in LTSLs (although this is not true for the slower release times of TTSLs). This is an important finding (supported by literature [e.g. 66]), as it means that this mechanism need not be included in spatially heterogeneous models, greatly simplifying the code required.

Considering the implications of this finding within the broader context of LTSL delivery of drugs, this does mean that there is no benefit in terms of tumour targeting to having LTSLs that have diameters on the order of 100 nm (while for TTSLs, this size was typically selected and justified on the grounds that it facilitated passive tumour targeting by the EPR effect). It is noted that there are other good reasons for liposomal size around 50 - 200 nm, which are that smaller liposomes are less stable, and larger liposomes are cleared more rapidly [179]. Despite this, it may be worth exploring further if there is a benefit to using larger carriers (which have a higher loading capacity) to deliver drugs with more rapid uptake kinetics, since this may facilitate a higher local concentration in the tumour

plasma; however it is acknowledged that there a complex range of factors at play with regards to the characteristics of nanoparticles, which are discussed more fully in [8]. In short, strategies such as PEGylation [63] reduce clearance by the MPS, but also reduce the interaction between the nanoparticles and the target cells. Non-spherical nanoparticles have been shown to be more prone to tumbling and oscillatory effects in the vasculature [8], which may increase the transit time of the nanoparticles in the tumour, which would be beneficial for thermosensitive nanoparticles. Surface charge also has an effect, with positively charged nanoparticles having increased interactions with cells [180].

5.3 Krogh Cylinder Models - An Introduction

Spatial variations in dose can be an important part of the problem of drug delivery to tumours, which have not been considered in this thesis until now. The spatial variations considered in this thesis are on the microvascular scale, and so do not extend to considering the macroscale differences in deposition across the tumour which will result from uneven heating. Further, for reasons described below, the simulations are limited to a single cylinder, rather than considering a complete microvascular geometry.

One of the simplest and most common approaches to include spatial variations is to use a similar approach to that first proposed by Krogh [181], in which the tissue is approximated as a capillary within a larger tissue cylinder, with no mass flux out of the boundaries of the outer (tissue) cylinder. In its simplest form, axial variations along the cylinder are neglected, so the radial diffusion equation is solved in the tissue space, usually with either a zero- or first-order reaction term. For these simple cases, analytical solutions exist, which were used to confirm that the numerical code was working correctly.

The first analytical solution is for the steady state case of a cylinder with zero-order uptake kinetics, in which the tissue concentration at the boundary with the capillary is taken to be equal to the capillary concentration (perhaps multiplied by some constant α). Mathematically, this is defined by the equation

$$\frac{\partial c_t}{\partial t} = D \left[\frac{1}{r} \frac{\partial}{\partial r} \left(r \frac{\partial c_t}{\partial r} \right) \right] - M \quad (5.1)$$

where M is some constant sink, with the boundary conditions

$$\left. \frac{\partial c}{\partial r} \right|_{r=R_0} = 0 \quad (5.2)$$

and

$$c(r = R_c) = \alpha c_c \quad (5.3)$$

where R_0 is the outer radius of the tissue, R_c is the capillary radius (and the inner radius of the tissue) and c_c is the concentration in the capillary. The analytical solution to this problem is given by [182]:

$$c_t = \alpha c_c + \frac{M}{4D}(r^2 - R_c^2) - \frac{MR_0^2}{2D} \ln \frac{r}{R_c} \quad (5.4)$$

The second test case used was the case of first-order uptake kinetics, which is useful as the uptake used in the doxorubicin model is concentration-dependent. In this case, where

$$\frac{\partial c_t}{\partial t} = D \left[\frac{1}{r} \frac{\partial}{\partial r} \left(r \frac{\partial c_t}{\partial r} \right) \right] - n c_t \quad (5.5)$$

this can be reformulated as a Sturm-Liouville problem [183] by setting $\bar{R} = \sqrt{\frac{n}{D}}r$

$$\frac{\partial}{\partial \bar{R}} \left(\bar{R} \frac{\partial c_t}{\partial \bar{R}} \right) - \bar{R} c_t = 0 \quad (5.6)$$

with the following solution:

$$c_t(R) = AI_0(R) + BK_0(R) \quad (5.7)$$

in which I_0 and K_0 are modified Bessel functions of the first and second kind (and order zero) respectively, where

$$A = \alpha c_c \frac{K_1(R_0)}{I_1(R_0) \left(\frac{K_1(R_0)}{I_1(R_1)} I_0(R_c) + K_0(R_c) \right)} \quad (5.8)$$

$$B = \alpha c_c \frac{1}{\frac{K_1(R_0)}{I_1(R_1)} I_0(R_c) + K_0(R_c)} \quad (5.9)$$

Plainly, use of this model to assess the spatial heterogeneity of dose following doxorubicin infusion requires a diffusion coefficient for free doxorubicin. While values exist in the literature, an attempt was made here to quantify this experimentally for free doxorubicin in *ex vivo* porcine pancreas in both hyperthermic and normothermic conditions. This was unfortunately not successful, and the approach is detailed in Appendix C. As a result, the literature value for doxorubicin of $5.01 \times 10^{-11} \text{ m}^2 \text{ s}^{-1}$

[34] is used. The same value is applied for 'idarubicin', since idarubicin and doxorubicin have been shown to have very similar transport properties in biomimetic hydrogels [184]. A biomimetic hydrogel is evidently not the same as biological tissue, however it provides a reassurance that the value for the diffusion coefficient is on the correct order of magnitude. Further, a major limiting factor in the transport of idarubicin has been identified as being its rapid binding to cells [85], which creates a challenge in measuring a diffusion coefficient in tissue; and as the mathematical model of transport includes a separate cellular uptake term, the use of data from a hydrogel remains valid.

Further parameters which must be chosen are those for the capillary and tissue radii, r_c and r_t respectively. Taking a typical capillary radius of $10\ \mu\text{m}$, two different values of tissue radii are used to explore the question of how different dosing and treatment regimens affect spatial variation of drug in the tissue. The first is the tissue radius which corresponds to the value of tumour vascular surface area/tumour volume which is used in the compartment models in this thesis, as well as the wider literature. This value of $15\ \text{mm}^2/\text{mm}^3$ corresponds to a tissue radius of $36.5\ \mu\text{m}$. The second tissue radius is used to provide an indication of what may be happening in the less well-vascularised regions of the tumour. Here, a tissue radius of $150\ \mu\text{m}$ is used, corresponding to an inter-capillary distance of $300\ \mu\text{m}$. In the following models, the compartment model is used to provide an approximate free plasma concentration profile to use as an input into the cylinder model.

5.4 Free Doxorubicin Infusion - A 1D Krogh Model

For an infusion of free doxorubicin under normothermic conditions, simulating $r_t = 36.5\ \mu\text{m}$ with an ideal infusion of 40 minutes, the peak values of intracellular concentration are (to 3 S.F.) $4.90\ \text{ng}/10^5$ cells in the tissue next to the capillary and $4.85\ \text{ng}/10^5$ cells at the outer edge of the cylinder. The spatial variation through the cylinder is plotted in Figure 5.9; although, as is apparent from the values quoted above, the spatial variation in this case is not large, with a decrease of only 0.86% in peak intracellular concentrations achieved across the cylinder. The compartment model predicted peak intracellular concentration ($4.86\ \text{ng}/10^5$ cells) falls within the peak values at the capillary boundary and tissue edge.

For a larger tissue radius however, the change in peak intracellular concentration across the tissue space becomes larger, with a 30.8% decrease from 2.01 to $1.39\ \text{ng}/10^5$ cells over the tissue space, as shown in Figure 5.10. The predicted peak intracellular concentration at the capillary boundary for

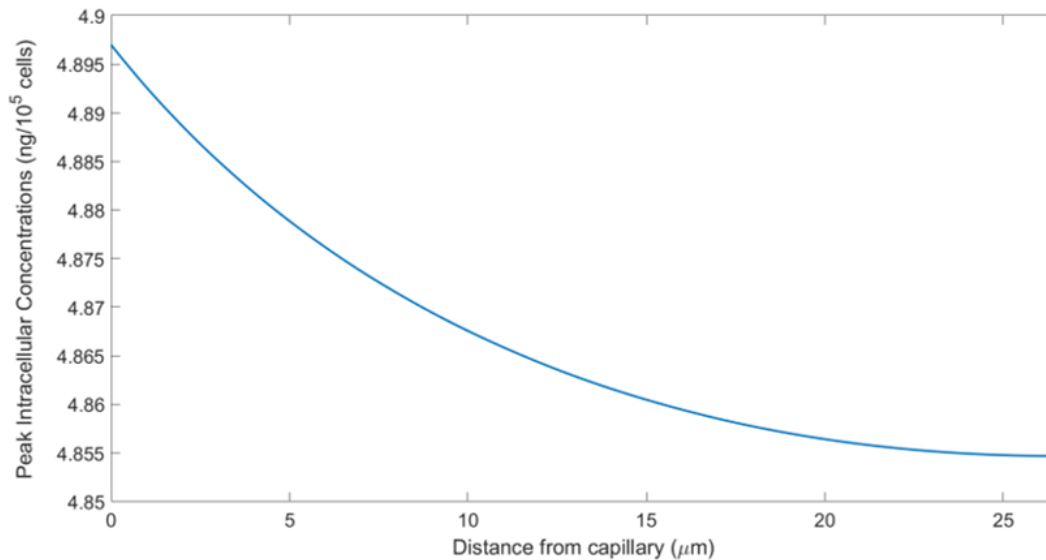


Figure 5.9. Obtained values of peak intracellular concentration following a 40 minute infusion of free doxorubicin, over a Krogh-style cylinder model with $r_c = 10\mu\text{m}$ and $r_t = 36.5\mu\text{m}$, using the combined uptake model. There is not a substantial decrease across the cylinder, which is consistent with *in vivo* literature, which shows fairly consistent levels of doxorubicin (total, not just intracellular) up to $100\mu\text{m}$ from a capillary following doxorubicin release from TSLs [89]. Note that values plotted do not correspond to a single point in time, but rather the maximum intracellular concentration achieved at that distance from the capillary.

this case is now only 41.4% of the compartment model predicted peak intracellular concentration, and the concentrations predicted across the full thickness of the cylinder are below the obtained normothermic intracellular IC50, with survival increasing over the tissue thickness from 56.2% to 77.6%.

The shape of this second plot can be explained by considering the timescales involved in this process which are tabulated in Table 5.2. The timescales associated with elimination and distribution are calculated based on a two compartment model, in which the plasma concentration follows a biexponential decay:

$$c_p(t) = Ae^{-\alpha t} + Be^{-\beta t} \quad (5.10)$$

where A , B , α and β can all be related to the rate constants in the compartment model [e.g. 46], and α and β , the half lives of distribution and elimination are given by

$$\alpha = \frac{1}{2} \left(k_t + k_p + k_{el} + [k_t^2 + k_p^2 + k_{el}^2 + 2(k_{el}k_p + k_p k_t - k_{el}k_t)]^{0.5} \right) \quad (5.11)$$

and

$$\beta = \frac{1}{2} \left(k_t + k_p + k_{el} - [k_t^2 + k_p^2 + k_{el}^2 + 2(k_{el}k_p + k_p k_t - k_{el}k_t)]^{0.5} \right) \quad (5.12)$$

respectively. Considering these timescales, it becomes apparent that the timescale associated with crossing the capillary membrane in the hypoxic, larger cylinder is 55 minutes, which is longer than the infusion duration of the drug. The shape of the plot of peak intracellular concentration achieved in this cylinder is therefore explained; it is not a single curve (as for the average-sized cylinder), but rather a curve which meets an almost horizontal line at a distance of $38 \mu\text{m}$ into the tissue. The reason for this is that, beyond $38 \mu\text{m}$, the peak intracellular concentration is reached during the elimination phase of the drug, in which concentrations in the plasma are relatively steady (compared to the distribution phase). The elimination phase can be seen (Figure 5.11) to last an order of magnitude longer than the other processes, and so this dominates the peak intracellular concentration beyond a certain penetration distance into the tumour tissue.

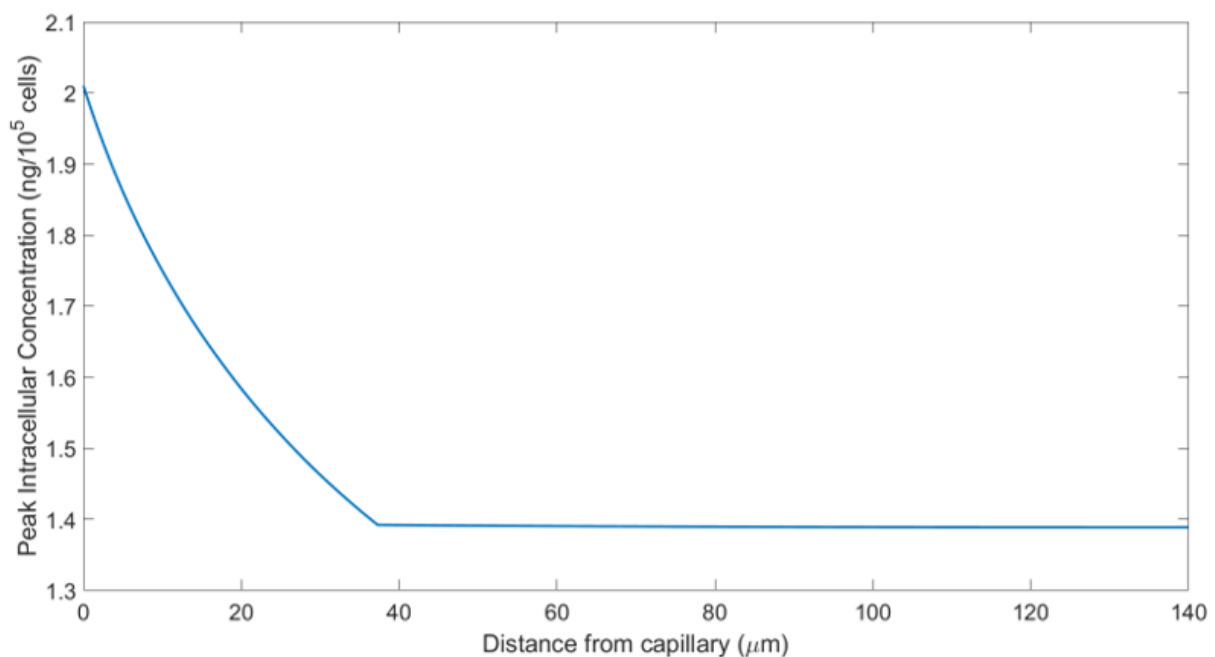


Figure 5.10. Obtained values of peak intracellular concentration following a 40 minute infusion of free doxorubicin, over a Krogh-style cylinder model with $r_c = 10 \mu\text{m}$ and $r_t = 150 \mu\text{m}$.

The fact that transport across the membrane is associated with a timescale larger in magnitude than the infusion timescale means that, in the case of the larger cylinder, the coupled Krogh-compartment model predicts peak intracellular concentrations that are somewhat lower than the prediction made for both the compartment model alone and the ‘average radius’ Krogh model (which is based on a value of $S = 15000 \text{ m}^{-1}$). This suggests that for the hypoxic regions of the tumour (and therefore, perhaps the tumour overall), optimisation based on a compartment model may be inaccurate. It is suggested that perhaps using a weighted sum of cylinder simulations might represent a compromise between computationally more complex methods (such as Green’s function simulation on microvas-

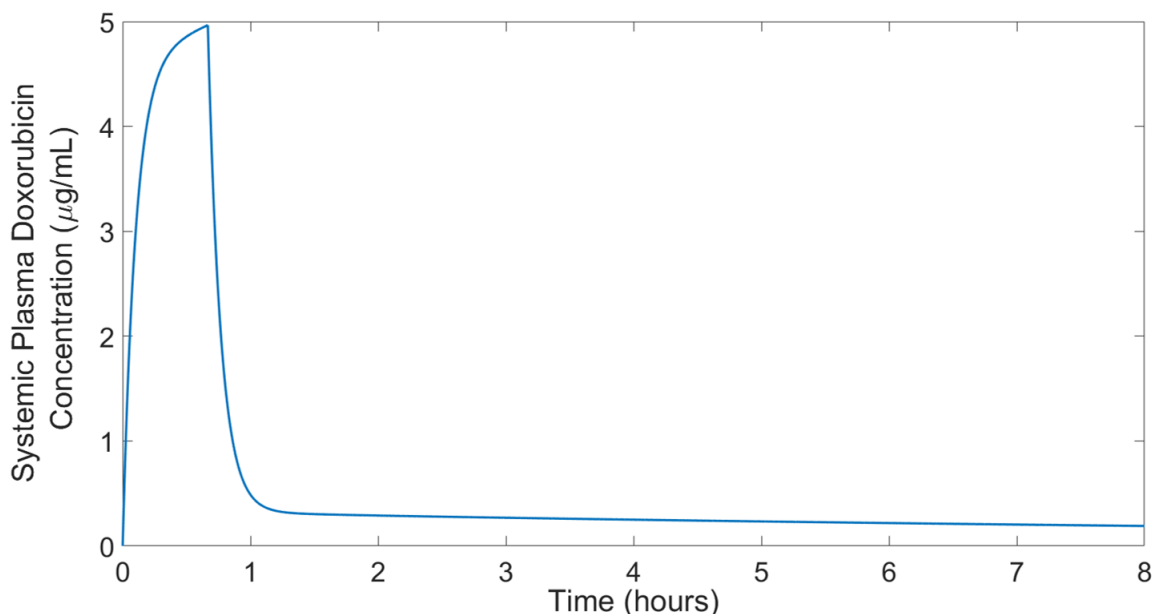


Figure 5.11. The systemic plasma concentration following a 40 minute infusion of free doxorubicin, showing that the concentration remains relatively steady during the elimination phase, which lasts several hours.

cular geometries [127, 128]) and a simpler compartment model approach.

One question posed by the different results for the two tissue radii examined from the 40 minute infusion (which is optimal in a compartment model-sense), is whether different cycles of chemotherapy should use different infusion durations to target proximal and distant cells. Figure 5.12 shows the predicted peak intracellular concentrations at the capillary, in the middle of the tissue, and at the edge of the cylinder for both the regular and larger tissue radius. For the regular tissue radius of $36.5 \mu\text{m}$, it can be seen that there is not a great deal of difference in the optimum infusion duration across the cylinder, and the durations are very close to the 40 minutes predicted by the compartment model. As the timescale associated with crossing the membrane for this average cylinder is just 3.3 minutes, the peak intracellular concentration profile is a single smooth curve (i.e., nowhere in this cylinder is the peak intracellular concentration achieved during the elimination phase of the drug). Considering the additional parameters and computational complexity associated with introducing spatial heterogeneity for this case, the compartment model optimisation therefore appears to be adequate across the tissue space (particularly given the uncertainty in the model parameters).

Considering the larger cylinder however, the values of peak intracellular concentration for the middle and edge cells appear almost independent of infusion duration. Again, this is also a result of the peak intracellular concentration beyond a certain point occurring during the elimination phase of the drug. As can be seen when considering the three infusion durations shown in Figure 5.13, the infusion

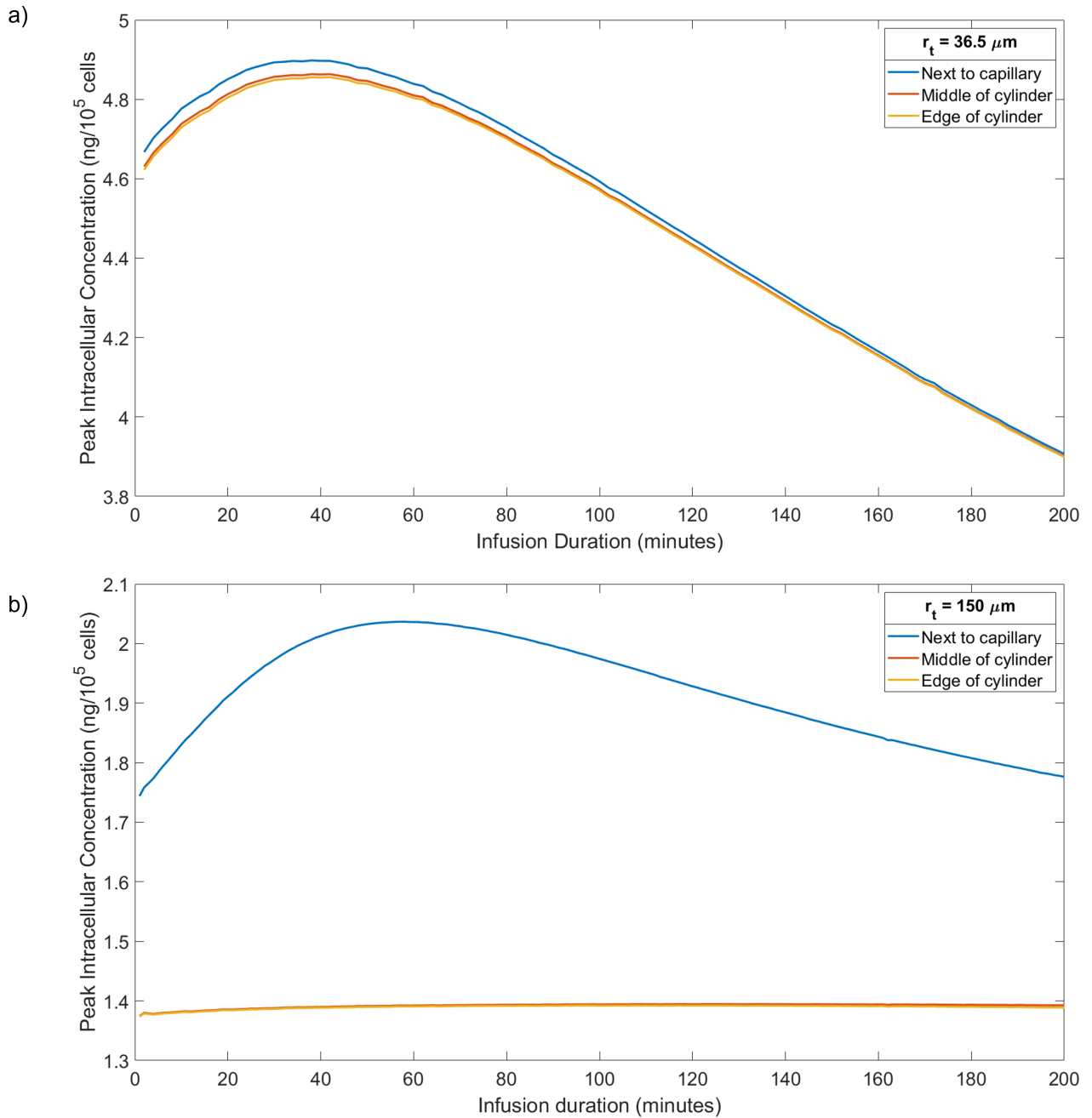


Figure 5.12. Plot showing how the infusion duration of free doxorubicin affects the peak intracellular concentration predicted next to the capillary, in the middle of the cylinder, and at the outer edge of the cylinder for tissue radii of a) $36.5 \mu\text{m}$ and b) $150 \mu\text{m}$.

Timescale	Calculation	Value (minutes)
Distribution of drug [46]	$\frac{1}{\alpha}$ (See Equations 5.10 to 5.12)	6.1
Elimination of drug [46]	$\frac{1}{\beta}$ (See Equations 5.10 to 5.12)	880
Infusion	Optimal Free Drug Infusion Duration	40
Diffusion [e.g. 67]	$T_{diff} = \frac{L^2}{D}$ $L = 26.5 \times 10^{-6}$ m (Average cylinder)	0.23 (Average cylinder)
	$L = 140 \times 10^{-6}$ m (Large cylinder) $D = 5.01 \times 10^{-11}$ m ² s ⁻¹	6.5 (Large cylinder)
Membrane permeability [67]	$\frac{1}{PS}$ $P = 3.4 \times 10^{-7}$ m s ⁻¹	3.3 (Average cylinder)
	$S = 15000$ m ⁻¹ (Average cylinder) $S = 889$ m ⁻¹ (Large cylinder)	55 (Large cylinder)

Table 5.2. The timescales involved in the spatially heterogeneous problem. Timescales are given to two significant figures.

duration of free doxorubicin makes little difference to the plasma concentration profile of the drug in the elimination phase. Prolonged infusion durations slightly move the point in the tissue where the two lines shown in Figure 5.10 intersect, but not in a way which is likely to substantially impact on treatment.

In summary, the work in this section suggests that the use of simple cylinders in the models does not radically alter the optimisation provided by compartment models for free doxorubicin treatment, although infusion durations should perhaps be slightly increased to allow for the lag occurring due to transport across the membrane and through the extracellular space. For more distant cells in poorly vascularised regions, the effect of infusion time on peak intracellular concentration for treatment with unencapsulated drug is minimal.

5.5 TSLs and spatial variations

While the above results suggest that including spatial distribution in the optimisation of free doxorubicin infusion duration is unlikely to have a substantial impact, the same analysis must be performed for TSL delivery, since the concentration-time profile of tumour doxorubicin becomes more complex.

When considering the variation in PIR_t on spatial variation of doxorubicin following TSL treatment with 90 minutes of heating, optimal infusion times were found using the compartment model with

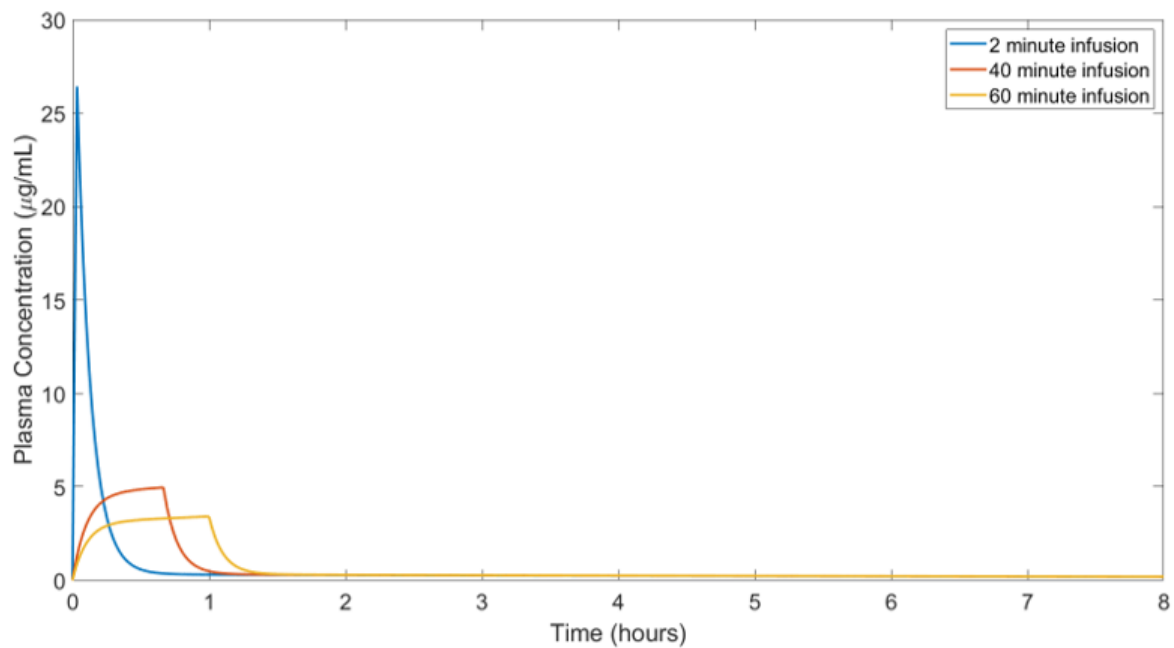


Figure 5.13. Plot of the predicted systemic free plasma concentration of doxorubicin (normothermic uptake model) for infusion durations of two minutes, 40 minutes, and 60 minutes. The concentration profile in the elimination phase is almost unaffected by the infusion duration.

$PIR_t = 0.5$ for time blocks of 5 and 15 minutes. The simulation was run modelling the hyperthermia as initially off, then as initially on. The lower of these two peak intracellular concentrations was stored as the lowest peak intracellular concentration achieved for that infusion duration. The infusion duration chosen was that which maximised the lower peak intracellular concentration. For a 5 minute time block, the optimum TSL infusion duration was found to be 26 minutes, while for a 15 minute time block, the optimum infusion time was longer, at 31 minutes. In all cases with TSLs, the combined cellular uptake model was used, and the results for both cylinders are as plotted in Figure 5.14.

As can be seen in the Figure, the differences in achieved peak intracellular concentrations are small in the regular cylinder, but more substantial in the hypoxic cylinder, with a larger tissue radius. In the larger cylinder, the time block has less influence on the peak intracellular concentration, but for the average cylinder, the hypothesis that prolonged hyperthermia might facilitate slightly elevated concentrations is proved correct. On the basis of these plots, it seems that recommending extended time blocks to guarantee the additional positive bioeffects of hyperthermia is valuable.

For 'idarubicin', the optimum TSL infusion durations for a fixed 90 minutes of hyperthermia, with 5 and 15 minute time blocks, were found to be 40 and 46 minutes respectively. In this case, the achieved peak intracellular concentrations are much more spatially heterogeneous, as can be seen in Figure 5.15. In the regular cylinder, this is not a particularly acute problem; the edge value is 95% of the capillary value (time block = 15 minutes, initially on). However, for the larger cylinder, the concen-

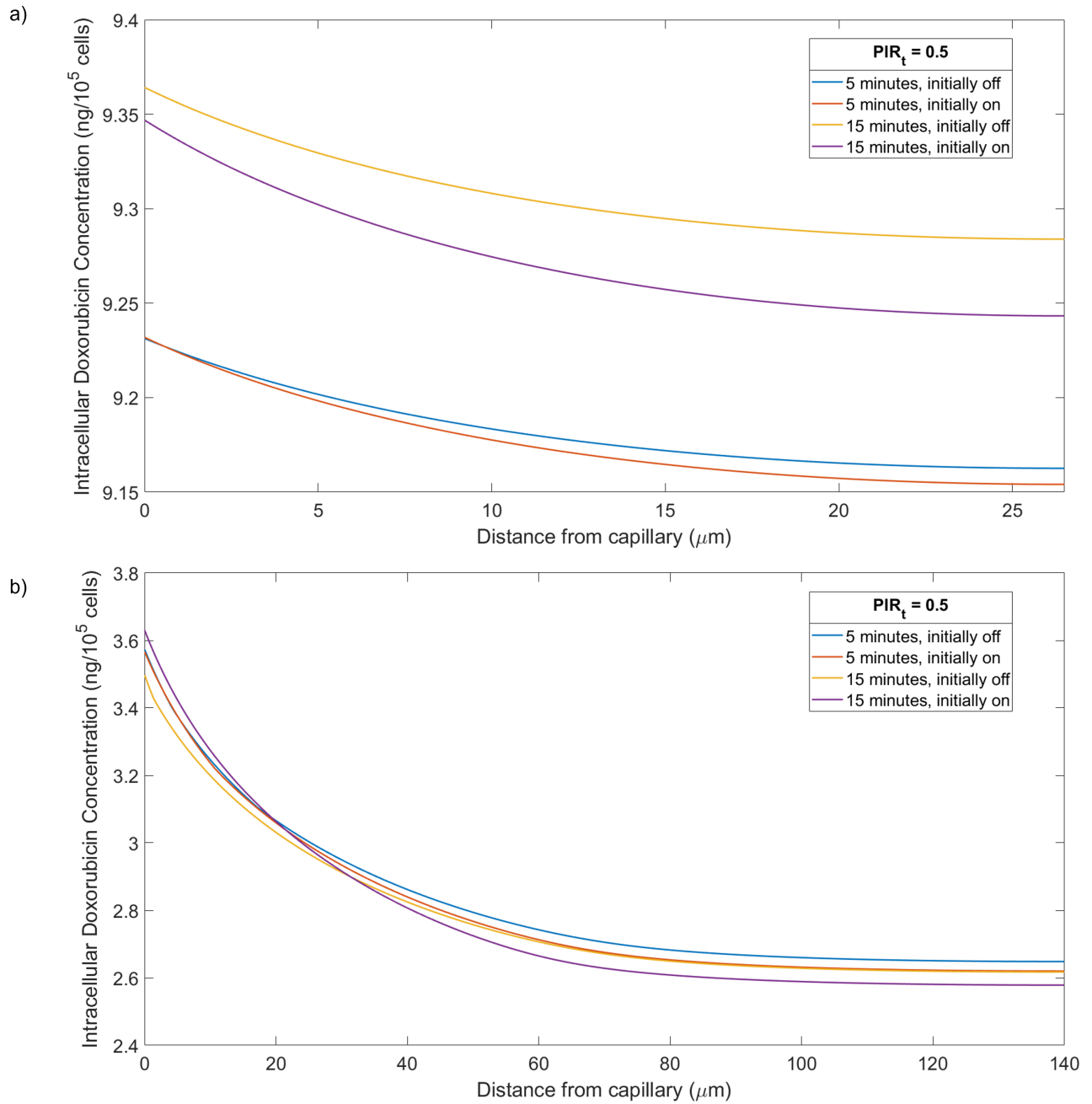


Figure 5.14. Plot showing how temporal PIR affects the spatial distribution of peak intracellular doxorubicin concentration in the regular cylinder (a) and the larger cylinder (b). The infusion durations in both cases were chosen as those that were optimal according to the compartment model - 26 minutes for 5 minute time blocks, and 31 minutes for 15 minute time blocks. Hyperthermia was assumed to start immediately and lasted for 90 minutes, and the combined model for cellular uptake was used in this simulation.

trations beyond $77\ \mu\text{m}$ are achieved during the elimination phase (and it is doubtful, considering the reported rapid plasma protein binding of idarubicin, that the concentrations there would even become that large). This greater spatial heterogeneity has been demonstrated *in vivo* [89], and may represent a limitation of idarubicin TSLs; however further work is required to determine whether or not this represents an issue, as no experimental work to determine an intracellular IC50 for idarubicin was done in this thesis; certainly, one cannot simply use the cell kill model derived for doxorubicin in this work here. Additionally, the choice of cellular volume will be a more important factor in modelling drugs with more rapid uptake kinetics, since smaller cell volumes (and thus greater cell densities) remove more drug from the extracellular space (as drug uptake is measured experimentally in units of $\text{ng}/10^5$ cells), limiting penetration of the drug. It is therefore suggested that cellular density is used as a variable in future works (rather than intracellular volume fraction and cell size).

The spatial variation in dose delivered in the hypoxic cylinder model suggests that LTSLs containing drugs with rapid cellular uptake kinetics may be less well-suited to treating poorly vascularised tumours. However, it is acknowledged that poorly vascularised cancers do sometimes respond well to chemotherapy over multiple cycles, which has been attributed to a treatment mechanism likened to 'peeling an onion from the inside out', in that successive layers of the tumour (onion) away from the vasculature are killed with each successive treatment [185].

Regardless, the incorporation of idarubicin into TSL delivery systems, is an exciting area of active research, since idarubicin is a highly potent drug, which could not previously be systemically administered to treat solid tumours.

Furthermore the work in this section finds that the recommendation (made on the basis of the compartment model, which did not incorporate any spatial heterogeneity) to use longer hyperthermia time blocks (segmenting the tumour for hyperthermia) remains valid when these specific spatial variations are also considered.

5.6 Cylinder Models with Axial Variations

The previous cylinder models were only 1D, and neglected axial variation due to the extravasation of drug along the capillary; for the case of delivery, the vascular (and therefore also the tissue) concentrations would decrease along the flow direction. Code implementing axial variation was cross-

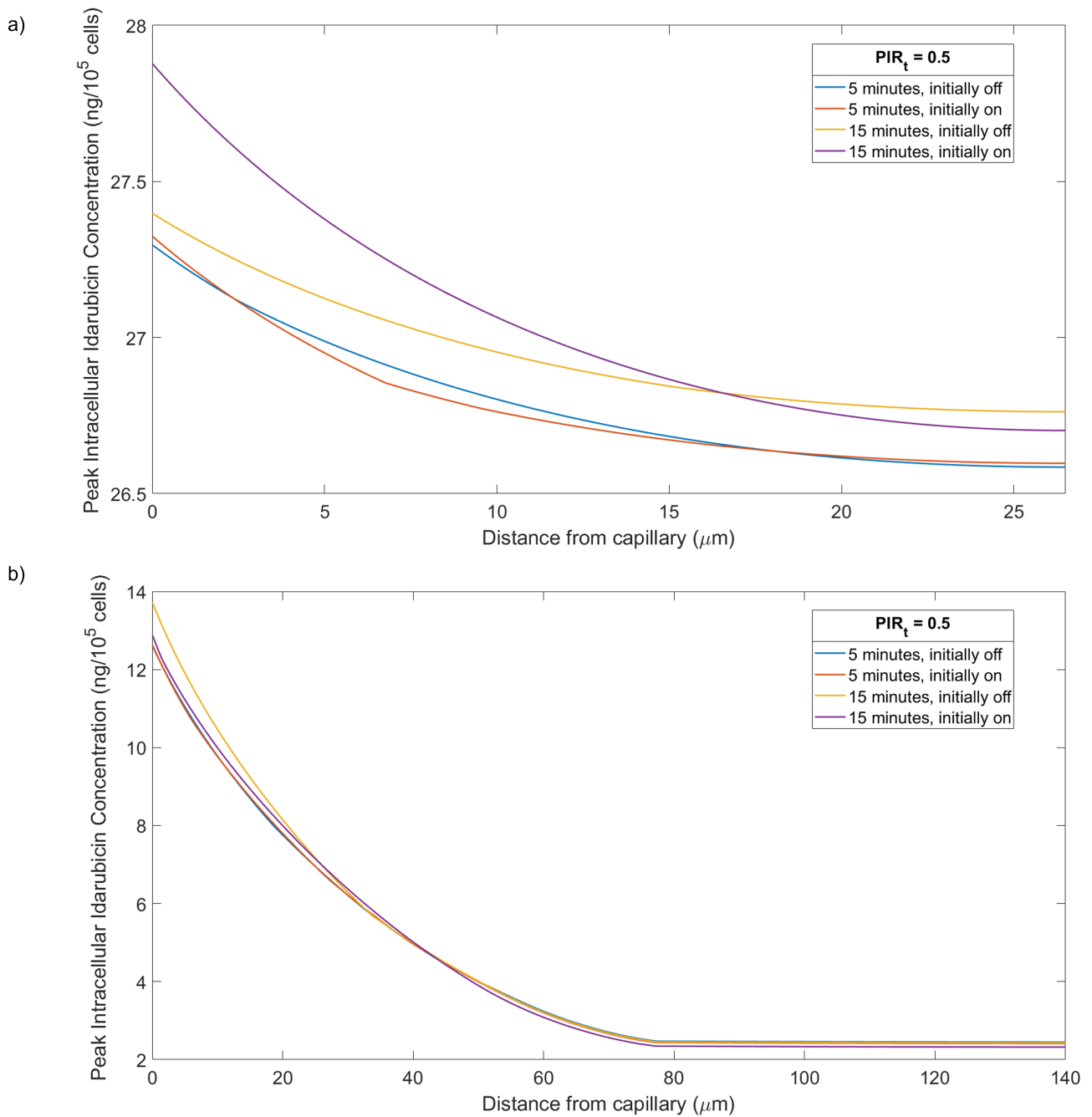


Figure 5.15. Plot showing how temporal PIR affects the spatial distribution of peak intracellular concentration of 'idarubicin' in the regular cylinder (a) and the larger cylinder (b). The infusion durations in both cases were chosen as those that were optimal according to the compartment model - 40 minutes for 5 minute time blocks, and 46 minutes for 15 minute time blocks. Hyperthermia was assumed to start immediately and lasted for 90 minutes.

referenced with the solutions provided by [186] for the washout problem. The washout problem describes a Krogh-style cylinder model, with a concentration initially in the tissue, with no solute in the inflowing blood. The governing equations are:

$$\frac{\partial C^t}{\partial t} - D \left[\frac{1}{r} \frac{\partial C^t}{\partial r} + \frac{\partial^2 C^t}{\partial r^2} + \frac{\partial^2 C^t}{\partial z^2} \right] = 0 \quad (5.13)$$

$$A \frac{\partial C^v}{\partial t} + Q \frac{\partial C^v}{\partial z} = -q \quad (5.14)$$

$$q = -2\pi r_c P (C^t(r_c) - C^v) \quad (5.15)$$

Equation 5.13 describes the concentration in the tissue (C^t), in which D is the diffusion coefficient. Equation 5.14 describes the area-averaged concentration in the vessel, in which A is the vessel cross-sectional area, Q is the volume flow rate, and $q(z, t)$ is the rate of diffusive efflux from the vessel per unit length. Although this formulation explores radial variation in the tissue space, radial variation is ignored in the capillary. This is justified due to the enhanced mass transport resulting from the convection of drug in the blood which is not present in the tissue space¹. Equation 5.15 describes the coupling condition.

The boundary conditions are, firstly, no radial flux at the outer edge of the cylinder:

$$\left. \frac{\partial C^t}{\partial r} \right|_{r=r_t} = 0 \quad (5.16)$$

Second and third, radial flux at the inside of the cylinder (the coupling conditions), are given by equation 5.15 and:

$$q = -2\pi r_c D \left. \frac{\partial C^t}{\partial r} \right|_{r=r_c} \quad (5.17)$$

There are constraints on the z-direction in the tissue space, which is that there is assumed to be no flux on the boundaries, i.e.

$$\left. \frac{\partial C^t}{\partial z} \right|_{z=0,L} = 0 \quad (5.18)$$

Finally, for the washout problem used in [186], and used here as a test case, there is the constraint on the in-flowing blood being free of solute:

¹Considering the $424.4 \mu\text{m s}^{-1}$ velocity over a length scale of $400 \mu\text{m}$ used in this section, with the stated doxorubicin diffusivity, the Péclet number in the vessel is over 3000; so convection dominates.

$$C^v(0, t) = 0 \quad (5.19)$$

although more generally, $C^v(0, t)$ is taken as the free drug concentration obtained from the appropriate compartment model.

An analytical solution is obtained in [186], however when this author applied separation of variables to the problem, a second exponential in z appears which is not present in the analytical solution by Secomb, as below:

$$C^t = (aJ_0(\mu r) + bY_0(\mu r))(e^{\kappa z} + k_1 e^{-\kappa z})e^{-\lambda t} \quad (5.20)$$

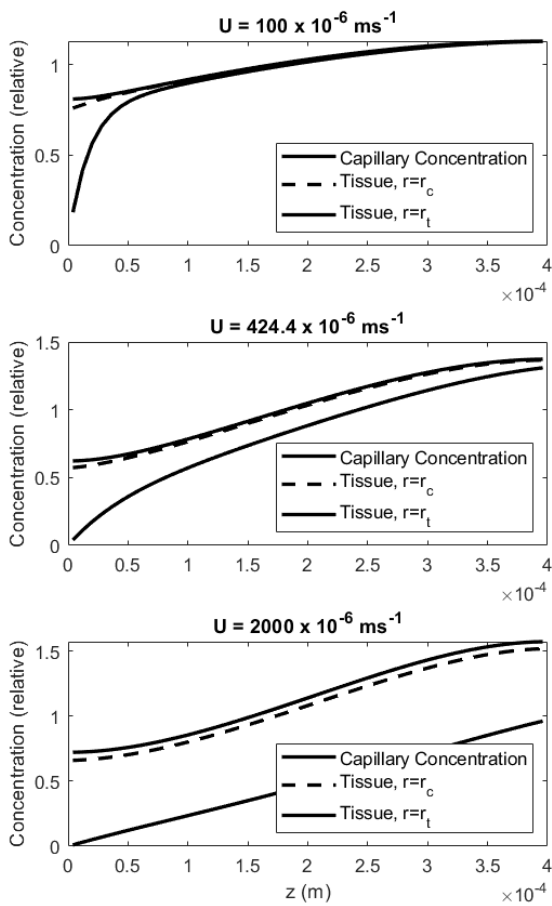
$$C^v = C_0^v(e^{\kappa z} + k_1 e^{-\kappa z})e^{-\lambda t} \quad (5.21)$$

$$q = q_0(e^{\kappa z} + k_1 e^{-\kappa z})e^{-\lambda t} \quad (5.22)$$

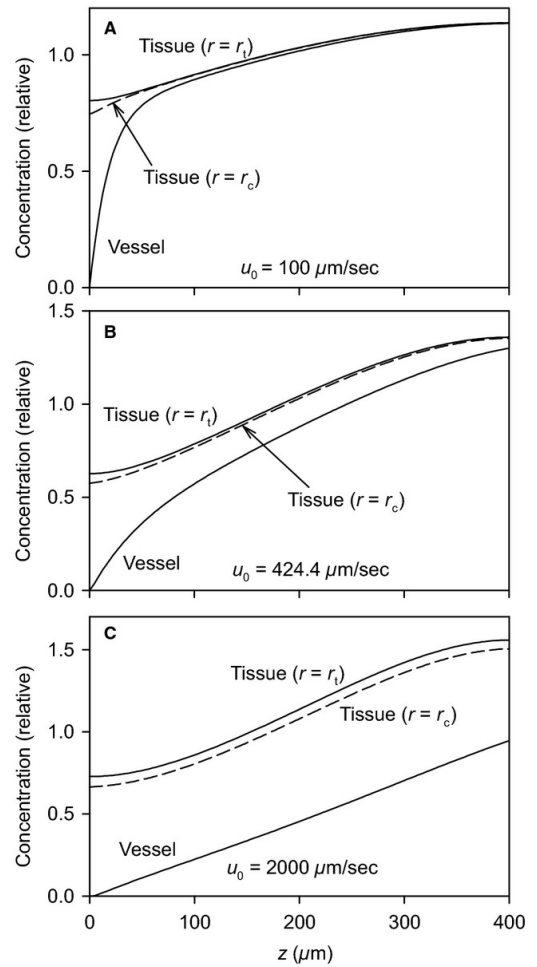
As a result a quantitative comparison to Figure 2 of [186] was used to confirm that the code was correct; this is shown in Figure 5.16.

For simulations of drug infusion, a capillary length of $600 \mu\text{m}$ was used [187], with a flow speed of $500 \mu\text{m s}^{-1}$, which is at the lower end of the reported range [188]; and so the effect of axial changes in concentration would be greater than for a faster flow. This was simulated using both the average and larger tissue cylinder radii given in the previous section, and the concentrations in the tissue and capillary at the end of a 40 minute infusion of free doxorubicin are shown in Figure 5.17.

It has been discussed in the literature that the choice of boundary conditions on the Krogh cylinder artificially decreases the concentrations in the tissue at the far end of the capillary, and that no net flux would be a more appropriate boundary condition to apply [186]. However, Figure 5.17 shows that the axial variation in concentration for the case of doxorubicin delivery to tissue is relatively small; and the impact of tissue radius on the predicted concentrations is much larger. In the average cylinder, the intracellular variation at the far end of the capillary is 98.7% of the value at the inlet, while in the larger cylinder, the equivalent value is 95.4%. Considering the extracellular concentrations at the edge of the tissue, the outlet concentrations represent 98.8% and 94.0% in the average and larger cylinder respectively, while for the capillary concentrations, the equivalent values are 98.6%



(a) Results from implemented finite volume code.



(b) Results from [186].

Figure 5.16. Plot of the concentrations resulting in the exponential phase of the washout problem, as defined in [186], which was used to confirm the implemented finite volume approach (the results from which are shown in Figure 5.16a) was working correctly. The literature results are reproduced from [186] with permission.

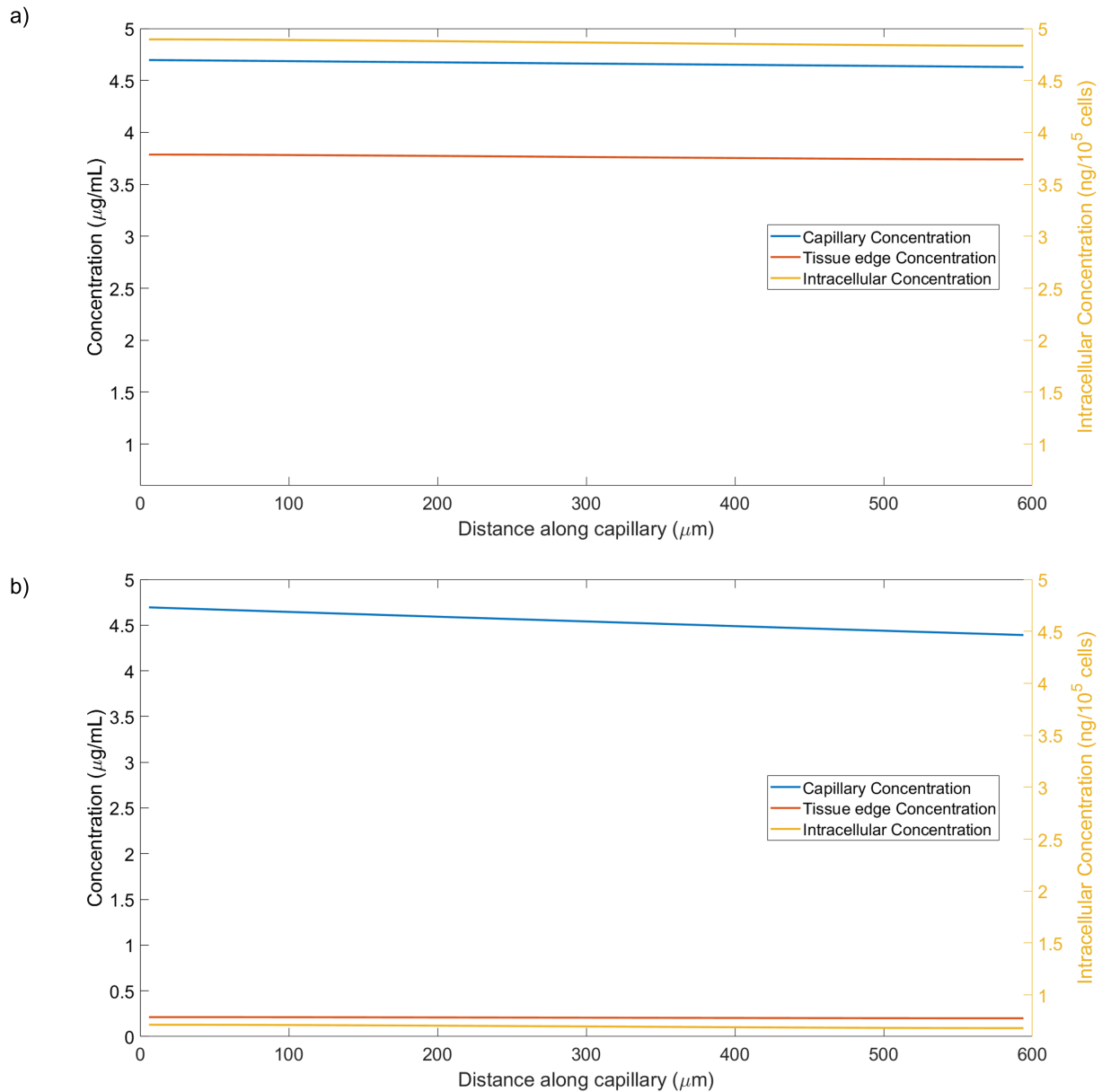


Figure 5.17. The concentrations at time $t = 40$ minutes into an infusion of free doxorubicin over 40 minutes, using the parameters from the compartment model in Chapter 3. The capillary flow speed was taken as $500 \mu\text{m s}^{-1}$, and a) shows the results from an ‘average’ tissue radius of $36.5 \mu\text{m}$, while b) shows the results from a larger tissue radius of $150 \mu\text{m}$.

and 93.5%. These reductions are modest compared to the reductions resulting from varying tissue thickness, and thus do not represent a major limitation of the work.

An attempt was made to introduce a no net flux version of the model, which implemented an additional volume element outside of the cylinder, which took the concentration at each timestep as the mean concentration in the outermost tissue element, but this caused stability issues for a drug infusion problem. The inclusion of no net flux is implemented in [186] using an ‘infinite’ cylinder around the tissue cylinder. This cylinder is required to be infinite for the derivation of an analytical solution to the washout problem, but is not required to be infinite for a stable finite volume code; although a large outer radius, around 10 times that of the tissue radius is required. A strict no flux boundary condition is then applied to the outer, ‘infinite’ cylinder, which contains a uniform source term, such that the boundary between the tissue cylinder and the outer cylinder satisfies no net flux at each timestep. Considering the relatively small reduction in axial concentrations, even applying a strict no flux boundary condition, the increased computational expense associated with simulating a domain 10 times larger was not considered worth pursuing. This decision is further justified by the fact that this could not be implemented in MATLAB’s ODE solvers owing to the time-dependent source term in the outer cylinder.

In summary, axial variations play a very small role in the transport problem when considering drug delivery of these small molecule therapeutics and can be neglected; the choice of radii is far more important.

5.7 Summary

In summary, the inclusion of spatial heterogeneity is a potentially important part of modelling drug delivery to solid tumours from LTSLs, especially for drugs with more rapid cellular uptake kinetics. The transport properties and behaviour of the drug are difficult to reduce to simple metrics which would facilitate knowing when the issue of transport was less important. For instance, reaction is concentration-dependent, which is in turn, a function of the drug’s pharmacokinetic profile, and the chosen infusion and heating parameters.

While spatial heterogeneity represents an important inclusion, the impact of the tissue radius on the predicted concentrations outcomes from a single cylinder mean that the use of a single cylinder

does not add any real benefit. The idea of a weighted sum of 1-D cylinders is perhaps a happy compromise between neglecting spatial heterogeneity and using complex models across microvascular geometry [127]. The cylinders need only be 1-D, as it is shown that consideration of the change in concentration along a capillary does not have a substantial impact on the predicted concentrations.

Treatment with doxorubicin TSLs would most likely benefit from the treatment volume (assuming ultrasound-mediated hyperthermia) being split and treated separately, so as to be more likely to achieve the positive bioeffects of hyperthermia, as well as localised release. It has been shown in this chapter that the peak intracellular drug concentrations achieved are similar for both prolonged hyperthermia time blocks of 15 minutes and shorter blocks of 5 minutes. The same conclusion is also reached for a drug with a more rapid cellular uptake, although a lack of experimental data on idarubicin in this thesis means that this cannot be confirmed.

The overwhelming conclusion from this chapter, however, is that even considering imperfect heating, doxorubicin TSLs are predicted to achieve greater intracellular concentrations than an optimised infusion of free doxorubicin. This suggests that the technology may yet provide real benefit to patients in the clinic. Furthermore, TSLs containing drugs which are otherwise unsuitable for the treatment of solid tumours (such as idarubicin) represent an exciting step, since the delivery platform facilitates the local delivery of drug which would otherwise never reach the tumour.

Chapter 6

Conclusions

The initial objective of this work was to use a combination of *in vitro* and *in silico* experiments to obtain a mathematical model for treatment with LTSLs. The first step was using literature data to demonstrate that compartment models can accurately predict the concentrations seen when the technology is used clinically. It was shown that incorporating non-ideal heating has a substantial effect on the predicted concentrations. Further, use of a temporal sense of non-ideal heating (i.e. the heating being turned on and off during the simulation) is necessary to produce extracellular concentration profiles which are more likely to represent the clinical situation.

A sensitivity analysis demonstrated that the predicted intracellular concentrations are highly dependent on the cellular uptake parameters. A new mathematical model for cellular uptake of doxorubicin in CT26 cells was therefore fitted to the experimental data found in the fourth chapter. Additionally, it was found that mild hyperthermia significantly ($p < 0.05$) increased uptake of and cell kill by doxorubicin in CT26 cells in a monolayer culture. Non-apoptotic mechanisms of cell death were also observed for the short doxorubicin exposure durations tested experimentally, which renders certain, more rapid, cell viability assays unsuitable for assessing cell kill in this instance.

In the final research chapter, the cellular uptake and cell kill models obtained from the experimental work in the preceding chapter were used in computational models. The first finding was that, of the two mechanisms by which mild hyperthermia increases cell kill by doxorubicin, the effect of increased cellular sensitivity to intracellular drug contributes more to the enhanced cell kill than the elevated uptake. It was demonstrated that the amount of drug which reaches the intracellular compartment having extravasated in its liposomal form is negligible for release rates which correspond to the studied LTSLs. Most importantly, the use of LTSL doxorubicin with non-ideal heating was pre-

dicted to result in a substantial improvement in cell kill compared to an optimised infusion of free doxorubicin with mild hyperthermia. Combinations of infusion and hyperthermia duration which are predicted to result in increased intracellular concentrations were presented for both free and LTSL doxorubicin, as well as an LTSL formulation of a drug with more rapid uptake kinetics.

The optimal infusion duration was found to be largely unaffected by including the spatial distribution of the drug in the tissue in a cylinder model in the optimisation. Considering a drug with more rapid cellular uptake, a more substantial variation was seen in achieved drug concentrations across the tissue space, which may represent a limitation of the use of these drugs in the clinic, although this still represents a step forwards, given that previously, using such drugs to treat solid tumours was unthinkable owing to their rapid protein-binding. More complex models to incorporate spatial heterogeneity were considered unnecessary, as axial variation along a capillary was found to have a negligible effect on delivered concentrations; and a weighted-sum of cylinders approach was recommended to avoid the variation in predictions associated with choosing different radii in a cylinder model.

Finally, for both doxorubicin and a drug with more rapid cellular uptake kinetics, it is shown in both a compartment and spatially heterogeneous model that segmenting the tumour into two distinct regions, and then heating each segment in turn for around 15 minutes may be beneficial, since the predicted peak intracellular concentrations are largely unaffected, but prolonged hyperthermia is more likely to induce the therapeutic benefits of elevated cellular uptake, increased cellular sensitivity, and improved perfusion and blood vessel permeability.

6.1 Future Work

For computational models to be of use in the further development of TSLs, more data on the cellular uptake of drugs are required to demonstrate a robustness of response across different cell lines. As is shown over the course of this work, there is limited benefit to using complex models with spatial heterogeneity to try and resolve the effects of treatment with TSLs, since the dependence on model parameters relating to pharmacokinetics and pharmacodynamics is a much greater source of uncertainty than that caused by the use of cylinder models rather than a realistic microvascular geometry.

Experimentally, it would be helpful to be able to refine the estimates for the parameter V_{max} (the maximum rate of cellular uptake associated with saturable transport), since the sensitivity analysis performed at the end of Chapter Four shows that this parameter (or at least the ratio between the hyperthermic and normothermic V_{max}) is that which results in the greatest variation in the predicted cell survival. This could be done using the same experiments as used in Chapter Four, but using a range of concentrations that are closer to the predicted value of K_m (the Michaelis constant), thus increasing the relative magnitude of the transport which is saturable and improving the estimate.

Similarly, k_{out} (the first order rate constant for cellular efflux of drug) could be better defined with an experiment focused purely on efflux, such as treating cells in a 6 well plate format, then, after treatment with drug, washing the wells and lysing the cells in half the wells, while adding fresh (non-spiked) media to the other half. The plate could then be returned to the incubator to facilitate a period of efflux in the latter group of cells. Subsequent analysis of the two samples side by side would help to quantify k_{out} . Further confidence in the mathematical model could also be achieved through applying step changes in concentration applied to the cells, such as by diluting the media in the wells part way through an incubation, or adding a stronger concentration of drug; this technique could also be used to assess the concentrations at which intracellular and extracellular doxorubicin are in equilibrium.

Considering that the increased cellular sensitivity to doxorubicin makes the larger contribution to increased cell kill than enhanced uptake of the drug, it would be informative to answer the specific question of whether the intracellular IC50 is different between normothermia and hyperthermia. While the difference between normothermic and hyperthermic IC50s was not significant in the experiments in this thesis, this is unsurprising given the broad range of concentrations assayed, which were not targeted to give intracellular concentrations close to the IC50, but rather to examine the full range of the cytotoxic effect of doxorubicin. Alternative techniques to those used in this work are better-suited to the problem of determining the intracellular IC50, such as the clonogenic flow cytometric assay developed by Maass et al. [175]. While the IC50 is the metric measured through fitting a Hill curve, using such a method to determine the change in intracellular IC90 or even IC95 may provide a more useful metric of the clinical benefits of using mild hyperthermia in conjunction with small molecule therapeutics, since it is necessary to know that hyperthermia also lowers the required intracellular drug concentrations for near-complete cell kill (as opposed to just 50%).

It is accepted that hyperthermia either before or after treatment increases cellular sensitivity to ra-

diotherapy, and that the closer in time the hyperthermia and treatment occur, the greater the benefit of hyperthermia [176]. The question of the timing of the hyperthermia for maximum benefit (in the absence of a TSL delivery system) with chemotherapy was not addressed in this work. It would be insightful to sample uptake and cytotoxicity at a range of temperatures from 36°C to 45°C before, during and after treatment to provide useful information on how long the effects last, and the variation observed as temperature varies, since non-uniform temperature fields are expected when the technology is used in the clinic.

Further studies on the effect of mild hyperthermia with doxorubicin should be performed using a more complex (i.e. 2.5D or 3D) cell culture model. The use of a more complex model will result in a higher degree of confidence in the obtained effects of hyperthermia, since the culture conditions more closely reflect the situation *in vivo* and in patients. For example, as discussed in the literature review, it has been shown that the cellular uptake of doxorubicin is modulated by the presence of extracellular matrix proteins [155], which are not present in 2D monolayer culture.

More broadly, the finding that liposomal extravasation does not contribute substantially to drug delivery with LTSLs suggests that it may also be worth exploring using different sizes of LTSLs, since there is no benefit to the 100 nm size range in terms of passive targeting via the EPR effect. However, this is a challenging area of study, much of which falls outside the scope of the current work, involving a complex interplay between factors such as nanoparticle size, shape, and surface charge. The computational model created in this thesis (or a similar model) would be a useful screening tool for assessing the required parameters to improve treatment. For example, if a smaller liposome with enhanced pharmacokinetics was produced, which was leakier (i.e. had a greater rate of release at 37°C, as smaller liposomes are typically less stable [179]), the computational model would be able to provide a quantitative answer as to what release rate at normothermic conditions was required to likely provide an improvement over the existing system.

Looking towards bringing the technology into clinical use, it is clear that LTSL technology requires more trials. A barrier to clinical adoption is that free doxorubicin alone is not usually used to treat solid tumours, so a comparison between clinical use of the free and LTSL drug would not demonstrate that LTSLs provided better outcomes than the standard of care.

To this end, a trial with an LTSL containing a drug which is a standard of care for a given indica-

tion would (if successful), represent a huge step towards the clinic. To maximise the chances of success, ultrasound-mediated hyperthermia should begin just before the infusion to ensure that the target is hyperthermic from the start of the infusion. The segmentation of the treatment volume into two smaller volumes which are more likely to be able to be maintained within the optimal release temperatures for the LTSLs for blocks of 15 minutes is recommended to maximise the therapeutic effect of the treatment.

Considering TSL technology with other heating modalities, such as microwave heating, there is a case to be made that certain heating modalities may be better suited for different applications of TSL technology than others. Considering the two different clinical cases of a single primary tumour, ultrasound heating may be beneficial, particularly in the case when the tumour needs shrinking before surgery to remove the tumour (termed neo-adjuvant chemotherapy). The focused nature of ultrasound is potentially useful when the surgery requires the tumour to be shrunk in a particular way (i.e. away from a major blood vessel, or functional part of an organ), such that the problematic part of the tumour cannot be safely reached with microwave heating probes. Conversely, for patients with metastatic disease, the multiple locations which can be targeted at once with microwave heating is potentially beneficial. Conversely, if there is a particular metastasis causing pain or threatening a vital function, such as nausea occurring as a result of a pancreatic tumour pressing on the stomach; ultrasound may represent a relieving localised treatment.

Appendices

Appendix A

Global Sensitivity Analysis and Lessons For Using Small Animal Models

A.1 Example Elementary Effects Test: Interpreting the Results

As stated in Chapter Three, sensitivity analyses were performed in MATLAB using the SAFE toolbox [143], with the elementary effects test, using Latin Hypercube Sampling to vary the model parameters within a given range. To provide an illustrative example to aid interpretation of the results, a global sensitivity analysis is performed here on the following simple model:

$$y = A_1 + B_1B_2 + C_1e^{C_2} + D_1e^3 \quad (\text{A.1})$$

with the parameter ranges as given in Table A.1. As given in Equations 3.14 and 3.15, the standard deviation (σ) is a measure of the interactions and non-linear effects, while the mean (μ) is an assessment of the overall importance of the variability of an individual input on the output of a model. This sensitivity analyses in this work use an adjusted mean, based on the magnitude of the elementary effect, rather than the sum of the elementary effects (which is not a good indicator for models which are non-monotonic) [189].

The results for the model are presented in Figure A.1, with the mean of the elementary effect plotted on the x-axis, and the standard deviation of the elementary effect plotted on the y-axis. It can be seen that A_1 and D_1 both have a standard deviation of zero, which makes sense, given that their relationship with model output is strictly linear, and neither parameter interacts in any way with another. The mean effect for D_1 is just over double that of A_1 since e^3 is just greater than 20, so a fluctuation in the value of D_1 by 5% (from 1 to 1.05) changes the output by just over 1; whereas a 5% fluctuation

Parameter	Value
A_1	9.5 - 10.5
B_1	9.5 - 10.5
B_2	0.95 - 1.05
C_1	0.95 - 1.05
C_2	0.95 - 1.05
D_1	0.95 - 1.05

Table A.1. Parameter ranges in the example sensitivity analysis.

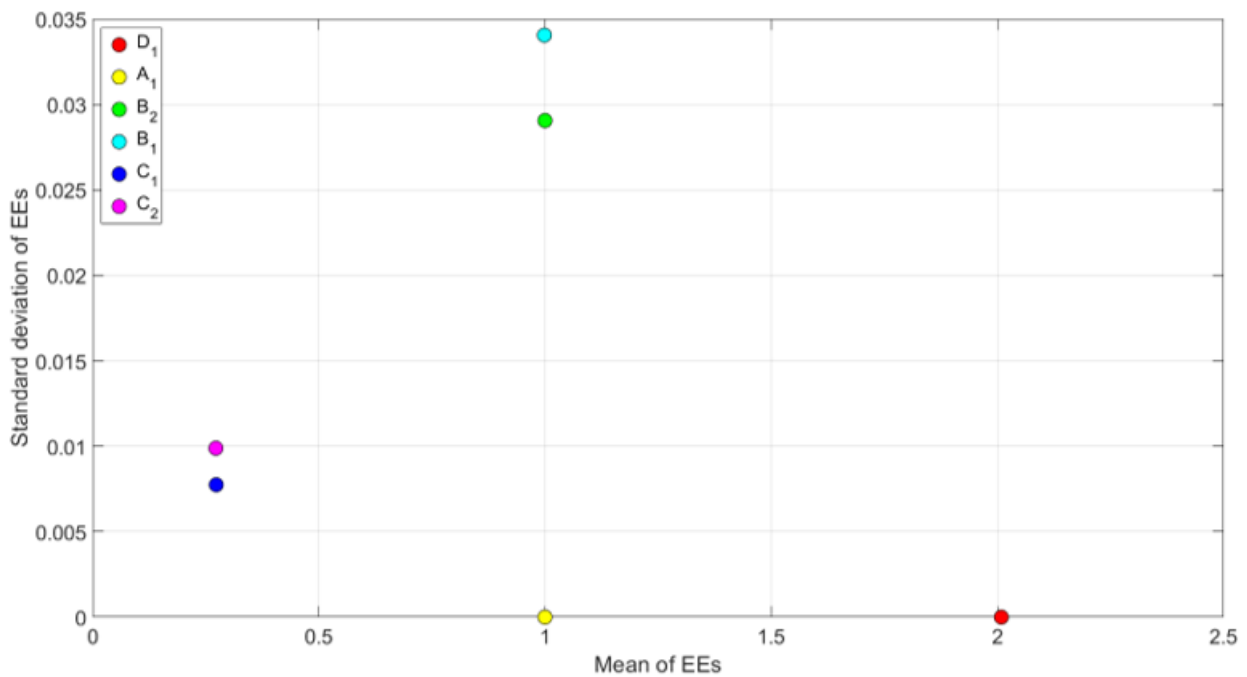


Figure A.1. Results of an example sensitivity analysis, for the output as described by Equation A.1, with variables as in Table A.1. $r=10$.

in A_1 changes the output by 0.5. Hence the mean of the elementary effects for D_1 is fractionally over double that of A_1 . If the range over which parameter A_1 is allowed to vary doubles (to $\pm 10\%$), the mean elementary effect of A_1 would become 2.

The other terms all have a measure of interaction and, in the case of C_2 , non-linearity, which is captured by the plot. The most general way of interpreting these plots is that the further from the origin the variables are, the more influence their variability has on the output. In all the results plots, variables are sorted in the legends in descending order of mean.

A.1.1 Sensitivity Analysis on Model Output

In addition to the sensitivity analysis performed using the peak intracellular concentration as an output, two other sensitivity analyses were performed on different model outputs. Firstly the area under the curve of the free doxorubicin concentration in the tumour plasma (from $t=0$ to $t=3$ hours), and secondly the area under the curve of the free doxorubicin in the systemic tissue. The first metric was selected as an alternative measure of treatment efficacy (since the cellular uptake model is subject to substantial uncertainty, the area under the curve was felt to be an appropriate second metric for drug delivered to target), while the final metric was chosen as a measure of the side effects (as the systemic free doxorubicin concentration is what is likely to result in off-target toxicity). $r = 1000$ in these simulations, and PIR_s was varied between 0.25 and 0.75. All other inputs were varied as described in Table 3.2 The results of these analyses are presented in Figures A.2 and A.3 respectively.

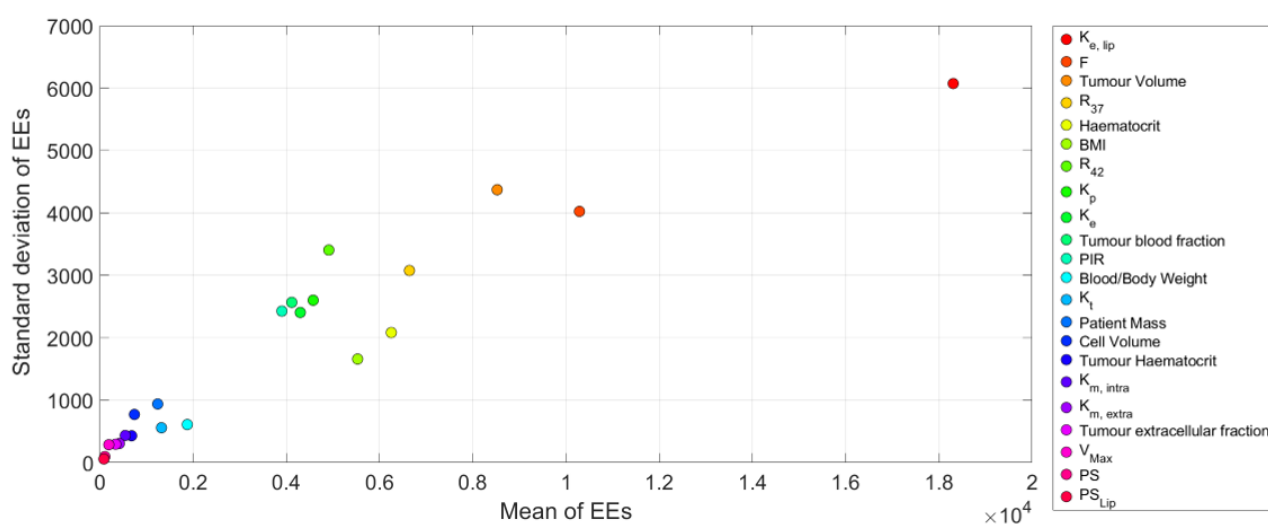


Figure A.2. Results of the elementary effects test using the area under the curve of tumour plasma concentration of free doxorubicin from $t=0$ to $t=3$ hours as an output. $r = 1000$.

The sensitivity analysis for the area under the curve (AUC) of the tumour plasma concentration-time plot (Figure A.2) shows that a parameter which is controllable (to some extent), the clearance rate of the liposome, has the most effect on the output. Beyond that, two parameters for which clinical measurement is possible have the second and third largest effects; the tumour volume, and the tumour perfusion. The effects of varying these parameters alone on both tumour plasma AUC and peak intracellular concentration are shown in Figure A.4.

The effect of varying the clearance rate of the liposomal form of the drug is as expected; increasing the circulation time of the drug increases the plasma AUC and the peak intracellular concentration.

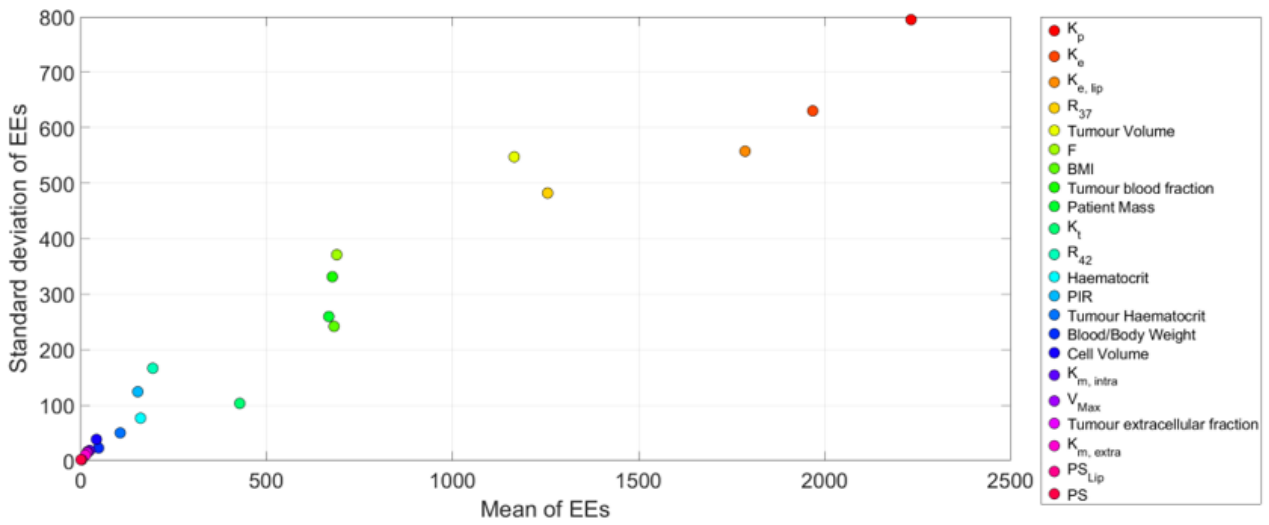


Figure A.3. Results of the elementary effects test using the area under the curve of systemic tissue concentration of free doxorubicin from $t=0$ to $t=3$ hours as an output. $r = 1000$.

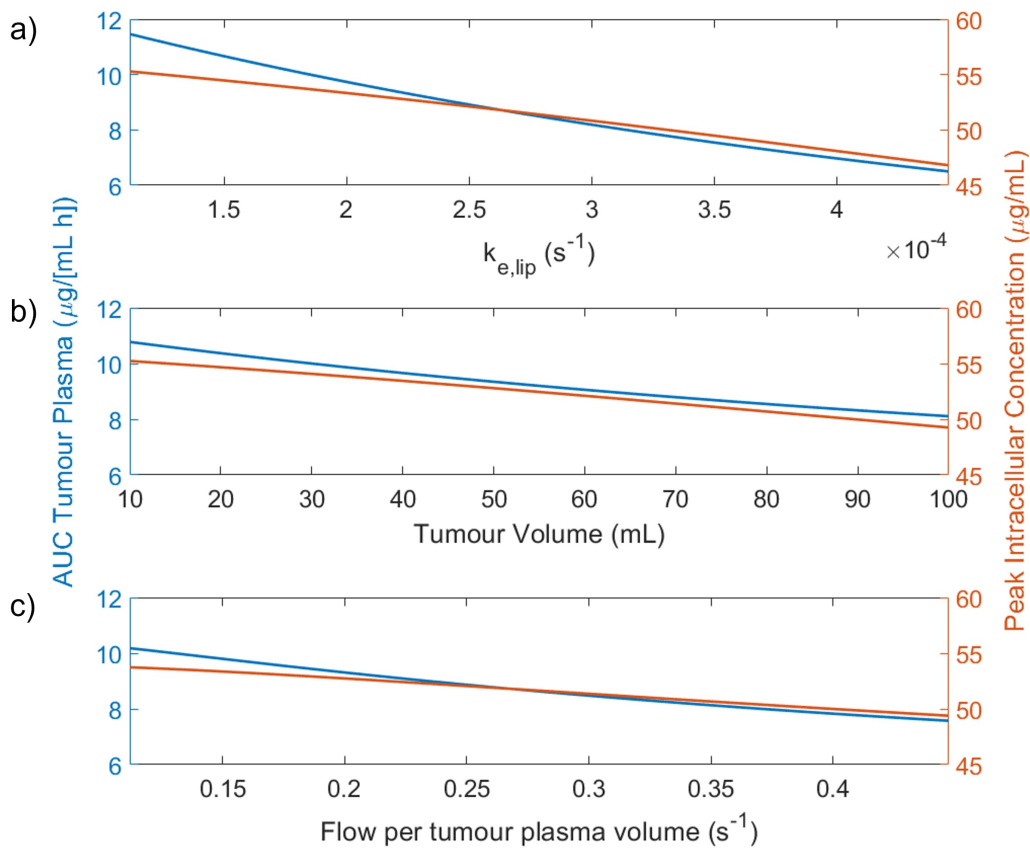


Figure A.4. Plot showing how varying different parameters affects the tumour plasma AUC (left Y axis) and peak intracellular doxorubicin concentrations (right Y axis) for a) liposomal doxorubicin clearance, $k_{e, lip}$, b) Flow per tumour plasma volume, F , and c) tumour volume, with all parameters varied between the range as given in Table 3.2.

Increasing tumour perfusion decreases both the plasma AUC and the measured peak intracellular concentration, however this result should not be over-interpreted, since this parameter attempts to group multiple effects which cannot be fully resolved by a compartment model.

The reason for the decreases in output concentrations as F is increased is that the elevated blood flow prevents accumulation of very high concentrations of free drug in the plasma, and also hastens the efflux of drug from the tumour (it has previously been shown that high rates of mass transport from the tumour back into the blood stream substantially limit sustained tumour accumulation [46]). Additionally, increased values of F will likely decrease the mean transit time of the liposomal form of the drug through the tumour, reducing the efficiency with which drug is released. However, the compartment model does not take into account the effect of an increased number of blood vessels which would occur in a more vascularised tumour, which would likely act to increase therapeutic effect, as the tissue will be less hypoxic, and transport through the extracellular space is less of a barrier to delivery.

In Figure A.4c, it can be seen that the increased tumour volume results in decreased tumour plasma AUC. Further examination of the concentration profiles in this case shows that this is due to increased drug release from the liposomes, with the free drug then being cleared more rapidly, resulting in a reduced AUC. This is not realistic, since above a certain size, the tumour volume which is being maintained at 42°C will be limited by the ultrasound heating and the cooling effect of tissue perfusion, so the percentage of drug release from the liposomes would not be so strongly related to tumour size - this is a further indicator of the limitations of PIR_s . Despite this, it is true to assume that larger tumours will be more difficult to treat owing to difficulties reaching and maintaining a state of mild hyperthermia over the treatment volume - but here the model shows this for the wrong reasons.

Finally, as a patient characteristic, it is interesting to see that BMI variation was responsible for one of the larger mean elementary effects. Although the discussion of the impact of BMI on chemotherapy is a separate area of study, which is somewhat outside the scope of the current work, the results are worthy of a brief discussion. The model clearly predicts that as BMI increases, both tumour plasma AUC and peak intracellular concentration decrease, as is shown in Figure A.5. This is due to the model predicting more drug in the peripheral tissue compartment, as the volume of this compartment relative to the tumour and plasma compartments is increased (there is no accounting, however, for the fact that k_p is likely affected by greater amounts of body fat). Additionally, the way that the dose is

calculated based on patient surface area means that larger patients see reduced systemic concentrations of free drug; a fact which is especially relevant given that many clinicians define a 'maximum' patient surface area, above which they will not further increase the dosage [190]. When it is further considered that another likely effect of elevated BMI is reduced hyperthermia (in the ultrasound-mediated case), since body fat associated with increased BMI attenuates ultrasound [191], it may be worth focusing initial clinical translation efforts on patients with healthy BMIs.

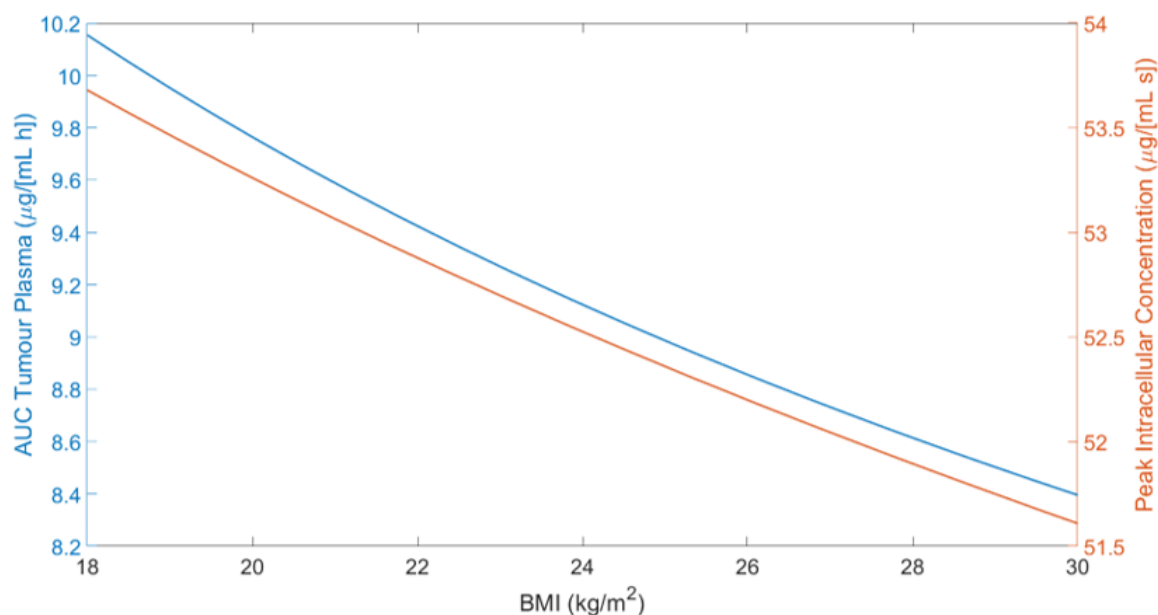


Figure A.5. Plot showing how variation in BMI impacts both tumour plasma AUC of free doxorubicin (left axis) and peak intracellular concentration (right axis).

The results of the sensitivity analysis for the systemic tissue concentration (Figure A.3) are as expected, being highly dependent on the value of k_p , the rate at which drug extravasates from the blood into the peripheral tissues. As this parameter covers so many different processes, it is highly challenging to obtain small confidence intervals for this parameter for a specific patient or patient group. Beyond this, it is largely dependent on the clearance of the free drug, and the encapsulated drug, which is as expected, since these parameters have the most affect on the concentration of drug in the blood. This is not necessarily true in some small animal models, in which the ratio of the heated volume to systemic tissue volume is much larger, and so associated parameters (i.e. heated tumour volume and PIR) would be expected to affect the tissue concentration more.

R_{37} (s^{-1}) (Optimal Infusion Duration in minutes)	Peak Intracellular Concentration ($\mu\text{g}/\text{mL}$) PANDOX protocol	Peak Intracellular Concentration ($\mu\text{g}/\text{mL}$) 'Average optimal protocol'	Peak Intracellular Concentration ($\mu\text{g}/\text{mL}$) Optimal Protocol
0.0001 (55)	63.9	64.3	64.4
0.0002 (66)	62.4	63.9	63.9
0.0003 (76)	60.7	63.4	63.4

Table A.2. The variation in peak intracellular concentration for different infusion times and values of R_{37} , with values rounded to the nearest $0.1 \mu\text{g}/\text{mL}$. Cell volume taken as 10^{-9} mL, $\text{PIR}_s = 0.5$.

A.2 Non-Optimal Infusion Durations - Effect on Intracellular Concentrations

The differences between using the optimal infusion duration based on the chosen and the extreme values of R_{37} are presented in Table A.2 for the case of 90 minutes of hyperthermia beginning with the infusion. The predicted peak intracellular concentrations from the idealised PANDOX protocol (30 minutes of infusion, with 90 minutes of hyperthermia) are also given for comparison.

The changes in peak intracellular concentration between the optimal infusion duration, and the infusion duration based on the original value of R_{37} are small, which demonstrates a good degree of robustness in using compartment models for treatment optimisation. In comparison, the use of the PANDOX protocol for the leakiest LTSLs result in 4.26% less intracellular drug compared to the optimum protocol.

A.3 *In vivo* models and Compartment Models

Previous literature studies [85, 120] have demonstrated good agreement between similar simulations and *in vivo* experiments in small animal models. Given the uncertainty in model output which results from the cellular uptake parameters, it is clear that part of the reason for their success has been using methods which do not rely on the intracellular concentration to validate the computational model. In [120], although a model was used to predict the tumour concentration profile, the comparison is made

between the fluorescence intensity of the tissue and the predicted spatial doxorubicin concentration profile following ultrasound-mediated hyperthermia. Similarly, in [85], experimentally derived parameters are used to create a predictive model which is shown to have a high accuracy in experiments using an LTSL containing a cell-impermeant dye (as opposed to doxorubicin), which thus meant cellular uptake terms in the model were neglected. In this section, an attempt is made to use literature data to compare the results of the computational model to a representative pre-clinical literature study.

The representative *in vivo* study of LTSL delivery chosen was that of Tagami et al. [192]. In this study, 3 mg/kg free or LTSL doxorubicin was given as a bolus to a mouse with a hind leg tumour, which was heated to 42°C for one hour post dose (with the heating initiated 10 minutes prior to the administration of drug). Tumour concentrations were established through sacrificing the mice after the hour, and analysing the tissue concentrations with an HPLC method. The resulting concentrations in the heated tumour increased by a factor of 3.8 between treatments with free and LTSL doxorubicin. The concentrations measured in the tumour (found from Figure 3 of [192]) were found to be 1.30 $\mu\text{g/g}$ and 4.91 $\mu\text{g/g}$ for unencapsulated and LTSL drug delivery respectively.

The parameter values used to simulate this pre-clinical study (which differ from those given in Table 3.1) are displayed in Table A.3. The results of the simulation are shown in Figure A.6. The predicted biopsy concentrations (a weighted sum of the components) are 6.78 $\mu\text{g/g}$ for free doxorubicin and 11.38 $\mu\text{g/g}$ for LTSL doxorubicin (assuming a tissue density of 1.05 g/mL [141]). Evidently, these results are both more than double the obtained *in vivo* results, although do correctly predict a greater concentration of intratumoural drug for treatment with LTSLs. Examining the plots in the figure provides a clearer indication as to why; the biopsy results at this time are almost entirely dependent on the predicted intracellular concentration¹, which is known to vary substantially between cell lines [e.g. 41, 95].

A further confounding factor is that the choice of cell volume/intracellular volume fraction has a large impact on the model output concentration in $\mu\text{g/g}$, since experiments to determine the cellular uptake of drug do so on a basis of ng/10⁵ cells (or some multiple thereof). The cell volume which has been used in much previous modelling work is 10⁻⁹ mL, however the Bionumbers database [141] suggests that a suitable range of cancer cell volumes (based on HeLa cells) is 1.2 - 4.3 x 10⁻⁹ mL, with a mean

¹The very low concentrations in the extracellular space reported in the Figure are not necessarily representative of what would be expected *in vivo*. This is due to the fact that binding to extracellular matrix proteins is not incorporated explicitly in this model.

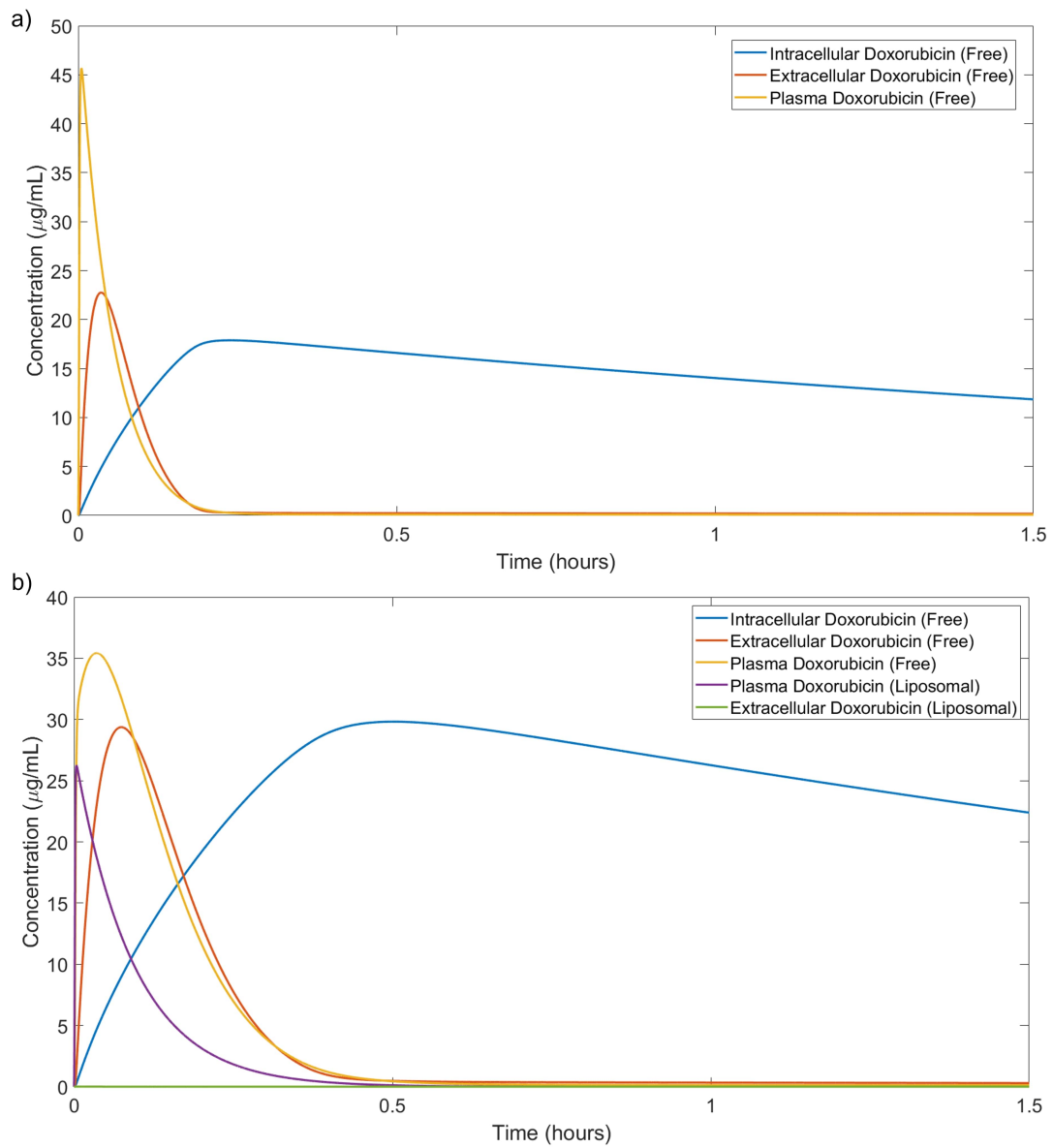


Figure A.6. Results of the compartment model simulation for a murine model for a bolus dose of free doxorubicin (a) and LTSL doxorubicin (b), followed by one hour of hyperthermia.

of 2.4×10^{-9} mL, so a cell volume of 10^{-9} mL clearly corresponds to a very small cell. To illustrate the impact of cell volume on predicted biopsy results (assuming that cellular volume fraction in the tumour is fixed), the cell volume range of [141] results in predicted biopsy concentrations (for free doxorubicin treatment) of $2.87 \mu\text{g/g}$ to $6.10 \mu\text{g/g}$; so varying this parameter within a reasonable range can change the predicted biopsy concentration by a factor greater than two.

A further reason for the inaccuracy of this simulation compared to the study results is likely that the pharmacokinetic parameters used are not accurate; Tagami et al. also took samples of blood to determine the concentration of drug in the systemic circulation at one hour, and reported higher concentrations than are predicted by the compartment model. This suggests that perhaps the clearance used in this model is too fast, or that the clearance of the drug is a saturable phenomenon. While it would certainly be possible to cherry-pick values from the literature here which provide a better fit to the chosen experiment, to do so would not provide a fair representation of how pre-clinical literature values often compare to model predictions.

There are two additional reasons why matching the results of pre-clinical studies is so challenging. The first is that the clearance of the liposomes is highly dose-dependent, and a saturable phenomenon [44]. The second source of increased variability in this model is that the tumour is far larger as a proportion of the mouse's volume (and indeed, the whole limb is heated). In this case, one would expect 'local' hyperthermia to have a notable effect on the plasma concentration profile of the drug. This is likely to increase the sensitivity of the modelling to the values of the parameters associated with liposomal release and blood flow.

A.3.1 Comparing LTSL and Free Drug Delivery *In Vivo*

One feature of some *in vivo* studies is the comparison of bolus doses of free and LTSL doxorubicin. Using the compartment model, it can be observed that comparing bolus doses of free and LTSL doxorubicin is not a good indicator of likely patient benefit, but rather an indication that liposomes circulate in the plasma for longer. This can be shown in the model in both the *in vivo* and in man case.

In vivo, using the parameters given above, the optimal infusion duration of LTSL with one hour of hyperthermia (as used by Tagami et al.) is 58 minutes, while the optimal infusion of free doxorubicin is found to be 78 minutes. The resulting intracellular concentrations from the optimal infusions and

Parameter	Value	Source
Dose (mg)	0.06	Based on a 3 mg/kg and a 20 g mouse.
V_p^s (mL)	18.4	Based on a 20 g mouse, subtracting blood, and assuming tissue density is approximately 1 g/mL.
Tumour Volume (mL)	0.268	Sphere with diameter 8 mm. [192].
V_p^S (mL)	0.88	Assumed 20 g mouse, with 80 mL/kg of blood [193] and a haematocrit of 0.45.
k_e (s ⁻¹)	6.1×10^{-3}	As in [194].
$k_{e,ip}$ (s ⁻¹)	2.78×10^{-5}	As in [46].
k_p (s ⁻¹)	8.08×10^{-4}	As in [194].
k_t (s ⁻¹)	1.30×10^{-5}	As in [194].

Table A.3. Parameters used in the mouse model of LTSL doxorubicin delivery. All parameters not shown are unchanged from the values in Table 3.1.

bolus doses are tabulated in Table A.4. From this, it can be observed that the relative improvement in treatment seen between the two bolus doses is 1.66; but between the two optimal infusions, it is lower at 1.24.

This is also true in the clinical case: Table A.5 shows the results of the model for comparing bolus and the idealised PANDOX protocol (30 minutes of infusion, 90 minutes of hyperthermia) which is taken as a clinically feasible usage of LTSLs. There is a more than three-fold increase in predicted peak intracellular concentration when the two bolus doses are compared, whereas the increase between the PANDOX protocol and optimal free drug infusion is much more modest. This shows that, if comparative efficacy is a desired study outcome *in vivo*, bolus doses should be avoided, and infusions used where possible.

Treatment Protocol (Mouse)	Infusion Duration (mins)	Start Hyperthermia (mins)	End Hyperthermia (mins)	Peak Intracellular Concentration ($\mu\text{g/mL}$)
LTSL (bolus)	0.1	0	60	29.8
Free (bolus)	0.1	N/A	N/A	17.9
LTSL (Optimal)	58	0	60	49.7
Free, optimal infusion	78	N/A	N/A	40.0

Table A.4. The results obtained from simulating a mouse model with different infusion durations of free and LTSL doxorubicin. The increase in efficacy which appears when comparing the two bolus doses appears far more impressive than the comparative increase between the optimal protocols.

Treatment Protocol (In Man)	Infusion Duration (mins)	Start Hyperthermia (mins)	End Hyperthermia (mins)	Peak Intracellular Concentration ($\mu\text{g/mL}$)
LTSL (bolus)	0.1	0	60	23.2
Free (bolus)	0.1	N/A	N/A	6.8
LTSL (PANDOX)	30	0	90	56.3
Free, optimal infusion	117	N/A	N/A	47.3

Table A.5. The results obtained from simulating (in man) different infusion durations of free and LTSL doxorubicin. The increase in efficacy which appears when comparing the two bolus doses appears far more impressive than the comparative increase between the PANDOX protocol and the optimal free doxorubicin infusion.

Appendix B

Justification of Experimental Parameters

In this Appendix, further experimental work performed to assess and optimise the cell viability assays performed in Chapter Four is presented.

B.1 Acceptable Level of Doxorubicin Solvent

Dimethyl sulphoxide (DMSO) is routinely used as a solvent for doxorubicin hydrochloride powder to make stock solutions, due to the high solubility of doxorubicin in DMSO (100 mg/mL, compared to 10 mg/mL in water [195]). In early experiments, medium was spiked from a 1 mg/mL stock solution of doxorubicin, resulting in a variable concentration of DMSO in the media, up to a maximum of 6.4%.

Use of DMSO in assays for small molecule therapeutics is very common, and according to Verheijen et al., 'the use of DMSO is so obvious that applied concentrations are often unreported. DMSO is generally accepted as nontoxic below 10% (v/v) and, in practice, it is assumed that effects of DMSO are negligible' [196]. It is generally accepted that higher concentrations have significant bioeffects; computational studies have shown that DMSO interacts with the lipid cell membranes [197], forming pores in the membrane at higher concentrations (>30%) while cytotoxicity has been demonstrated experimentally; de Ménorval et al. [198] showed that in Chinese Hamster Lung Fibroblast cells (DC-3F) cells, blebbing could clearly be observed at 30 vol-% DMSO. The authors also observed that the transport of a cell permeant entered the cell more readily at just 5 vol-% DMSO than with no DMSO in the media. The cell membrane even became permeable to a membrane impermeant, Yo-Pro-1 at around 20 vol-% DMSO. This, in combination with de Ménorval demonstrating that at 10 vol-% DMSO, undulations of the plasma membrane can be observed suggest that such concentrations are inappropriate for experiments dealing with cellular uptake of a drug.

At lower concentrations (1 vol-% and below) of DMSO, again, there are reports of bioeffects, however there is less agreement in the literature: Verheijen et al., found that 0.1 vol-% DMSO altered microRNAs in an iPSC-derived cardiac model, however Wen et al. [199] described low levels (<1 vol-%) of DMSO increasing cell growth rates in myeloma. To determine if 1 vol-% was an acceptable concentration to take forwards, two MTS assays were performed; one assessing the effect of a two hour exposure to DMSO, and the second assessing the impact of a 24 hour exposure.

The results of the two hours exposure (Figure B.1) seem to suggest that the addition of DMSO at both 1 and 6.4 vol-% does not have a significant impact on cell viability as measured by MTS. However with a 24 hour exposure (Figure B.2), viability of cells in 6.4% DMSO dropped to 59.8%; clearly showing that such a concentration should be considered toxic; in many ways, it is surprising that this effect is not seen with a two hour exposure. As well as the results of the MTS assay, microscopy images are perhaps the clearest indicator of the effect that DMSO is having on cells. Figure B.3 shows loss of adhesion and rounding of the cells after just one hour of exposure to 6.4 vol-% DMSO.

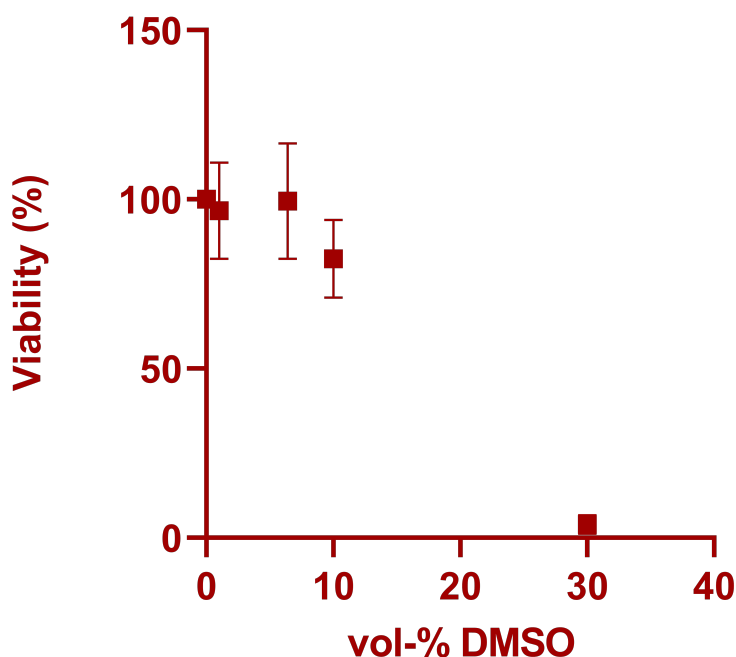


Figure B.1. Analysis of the impact of a 2 hour exposure to DMSO on cell viability assessed by MTS assay 24 hours following removal of DMSO (Method: Section 4.3.2). Brown squares represent the mean of five independent wells, error bars represent standard deviations.

As a result of the visible changes in cell morphology (from spread and fibrous to raised and rounding) after only a 1 hour exposure to 6.4 vol-% DMSO, it was decided that all experiments would be performed with a 1 vol-% DMSO concentration. Cells exposed to 1 vol-% DMSO for 2 hours were imaged

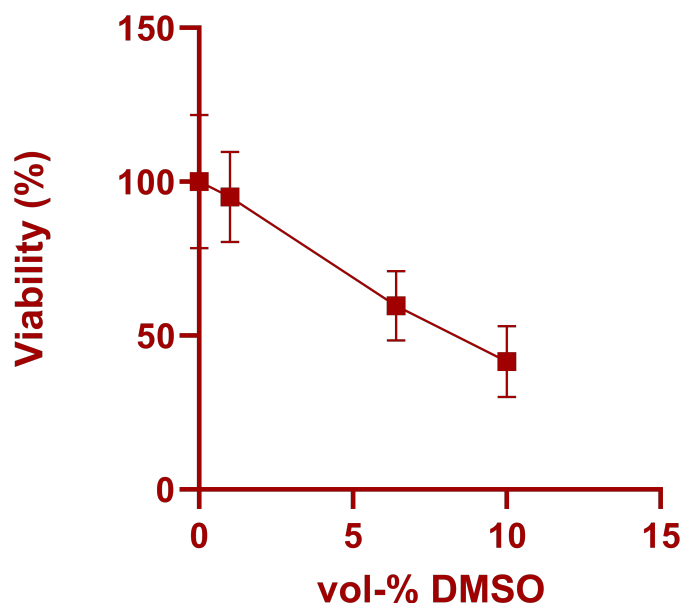


Figure B.2. Analysis of the impact of a 24 hour exposure to DMSO on cell viability assessed by MTS assay immediately following removal of DMSO (Method: Section 4.3.2). Brown squares represent the mean of five independent wells, error bars represent standard deviations.

using the Celigo - as shown in Figure B.4, demonstrating that morphological changes are negligible (while the MTS viability for a 24 hour exposure to 1 vol-% DMSO is not significantly different to the negative control).

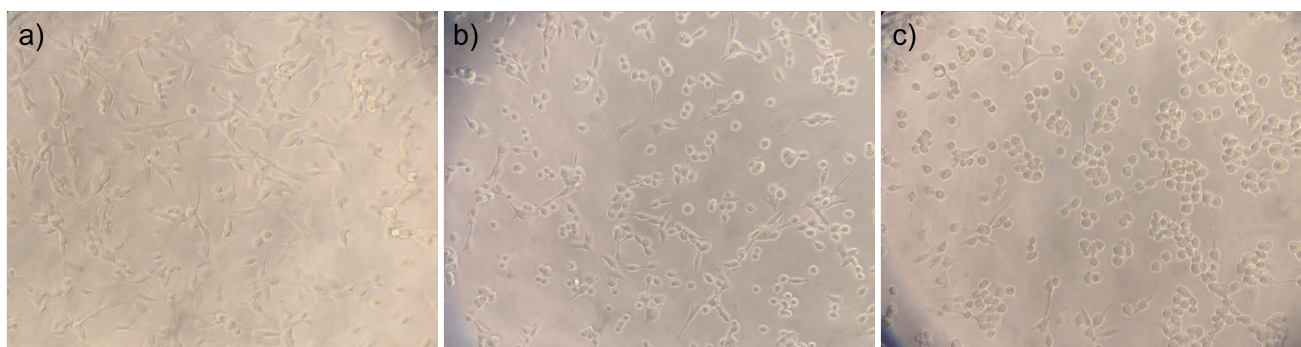


Figure B.3. 20x Magnification of cells after 1 hour of exposure to different concentrations of DMSO. A) DMSO-free control, B) 6.4 vol-% DMSO, C) 30 vol-% DMSO.

B.2 Consideration of Doxorubicin-Protein Binding

When administering drugs systemically, a portion of the drug will bind to proteins in the blood; this proportion can have a significant effect on the pharmacokinetics and pharmacodynamics of the drug, as bound drug may not undergo the same degree of renal clearance, nor interact with its target in the same way as the unbound drug [48]. The same protein-binding can also affect the results of *in vitro* work, as drug binds to proteins in the FBS.

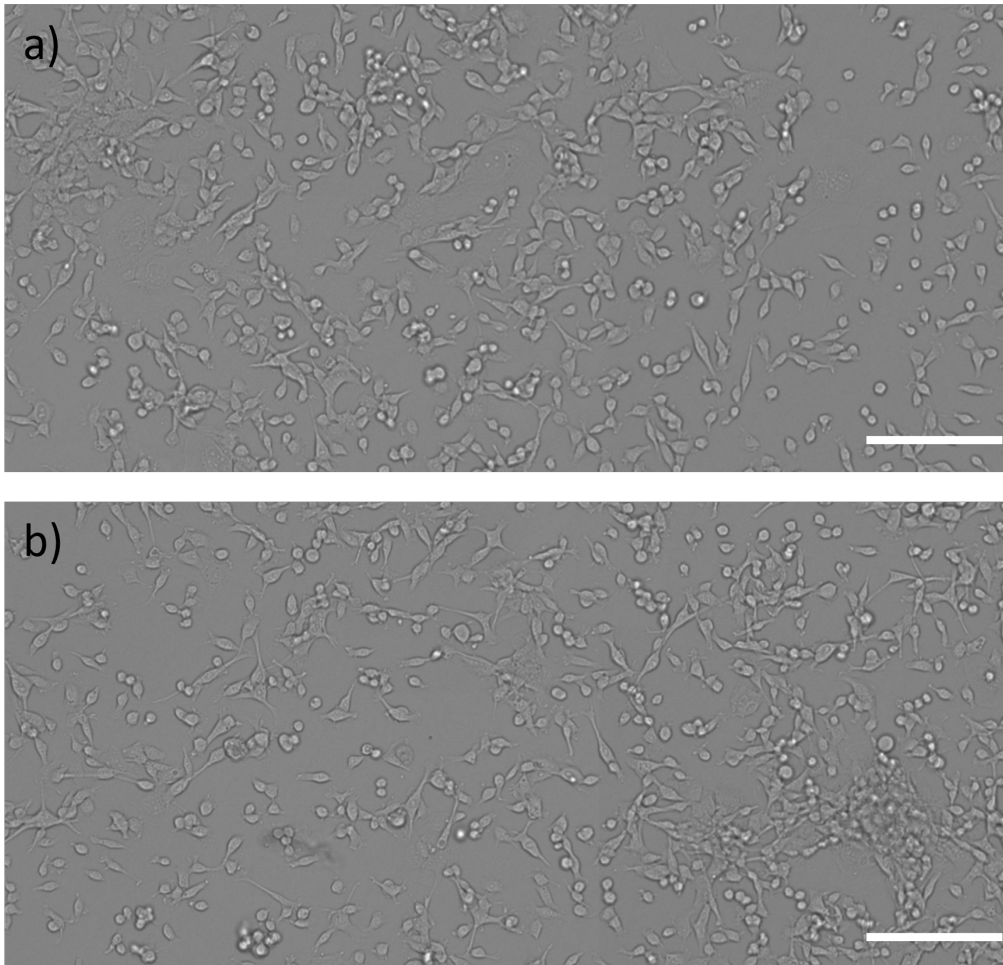


Figure B.4. Representative brightfield Celigo images of cells in a 96 well plate with CT26 cells which have been exposed to 1 vol-% DMSO for 120 minutes (a), or DMSO-free control (b). Scale bar in both images is 200 μm .

The results of two preliminary studies are included here to demonstrate the impact of including FBS in media on the viability of cells. Firstly, the relative viability of cells that had spent two hours in serum free media compared to complete media was tested with an MTS assay, 28 hours following exposure. The results of this experiment are shown in Figure B.5. Secondly, an MTS assay was performed after treating cells for 30 minutes with complete media (negative control), serum-free media with 10 $\mu\text{g}/\text{mL}$ doxorubicin, and complete media with 10 $\mu\text{g}/\text{mL}$ doxorubicin ($n = 5$). The MTS assay was performed 24 hours following removal of the treatment. The results are as shown in Figure B.6.

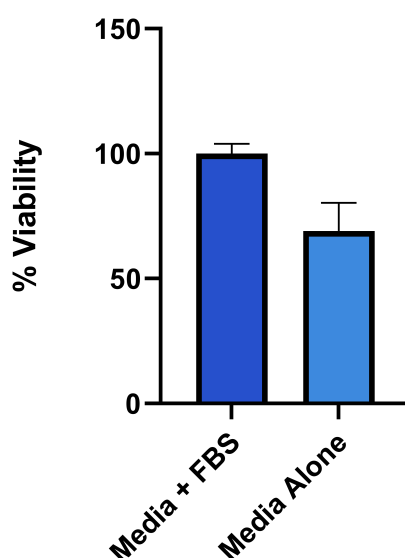


Figure B.5. Viability measured by MTS, 28 hours after two hours in serum-free media (or complete media as a negative control). The cells were incubated with MTS reagent for 105 minutes. The error bars represent the standard deviation, $n = 5$. The difference between the groups was found to be significant ($p < 0.01$) with an unpaired t-test.

It is clear in both cases that the absence of FBS causes a substantial reduction in cell viability. Such a reduction in viability was considered a greater confounding factor than the binding of doxorubicin to serum proteins, so complete media was used in all studies in Chapter Four.

The predicted unbound fraction of drug in media supplemented with 10% FBS is predicted to be around 0.8 [e.g. 200]. A scaling rule provided by McNamara and Alcorn [201] for determining the unbound fraction of a drug gives a similar value of 0.833 (when scaled from the very well documented binding of doxorubicin to Human Serum Albumin (HSA) in plasma):

$$f_{u,est} = \left(1 + \frac{P(1 - f_{u,known})}{P_{known} f_{u,known}} \right)^{-1} \quad (\text{B.1})$$

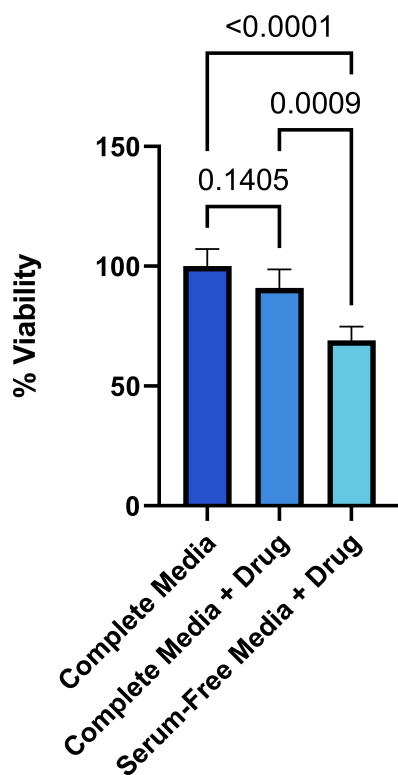


Figure B.6. Viability measured by MTS 24 hours after 30 minutes in 10 $\mu\text{g}/\text{mL}$ doxorubicin in both serum-free and complete media compared to a negative control. The error bars represent the standard deviation, $n = 5$. P values from a one-way ANOVA (calculated in GraphPad PRISM) are included on the plot.

in which:

- $f_{u,est}$ is the estimated unbound fraction of drug
- P is the protein concentration in the solution, in this case the concentration of BSA, the major protein in FBS. At 10% FBS, the concentration of BSA in media is about 3 mg/mL [202].
- P_{known} is the concentration of HSA in plasma; 39.24 mg/mL [203]
- $f_{u,known}$ is the binding fraction of doxorubicin to HSA in plasma, 0.2767 [203]

These values are similar, so while there is an argument that a full model would include binding terms such as these, the additional use of lumped element parameters (such as diffusivity), and the estimated nature of permeability values means that there is no clear reason to believe that the model would be made more accurate by including this term; but it was thought important to check that the concentration the cells were being exposed to was not inaccurate by orders of magnitude.

B.3 When to Assay for Cell Viability

To determine the optimal time-point after drug exposure to perform the trypan blue, MTS, and Celigo assays, cell counts were performed with trypan blue exclusion and compared to negative control flasks 0, 6, 24, 48, and 72 hours after removal of the drug. The results are shown in Figure B.7, from which it can be seen that counting at 48 hours provides the lowest viability. This therefore seems to represent the point of maximal drug impact and therefore the optimal time to perform the assay, as it is before cells in the negative control reach confluency and stop dividing so rapidly and at such a time that the doxorubicin has clearly had an effect (which can not be seen at the earliest two time points).

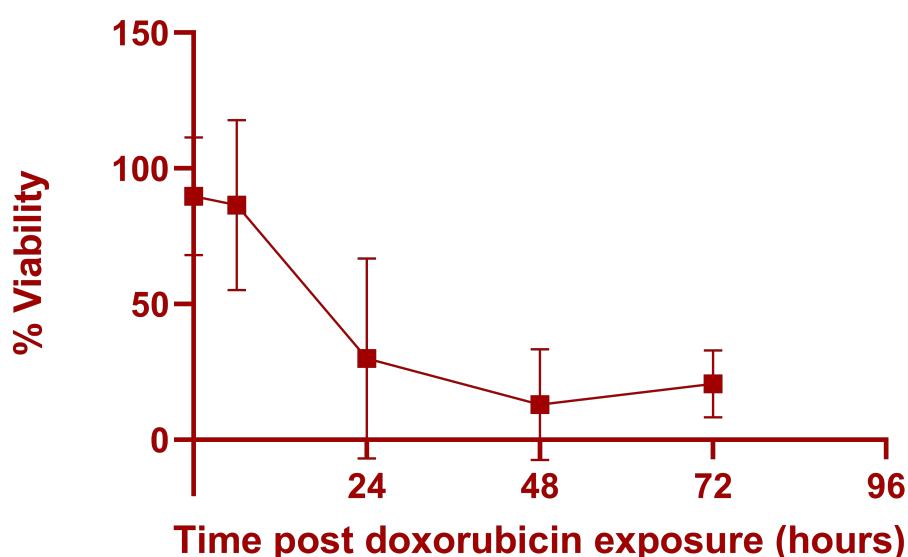


Figure B.7. Graph of cell viability as obtained by trypan blue exclusion (Method: Section 4.3.1) assayed at the stated times post-exposure to 10 $\mu\text{g/mL}$ doxorubicin (0.1 vol-% DMSO) for 90 minutes. Error bars represent the standard deviation, $n = 3$.

A similar study was performed with an MTS assay, but using the full range of concentrations with two hours of exposure. The plates were assayed at 24, 48, and 72 hours after treatment (the results from trypan blue exposure and a first run through with MTS clearly showed that the cytotoxic effect of doxorubicin could not be resolved 6 hours after treatment). A representative set of results at 24 and 72 hours are displayed in Figure B.8. Unfortunately, the 48 hour plate had become saturated; it is not clear why this happened. Nevertheless, the 24 and 72 hour results were similar enough to each other that it was also decided to perform both the MTS and trypan blue survival assays 48 hours post doxorubicin exposure. The arguments around reaching confluency also hold true for the MTS assay, with confluency being observed in the healthy control around 3-4 days after plating, suggesting that 72 hours post exposure is too long.

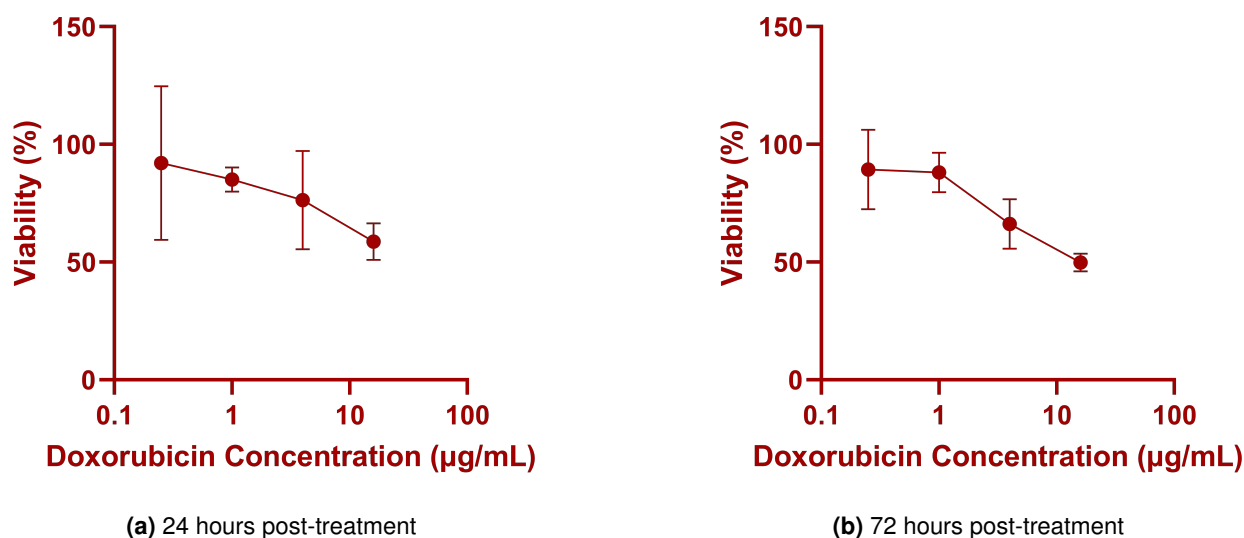


Figure B.8. Viability of cells by MTS assay (method as described in Section 4.3.2), 24 hours (left) and 72 hours (right) after a 60 minute exposure to varying concentrations of doxorubicin as shown. Circles represent the mean of five independent wells, and the error bars the standard deviation. The standard deviations of the doxorubicin free wells (not shown due to logarithmic scale) were 26.29% and 18.02% for the 24 hour and 72 hour plates respectively.

B.4 Demonstrating Linearity and Choosing Incubation Period for the MTS Assay

There is some debate in the literature as to the conditions under which the MTS assay provides a linear relationship between the number of viable cells and the absorbance reading. For example Huang et al. [204] compared the results of an MTS assay performed on wells with different numbers of cells with either Dulbecco's Modified Eagle's Medium (DMEM), RPMI, or DPBS, with or without FBS at different concentrations in a murine mammary epithelial cell line, HC11. They reported that 'ten percent serum, for example, can eliminate the difference between 2000 and 4000 cells after a 4 hours incubation'. As a result, it was important to check that a linear relationship between cell number and absorbance existed under the conditions that would be used to determine the cytotoxic effect of doxorubicin.

To establish this, $n = 5$ wells of a 96 well plate were plated with 0, 1250, 2500, 5000, 10,000, and 20,000 cells in 100 μL of complete media, and left for 24 hours to ensure that the cells had fully adhered to the plate. The media was then aspirated, the wells were washed with 100μL of DPBS, before 100 μl of complete media and 20 μL of CellTiter 96® AQueous One Solution (MTS assay reagent) was added to each well. This was incubated for 30 minutes before being read on the plate reader, then returned to the incubator for another hour, before another reading was taken. The results are shown in Figure B.9.

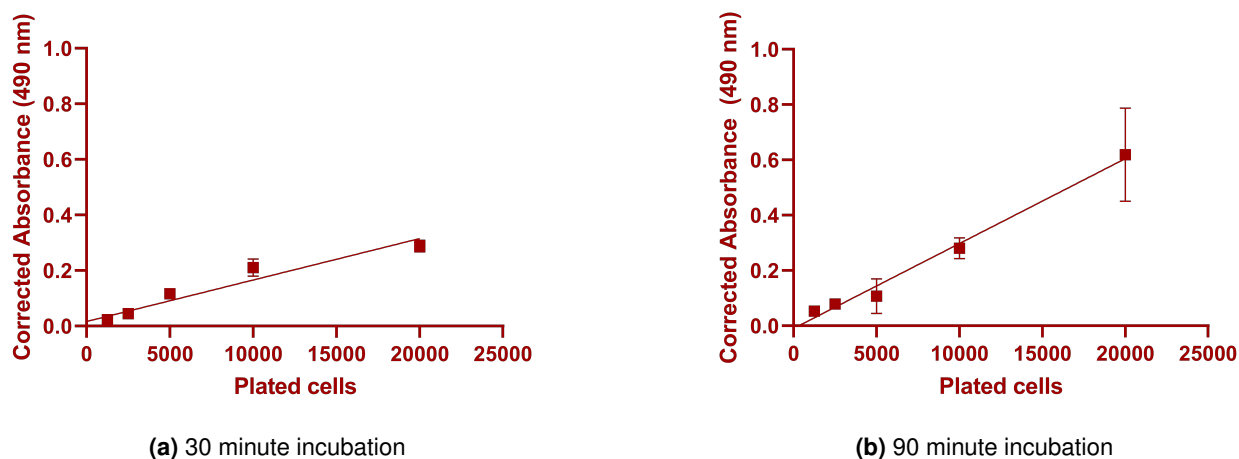


Figure B.9. Analysis of the impact of cell number plated on MTS absorbance signal generated. CT26 cells were plated at the stated densities in 96 well plates and exposed (24 hours later) to MTS reagent for 30 minutes (left) or 90 minutes (right) and measured for absorbance as described in Section 4.3.2. The absorbance was corrected by subtracting the background absorbance of the well (the mean value between 850 and 900 nm) from all wells, then subtracting the mean and two standard deviations of the resulting signal at 490 nm in the negative control wells. Brown squares represent the mean of five independent wells, error bars represent standard deviations, line of best fit as calculated using PRISM (using the standard deviations), $R^2 = 0.9204$ for the 30 minute incubation, and $R^2 = 0.8990$ for the 90 minute incubation.

Longer incubation times can increase the signal to noise ratio associated with the assay – however incubation for too long will result in saturation of the absorbance reading. It can be seen from the results in Figure B.9b that a 90 minute incubation period does not give readings above the limit of linearity for 10,000 cells, so treatment plates used 10,000 cells and such an incubation time of 90 minutes. Although the R^2 value (based on both the mean and standard deviation, calculated using GraphPad PRISM) is higher at 30 minutes, a 90 minute incubation was used in this thesis, as the steeper gradient gave the greatest chance of small survival fractions being resolved. A subsequent repeat (results not shown) of an MTS assay at 20,000 cells per well suggested that the large variance at 20,000 cells shown here was a feature of this particular experiment.

B.5 Determination of Seeding Density and Incubation Time for the Clonogenic Assay

A preliminary clonogenic assay was performed plating 200 and 400 cells respectively, and ‘treating’ both with complete media for an hour, before washing twice and returning to the incubator. The plate was then fixed and stained after seven days - the results of which can be seen in Figure B.10. These colonies were counted by hand, returning: 107, 117, 111 and 173, 200, 209 colonies respectively. The ratio of colony numbers between 200 and 400 cells was found to be $0.576 \pm 0.050 : 1$.

From counting this plate, it was clear that seeding 400 cells for the negative control was too many, as colony merging made it difficult to obtain an accurate count (for instance, in the south-west of the bottom right well in Figure B.10). 200 provided a number of colonies amenable to counting without merging which was sufficient to detect toxic effects, so this number was taken forward as an appropriate negative control seeding density. Although 0.57 ± 0.05 was not within one standard deviation of the ratio (0.57 ± 0.05), the result is close enough to 0.5 considering two factors. Firstly, that the nature of seeding small numbers of cells means that it would be very easy to seed a ratio which was not exactly 0.5 to begin with, and secondly, the likely impact of colony merging (which is more likely to have occurred in the 400 cell wells) would be a slight under-count; correcting for which would bring the ratio down towards 0.5.

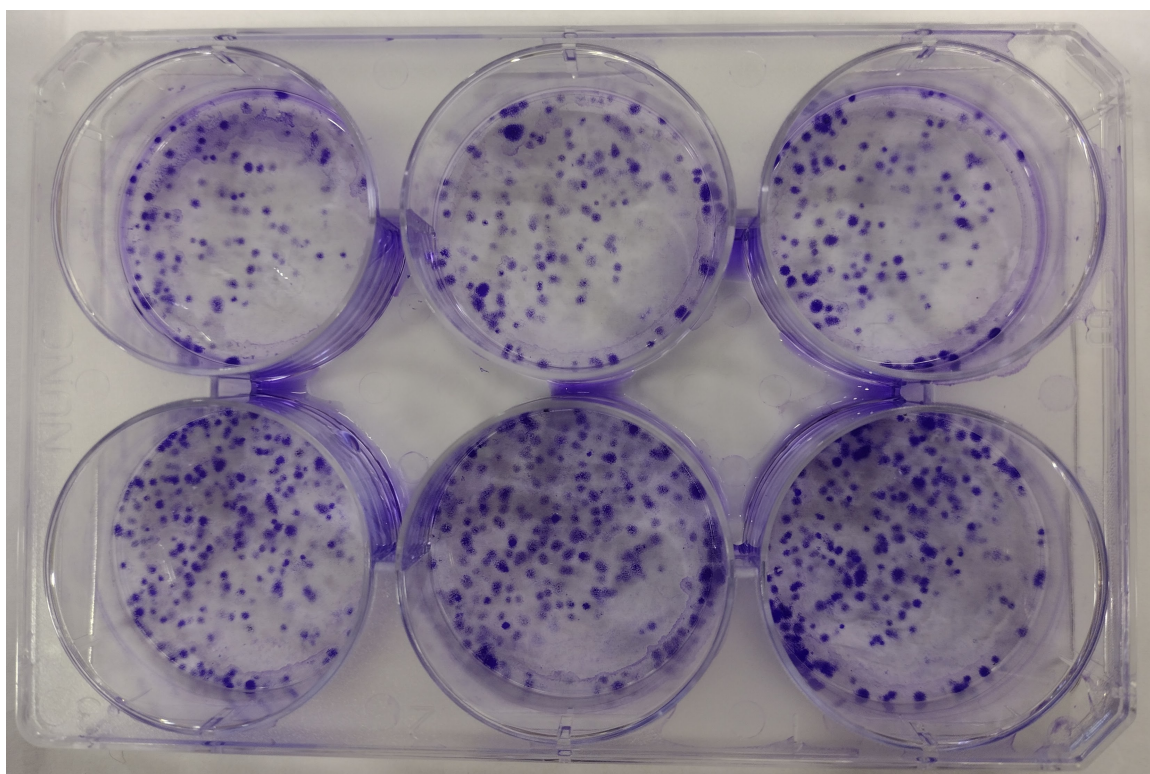


Figure B.10. Photograph of clonogenic assay plate to determine appropriate seeding density. The top three wells had 200 cells seeded, while the bottom wells had 400 cells seeded. The plate was incubated for 24 hours before being washed, returned to the incubator for an hour, then washed twice again before being returned to the incubator in complete media for seven days, and fixed and stained, as described in Section 4.4.

Considering the incubation time of the assay, a rule of thumb for colony counting under a microscope is that colonies are clusters of more than 50 cells [163], which would require seven doubling times. CT26 cells have a doubling time of around 22 hours [205]; so seven days incubation post exposure represents around 7.6 doubling times, which should allow for sufficient colony formation (especially considering the initial 24 hour incubation before the addition of drug).

Initially, in plates with a negative control and treatment group, it seemed that 7 days might not be

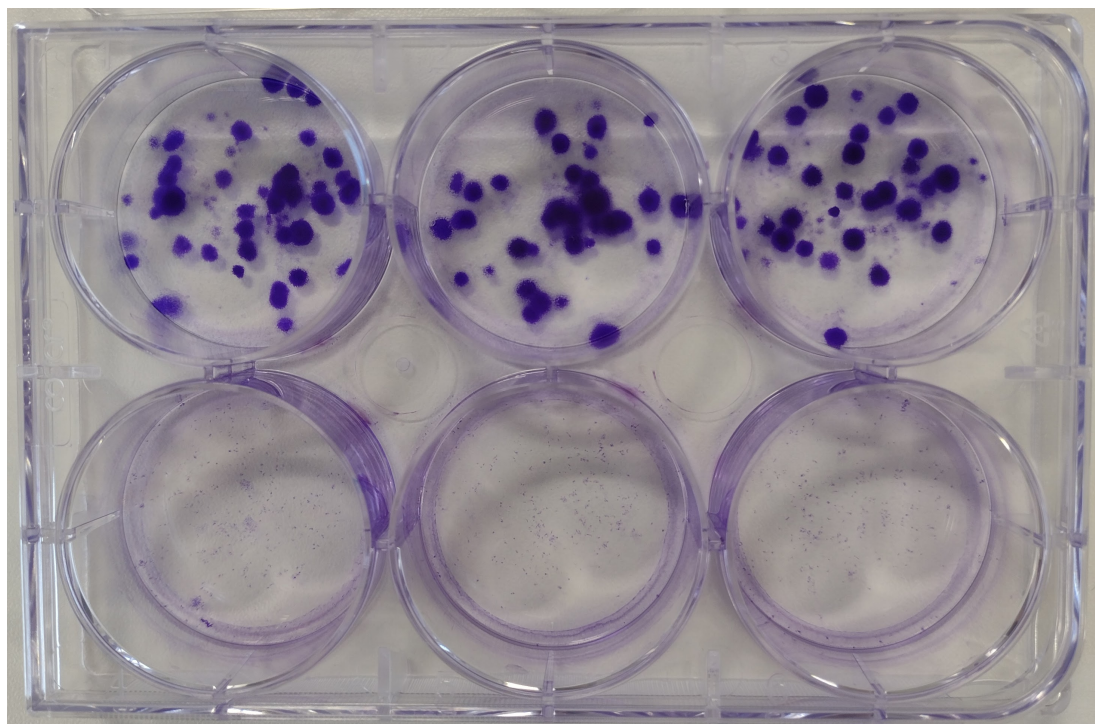


Figure B.11. Photograph of a clonogenic plate that has been allowed 10 days to form colonies, rather than 7 days. 200 cells were plated in the top three wells, while 2000 cells were plated in the lower three wells, which were treated with 4 $\mu\text{g/mL}$ of doxorubicin for 2 hours at 37°C, as per the protocol described in Section 4.4 (except the incubation time).

sufficient, since colonies in the treatment group often expressed phenotypic changes which made the colonies notably smaller, and made it more difficult to assess if a colony should or should not be counted. To try to overcome this difficulty, a few plates were imaged at day seven using the Celigo, before being returned to the incubator, and not stained until day 10. However, as can clearly be seen in Figure B.11, colonies from untreated cells became too large for accurate counting at day 10 compared to day 7, and additionally, the colonies in the treatment wells are no larger - however the Celigo images were useful in determining the sizes of valid colonies; as a measurement of cell size was used to provide a minimum colony size estimate for the automated colony counting.

Appendix C

Microdialysis as a Method to Quantify Transport of Doxorubicin in *Ex Vivo* Porcine Tissue

C.1 Microdialysis

Microdialysis probes, as used in this appendix, can be used to sample or deliver analytes to target tissue, usually *in vivo*. In these experiments, CMA 20 High Cut Off Microdialysis Probes (Harvard Apparatus, CMA8010436) were used, which consist of an inlet tube, which connects to an inner cannula, from where perfusion fluid flows into the tip of the probe, which is 10 mm in length, and has a semi-permeable membrane which allows analytes through. Fluid continues back up around the outside of the inner cannula, up to an outlet tube, where the output fluid, called the dialysate, can be collected.

C.1.1 Extraction Efficiency

The initial idea was to use microdialysis probes to both deliver and extract doxorubicin from the tissue, using a probe with a high cut-off, such that protein-bound doxorubicin could also pass through the membrane; in this case, high cut-off refers to a 100 kDa size limit. It is important to quantify extraction efficiencies when using microdialysis probes; these quantify the amount of drug in the perfusate which is entering the tissue (for delivery) and the amount of drug in the tissue which is reaching the outlet (for recovery). These fractions are not necessarily the same [206]. The extraction efficiencies are also highly dependent on probe flow rate and temperature, meaning that separate calibrations would be needed for different conditions.

The extraction efficiency for delivery was deemed unnecessary to determine, since a comparison of the fluorescence signals of the perfusate and dialysate for a given experiment would give a more accurate measurement of the doxorubicin delivery over the time course. To establish the extraction efficiency of recovery, the CMA 20 probe circuit was prepared by infusing deionised water in a 1 mL syringe using a syringe pump (Cole-Parmer, model number 110) at 12 $\mu\text{L}/\text{min}$ for 20 minutes, with the probe securely fixed in a beaker of deionised water. This ensures that there is no air in the system. A photo of the set-up is shown (during flushing) in Figure C.1. 50 mL of 5 $\mu\text{g}/\text{mL}$ doxorubicin hydrochloride solution (Fisher BioReagents) in deionised water was warmed and stirred using a magnetic hotplate (Corning PC-420D), with the temperature setting adjusted throughout to try and maintain a temperature around 37°C. This beaker was protected from light during the experiment with metal foil. The temperature of the water was measured at 10 minute intervals between sampling and varied between 35°C and 38°C.

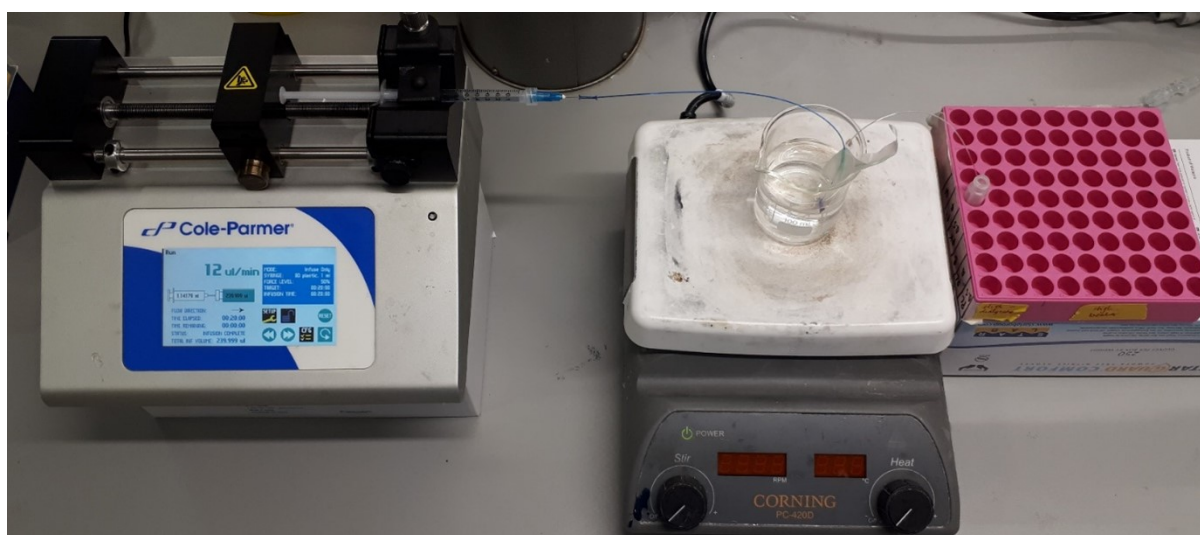


Figure C.1. The set up of the experiment designed to determine the extraction efficiency of recovery of the microdialysis probes for doxorubicin at 37°.

Using a similar set up as the preparation in Figure C.1, the CMA 20 probe was secured in the doxorubicin solution and protected from light. The syringe pump was set to 2 $\mu\text{L}/\text{min}$. Dialysate was collected every 10 minutes directly into a clear polypropylene short thread autosampler vial with integrated 0.3 mL insert (Sigma Aldrich). Every 10 minutes, from 5 minutes onwards, a 20 μL sample was taken from the doxorubicin beaker, using Lo-bind pipette tips. Dialysate and beaker samples were placed into an ice box, protected from light. After 120 minutes, sample collection was stopped and doxorubicin beaker swapped for deionised water to flush the CMA 20 probe. The doxorubicin concentrations were compared to the mean beaker concentration using a flow injection analysis with

the same HPLC devices and fluorescence detector as in Chapter 4. The resulting extraction efficiency is plotted as a function of time in Figure C.2 (the 50 minute vial was lost due to experimental error). It can be seen that with the low flow rate of $2 \mu\text{L}/\text{min}$, the extraction efficiency nears 50%, but does not reach this level until between 30 to 40 minutes.

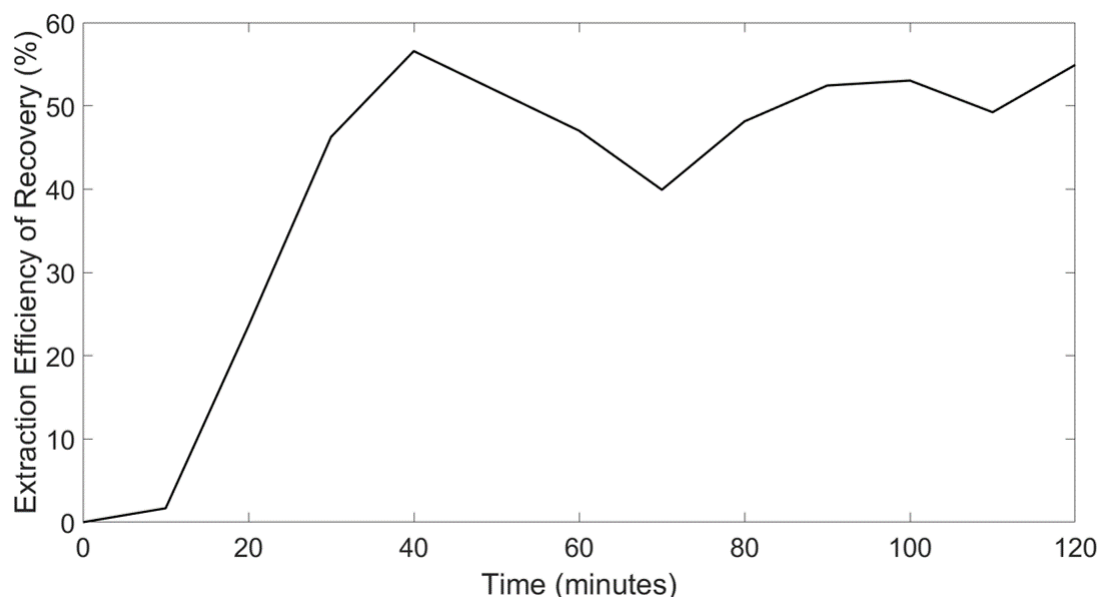


Figure C.2. Extraction efficiency of $5 \mu\text{g}/\text{mL}$ doxorubicin in stirred, deionised water at 37°C as a function of time. Samples every 10 minutes, with no sample at 50 minutes due to experimental error.

This lagging behaviour is fairly typical of lipophilic analytes, and the authors of one study [207] also demonstrate (Figure 5a of [207]) that microdialysis is not able to resolve well step changes in concentration of doxorubicin, whereas the same changes in concentration are well-resolved for a non-lipophilic analyte, antipyrine. This lag is problematic for using microdialysis probes to recover varying concentrations of doxorubicin from tissue, with the aim of calculating a diffusion coefficient. Other associated inaccuracies which would result from using microdialysis to recover doxorubicin from *ex vivo* tissue is that recovery efficiency may be lower in tissue (compared to water), especially as the beaker in this case is stirred, and there is also no consideration of the lower efficiency associated with the extraction of protein-bound doxorubicin.

As a result, it was decided that although microdialysis represents an acceptable possible delivery mechanism (as it would be possible to quantify exactly how much drug had been delivered through comparing the dialysate and perfusate signals, thus eliminating the need for the exact calculation of the delivery and recovery efficiencies), this lag makes it an unsuitable technique for drug recovery. Biopsies, although destructive, were chosen as an alternative method to try and quantify tissue

concentrations at different timepoints to avoid these issues.

C.2 Porcine Pancreas

In the following *ex vivo* protocols, the same approach as would be taken for *in vivo* use was followed to insert the probe into the tissue: split tubing was slid over the end of a blunt 23G needle. The needle was inserted into the tissue, then withdrawn, leaving only the tubing in the remaining hole. The microdialysis probe was then inserted into the tubing and the outer wing of each probe was sutured using Surgipro™ monofilament polypropylene 2-0 on a Surgalloy™ V-20 taper needle (Covidien™), to keep the probes in place whilst minimising tissue trauma. Once the probe was secured, the split tubing was removed.

The first preliminary experiment was performed using a section of frozen porcine pancreas measuring approximately 68 mm x 35 mm x 27 mm, which had been gently thawed. For this experiment, following the insertion of the probes, the pancreas was placed in a beaker containing PBS and placed on a hot plate, with the temperature set to achieve a temperature in the PBS which was close to 37 °C. Following two hours of probe perfusion (in this preliminary test, one probe was used for delivery, the other was used for recovery, as this experiment pre-dated the conclusion that microdialysis recovery was unnecessarily complex), the pancreas had almost begun to fragment, and was not in good condition. Photos of the pancreas sample before and after this experiment can be seen in Figure C.3. This is particularly problematic around the probe used for delivery, since it couldn't be guaranteed that the doxorubicin delivered was all going into the tissue (rather than the surrounding PBS, due to the separation of the pancreas around the probe's insertion point).

Following this, future experiments were performed using either fresh, whole porcine pancreata, which had not been frozen, or with frozen porcine pancreas which was embedded in agar in a holder which had been previously designed for flow channel experiments in tissue phantoms. A picture of this sort of set up is shown in Figure C.4 (although no scale bar is shown, the pancreas sample is a similar size to that used in Figure C.3).

C.3 Biopsies

200 µg/mL of doxorubicin in water was delivered to a fresh porcine pancreas using the microdialysis probe at a flow rate of 2 µL/min. Biopsies were taken with a biopsy punch, as shown in Figure C.5.

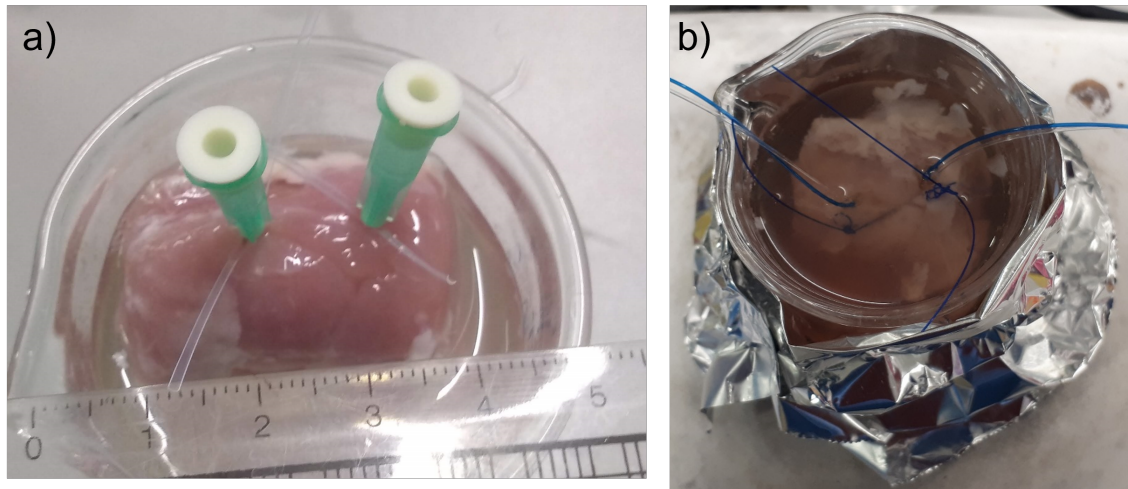


Figure C.3. Photos which show how the condition of the pancreas section deteriorated over 2 hours immersed in PBS which was kept between 35.8°C and 38.3°C: a) shows the pancreas before the experiment, with the introducer needles and split tubing inserted, b) shows the pancreas after 2 hours, with the probes in place.

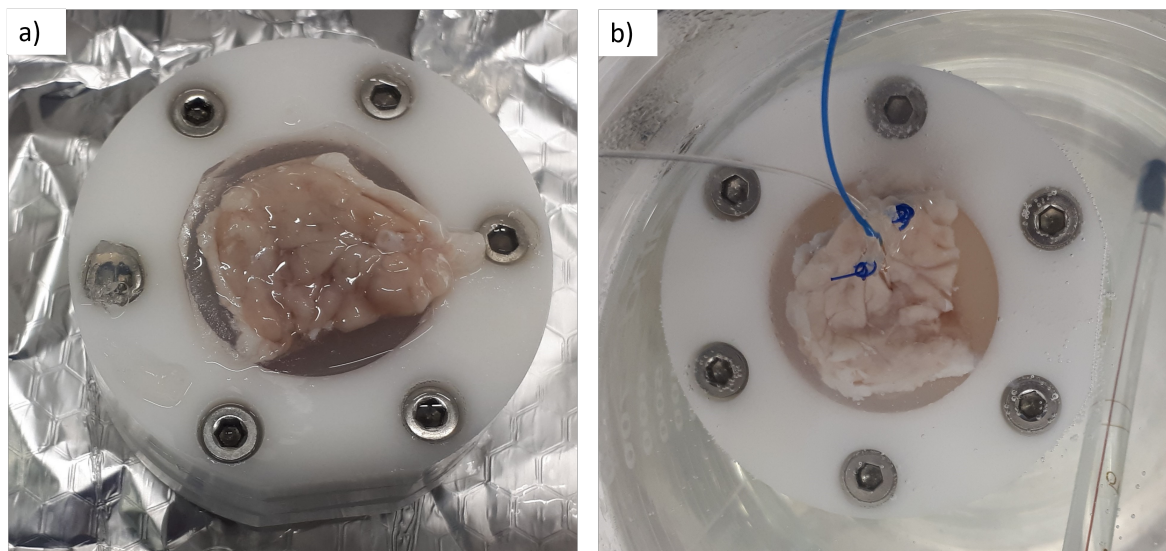


Figure C.4. Photos which show a section of frozen pancreas embedded in agar in a holder: a) shows the pancreas prior to a two hour experiment, and b) shows the pancreas at the end of the experiment. Visually, there is much less change in the condition of the tissue than in the case in which the pancreas was unconstrained.

Biopsies were taken in 'round-the-clock' fashion, as shown in Figure C.6, maintaining a similar distance (approximately 10 mm) from the infusion point with each sample. A sample was taken every 20 minutes for 2 hours. At the end of the experiment, the probe was removed, and the distances between the probe and the biopsies were measured, and a biopsy of the probe's location was also taken.

The tissue samples were each weighed and prepared for HPLC analysis. Briefly, this involved homogenisation (with a Precellys 24 Tissue Homogeniser), protein precipitation using acetonitrile, and concentration using a centrifuge concentrator. No doxorubicin was detectable from the biopsied tissue during the analysis.



Figure C.5. A biopsy punch used for tissue sampling, next to a 1.5 mL eppendorf for scale.

Taking 10 mm as a reasonable distance from the probe given the size of the biopsy, using the literature value for diffusion coefficient given in Chapter 5 ($5.01 \times 10^{-11} \text{ m}^2\text{s}^{-1}$), the diffusion timescale is around 554 hours, so it is not surprising that no doxorubicin is detectable this far from the probe. Given the size of the biopsy punch, this approach was not continued.



Figure C.6. The holes left from ‘round-the-clock’ biopsy punch sampling in the experiment on a fresh, whole porcine pancreas.

C.4 Fluorescence Imaging

A brief attempt was made to quantify doxorubicin transport via fluorescence imaging using the Celigo Imaging Cytometer (Nexcelom). With the delivery of the concentrations which had been used, there was insufficient signal from the doxorubicin to resolve the drug in the tissue samples.

Fluorescence imaging-based quantification remains the most promising technique which might allow for successful quantification of the doxorubicin concentrations in the tissue sample. A possible route forward would be to use larger concentrations of drug and a more powerful fluorescence microscope, with careful sectioning of the tissue. Use of a fluorescence microscope also facilitates examining transport on much smaller length scales, which require more reasonable timescales. For example, establishing a fluorescence baseline of 100% at the probe boundary, where the fluorescence signal would be expected to be strongest, it would be possible to use multiple experiments, sectioning new samples at (for example) 10 minute intervals, to approximate the diffusion coefficient. This was not pursued due to project time constraints and the challenges associated with obtaining a section of tissue level with the probe's membrane.

C.5 Summary

Microdialysis is a challenging modality to use for the study of the delivery of lipophilic analytes. It is possible to deliver a known quantity of doxorubicin using a microdialysis probe, however quantitative assessment of its transport remains challenging due to the contradictory requirements of achieving good spatial resolution and having a sample which contains a quantifiable amount of doxorubicin, without having treated for such a prolonged duration that doxorubicin degradation becomes an additional consideration. In light of these issues, it was decided to use literature values in the spatial modelling section of this thesis.

Bibliography

- [1] Cancer Research UK. Cancer Statistics for the UK, Mar 2020. URL <https://www.cancerresearchuk.org/health-professional/cancer-statistics-for-the-uk>.
- [2] Agamemnon A Epenetos, Deborah Snook, Helga Durbin, Peter M Johnson, and Joyce Taylor-Papadimitriou. Limitations of Radiolabeled Monoclonal Antibodies for Localization of Human Neoplasms. *Cancer Research*, 46(6):3183–3191, 1986.
- [3] Emma Hope. Chemotherapy, Radiotherapy and Surgical Tumour Resections in England, Apr 2020. URL <https://www.gov.uk/government/statistics/chemotherapy-radiotherapy-and-surgical-tumour-resections-in-england/chemotherapy-radiotherapy-and-surgical-tumour-resections-in-england#authors>.
- [4] Vincent T DeVita and Edward Chu. A History of Cancer Chemotherapy. *Cancer Research*, 68(21):8643–8653, 2008.
- [5] Jane C Wright, Aaron Prigot, Barbara P Wright, Solomon Weintraub, and Louis T Wright. An Evaluation of Folic Acid Antagonists in Adults with Neoplastic Diseases. *Journal of the National Medical Association*, 43(4):211, 1951.
- [6] Min Chiu Li, Roy Hertz, and Delbert M Bergenstal. Therapy of Choriocarcinoma and Related Trophoblastic Tumors with Folic Acid and Purine Antagonists. *New England Journal of Medicine*, 259(2):66–74, 1958.
- [7] Chi Heem Wong, Kien Wei Siah, and Andrew W Lo. Estimation of Clinical Trial Success Rates and Related Parameters. *Biostatistics*, 20(2):273–286, 2019.
- [8] Elvin Blanco, Haifa Shen, and Mauro Ferrari. Principles of Nanoparticle Design for Overcoming Biological Barriers to Drug Delivery. *Nature Biotechnology*, 33(9):941, 2015.
- [9] Martin Hossann, Tungte Wang, Michael Wiggenhorn, Rebecca Schmidt, Anja Zengerle, Gerhard Winter, Hansjörg Eibl, Michael Peller, Maximilian Reiser, Rolf D Issels, et al. Size of

- Thermosensitive Liposomes Influences Content Release. *Journal of Controlled Release*, 147 (3):436–443, 2010.
- [10] Immunotherapy to Treat Cancer, Sep 2019. URL <https://www.cancer.gov/about-cancer/treatment/types/immunotherapy#:~:text=The%20immune%20system%20helps%20your,living%20organisms%20to%20treat%20cancer>.
- [11] Mark C Pettinato. Introduction to Antibody-Drug Conjugates. *Antibodies*, 10(4):42, 2021.
- [12] Stanley J Oiseth and Mohamed S Aziz. Cancer Immunotherapy: A Brief Review of the History, Possibilities, and Challenges Ahead. *J Cancer Metastasis Treat*, 3(10):250–261, 2017.
- [13] Paul Polakis. Antibody Drug Conjugates for Cancer Therapy. *Pharmacological Reviews*, 68(1):3–19, 2016.
- [14] Zhiwen Fu, Shijun Li, Sifei Han, Chen Shi, and Yu Zhang. Antibody Drug Conjugate: The “Biological Missile” for Targeted Cancer Therapy. *Signal Transduction and Targeted Therapy*, 7(1):93, 2022.
- [15] Allen Shaughnessy. Magic Bullets With A Hefty Price Tag. *BMJ: British Medical Journal*, 345 (7887):18–19, 2012.
- [16] Kandice A Kapinos, Ellen Hu, Jigar Trivedi, Praveen Ramakrishnan Geethakumari, and Ankit Kansagra. Cost-Effectiveness Analysis of CAR T-Cell Therapies vs Antibody Drug Conjugates for Patients with Advanced Multiple Myeloma. *Cancer Control*, 30:10732748221142945, 2023.
- [17] Non-Hodgkin’s Lymphoma: Diagnosis and Management, January 2016. URL <https://www.nice.org.uk/guidance/ng52/documents/guideline-appendices>.
- [18] Etienne Cabane, Xiaoyan Zhang, Karolina Langowska, Cornelia G Palivan, and Wolfgang Meier. Stimuli-Responsive Polymers and Their Applications in Nanomedicine. *Biointerphases*, 7(1-4):9, 2012.
- [19] Christoph Alexiou, Wolfgang Arnold, Roswitha J Klein, Fritz G Parak, Peter Hulin, Christian Bergemann, Wolfgang Erhardt, Stefan Wagenpfeil, and Andreas S Luebbe. Locoregional Cancer Treatment with Magnetic Drug Targeting. *Cancer Research*, 60(23):6641–6648, 2000.
- [20] Milton B Yatvin, John N Weinstein, Warren H Dennis, and Robert Blumenthal. Design of Liposomes for Enhanced Local Release of Drugs by Hyperthermia. *Science*, 202(4374):1290–1293, 1978.

- [21] Paul C Lyon, Michael D Gray, Christophoros Mannaris, Lisa K Folkes, Michael Stratford, Leticia Campo, Daniel YF Chung, Shaun Scott, Mark Anderson, Robert Goldin, et al. Safety and Feasibility of Ultrasound-Triggered Targeted Drug Delivery of Doxorubicin from Thermosensitive Liposomes in Liver Lumours (TARDOX): A Single-Centre, Open-Label, Phase 1 Trial. *The Lancet Oncology*, 19(8):1027–1039, 2018.
- [22] Li Li, Timo LM ten Hagen, Michiel Bolkestein, Astrid Gasselhuber, Jeremy Yatvin, Gerard C van Rhoo, Alexander MM Eggermont, Dieter Haemmerich, and Gerben A Koning. Improved Intratumoral Nanoparticle Extravasation and Penetration by Mild Hyperthermia. *Journal of Controlled Release*, 167(2):130–137, 2013.
- [23] Dickson K Kirui, Eugene J Koay, Xiaojing Guo, Vittorio Cristini, Haifa Shen, and Mauro Ferrari. Tumor Vascular Permeabilization using Localized Mild Hyperthermia to Improve Macromolecule Transport. *Nanomedicine: Nanotechnology, Biology and Medicine*, 10(7):1487–1496, 2014.
- [24] Anirudh Sharma, Sanem Özayral, Julia S Caserto, Rosemarie Ten Cate, Nicole M Anders, James D Barnett, Sri Kamal Kandala, Elizabeth Henderson, Jacqueline Stewart, Eleni Liapi, et al. Increased Uptake of Doxorubicin by Cells Undergoing Heat Stress does not Explain its Synergistic Cytotoxicity with Hyperthermia. *International Journal of Hyperthermia*, 36(1):711–719, 2019.
- [25] Yu Huang, Boram Gu, Cong Liu, Justin Stebbing, Wladyslaw Gedroyc, Maya Thanou, and Xiao Yun Xu. Thermosensitive Liposome-Mediated Drug Delivery in Chemotherapy: Mathematical Modelling for Spatio-temporal Drug Distribution and Model-Based Optimisation. *Pharmaceutics*, 11(12):637, 2019.
- [26] 2023. URL <https://www.cancer.gov/publications/dictionaries/cancer-terms/def/solid-tumor>.
- [27] Jul 2020. URL <https://www.cancerresearchuk.org/what-is-cancer/how-cancer-starts/types-of-cancer>.
- [28] Robin Hesketh. *Introduction to Cancer Biology*. Cambridge University Press, 2013.
- [29] Andrew I Minchinton and Ian F Tannock. Drug Penetration in Solid Tumours. *Nature Reviews Cancer*, 6(8):583–592, 2006.

- [30] Triantafyllos Stylianopoulos. The Solid Mechanics of Cancer and Strategies for Improved Therapy. *Journal of Biomechanical Engineering*, 139(2):021004, 2017.
- [31] Timothy P Padera, Brian R Stoll, Jessica B Tooredman, Diane Capen, Emmanuelle di Tomaso, and Rakesh K Jain. Cancer Cells Compress Intratumour Vessels. *Nature*, 427(6976):695–695, 2004.
- [32] Carl-Henrik Heldin, Kristofer Rubin, Kristian Pietras, and Arne Östman. High Interstitial Fluid Pressure — An Obstacle in Cancer Therapy. *Nature Reviews Cancer*, 4(10):806–813, 2004.
- [33] Mark W Dewhirst and Timothy W Secomb. Transport of Drugs from Blood Vessels to Tumour Tissue. *Nature Reviews Cancer*, 17(12):738–750, 2017.
- [34] Brent D Weinberg, Ravi B Patel, Agata A Exner, Gerald M Saidel, and Jinming Gao. Modeling Doxorubicin Transport to Improve Intratumoral Drug Delivery to RF Ablated Tumors. *Journal of Controlled Release*, 124(1-2):11–19, 2007.
- [35] James W Baish, Triantafyllos Stylianopoulos, Ryan M Lanning, Walid S Kamoun, Dai Fukumura, Lance L Munn, and Rakesh K Jain. Scaling Rules for Diffusive Drug Delivery in Tumor and Normal Tissues. *Proceedings of the National Academy of Sciences*, 108(5):1799–1803, 2011.
- [36] James J Kwan, Rachel Myers, Christian M Coviello, Susan M Graham, Apurva R Shah, Eleanor Stride, Robert C Carlisle, and Constantin C Coussios. Ultrasound-Propelled Nanocups for Drug Delivery. *Small*, 11(39):5305–5314, 2015.
- [37] Xinming Jing, Fengming Yang, Chuchu Shao, Ke Wei, Mengyan Xie, Hua Shen, and Yongqian Shu. Role of Hypoxia in Cancer Therapy by Regulating the Tumor Microenvironment. *Molecular Cancer*, 18:1–15, 2019.
- [38] Vincent M Perez, Joseph F Kearney, and Jen Jen Yeh. The PDAC Extracellular Matrix: A Review of the ECM Protein Composition, Tumor Cell Interaction, and Therapeutic Strategies. *Frontiers in Oncology*, 11:751311, 2021.
- [39] Maximilian Weniger, Kim C Honselmann, and Andrew S Liss. The Extracellular Matrix and Pancreatic Cancer: A Complex Relationship. *Cancers*, 10(9):316, 2018.
- [40] Qing Chang, Olga I Ornatsky, Iram Siddiqui, Rita Straus, Vladimir I Baranov, and David W Hedley. Biodistribution of Cisplatin Revealed by Imaging Mass Cytometry Identifies Extensive Collagen Binding in Tumor and Normal Tissues. *Scientific Reports*, 6:36641, 2016.

- [41] Krishna K Ramajayam, Danforth A Newton, and Dieter Haemmerich. Selecting Ideal Drugs for Encapsulation in Thermosensitive Liposomes and Other Triggered Nanoparticles. *International Journal of Hyperthermia*, 39(1):998–1009, 2022.
- [42] Andrew J Primeau, Augusto Rendon, David Hedley, Lothar Lilge, and Ian F Tannock. The Distribution of the Anticancer Drug Doxorubicin in Relation to Blood Vessels in Solid Tumors. *Clinical Cancer Research*, 11(24):8782–8788, 2005.
- [43] Howard L. Johnson and Howard I. Maibach. Drug Excretion in Human Eccrine Sweat. *Journal of Investigative Dermatology*, 56(3):182–188, 1971. ISSN 0022-202X. doi: <https://doi.org/10.1111/1523-1747.ep12260784>. URL <https://www.sciencedirect.com/science/article/pii/S0022202X15479643>.
- [44] Alberto Gabizon, Dinah Tzemach, Lidia Mak, Moshe Bronstein, and Aviva T Horowitz. Dose Dependency of Pharmacokinetics and Therapeutic Efficacy of PEGylated Liposomal Doxorubicin (Doxil) in Murine Models. *Journal of Drug Targeting*, 10(7):539–548, 2002.
- [45] TM Allen and C Hansen. Pharmacokinetics of Stealth versus Conventional Liposomes: Effect of Dose. *Biochimica et Biophysica Acta (BBA)-Biomembranes*, 1068(2):133–141, 1991.
- [46] Charlene M Dawidczyk, Luisa M Russell, Margot Hultz, and Peter C Searson. Tumor Accumulation of Liposomal Doxorubicin in Three Murine Models: Optimizing Delivery Efficiency. *Nanomedicine: Nanotechnology, Biology and Medicine*, 13(5):1637–1644, 2017.
- [47] Tamsyn Clark, Georg Ebeling, Luca Bau, Daniel Voyce, Constantin Coussios, and Peter Friend. HPB O03 Preclinical Safety and Feasibility of In Situ Isolated Normothermic Liver Chemoperfusion (INLiC) for Enhanced Drug Delivery. *British Journal of Surgery*, 109(Supplement_9):znac404–017, 2022.
- [48] Stephan T Stern, Marilyn N Martinez, and David M Stevens. When is it Important to Measure Unbound Drug in Evaluating Nanomedicine Pharmacokinetics? *Drug Metabolism and Disposition*, 44(12):1934–1939, 2016.
- [49] CG Koedoot, RJ De Haan, AM Stiggelbout, PFM Stalmeier, A De Graeff, PJM Bakker, and JCJM de Haes. Palliative Chemotherapy or Best Supportive Care? A Prospective Study Explaining Patients' Treatment Preference and Choice. *British Journal of Cancer*, 89(12):2219–2226, 2003.

- [50] Mark W Dewhirst and Kathleen A Ashcraft. Implications of Increase in Vascular Permeability in Tumors by VEGF: A Commentary on the Pioneering Work of Harold Dvorak. *Cancer Research*, 76(11):3118–3120, 2016.
- [51] Domenico Ribatti, Beatrice Nico, Enrico Crivellato, and Angelo Vacca. The Structure of the Vascular Network of Tumors. *Cancer Letters*, 248(1):18–23, 2007.
- [52] Yechezkel Chezy Barenholz. Doxil®—The First FDA-Approved Nano-Drug: Lessons Learned. *Journal of Controlled Release*, 160(2):117–134, 2012.
- [53] Joseph W Nichols and You Han Bae. EPR: Evidence and Fallacy. *Journal of Controlled Release*, 190:451–464, 2014.
- [54] Atiar M Rahman, Syed Wamique Yusuf, and Michael S Ewer. Anthracycline-Induced Cardiotoxicity and the Cardiac-Sparing Effect of Liposomal Formulation. *International Journal of Nanomedicine*, 2(4):567, 2007.
- [55] Björnmalm, Mattias and Thurecht, Kristofer J and Michael, Michael and Scott, Andrew M and Caruso, Frank. Bridging Bio-Nano Science and Cancer Nanomedicine. *ACS Nano*, 11(10): 9594–9613, 2017.
- [56] Shrey Sindhwani, Abdullah Muhammad Syed, Jessica Ngai, Benjamin R Kingston, Laura Maiorino, Jeremy Rothschild, Presley MacMillan, Yuwei Zhang, Netra Unni Rajesh, Tran Hoang, et al. The Entry of Nanoparticles into Solid Tumours. *Nature Materials*, 19(5):566–575, 2020.
- [57] Il Keun Kwon, Sang Cheon Lee, Bumsoo Han, and Kinam Park. Analysis on the Current Status of Targeted Drug Delivery to Tumors. *Journal of Controlled Release*, 164(2):108–114, 2012.
- [58] Grant H Petersen, Saeed K Alzghari, Wayne Chee, Sana S Sankari, and Ninh M La-Beck. Meta-Analysis of Clinical and Preclinical Studies Comparing the Anticancer Efficacy of Liposomal Versus Conventional Non-Liposomal Doxorubicin. *Journal of Controlled Release*, 232: 255–264, 2016.
- [59] João Paulo F Longo, Carolina M Lucci, Luís A Muehlmann, and Ricardo B Azevedo. Nanomedicine for Cutaneous Tumors- Lessons Since the Successful Treatment of the Kaposi Sarcoma, 2018.
- [60] Fredrik Kullenberg, Oliver Degerstedt, Carlemi Calitz, Nataša Pavlović, David Balgoma, Johan Gråsjö, Erik Sjögren, Mikael Hedeland, Femke Heindryckx, and Hans Lennernäs. In Vitro

- Cell Toxicity and Intracellular Uptake of Doxorubicin Exposed as a Solution or Liposomes: Implications for Treatment of Hepatocellular Carcinoma. *Cells*, 10(7):1717, 2021.
- [61] Ann L.B. Seynhaeve, Bilyana M. Dicheva, Saske Hoving, Gerben A. Koning, and Timo L.M. ten Hagen. Intact Doxil is taken up intracellularly and released doxorubicin sequesters in the lysosome: Evaluated by in vitro/in vivo live cell imaging. *Journal of Controlled Release*, 172(1):330–340, 2013. ISSN 0168-3659. doi: <https://doi.org/10.1016/j.jconrel.2013.08.034>. URL <https://www.sciencedirect.com/science/article/pii/S0168365913005038>.
- [62] Suzan Bandak, Dorit Goren, Aviva Horowitz, Dina Tzemach, and Alberto Gabizon. Pharmacological Studies of Cisplatin Encapsulated in Long-Circulating Liposomes in Mouse Tumor Models. *Anti-Cancer Drugs*, 10(10):911–920, 1999.
- [63] Sara Zalba, Timo LM Ten Hagen, Carmen Burgui, and María J Garrido. Stealth Nanoparticles in Oncology: Facing the PEG Dilemma. *Journal of Controlled Release*, 351:22–36, 2022.
- [64] Alexey Bogdanov, Andrey Bogdanov, Viacheslav Chubenko, Nikita Volkov, Fedor Moiseenko, and Vladimir Moiseyenko. Tumor Acidity: From Hallmark of Cancer to Target of Treatment. *Frontiers in Oncology*, 12, 2022.
- [65] Astrid Gasselhuber, Matthew R Dreher, Ayele Negussie, Bradford J Wood, Frank Rattay, and Dieter Haemmerich. Mathematical Spatio-Temporal Model of Drug Delivery From Low Temperature Sensitive Liposomes During Radiofrequency Tumour Ablation. *International Journal of Hyperthermia*, 26(5):499–513, 2010.
- [66] Astrid Gasselhuber, Matthew R Dreher, Frank Rattay, Bradford J Wood, and Dieter Haemmerich. Comparison of Conventional Chemotherapy, Stealth Liposomes and Temperature-Sensitive Liposomes in a Mathematical Model. *PLoS one*, 7(10):e47453, 2012.
- [67] Ardith W El-Kareh and Timothy W Secomb. A Mathematical Model for Comparison of Bolus Injection, Continuous Infusion, and Liposomal Delivery of Doxorubicin to Tumor Cells. *Neoplasia (New York, NY)*, 2(4):325, 2000.
- [68] Roger Von Moos, Beat JK Thuerlimann, Matti Aapro, Daniel Rayson, Karen Harrold, Jalid Sehouli, Florian Scotte, Domenica Lorusso, Reinhard Dummer, Mario E Lacouture, et al. Pegylated liposomal doxorubicin-associated hand–foot syndrome: recommendations of an international panel of experts. *European journal of cancer*, 44(6):781–790, 2008.

- [69] Siraj Saadaldin Abdullah, Jean Baptiste Pialat, Marlene Wiart, François Duboeuf, Jean-Yves Mabrut, Brigitte Bancel, Agnès Rode, Christian Ducerf, Jacques Baulieux, and Yves Berthezene. Characterization of Hepatocellular Carcinoma and Colorectal Liver Metastasis by Means of Perfusion MRI. *Journal of Magnetic Resonance Imaging: An Official Journal of the International Society for Magnetic Resonance in Medicine*, 28(2):390–395, 2008.
- [70] Barbara Kneidl, Michael Peller, Gerhard Winter, Lars H Lindner, and Martin Hossann. Thermosensitive Liposomal Drug Delivery Systems: State of the Art Review. *International Journal of Nanomedicine*, 9:4387, 2014.
- [71] David Needham, Gopal Anyarambhatla, Garheng Kong, and Mark W Dewhurst. A New Temperature-Sensitive Liposome for Use with Mild Hyperthermia: Characterization and Testing in a Human Tumor Xenograft Model. *Cancer Research*, 60(5):1197–1201, 2000.
- [72] Caitlin Burke, Matthew R Dreher, Ayele H Negussie, Andrew S Mikhail, Pavel Yarmolenko, Aakash Patel, Brenden Skilskyj, Bradford J Wood, and Dieter Haemmerich. Drug Release Kinetics of Temperature Sensitive Liposomes Measured at High-Temporal Resolution with a Millifluidic Device. *International Journal of Hyperthermia*, 34(6):786–794, 2018.
- [73] Lukas Christian Sebeke, Juan Daniel Castillo Gómez, Edwin Heijman, Pia Rademann, Alexandra Claudia Simon, Sandra Ekdawi, Susan Vlachakis, Dennis Toker, Ben Lasse Mink, Claudia Schubert-Quecke, et al. Hyperthermia-Induced Doxorubicin Delivery from Thermosensitive Liposomes via MR-HIFU in a Pig Model. *Journal of Controlled Release*, 343:798–812, 2022.
- [74] N Borys. Phase 1/2 Study of ThermoDox With Approved Hyperthermia in Treatment of Breast Cancer Recurrence at the Chest Wall (DIGNITY). *ClinicalTrials.gov Identifier: NCT00826085*, 2009.
- [75] R T Poon and R Lencioni. Phase 3 Study of ThermoDox With Radiofrequency Ablation (RFA) in Treatment of Hepatocellular Carcinoma (HCC). *ClinicalTrials.gov Identifier: NCT00617981*, 2008.
- [76] R T Poon, R Lencioni, and C M Hua. A Phase III, Randomized, Double Blind, Dummy-Controlled Study of ThermoDox ® (Lyso-Thermosensitive Liposomal Doxorubicin-LTLD) in Hepatocellular Carcinoma (HCC) Using Standardized Radiofrequency Ablation (RFA) Treatment Time ≥ 45 Minutes for Solitary Lesions ≥ 3 cm to ≤ 7 cm. *ClinicalTrials.gov Identifier: NCT02112656*, 2014.

- [77] Rugo, H and Pabbathi, H and Shrestha, S and Aithal, S and Borys, N and Zoberi, I. Lyso-Thermosensitive Liposomal Doxorubicin Shows Efficacy with Minimal Adverse Events in Patients with Breast Cancer Recurrence at the Chest Wall. *San Antonio Breast Cancer Symposium*, Dec 2015. URL <https://investor.celsion.com/static-files/3b38d644-a483-4cba-8f49-02f124e680f0>.
- [78] Riccardo Lencioni and Dania Cioni. RFA plus Lyso-Thermosensitive Liposomal Doxorubicin: In Search of the Optimal Approach to Cure Intermediate-Size Hepatocellular Carcinoma. *Hepatic Oncology*, 3(3):193–200, 2016.
- [79] Celsion Corporation Receives Recommendation from Independent Data Monitoring Committee to Consider Stopping the Phase III OPTIMA Study, Jul 2020. URL <https://investor.celsion.com/news-releases/news-release-details/celsion-corporation-receives-recommendation-independent-data>.
- [80] Maximilian Regenold, Pauric Bannigan, James C Evans, Adam Waspe, Michael J Temple, and Christine Allen. Turning Down the Heat: The Case for Mild Hyperthermia and Thermosensitive Liposomes. *Nanomedicine: Nanotechnology, Biology and Medicine*, 40:102484, 2022.
- [81] Yannan Dou, Kullervo Hynynen, and Christine Allen. To Heat or Not to Heat: Challenges with Clinical Translation of Thermosensitive Liposomes. *Journal of Controlled Release*, 249:63–73, 2017.
- [82] Mohammad Souri, Madjid Soltani, and Farshad Moradi Kashkooli. Computational Modeling of Thermal Combination Therapies by Magneto-Ultrasonic Heating to Enhance Drug Delivery to Solid Tumors. *Scientific Reports*, 11(1):19539, 2021.
- [83] Martin Hossann, Johannes Hirschberger, Rebecca Schmidt, Christine Baumgartner, Katja Zimmermann, Silke Baer, Christina Ratzlaff, Michael Peller, Karin Troedson, Simone Limmer, et al. A Heat-Activated Drug-Delivery Platform Based on Phosphatidyl-(oligo)-glycerol Nanocarrier for Effective Cancer Treatment. *Advanced NanoBiomed Research*, 1(6):2000089, 2021.
- [84] Tao Lu, Wouter JM Lokerse, Ann LB Seynhaeve, Gerben A Koning, and Timo LM Ten Hagen. Formulation and Optimization of Idarubicin Thermosensitive Liposomes Provides Ultrafast Triggered Release at Mild Hyperthermia and Improves Tumor Response. *Journal of Controlled Release*, 220:425–437, 2015.
- [85] Timo LM Ten Hagen, Matthew R Dreher, Sara Zalba, Ann LB Seynhaeve, Mohamadreza Amin,

- Li Li, and Dieter Haemmerich. Drug Transport Kinetics of Intravascular Triggered Drug Delivery Systems. *Communications Biology*, 4(1):1–17, 2021.
- [86] Chelsea D Landon, Ji-Young Park, David Needham, and Mark W Dewhirst. Nanoscale Drug Delivery and Hyperthermia: The Materials Design and Preclinical and Clinical Testing of Low Temperature-Sensitive Liposomes used in Combination with Mild Hyperthermia in the Treatment of Local Cancer. *The Open Nanomedicine Journal*, 3:38, 2011.
- [87] Michael D Gray, Paul C Lyon, Christophoros Mannaris, Lisa K Folkes, Michael Stratford, Leticia Campo, Daniel YF Chung, Shaun Scott, Mark Anderson, Robert Goldin, et al. Focused Ultrasound Hyperthermia for Targeted Drug Release from Thermosensitive Liposomes: Results from a Phase I Trial. *Radiology*, 291(1):232–238, 2019.
- [88] Paul Christopher Lyon, Christophoros Mannaris, Michael Gray, Robert Carlisle, Fergus V Gleeson, David Cranston, Feng Wu, and Constantin C Coussios. Large-Volume Hyperthermia for Safe and Cost-Effective Targeted Drug Delivery Using a Clinical Ultrasound-Guided Focused Ultrasound Device. *Ultrasound in Medicine & Biology*, 47(4):982–997, 2021.
- [89] Tao Lu, Dieter Haemmerich, Hui Liu, Ann LB Seynhaeve, Gerard C van Rhoon, Adriaan B Houtsmuller, and Timo LM Ten Hagen. Externally Triggered Smart Drug Delivery System Encapsulating Idarubicin Shows Superior Kinetics and Enhances Tumoral Drug Uptake and Response. *Theranostics*, 11(12):5700, 2021.
- [90] David A Gewirtz. A Critical Evaluation of the Mechanisms of Action Proposed for the Antitumor Effects of the Anthracycline Antibiotics Adriamycin and Daunorubicin. *Biochemical Pharmacology*, 57(7):727–741, 1999.
- [91] KM Tewey, TC Rowe, L Yang, BD Halligan, and Leroy-Fong Liu. Adriamycin-Induced DNA Damage Mediated by Mammalian DNA Topoisomerase II. *Science*, 226(4673):466–468, 1984.
- [92] SH Kim and JH Kim. Lethal Effect of Adriamycin on the Division Cycle of HeLa Cells. *Cancer Research*, 32(2):323–325, 1972.
- [93] Ralph E Durand and Peggy L Olive. Flow Cytometry Studies of Intracellular Adriamycin in Single Cells In Vitro. *Cancer Research*, 41(9 Part 1):3489–3494, 1981.
- [94] Kathryn E Rogers, Brian I Carr, and Zoltán A Tökés. Cell Surface-Mediated Cytotoxicity of Polymer-Bound Adriamycin against Drug-Resistant Hepatocytes. *Cancer Research*, 43(6): 2741–2748, 1983.

- [95] Ardith W El-Kareh and Timothy W Secomb. Two-Mechanism Peak Concentration Model for Cellular Pharmacodynamics of Doxorubicin. *Neoplasia*, 7(7):705, 2005.
- [96] Nicolas Maestre, Thomas R Tritton, Guy Laurent, and Jean-Pierre Jaffr  zou. Cell Surface-Directed Interaction of Anthracyclines Leads to Cytotoxicity and Nuclear Factor κ B Activation But Not Apoptosis Signalling. *Cancer Research*, 61(6):2558–2561, 2001.
- [97] Kanu Chatterjee, Jianqing Zhang, Norman Honbo, and Joel S Karliner. Doxorubicin Cardiomyopathy. *Cardiology*, 115(2):155–162, 2010.
- [98] Liqun Zhao and Baolin Zhang. Doxorubicin Induces Cardiotoxicity Through Upregulation of Death Receptors Mediated Apoptosis in Cardiomyocytes. *Scientific Reports*, 7(1):1–11, 2017.
- [99] Joint Formulary Committee. Doxorubicin Hydrochloride- British National Formulary (online), accessed 02/06/2020, 2020. URL <https://bnf.nice.org.uk/drug/doxorubicin-hydrochloride.html>.
- [100] P Workman. Infusional Anthracyclines: Is Slower Better? If So, Why? *Annals of Oncology*, 3(8):591–594, 1992.
- [101] Mads Dalmark and HH Storm. A Fickian Diffusion Transport Process with Features of Transport Catalysis. Doxorubicin Transport in Human Red Blood Cells. *The Journal of General Physiology*, 78(4):349–364, 1981.
- [102] David J Kerr, Anne M Kerr, R Ian Freshney, and Stanley B Kaye. Comparative Intracellular Uptake of Adriamycin and 4'-Deoxydoxorubicin by Non-Small Cell Lung Tumor Cells in Culture and its Relationship to Cell Survival. *Biochemical Pharmacology*, 35(16):2817–2823, 1986.
- [103] Praveena Mohan and Natalya Rapoport. Doxorubicin as a Molecular Nanotheranostic Agent: Effect of Doxorubicin Encapsulation in Micelles or Nanoemulsions on the Ultrasound-Mediated Intracellular Delivery and Nuclear Trafficking. *Molecular Pharmaceutics*, 7(6):1959–1973, 2010.
- [104] Matthew T McKenna, Jared A Weis, Stephanie L Barnes, Darren R Tyson, Michael I Miga, Vito Quaranta, and Thomas E Yankeelov. A Predictive Mathematical Modeling Approach for the Study of Doxorubicin Treatment in Triple Negative Breast Cancer. *Scientific Reports*, 7(1):1–14, 2017.

- [105] Pawel Swietach, Alzbeta Hulikova, Shalini Patiar, Richard D Vaughan-Jones, and Adrian L Harris. Importance of Intracellular pH in Determining the Uptake and Efficacy of the Weakly Basic Chemotherapeutic Drug, Doxorubicin. *PLoS one*, 7(4):e35949, 2012.
- [106] H Peeters, EM van Zwol, L Brancato, MG MC da Cunha, and J Bogers. Systematic Review of the Registered Clinical Trials for Oncological Hyperthermia Treatment. *International Journal of Hyperthermia*, 39(1):806–812, 2022.
- [107] GC Van Rhoon, Martine Franckena, and TLM Ten Hagen. A Moderate Thermal Dose is Sufficient for Effective Free and TSL based Thermochemotherapy. *Advanced Drug Delivery Reviews*, 163:145–156, 2020.
- [108] Mark W Dewhirst, Zeljko Vujaskovic, Ellen Jones, and Donald Thrall. Re-setting the Biologic Rationale for Thermal Therapy. *International Journal of Hyperthermia*, 21(8):779–790, 2005.
- [109] Peter Vaupel, Helmut Piazena, Markus Notter, Andreas R Thomsen, Anca-L Grosu, Felix Scholkmann, Alan Graham Pockley, and Gabriele Multhoff. From Localized Mild Hyperthermia to Improved Tumor Oxygenation: Physiological Mechanisms Critically Involved in Oncologic Thermo-Radio-Immunotherapy. *Cancers*, 15(5):1394, 2023.
- [110] Arlene L Oei, Lianne EM Vriend, Johannes Crezee, Nicolaas AP Franken, and Przemek M Krawczyk. Effects of Hyperthermia on DNA Repair Pathways: One Treatment to Inhibit Them All. *Radiation Oncology*, 10(1):1–13, 2015.
- [111] Simon N Powell and Lisa A Kachnic. Homologous Recombination Research is Heating Up and Ready for Therapy. *Proceedings of the National Academy of Sciences*, 108(24):9731–9732, 2011.
- [112] Diana Salvador, Verónica Bastos, and Helena Oliveira. Hyperthermia Enhances Doxorubicin Therapeutic Efficacy Against A375 and MNT-1 Melanoma Cells. *International Journal of Molecular Sciences*, 23(1):35, 2022.
- [113] Costanza E Maurici, Robin Colenbier, Britta Wylleman, Luigi Brancato, Eke van Zwol, Johan Van den Bossche, Jean-Pierre Timmermans, Elisa Giovannetti, Marina GMC Mori da Cunha, and Johannes Bogers. Hyperthermia Enhances Efficacy of Chemotherapeutic Agents in Pancreatic Cancer Cell Lines. *Biomolecules*, 12(5):651, 2022.
- [114] Enzo M Scutigliani, Yongxin Liang, Hans Crezee, Roland Kanaar, and Przemek M Krawczyk.

- Modulating the Heat Stress Response to Improve Hyperthermia-Based Anticancer Treatments. *Cancers*, 13(6):1243, 2021.
- [115] Denis Lecavalier and William J Mackillop. The Effect of Hyperthermia on Glucose Transport in Normal and Thermal-Tolerant Chinese Hamster Ovary Cells. *Cancer Letters*, 29(2):223–231, 1985.
- [116] Yang Liu, Cheong-Weon Cho, Xiangdong Yan, Thomas K Henthorn, Kevin O Lillehei, Wesley N Cobb, and Ka-yun Ng. Ultrasound-Induced Hyperthermia Increases Cellular Uptake and Cytotoxicity of P-glycoprotein Substrates in Multi-Drug Resistant Cells. *Pharmaceutical Research*, 18:1255–1261, 2001.
- [117] Terence Ta and Tyrone M Porter. Thermosensitive Liposomes for Localized Delivery and Triggered Release of Chemotherapy. *Journal of Controlled Release*, 169(1-2):112–125, 2013.
- [118] Paul C Lyon, Lucy F Griffiths, Jenni Lee, Daniel Chung, Robert Carlisle, Feng Wu, Mark R Middleton, Fergus V Gleeson, and Constantin C Coussios. Clinical Trial Protocol for TARDOX: A Phase I Study to Investigate the Feasibility of Targeted Release of Lyso-Thermosensitive Liposomal Doxorubicin (ThermoDox®) using Focused Ultrasound in Patients with Liver Tumours. *Journal of Therapeutic Ultrasound*, 5(1):1–8, 2017.
- [119] Jay L Dinerman, Ronald D Berger, and Hugh Galkins. Temperature Monitoring During Radiofrequency Ablation. *Journal of Cardiovascular Electrophysiology*, 7(2):163–173, 1996.
- [120] Astrid Gasselhuber, Matthew R Dreher, Ari Partanen, Pavel S Yarmolenko, David Woods, Bradford J Wood, and Dieter Haemmerich. Targeted Drug Delivery by High Intensity Focused Ultrasound Mediated Hyperthermia Combined with Temperature-Sensitive Liposomes: Computational Modelling and Preliminary In Vivo Validation. *International Journal of Hyperthermia*, 28(4):337–348, 2012.
- [121] Cong Liu and Xiao Yun Xu. A Systematic Study of Temperature Sensitive Liposomal Delivery of Doxorubicin using a Mathematical Model. *Computers in Biology and Medicine*, 60:107–116, 2015.
- [122] Davud Asemani and Dieter Haemmerich. A Unified Mathematical Model for Nano-Liposomal Drug Delivery to Solid Tumors. *IEEE Transactions on Nanobioscience*, 17(1):3–11, 2017.
- [123] Tao Lu and Timo LM Ten Hagen. A Novel Kinetic Model to Describe the Ultra-Fast Triggered

- Release of Thermosensitive Liposomal Drug Delivery Systems. *Journal of Controlled Release*, 324:669–678, 2020.
- [124] Rebecca J Shipley and S Jonathan Chapman. Multiscale Modelling of Fluid and Drug Transport in Vascular Tumours. *Bulletin of Mathematical Biology*, 72(6):1464–1491, 2010.
- [125] Moath Alamer and Xiao Yun Xu. Investigating the Effect of Tumor Microvascular Architecture on Drug Transport and Distribution. *Proceedings of the 4th World Congress on Electrical Engineering and Computer Systems and Sciences (EECSS'18)*, 2018.
- [126] Randall J LeVeque et al. *Finite Volume Methods for Hyperbolic Problems*, volume 31. Cambridge University Press, 2002.
- [127] Timothy W Secomb. A Green's Function Method for Simulation of Time-Dependent Solute Transport and Reaction in Realistic Microvascular Geometries. *Mathematical Medicine and Biology: A Journal of the IMA*, 33(4):475–494, 2016.
- [128] Timothy W Secomb, Richard Hsu, Eric YH Park, and Mark W Dewhirst. Green's Function Methods for Analysis of Oxygen Delivery to Tissue by Microvascular Networks. *Annals of Biomedical Engineering*, 32(11):1519–1529, 2004.
- [129] Daniel L Gustafson, Jeffrey C Rastatter, Tina Colombo, and Michael E Long. Doxorubicin Pharmacokinetics: Macromolecule Binding, Metabolism, and Excretion in the Context of a Physiologic Model. *Journal of Pharmaceutical Sciences*, 91(6):1488–1501, 2002.
- [130] Dominic J Vitello, Richard M Ripper, Michael R Fettiplace, Guy L Weinberg, and Joseph M Vitello. Blood Density is Nearly Equal to Water Density: A Validation Study of the Gravimetric Method of Measuring Intraoperative Blood Loss. *Journal of Veterinary Medicine*, 2015, 2015.
- [131] H H Billett. *Hemoglobin and Hematocrit*. Butterworths, 1990.
- [132] Bernard E Van Beers, Isabelle Leconte, Roland Materne, Anne M Smith, Jacques Jamart, and Yves Horsmans. Hepatic Perfusion Parameters in Chronic Liver Disease: Dynamic CT Measurements Correlated with Disease Severity. *American Journal of Roentgenology*, 176(3):667–673, 2001.
- [133] David M Brizel, Bruce Klitzman, J Michael Cook, Jeri Edwards, Gary Rosner, and Mark W Dewhirst. A Comparison of Tumor and Normal Tissue Microvascular Hematocrits and Red Cell Fluxes in a Rat Window Chamber Model. *International Journal of Radiation Oncology, Biology, Physics*, 25(2):269–276, 1993.

- [134] Ning Z Wu, Daphne Da, Tracy L Rudoll, David Needham, A Richard Whorton, and Mark W Dewhirst. Increased Microvascular Permeability Contributes to Preferential Accumulation of Stealth Liposomes in Tumor Tissue. *Cancer Research*, 53(16):3765–3770, 1993.
- [135] Ning Z Wu, Bruce Klitzman, Gary Rosner, David Needham, and Mark W Dewhirst. Measurement of Material Extravasation in Microvascular Networks using Fluorescence Video-Microscopy. *Microvascular Research*, 46(2):231–253, 1993.
- [136] Duane E Hilmas and Edward L Gillette. Morphometric Analyses of the Microvasculature of Tumors during Growth and After X-Irradiation. *Cancer*, 33(1):103–110, 1974.
- [137] Rakesh K Jain. Transport of molecules in the tumor interstitium: a review. *Cancer research*, 47(12):3039–3051, 1987.
- [138] Joseph A Sparano, James Speyer, William J Gradishar, Leonard Liebes, Rajeshwari Sridhara, Sandra Mendoza, David Fry, and Merrill J Egorin. Phase I Trial of Escalating Doses of Paclitaxel plus Doxorubicin and Dexrazoxane in Patients with Advanced Breast Cancer. *Journal of Clinical Oncology*, 17(3):880–880, 1999.
- [139] Ronnie TP Poon and Nicholas Borys. Lyso-Thermosensitive Liposomal Doxorubicin: A Novel Approach to Enhance Efficacy of Thermal Ablation of Liver Cancer. *Expert Opinion on Pharmacotherapy*, 10(2):333–343, 2009.
- [140] Ari Partanen, Pavel S Yarmolenko, Antti Viitala, Sunil Appanaboyina, Dieter Haemmerich, Ashish Ranjan, Genevieve Jacobs, David Woods, Julia Enholm, Bradford J Wood, et al. Mild hyperthermia with magnetic resonance-guided high-intensity focused ultrasound for applications in drug delivery. *International journal of hyperthermia*, 28(4):320–336, 2012.
- [141] Ron Milo, Paul Jorgensen, Uri Moran, Griffin Weber, and Michael Springer. BioNumbers — The Database of Key Numbers in Molecular and Cell Biology. *Nucleic Acids Research*, 38(suppl_1):D750–D753, 2010.
- [142] Alberto Zaniboni, Swapna Prabhu, and Riccardo A Audisio. Chemotherapy and Anaesthetic Drugs: Too Little is Known. *The Lancet Oncology*, 6(3):176–181, 2005.
- [143] Francesca Pianosi, Fanny Sarrazin, and Thorsten Wagener. A MATLAB Toolbox for Global Sensitivity Analysis. *Environmental Modelling & Software*, 70:80–85, 2015.

- [144] Francesca Campolongo, Andrea Saltelli, and Jessica Cariboni. From Screening to Quantitative Sensitivity Analysis. A Unified Approach. *Computer Physics Communications*, 182(4):978–988, 2011.
- [145] Andrea Saltelli, Paola Annoni, Ivano Azzini, Francesca Campolongo, Marco Ratto, and Stefano Tarantola. Variance Based Sensitivity Analysis of Model Output. Design and Estimator for the Total Sensitivity Index. *Computer Physics Communications*, 181(2):259–270, 2010.
- [146] Howard Gurney. How to Calculate the Dose of Chemotherapy. *British Journal of Cancer*, 86(8):1297–1302, 2002.
- [147] Delafield Du Bois and Eugene F Du Bois. Clinical Calorimetry: Tenth Paper A Formula to Estimate the Approximate Surface Area if Height and Weight be Known. *Archives of Internal Medicine*, 17(6_2):863–871, 1916.
- [148] Fan Yuan, Michael Leunig, David A Berk, and Rakesh K Jain. Microvascular Permeability of Albumin, Vascular Surface Area, and Vascular Volume Measured in Human Adenocarcinoma LS174T using Dorsal Chamber in SCID Mice. *Microvascular Research*, 45(3):269–289, 1993.
- [149] V Goh and R Glynne-Jones. Perfusion CT Imaging of Colorectal Cancer. *The British Journal of Radiology*, 87(1034):20130811, 2014.
- [150] Maximum Allowable Blood Loss, 2017. URL <https://medicine.uiowa.edu/iowaprotocols/maximum-allowable-blood-loss>.
- [151] Hematocrit: Medlineplus Medical Encyclopedia, 2023. URL <https://medlineplus.gov/ency/article/003646.htm>.
- [152] Mark Middleton. PanDox: Targeted Doxorubicin in Pancreatic Tumours (PanDox), Mar 2023. URL <https://clinicaltrials.gov/ct2/show/NCT04852367>.
- [153] Amalia Ruiz, Guanglong Ma, Jani Seitsonen, Sara GT Pereira, Janne Ruokolainen, and Wafa T Al-Jamal. Encapsulated Doxorubicin Crystals Influence Lysolipid Temperature-Sensitive Liposomes Release and Therapeutic Efficacy In Vitro and In Vivo. *Journal of Controlled Release*, 328:665–678, 2020.
- [154] Adi de la Zerda, Michael J Kratochvil, Nicholas A Suhar, and Sarah C Heilshorn. Bioengineering Strategies to Probe T Cell Mechanobiology. *APL Bioengineering*, 2(2):021501, 2018.
- [155] Carrie J Lovitt, Todd B Shelper, and Vicky M Avery. Doxorubicin Resistance in Breast Cancer Cells is Mediated by Extracellular Matrix Proteins. *BMC Cancer*, 18(1):41, 2018.

- [156] Ami Yamamoto, Yin Huang, Brad A Krajina, Margaux McBirney, Andrea E Doak, Sixuan Qu, Carolyn L Wang, Michael C Haffner, and Kevin J Cheung. Metastasis from the Tumor Interior and Necrotic Core Formation are Regulated by Breast Cancer-Derived Angiopoietin-Like 7. *Proceedings of the National Academy of Sciences*, 120(10):e2214888120, 2023.
- [157] Yutaka Shimoyama, Tetsuro Kubota, Masahiko Watanabe, Kyuya Ishibiki, and Osahiko Abe. Predictability of In Vivo Chemosensitivity by In Vitro MTT Assay with Reference to the Clonogenic Assay. *Journal of Surgical Oncology*, 41(1):12–18, 1989.
- [158] Aysun Adan, Yagmur Kiraz, and Yusuf Baran. Cell Proliferation and Cytotoxicity Assays. *Current Pharmaceutical Biotechnology*, 17(14):1213–1221, 2016.
- [159] Nikko Brix, Daniel Samaga, Roman Hennel, Katharina Gehr, Horst Zitzelsberger, and Kirsten Lauber. The Clonogenic Assay: Robustness of Plating Efficiency-Based Analysis is Strongly Compromised by Cellular Cooperation. *Radiation Oncology*, 15:1–12, 2020.
- [160] Su-Wen Lim, Hwei-San Loh, Kang-Nee Ting, Tracey Dawn Bradshaw, and Zeenathul Nazariah Allaudin. Reduction of MTT to Purple Formazan by Vitamin E Isomers in the Absence of Cells. *Tropical Life Sciences Research*, 26(1):111, 2015.
- [161] Hee Sam Na, Yeun Keun Lim, Young-Il Jeong, Hyun Sook Lee, You Jin Lim, Mi Sun Kang, Chong-Su Cho, and Hyun Chul Lee. Combination Antitumor Effects of Micelle-Loaded Anti-cancer Drugs in a CT-26 Murine Colorectal Carcinoma Model. *International Journal of Pharmaceutics*, 383(1-2):192–200, 2010.
- [162] Andrey V Shubin, Ilya V Demidyuk, Alexey A Komissarov, Lola M Rafieva, and Sergey V Kostrov. Cytoplasmic Vacuolization in Cell Death and Survival. *Oncotarget*, 7(34):55863, 2016.
- [163] Nicolaas AP Franken, Hans M Rodermond, Jan Stap, Jaap Haveman, and Chris Van Bree. Clonogenic Assay of Cells In Vitro. *Nature Protocols*, 1(5):2315–2319, 2006.
- [164] Beata Brzozowska, Maciej Gałeczki, Adrianna Tartas, Józef Ginter, Urszula Kaźmierczak, and Lovisa Lundholm. Freeware Tool for Analysing Numbers and Sizes of Cell Colonies. *Radiation and Environmental Biophysics*, 58(1):109–117, 2019.
- [165] Paul Christopher Lyon, Visa Suomi, Philip Jakeman, Leticia Campo, Constantin Coussios, and Robert Carlisle. Quantifying Cell Death Induced by Doxorubicin, Hyperthermia or HIFU Ablation with Flow Cytometry. *Scientific Reports*, 11(1):1–19, 2021.

- [166] H Vakifahmetoglu, M Olsson, and B Zhitovskiy. Death Through a Tragedy: Mitotic Catastrophe. *Cell Death & Differentiation*, 15(7):1153–1162, 2008.
- [167] Michalis Fragkos and Peter Beard. Mitotic Catastrophe Occurs in the Absence of Apoptosis in p53-null Cells with a Defective G1 Checkpoint. *PLoS One*, 6(8):e22946, 2011.
- [168] D Grzanka, A Grzanka, M Izdebska, L Gackowska, A Stepien, and A Marszalek. Actin Reorganization in CHO AA8 Cells Undergoing Mitotic Catastrophe and Apoptosis Induced by Doxorubicin. *Oncology Reports*, 23(3):655–663, 2010.
- [169] Malgorzata A Sliwinska, Grazyna Mosieniak, Kamila Wolanin, Aneta Babik, Katarzyna Piwocka, Adriana Magalska, Joanna Szczepanowska, Jan Fronk, and Ewa Sikora. Induction of Senescence with Doxorubicin Leads to Increased Genomic Instability of HCT116 Cells. *Mechanisms of Ageing and Development*, 130(1-2):24–32, 2009.
- [170] Abdelhadi Rebbaa, Xin Zheng, Pauline M Chou, and Bernard L Mirkin. Caspase Inhibition Switches Doxorubicin-Induced Apoptosis to Senescence. *Oncogene*, 22(18):2805–2811, 2003.
- [171] Razmik Mirzayans, Bonnie Andraiss, and David Murray. Roles of Polyploid/Multinucleated Giant Cancer Cells in Metastasis and Disease Relapse following Anticancer Treatment. *Cancers*, 10(4):118, 2018.
- [172] Young-Woo Eom, MI Kim, Seok Soon Park, Mi Jin Goo, Hyuk Jae Kwon, Seonghyang Sohn, Wook-Hwan Kim, Gyesoon Yoon, and Kyeong Sook Choi. Two Distinct Modes of Cell Death Induced by Doxorubicin: Apoptosis and Cell Death Through Mitotic Catastrophe Accompanied by Senescence-Like Phenotype. *Oncogene*, 24(30):4765–4777, 2005.
- [173] Albert N Ngo, Miezan JM Ezoulin, Ibrahima Youm, and Bi-Botti C Youan. Optimal Concentration of 2, 2, 2-Trichloroacetic Acid for Protein Precipitation Based on Response Surface Methodology. *Journal of Analytical & Bioanalytical Techniques*, 5(4), 2014.
- [174] Clifford M Hurvich and Chih-Ling Tsai. Regression and Time Series Model Selection in Small Samples. *Biometrika*, 76(2):297–307, 1989.
- [175] Katie F Maass, Chethana Kulkarni, Mohiuddin A Quadir, Paula T Hammond, Alison M Betts, and Karl Dane Wittrup. A Flow Cytometric Clonogenic Assay Reveals the Single-Cell Potency of Doxorubicin. *Journal of Pharmaceutical Sciences*, 104(12):4409–4416, 2015.

- [176] Xionge Mei, Hans M Rodermond, Nicolaas AP Franken, Lukas JA Stalpers, Johannes Crezee, H. Petra Kok, and Arlene L Oei. Poster: A Short Time Interval Between Radiotherapy and Hyperthermia Leads to Better Tumor Control in Cervical Cancer Models. In *European Society for Hyperthermic Oncology, Gothenburg, Sweden, September 2022*.
- [177] Kenneth R Hande. Clinical Applications of Anticancer Drugs Targeted to Topoisomerase II. *Biochimica et Biophysica Acta (BBA) - Gene Structure and Expression*, 1400(1-3):173–184, 1998.
- [178] HC Gillies, D Herriott, R Liang, K Ohashi, HJ Rogers, and PG Harper. Pharmacokinetics of Idarubicin (4-demethoxydaunorubicin; IMI-30; NSC 256439) Following Intravenous and Oral Administration in Patients with Advanced Cancer. *British Journal of Clinical Pharmacology*, 23(3):303–310, 1987.
- [179] Richard L Magin, Jane M Hunter, Michael R Niesman, and George A Bark. Effect of Vesicle Size on the Clearance, Distribution, and Tumor Uptake of Temperature-Sensitive Liposomes. *Cancer Drug Delivery*, 3(4):223–237, 1986.
- [180] Christina R Miller, Bruce Bondurant, Shannon D McLean, Kathy A McGovern, and David F O'Brien. Liposome-Cell Interactions In Vitro: Effect of Liposome Surface Charge on the Binding and Endocytosis of Conventional and Sterically Stabilized Liposomes. *Biochemistry*, 37(37):12875–12883, 1998.
- [181] August Krogh. The Number and Distribution of Capillaries in Muscles with Calculations of the Oxygen Pressure Head Necessary for Supplying the Tissue. *The Journal of Physiology*, 52(6):409, 1919.
- [182] Daniel Goldman. Theoretical Models of Microvascular Oxygen Transport to Tissue. *Microcirculation*, 15(8):795–811, 2008.
- [183] John P Kirkpatrick and Mark W Dewhirst. Analytic Solution to Steady-State Radial Diffusion of a Substrate with First-Order Reaction Kinetics in the Tissue of a Krogh's Cylinder. *Radiation research*, 169(3):350–354, 2008.
- [184] Oliver Degerstedt, Johan Gråsjö, Anton Norberg, Erik Sjögren, Per Hansson, and Hans Lennernäs. Drug Diffusion in Biomimetic Hydrogels: Importance for Drug Transport and Delivery in Non-Vascular Tumor Tissue. *European Journal of Pharmaceutical Sciences*, 172:106150, 2022.

- [185] Ian F Tannock, Carol M Lee, Jonathon K Tunggal, David SM Cowan, and Merrill J Egorin. Limited Penetration of Anticancer Drugs Through Tumor Tissue: A Potential Cause of Resistance of Solid Tumors to Chemotherapy. *Clinical Cancer Research*, 8(3):878–884, 2002.
- [186] Timothy W Secomb. Krogh-Cylinder and Infinite-Domain Models for Washout of an Inert Diffusible Solute from Tissue. *Microcirculation*, 22(1):91–98, 2015.
- [187] Sanjay Batra and Karel Rakusan. Capillary Length, Tortuosity, and Spacing in Rat Myocardium during Cardiac Cycle. *American Journal of Physiology-Heart and Circulatory Physiology*, 263(5):H1369–H1376, 1992.
- [188] KP Ivanov, MK Kalinina, and Yu I Levkovich. Blood Flow Velocity in Capillaries of Brain and Muscles and its Physiological Significance. *Microvascular Research*, 22(2):143–155, 1981.
- [189] Francesca Campolongo, Jessica Cariboni, and Andrea Saltelli. An Effective Screening Design for Sensitivity Analysis of Large Models. *Environmental Modelling & Software*, 22(10):1509–1518, 2007.
- [190] Kathryn M Field, Suzanne Kosmider, Michael Jefford, Michael Michael, Ross Jennens, Michael Green, and Peter Gibbs. Chemotherapy Dosing Strategies in the Obese, Elderly, and Thin Patient: Results of a Nationwide Survey. *Journal of Oncology Practice*, 4(3):108–113, 2008.
- [191] Gail ter Haar and Constantin Coussios. High Intensity Focused Ultrasound: Physical Principles and Devices. *International Journal of Hyperthermia*, 23(2):89–104, 2007.
- [192] Tatsuaki Tagami, Mark J Ernsting, and Shyh-Dar Li. Efficient Tumor Regression by a Single and Low Dose Treatment with a Novel and Enhanced Formulation of Thermosensitive Liposomal Doxorubicin. *Journal of Controlled Release*, 152(2):303–309, 2011.
- [193] Jennifer Martin. Blood Collection in the Pet Mouse, Nov 2021. URL https://ksvdl.org/resources/news/diagnostic_insights_for_technicians/october2015/blood-collection-in-mouse.html.
- [194] Mari Tsuchihashi, Hideyoshi Harashima, and Hiroshi Kiwada. Development of a Pharmacokinetic/Pharmacodynamic (PK/PD)-Simulation System for Doxorubicin in Long Circulating Liposomes in Mice using Peritoneal P388. *Journal of Controlled Release*, 61(1-2):9–19, 1999.
- [195] Cell Signalling Technology, Inc. Doxorubicin, accessed 02/05/2022, 2022. URL <https://www.cellsignal.com/products/activators-inhibitors/doxorubicin/5927>.

- [196] M Verheijen, Matthias Lienhard, Yannick Schrooders, Olivia Clayton, Ramona Nudischer, Stefan Boerno, Bernd Timmermann, Nathalie Selevsek, Ralph Schlapbach, Hans Gmuender, et al. DMSO Induces Drastic Changes in Human Cellular Processes and Epigenetic Landscape In Vitro. *Scientific Reports*, 9(1):1–12, 2019.
- [197] Andrey A Gurtovenko and Jamshed Anwar. Modulating the Structure and Properties of Cell Membranes: The Molecular Mechanism of Action of Dimethyl Sulfoxide. *The Journal of Physical Chemistry B*, 111(35):10453–10460, 2007.
- [198] Marie-Amelie de Menorval, Lluís M Mir, M Laura Fernández, and Ramon Reigada. Effects of Dimethyl Sulfoxide in Cholesterol-Containing Lipid Membranes: A Comparative Study of Experiments In Silico and with Cells. *PloS One*, 7(7):e41733, 2012.
- [199] Jianguo Wen, Yijiu Tong, and Youli Zu. Low Concentration DMSO Stimulates Cell Growth and In Vitro Transformation of Human Multiple Myeloma Cells. *British Journal of Medicine and Medical Research*, 5(1):65, 2015.
- [200] Graeme J Finlay and Bruce C Baguley. Effects of Protein Binding on the In Vitro Activity of Antitumour Acridine Derivatives and Related Anticancer Drugs. *Cancer Chemotherapy and Pharmacology*, 45(5):417–422, 2000.
- [201] Patrick J McNamara and Jane Alcorn. Protein Binding Predictions in Infants. *AAPS PharmSci*, 4(1):19–26, 2002.
- [202] Fetal Bovine Serum (FBS), Accessed 03/05/2022, 2022. URL <https://rmbio.com/collections/summer/products/fbs>.
- [203] Staffan Eksborg, Hans Ehrsson, and Britta Ekqvist. Protein Binding of Anthraquinone Glycosides, with Special Reference to Adriamycin. *Cancer Chemotherapy and Pharmacology*, 10(1):7–10, 1982.
- [204] Kuang Tzu Huang, Yen Hao Chen, and Ameae M Walker. Inaccuracies in MTS Assays: Major Distorting Effects of Medium, Serum Albumin, and Fatty Acids. *Biotechniques*, 37(3):406–412, 2004.
- [205] Georgina L Dobek, Xiujuan Zhang, Daniel A Balazs, and WT Godbey. Analysis of Promoters and Expression-Targeted Gene Therapy Optimization Based on Doubling Time and Transfectability. *The FASEB Journal*, 25(9):3219–3228, 2011.

- [206] Julie A Stenken. Methods and Issues in Microdialysis Calibration. *Analytica Chimica Acta*, 379 (3):337–358, 1999.
- [207] Gillian Whitaker and Craig E Lunte. Investigation of Microdialysis Sampling Calibration Approaches for Lipophilic Analytes: Doxorubicin. *Journal of Pharmaceutical and Biomedical Analysis*, 53(3):490–496, 2010.